Annual Report 2017

Institute for Nuclear Waste Disposal
Institut für Nukleare Entsorgung

H. Geckeis, M. Altmaier, S. Fanghänel (Eds.)

KIT
Karlsruhe Institute of Technology

Table of contents

1 Introduction to the Institute for Nuclear Waste Disposal (INE)

The **Institute for Nuclear Waste Disposal** (INE), at the Karlsruhe Institute of Technology **KIT** performs R&D focusing on

(i) **Long-term safety research for nuclear waste disposal (key focus of INE research),**
(ii) **Radiation protection**
(iii) **Decommissioning of nuclear facilities**
(iv) **Geoenergy.**

All R&D activities of INE are integrated into the program Nuclear Safety Research within the KIT-Energy Center and the program Nuclear Waste Management, Safety and Radiation Research (NUSAFE) within the Helmholtz Association. INE contributes to German provident research for the safety of nuclear waste disposal, which is the responsibility of the Federal Government.

Following the decision taken by Germany to phase out the use of nuclear energy, the safe disposal of long-lived nuclear waste remains as a key topic of highest priority. Projections based on scheduled operation times for nuclear power plants (Amendment to German Atomic Energy Act, August 2011) in Germany indicate that about a total of 17,770 tons of spent nuclear fuel will be generated. About 6,670 tons have been shipped to France and the UK until 2005 for reprocessing, to recover plutonium and uranium. Consequently, two types of high level, heat producing radioactive waste (HLW) have to be disposed of safely: spent nuclear fuel and vitrified high level waste from reprocessing (HLW glass). The disposal of low- and intermediate level waste present in much larger quantities likewise needs to be addressed.

Over the last decades, a consensus within the international scientific/technical community was established, clearly emphasizing that disposal in deep geological formations is the safest way to dispose of high level, heat producing radioactive waste. Disposal concepts with strong inherent passive safety features ensure the effective protection of the population and the biosphere against radiation exposure over very long periods of time. The isolation and immobilization of nuclear waste in a repository is ensured by the appropriate combination of redundant barriers (multi-barrier system).

Long term safety research for nuclear waste disposal at INE establishes geochemical expertise and models to be used in the disposal Safety Case, focusing primarily on the detailed scientific description of aquatic radionuclide chemistry in the geochemical environment of a repository. Work concentrates on the disposal of spent nuclear fuel and HLW-glass in the relevant potential host rock formations currently considered: rock salt, clay and crystalline rock formations. Actinides and long-lived fission and activation products play a central role, as they dominate HLW radiotoxicity over long periods of time. Long-lived anionic fission and activation products are likewise investigated as significant contributors to the maximum radiation dose projected for relevant scenarios.

Relevant long-term scenarios for nuclear repositories in deep geological formations have to take into account possible radionuclide transport via the groundwater pathway. Possible groundwater intrusion into emplacement caverns is assumed to cause waste form corrosion and eventually radionuclide release. Radionuclide mobility is then determined by the various geochemical reactions in complex aquatic systems: i.e. dissolution of the nuclear waste form (HLW glass, spent nuclear fuel), radiolysis phenomena, redox reactions, complexation with inorganic and organic ligands, colloid formation, surface reactions at mineral surfaces, precipitation of solid phases and solid solutions.

Prediction and quantification of all these processes require fundamental thermodynamic data and comprehensive process understanding at the molecular scale. Radionuclide concentrations in relevant aqueous systems typically lie in the nano-molar range, which is exceedingly small in relation to main groundwater components. Quantification of chemical reactions occurring in these systems require the application and development of advanced tools and experimental approaches, to provide insight into the chemical speciation of radionuclides at trace concentrations. Innovative laser and X-ray spectroscopic techniques are continuously developed and applied to this end. A specialized working group performing state-of-art theoretical quantum chemical calculations for actinide chemistry support both interpretation of experimental results and optimized experiment design.

The long-term safety of a nuclear waste repository must be demonstrated by application of modelling tools on real natural systems over geological time scales. Geochemical models and thermodynamic databases are developed at INE as basis for the description of radionuclide geochemical behavior in complex natural aquatic systems. The prediction of radionuclide migration in the geosphere necessitates coupled modelling of geochemistry and transport. Transferability and applicability of model predictions are examined by designing dedicated laboratory experiments, field studies in underground laboratories and by studying natural analog systems. This strategy allows to identify and analyze key uncertainties and continuously optimize the developed models.

The R&D topic **radiation protection** at INE focuses on the assessment of radiation exposures on man by estimating doses from external radiation

fields. The strategy driving this work is to provide techniques and models for an individualized dosimetry, which goes beyond the current approach of applying reference models in dose assessment. Both the specific anatomical and physiological features of the exposed individual and the specific effective radiation fields are considered in the frame of an individualized dosimetry. Work is performed in close cooperation with the KIT safety management SUM.

The R&D topic **decommissioning of nuclear and conventional facilities** at INE expands the existing activities at the Institute of Technology and Management in Construction (KIT-TMB). Research in this field is focusing on a better understanding of the complete decommissioning process in Germany as well as on a global level.

The topic **geoenergy** is mainly focusing on geothermal energy research in fractured reservoir systems with special focus on Enhanced Geothermal Systems (EGS).

INE laboratories are equipped with all necessary infrastructures to perform radionuclide/actinide research, including hot cells, alpha glove boxes, inert gas alpha glove boxes and radionuclide laboratories. State-of-the-art analytical instruments and methods are applied for analysis and speciation of radionuclides and radioactive materials. Advanced spectroscopic tools exist for the sensitive detection and analysis of radionuclides. Trace element and isotope analysis is made by instrumental analytical techniques such as atomic absorption spectroscopy (AAS), ICP-atomic emission spectroscopy (ICP-AES) and ICP-mass spectrometry (Quadrupole-ICP-MS and high resolution ICP-MS). Methods available for surface sensitive analysis and characterization of solid samples include X-ray diffraction (XRD), atomic force microscopy (AFM) and laser-ablation coupled with ICP-MS. A modern X-ray photoelectron spectrometer (XPS) and an environmental scanning electron microscope (ESEM) are installed. INE has direct access to a TEM instrument on the KIT Campus North site

(Institute for Applied Materials, IAM). Laser spectroscopic techniques are developed and applied for sensitive actinide and fission product speciation such as time-resolved laser fluorescence spectroscopy (TRLFS), laser-induced breakdown spectroscopy (LIBS) and Raman spectroscopy. Insight into structural and electronic properties of radionuclide species is obtained by X-ray absorption fine structure (XAFS) spectroscopy and related techniques available at the INE-Beamline and the ACT experimental station at the KIT synchrotron source KARA. The ACT laboratory for radionuclide research at the new CAT-ACT beamline – a state-of the art facility jointly operated by INE and ITCP/IKFT – became fully operational in 2016. INE's beamlines, in close proximity to INE controlled area laboratories, represent in combination with the other analytical methods a unique experimental infrastructure, which both profits from and contributes to INE's leading expertise in the field of actinide chemistry and spectroscopy. A 400 MHz-NMR spectrometer adapted to measuring radioactive liquid samples adds to the analytical and speciation portfolio of INE. Quantum chemical calculations are performed on INE's computing cluster, which is equipped with 17 nodes and 76 processors. The INE CAD workstations enable construction and planning of hardware components, process layout and flow sheets. The institute workshop is equipped with modern machine tools to manufacture components for specific experimental and analytical devices in hot laboratories.

In 2017, the **Institute for Nuclear Waste Disposal** had around **90 employees** working in the six departments, which reflect the R&D and organizational tasks of the institute (Fig. 1):

(i) Technical infrastructure / analytical chemistry
(ii) Safety of nuclear waste disposal
(iii) Radiochemistry
(iv) Radionuclide speciation
(v) Geochemistry
(vi) Decommissioning of nuclear and conventional facilities.

Institute for Nuclear Waste Disposal (INE)

Director: Prof. Dr. H. Geckeis
Deputy Director: Prof. Dr. Th. Schäfer

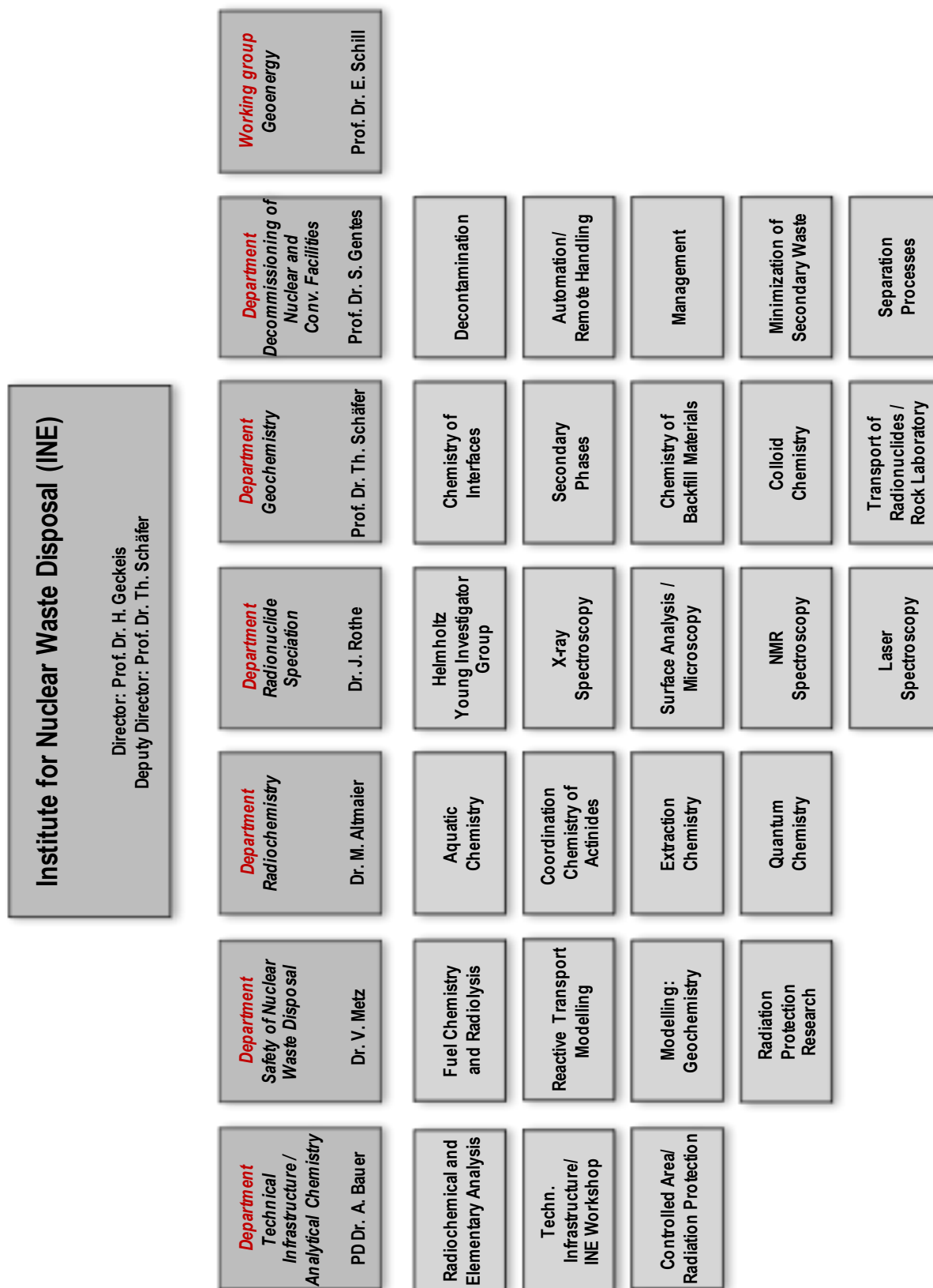| Department Technical Infrastructure / Analytical Chemistry — PD Dr. A. Bauer	Department Safety of Nuclear Waste Disposal — Dr. V. Metz	Department Radiochemistry — Dr. M. Altmaier	Department Radionuclide Speciation — Dr. J. Rothe	Department Geochemistry — Prof. Dr. Th. Schäfer	Department Decommissioning of Nuclear and Conv. Facilities — Prof. Dr. S. Gentes	Working group Geoenergy — Prof. Dr. E. Schill
Radiochemical and Elementary Analysis	Fuel Chemistry and Radiolysis	Aquatic Chemistry	Helmholtz Young Investigator Group	Chemistry of Interfaces	Decontamination	
Techn. Infrastructure/ INE Workshop	Reactive Transport Modelling	Coordination Chemistry of Actinides	X-ray Spectroscopy	Secondary Phases	Automation/ Remote Handling	
Controlled Area/ Radiation Protection	Modelling: Geochemistry	Extraction Chemistry	Surface Analysis / Microscopy	Chemistry of Backfill Materials	Management	
	Radiation Protection Research	Quantum Chemistry	NMR Spectroscopy	Colloid Chemistry	Minimization of Secondary Waste	
			Laser Spectroscopy	Transport of Radionuclides / Rock Laboratory	Separation Processes	

Fig. 1: Organizational chart of the Institute for Nuclear Waste Disposal (INE)

2 Education and training

Teaching of students and promotion of young scientists is of fundamental importance to ensure high-level competence and to maintain a leading international position in the fields of nuclear and radiochemistry. INE scientists are strongly involved in teaching at KIT Campus South and the Universities of Heidelberg, Jena and Strasbourg as well as the TU Darmstadt.

Prof. Dr. **Horst Geckeis**, director of INE, holds a professorship for radiochemistry at KIT Campus South, Department of Chemistry and Biosciences. He teaches fundamental and applied radiochemistry for chemistry students in bachelor and master courses. A radiochemistry module consisting of basic and advanced lectures on nuclear chemistry topics and laboratory courses has been set up for master students in Karlsruhe. In addition, Dr. **Marcus Altmaier**, head of the department radiochemistry, gives a lecture concerning the chemistry of f-elements.

Prof. Dr. **Sascha Gentes** head of the department decommissioning of nuclear and conventional facilities holds a professorship at the Institute for Technology and Management in Construction at the KIT-Department of Civil Engineering, Geo and Environmental Sciences and gives lectures in the field of decommissioning of nuclear facilities, environmentally-friendly Recycling and Disassembly of Buildings, Machinery and Process Engineering as well as construction technology.

Prof. Dr. **Petra Panak**, heading a working group on actinide speciation at INE, holds a professorship of radiochemistry at the Heidelberg University. A basic course in radiochemistry is offered for bachelor and/or master students. An advanced course comprised of the chemistry of f-elements and medical applications of radionuclides is also offered. The advanced radiochemistry lectures are supplemented by scientific internships at the INE radioactive laboratories.

Around 30 students from Karlsruhe and Heidelberg participated in two 3-week radiochemistry laboratory courses in 2017 held at KIT Campus North in the FTU radiochemistry and hot laboratories at INE. Some students are intensifying their knowledge in nuclear/radiochemistry topics during scientific internships at INE. Obviously, students are very interested in nuclear chemistry topics and appreciate the various semester courses.

In 2017 Dr. **Tonya Vitova** gives lectures at the KIT Campus South, Department of Chemistry and Biosciences, in the field of instrumental analytics and Prof. Dr. **Eva Schill** at the Department of Civil Engineering, Geo and Environmental Sciences in the field of geothermal energy. Dr. **Volker Metz** gives lectures at the Department of Mechanical Engineering in the field of nuclear fuel cycle. Lectures and practical units are taught by Dr. **Frank Heberling** and Dr. **Volker Metz** at KIT Campus South, Department of Civil Engineering, Geo and Environmental Sciences, focused in 2017 on "environmental geology: radio- and chemotoxic elements".

Dr. **Andreas Bauer** is lecturing Clay Mineralogy at the University of Jena. His lecture deals with the mineralogical characterization of these fine materials and the importance of quantifying surface reactions. In the second part of the lectures sound, practical advice on powder X-ray diffraction in general is provided, as well as a useful set of step-by step instructions for the novice.

Dr. **Andreas Geist** gives lectures at the École européenne de chimie, polymères et matériaux in Strasbourg concerning the Solvent Extraction of Metal Ions.

Prof. Dr. **Eva Schill** and Prof. Dr. **Thorsten Schäfer** received a call to a chair at the universities of Darmstadt and Jena.

Moreover, INE was involved in many schools and workshops concerning the education and teaching of students and young scientists.

Through this close cooperation with universities, students are educated in the field of nuclear and actinide chemistry, which most universities can no longer offer. Hence, INE makes a vital contribution to the intermediate and long perspective of maintaining nuclear science competence. Moreover, INE is involved in the education of trainees (chemical lab technicians, industrial mechanics and product designers) as well as student internships like BORS and BOGY.

PhD students

In 2017, 20 doctoral students worked at INE on their dissertations; three of them were awarded their doctorate. Topics of the theses are:

- Experimental and modelling studies of cement/clay interface process

- Advanced spectroscopic and microscopic structural investigations of nuclear waste glass forms

- Technetium interaction with inorganic ligands and retention processes in the sulfide system

- Application of high-resolution x-ray absorption (HR-XAS) spectroscopy for the investigation of the release and solubility of radionuclide species originating from highly radioactive waste in aquatic media

- Experimental investigation of the separation process of particle mixtures within a rod magnetic filter

- Solubility, speciation and thermodynamics of tetravalent and hexavalent Uranium

- Characterization of geothermal reservoirs with the help of radionuclide analysis

- Electromagnetical und Eigenpotential monitoring of fluid injections in crystalline rock

- Potential Influence of oxygenated Glacial Meltwater on Radionuclide (re)mobilization in fractured rock

- Joint inversion of magnetotelluric and gravity data from Mt. Viilarica area (S-Chile)

- Behavior of natural radionuclides in soil/groundwater systems

- Impact of anions on the retention of actinides on clay minerals under slightly alkaline to hyper alkaline pH conditions

- Bentonite erosion and colloid mediated radionuclide transport in advection controlled systems

- Development of methods for the individual dosimetry of the staff in disposal facilities

- Investigation of solubility and complexation of Plutonium and Neptunium in highly reducing aquatic systems

- Impact of the flow channel geometry on the agglomeration of colloids and the reduction of permeability in altered granites of potential geothermic reservoir rocks

- Redox behavior, solubility and sorption of Pu(III/IV) in the presence of ISA

- Steel corrosion and actinides sorption by iron corrosion products under saline conditions

- Spectroscopic and thermodynamic investigations of the complexation of An(III) and Ln(III) with hydrophilic Bis-triazinylpyridines

- Accurate neutron scattering based Monte Carlo Simulations of Radiation Fields and Dosimetry imposed by stored High-Level Nuclear Fuel Waste

3 National and international cooperation, conferences and workshops

3.1 National and international cooperation

INE R&D involves numerous national and international collaborations and projects. These are described in the following.

National

INE is involved in various bi- and multilateral collaborations with national research centers, universities and industrial partners on different topics. The projects are partly supported by the German Federal Ministry for Economics and Technology (BMWi), the Federal Ministry for Education and Research (BMBF), the Federal Ministry for the Environment, Nature Conservation, Building and Nuclear Safety (BMUB), the German Research Foundation (DFG) and the Helmholtz Association (HGF).

The **ThermAc** project aims at extending the chemical understanding and available thermodynamic database for actinides, long-lived fission products and relevant matrix elements in aquatic systems at elevated temperatures. To this end, a systematic use of estimation methods, new experimental investigations and quantum-chemistry-based information is intended. ThermAc has started in March 2015 and is projected for three years with an additional 1.5 year extension phase. The project is funded by the German Federal Ministry for Education and Research (BMBF) and is coordinated by KIT-INE. The ThermAc project is developed in order to improve the scientific basis for assessing nuclear waste disposal scenarios at elevated temperature conditions.

The work of KIT-INE within **VESPA II** (initiated in September 2017) is highlighting the key relevance of geochemical research for evaluating radionuclide retention and mobilization in the frame of nuclear waste disposal. Based upon new systematic experimental studies, a significant increase of understanding regarding the behavior of long-lived fission and activation products, i.e. ^{99}Tc, ^{79}Se and ^{129}I, has been obtained. Fundamental site- and host-rock independent thermodynamic data derived within VESPA allow a better modeling and prediction of radionuclide chemistry in aquatic systems. The retention of radionuclides on several relevant mineral phases is analyzed and quantified. As a result of the work performed by KIT-INE within VESPA II, the long-term safety of different repository concepts and scenarios can be assessed on a decisively improved scientific level.

Within the **THEREDA** project, KIT-INE generates and evaluates thermodynamic data – complex formation constants, solubility data – for selected radionuclides from experiments and literature. The data are incorporated into a centrally managed and administered database of evaluated thermodynamic parameters after passing an evaluation process. This database is open for registered user. Thermodynamic data are required for environmental applications in general and radiochemical issues in particular. THEREDA, funded by the Bundesamt für Strahlenschutz (BfS), is developed to be a national (reference) standard and will be the basis for performance assessment calculations for a national nuclear waste repository.

The **GRaZ** project deals with the migration of radionuclides in the near field of a repository for radioactive waste in clay formations with focus on the hyper-alkaline water-cement-system. KIT-INE investigates the retention of actinides and lanthanides by clay minerals in presence of relevant inorganic and organic ligands. The project focusses on carbonate, and cement additives (e.g. plasticizer and superplasticizer) like gluconic acid and citric acid. The impact of these ligands on the sorption and solubility of actinides is studied in a wide pH range up to hyperalkaline pH values. One important issue of the project is the consistent thermodynamic modelling of experimental solubility, complexation, and sorption data. The project provides basic knowledge and thermodynamic data needed in the frame of a long-term safety analysis of different repository concepts.

The disassembly of the reactor pressure vessel and internals poses one of the most demanding challenges in the decommissioning of a nuclear power plant. For this purpose, a waterjet cutting technique (WASS) is used, employing a high-pressure water jet and a sharp-edged abrasive medium directed to the cutting material. Advantages of WASS among other conventional cutting techniques are the compact design of the setup, the ease of remote manipulation (also at difficult positions) and the "cold" operation under water, which also serves as shielding. However, this technique produces a considerable amount of expensive secondary waste, a water suspension containing small-grained radioactive metal cuttings and abrasive grains. The **MASK** project is initialized to overcome this limitation. Metal cuttings are separated by a magnetic filter in order to substantially minimize the radioactivity of the secondary waste.

The **KOLLORADO-e2** project focuses on the erosion stability of compacted bentonite (geotechnical barrier) as a function of the contact water chemistry/hydraulics and the formation of near-field colloids/nanoparticles as potential carriers for actinides/radionuclides. Both, a detailed experimental program quantifying the bentonite erosion and investigating the influence of surface roughness/charge heterogeneity on nanoparticle mobility and actinide bentonite nanoparticle sorption reversibility (including AMS method development), as well as approaches to implement the acquired process understanding in reactive transport modelling codes comprise the project activities.

ENTRIA aims at evaluating criteria for the management of highly radioactive waste from the viewpoint of all involved academic disciplines such as natural sciences, engineering, law and social science. ENTRIA is

addressing the three most important options in storing and disposing of highly radioactive waste products: prolonged surface storage prior to disposal; disposal in deep geological formations with arrangements for monitoring and retrieval; final disposal in a maintenance-free deep geological disposal repository. A major goal of ENTRIA is the strong interaction between young and senior scientists of various disciplines (civil engineering, law, natural sciences, philosophy, political and social sciences). Within the project, INE is responsible for work packages on developing radionuclide source terms and developing individual dosimetry for personnel with respect to deep geological disposal in various rock formations.

The collaborative project **EDUKEM** aims at an improved understanding of uranium chemistry in saline systems and establishing targeted experimental techniques. Work of KIT-INE within EUDKEM focusses on the aquatic chemistry and thermodynamics of hexavalent and tetravalent uranium in relevant saline solutions. Based upon new solubility studies, spectroscopic evidence and literature, a comprehensive description of U(IV) and U(VI) solubility and speciation in key saline systems relevant for nuclear waste disposal in salt-based repositories will be established.

The mechanical and chemical stability of steel containers containing nuclear waste play an important role in performance assessment of disposal sites. The project **KORSO** aims at improving the understanding of steel corrosion in saline environments under conditions representative of disposal sites for heat generating waste. Microscopic and spectroscopic techniques are applied to identify the underlying corrosion mechanisms and their kinetics in dedicated experiments in saline, anoxic and elevated temperature conditions. The second aim is to investigate the retention of radionuclides by secondary phases identified in corrosion experiments by applying spectroscopic and chemical methods. The ultimate goal is to reduce uncertainties concerning interaction mechanisms between radionuclides and corrosion products, and thereby improve confidence in the long-term prediction of radionuclide mobility.

The Helmholtz young investigators group (HYIG) **"Advanced synchrotron-based systematic investigations of actinide (An) and lanthanide (Ln) systems to understand and predict their reactivity"** systematically investigates the electronic and coordination structures of actinide (An) and chemical homologue lanthanide (Ln) systems with novel synchrotron-based high energy resolution X-ray emission/absorption/inelastic scattering techniques. The experimental results are supported by theoretical calculations and simulations with quantum chemical codes. These investigations improve the understanding of An/Ln reactivity in repository systems and waste matrices on a molecular scale and thereby support the reliability of safety case evaluation of the repository long term safety. The elucidation of electronic and coordination structures of An/Ln systems provide basic insight into structure-reactivity relationships of actinide elements, which is a present scientific frontier.

In the framework of measures for retrieval of radioactive waste and decommissioning of the **Asse II salt mine**, provisions for emergency preparedness are taken. Therefore, the operator of Asse II, the Federal Company for Radioactive Waste Disposal (BGE), drilled an exploration drilling in the overlaying sedimentary rocks of the salt diapir and coordinates studies with respect to the near-field of the radioactive waste. INE contributes both to the studies on radionuclide retention by rocks of the overlaying sediments as well as to studies on the geochemical milieu and radionuclide solubility in the near-field of the radioactive waste. Drill cores and a pore water sample of the exploration borehole, comprising Triassic shell limestone (Muschelkalk) and Bunter sandstone (Buntsandstein) were used in sorption experiments with a variety of actinides, fission and decay products. Based on the experimental results, sorption coefficients are derived, which are important input parameters for the assessment of the radionuclide retention capability of the sedimentary rocks overlaying the Asse II salt mine. With respect to the near field of the waste within Asse II, INE compiles the present state of knowledge on geochemical processes in the waste emplacement rooms and develops a conceptual model to derive near-field radionuclide source terms.

International

The international Colloid Formation and Migration (**CFM**) project focuses on the stability of the bentonite buffer/backfill in contact with water conducting features and the influence of colloids on radionuclide migration in crystalline host rocks coordinated by NAGRA (National Cooperative for the Disposal of Radioactive Waste, Switzerland). The project uses the experimental set-up in the controlled zone at the Grimsel Test Site (Switzerland). Additional partners involved are from Japan (JAEA, NUMO, CRIEPI), South Korea (KAERI), Finland (POSIVA Oy and Helsinki University), Switzerland (NAGRA, PSI-LES), Spain (CIEMAT), Sweden (SKB, KTH), United Kingdom (NDA RWMD) and United States (LANL). INE plays a decisive role in the laboratory program and is mainly carrying out the field activities.

EURATOM FP7 and Horizon 2020

A follow-up of the FP7 project SACSESS, **GENIORS** focuses on actinide separations related to future multiple recycling strategies. GENIORS is expected to provide the EU with science-based strategies for nuclear fuel management and contribute significantly to its energy independence. In the longer term, the project's results will facilitate radioactive waste management by reducing its volume and radiotoxicity, and support a more efficient utilization of natural resources. 24 Partners from 10 countries contribute to GENIORS; a formal collaboration with US-DOE is established. The project is coordinated by CEA; KIT is in charge of the hydrometallurgy domain.

The separation of rare earth elements (REE) from secondary sources such as mine tailings is studied in the ERA-MIN project **ENVIREE**. The project is

coordinated by CHALMERS (Sweden). Eleven partners form eight counties contribute to the following areas: assessment of sources, development of innovative, efficient and environmentally benign leaching and separation methods, life cycle assessment and economic feasibility studies.

The overall objective of the Horizon 2020 project **BEACON** is to develop and test the tools necessary for the assessment of the mechanical evolution of an installed bentonite barrier and the resulting performance of the barrier. This will be achieved by cooperation between design and engineering, science and performance assessment. The evolution from an installed engineered system to a fully functioning barrier will be assessed. This will require a more detailed understanding of material properties, of the fundamental processes that lead to homogenization via water saturation, of the role of scale effects and improved capabilities for numerical modelling. The goal is to verify the performance of current designs for buffers, backfills, seals and plugs. For some repository designs mainly in crystalline host rock, the results can also be used for the assessment of consequences of mass loss from a bentonite barrier in long-term perspective.

The EURATOM FP7 Collaborative Project **CAST** aims to develop understanding of the generation and release of C-14 from radioactive waste materials under conditions of underground geological repositories. INE contributes with experimental studies to work packages "Steels" and "Zircaloy" as well as to the work package "Dissemination of knowledge". Within the two experimental work packages, INE conducts studies with highly active stainless steel and Zircaloy-4 samples in the shielded box-line of INE. In our experiments, the content of organic and inorganic C-14 both in gaseous and liquid samples are determined. These studies are of high relevance for the role of C-14 in safety assessments for SNF repositories, because volatile and dissolved C-14 bearing organic species possess a high mobility through various geo-engineered and geological barriers.

Within the European Commission Horizon 2020 frame, the study of modern spent nuclear fuel dissolution and chemistry in failed container conditions is included in the **DISCO** collaborative project. The aims of this project are, first, to enhance the understanding of spent fuel matrix dissolution under conditions representative of failed containers in reducing repository environments and, second, to assess whether novel types of fuel (MOX, UO_2 doped with additives such as Cr, Gd) behave like the conventional ones (UO_2). INE provides results on the dissolution of MOX fuel under reducing conditions and, in addition, is the leader of work package 3 "Spent fuel dissolution experiment" supervising the spent nuclear fuel dissolution experiments that will be performed by the different partners within the project. INE also contributes to work package 2 "Preparation and characterization of samples and experimental systems".

INE contributes actively to international organizations, such as the Thermodynamic Database Project of the Nuclear Energy Agency (NEA).

CEBAMA is a collaborative project investigating cement-based materials, properties, evolution and barrier functions within the European Commission Horizon 2020 frame (www.cebama.eu). Scientific and technical research in CEBAMA is largely independent of specific disposal concepts and addresses different types of host rocks, as well as bentonite. CEBAMA is not focusing on one specific cementitious material, but aims at studying a variety of important cement-based materials in order to provide insight on general processes and phenomena. CEBAMA is coordinated by INE.

The H2020 project EU project **ANNETTE** (Advanced Networking for Nuclear Education and Training and Transfer of Expertise) intends to assure qualified workforce in the next decades and focuses on education of under-graduate and graduate students of European academic institutions. In this Education and Training action, INE organizes two intersemester courses on management of spent nuclear fuel and deep geological disposal of highly radioactive waste. Access of students to nuclear laboratories and interim storage facilities are prepared.

The goal of the H2020 project **DEEPEGS** is to demonstrate the feasibility of enhanced geothermal systems (EGS) for delivering energy from renewable resources in Europe. Testing of stimulating technologies for EGS in deep wells in different geologies will deliver new innovative solutions and models for wider deployments of EGS reservoirs across Europe. DEEPEGS will demonstrate advanced technologies for widespread exploitation of high enthalpy heat (i) beneath existing hydrothermal field at Reykjanes (volcanic environment) with temperature up to 550°C and (ii) very deep hydrothermal reservoirs in France with temperatures up to 220°C. The focus on business cases will demonstrate advances in bringing EGS derived energy (TRL6-7) to market exploitation. We seek to understand and address social concerns about EGS deployments. We will through risk analysis and hazard mitigation plans ensure that relevant understanding and minimization of the risks will be implemented as part of the RTD business case development.

The **GEMex** project is a EU-Mexico joint effort in development of Enhanced Geothermal Systems (EGS) and Superhot Geothermal Systems (SHGS) at Acoculco and Los Humeros that bases on three pillars:

1 – Resource assessment of these geothermal sites by understanding the tectonic evolution, fracture distribution and hydrogeology and predicting in-situ stresses and temperatures at depth.

2 – Reservoir characterization including novel geophysical and geological methods to be advanced for the specific condition. Accompanying high-pressure/ high-temperature laboratory experiments will provide the input parameters.

3 – Concepts for site development will include definition of drill paths, a design for well completion including suitable material selection, and optimum stimulation and operation procedures for safe and economic exploitation. In these steps, we will address issues of public acceptance and outreach as well as the monitoring and control of environmental impact.

3.2   Migration'17 conference

The 16th International Conference on the Chemistry and Migration Behavior of Actinides and Fission Products in the Geosphere, Migration '17, was held from September 10 – 15, 2017, in Barcelona, Spain. The highly successful conference was organized by Amphos21 as local organizer in cooperation with KIT-INE and with support of the International Steering Committee and the International Scientific Committee. As in the several previous Migration conferences, Migration 2017 served as a high visibility international forum to present and discuss a wide range of topics relevant for understanding and predicting radionuclide migration processes. More than 250 participants (including ~ 60 students) from 22 countries were joining the conference, showing that radionuclide migration is a topic of wide international interest.

The Migration '17 conference was opened on Sunday afternoon with an interesting plenary discussion panel on "science in radionuclide migration: the needs of the end users". Panelists were representing international waste management organizations (ONDRAF-NIRAS, SKB, ANDRA, ENRESA, NUMO) with Jordi Bruno, CEO of Amphos21, moderating the discussions.

The Main Session topics of Migration '17 were addressing the aquatic chemistry of actinides and fission products, migration behavior of radionuclides, geochemical and transport modelling, selected case studies and a specific topic focusing on cementitious systems / radionuclide behavior in hyperalkaline solutions.
The two extended Poster Sessions, which were held on two days and gave ample time for discussions and scientific exchange, were a key event of Migration '17, showing an impressive range of excellent scientific research especially from young researchers. A total of more than 230 posters were on display. The International Steering and Scientific Committee awarded three Best Poster Awards; one of them to Nese Cevirim-Papaioannou of KIT-INE.

In addition to the poster Sessions, a total of 60 oral presentations were held from Monday to Friday. Selected invited talks highlighted topics of specific importance. In total, the numerous contributions at Migration '17 evidenced significant advance on several topics and emphasized the quality, variety and impact of RD&D in the field of radionuclide migration.

The 17th Migration Conference has been announced for September 2019, to be held in Kyoto, Japan.

Prof. Horst Geckeis, Chairman of the Migration International Steering Committee, speaking at the Migration '17 Opening Session.
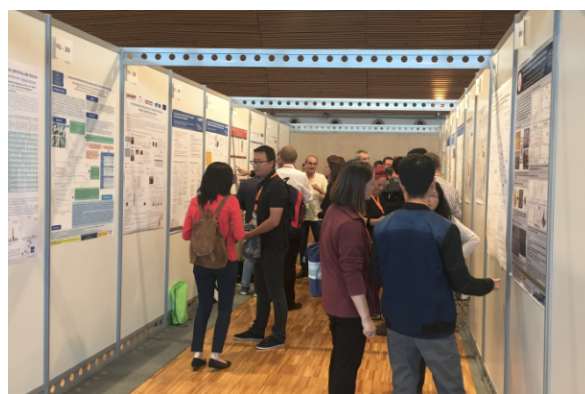
Poster Session at the Migration '17 Conference.

3.3 Inauguration workshop of the CAT-ACT beamline for catalysis and radionuclide research

On September 20 and 21, 2017, a two day workshop dedicated to the inauguration of the new beamline for catalysis and radionuclide research (CAT-ACT) at the Karlsruhe Institute of Technology (KIT) synchrotron light source took place in Eggenstein-Leopoldshafen on KIT Campus North. The workshop was co-organized by the three KIT institutes which have conceived and are jointly operating the beamline - the Institutes for Chemical Technology and Polymer Chemistry (ITCP), Nuclear Waste Disposal (INE) and Catalysis Research and Technology (IKFT) - and highlighted research activities and access possibilities at two in line experimental stations [1]. More than 60 national and international delegates attended the two day symposium which also featured oral contributions from industrial synchrotron users and, of course, researchers from Karlsruhe (Figure 1).

[1] J.-D. Grunwaldt, H. Lichtenberg, J. Rothe, *Synchr. Rad. News* Vol. 31(1), 2018.

Fig. 1: *Participants of the CAT-ACT beamline inauguration workshop grouped in front of the KARA accelerator building.*

4 Fundamental Studies: Process understanding on a molecular scale

In order to develop fundamental scientific understanding on a molecular scale and ensure the reliable quantitative prediction of key processes in aquatic chemistry, several R&D studies on radionuclide chemistry and geochemistry are performed at KIT-INE. Aiming at a comprehensive assessment of radionuclide behavior and mobility in aquatic systems relevant for nuclear waste disposal, experimental studies with actinides, long-lived fission and activation products and selected non-radioactive elements of interest are performed. The investigated aqueous systems cover from dilute solutions to highly saline salt brine systems and establish essential site-independent data and process understanding. Work is focusing both on detailed experimental investigations using the unique facilities available at KIT-INE, and subsequently developing reliable chemical models and consistent thermodynamic data. This combined approach allows a systematic and reliable evaluation of key processes such as radionuclide solubility, radionuclide speciation, radionuclide retention and transport processes in relevant near- and far-field scenarios.

The fundamental studies summarized in this section are related to the (i) chemistry and thermodynamics of actinides and fission products in aqueous solution, (ii) radionuclide sorption on mineral phases, and (iii) retention of radionuclides by secondary phase formation. The studies aim at identifying relevant radionuclide retention/retardation mechanisms on a molecular level and their robust thermodynamic quantification in support of the Nuclear Waste Disposal Safety Case. The fundamental studies on aqueous radionuclide chemistry described in Chapter 4 are supporting the applied studies (see Chapter 5) performed at KIT-INE.

4.1 Chemistry and thermodynamics of actinides and fission products in aqueous solution

N. Adam, M. Altmaier, A. Baumann, M. Böttle, N. Cevirim-Papaioannou, K. Dardenne, F. Endrizzi,
D. Fellhauer, X. Gaona, J.-Y. Lee, M. Maiwald, P.J. Panak, J. Rothe, J. Schepperle, D. Schild, T. Schramm,
A. Skerencak-Frech, A. Tasi, E. Yalcintas

Introduction

Accurate knowledge of the aquatic chemistry and thermodynamics of actinides, fission and activation products is mandatory in the context of nuclear waste disposal. The availability of complete and correct chemical and thermodynamic models represents the fundamental basis for geochemical model calculations and source-term estimations. The studies summarized in this section highlight examples from the fundamental research performed at KIT-INE in 2017 within this broad topic.

In addition to the experimental R&D activities described in this chapter, KIT-INE continuously contributes to several national and international projects, e.g. the development of national (THEREDA) and international (NEA-TDB) thermodynamic reference databases for actinides and fission products.

Redox behavior of Tc(IV) in alkaline, dilute to concentrated NaCl-NaNO₃ systems

Technetium-99 is a β-emitting fission product highly relevant for the safety assessment of nuclear waste repositories due to its significant inventory in radioactive waste, long half-life ($t_{1/2} \sim 2.1 \cdot 10^5$ a) and redox sensitivity. The two most stable oxidation states of ^{99}Tc are (i) Tc(VII) which exists as soluble and mobile pertechnetate (TcO_4^-) under oxidizing and anoxic conditions, and (ii) Tc(IV) which forms sparingly soluble hydrous oxides under the reducing conditions expected to prevail in deep underground repositories.

Large nitrate inventories are expected in certain types of radioactive wastes, mostly arising from the neutralization of HNO₃ used in the reprocessing of spent fuel. Upon contact with intruding groundwater, concentrated nitrate plumes may be generated in the near-field of the disposed waste, affecting the redox milieu, and potentially contributing to the oxidation and subsequent mobilization of redox-sensitive radionuclides. A reliable knowledge on the impact of nitrate on the redox behavior of Tc in dilute to concentrated saline systems is very relevant for the safety assessment of repositories for radioactive waste. Studies developed within this framework can also provide relevant insights for the understanding of Tc behavior in legacy sites such as Hanford nuclear tank wastes.

The redox behavior and solubility of ^{99}Tc was investigated in 0.1 and 5.0 M NaCl-NaNO₃-NaOH solutions with $[NO_3^-]$ = 0.1-1.0 M and $8.5 \leq pH_m \leq 14.5$ (with pH_m = -log $[H^+]$). Three reducing chemicals were used in independent batch series: Sn(II), Na₂S₂O₄ and Fe(0). In the absence of nitrate, these reducing chemicals have been shown to stabilize Tc(IV) [1, 2]. Two series of samples were prepared in the absence and presence of $TcO_2 \cdot 0.6H_2O$(am). pH_m, E_h and [Tc] (in the active samples) were monitored at regular time intervals for up to 300 days. The redox state of Tc in both solid and aqueous phases was determined for selected samples by XANES spectroscopy and solvent extraction with TPPC. Colorimetric nitrate/nitrite
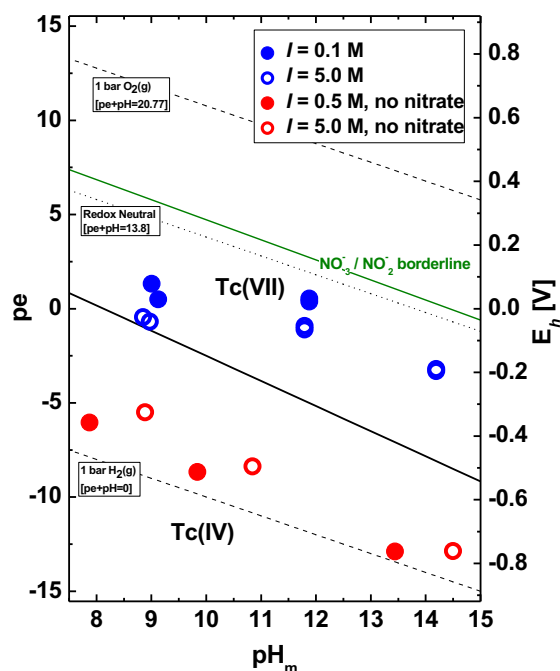
Fig. 1: *Pourbaix diagrams of Tc and N, and experimental pH_m-E_h data measured in Sn(II) systems in the absence (red symbols) and presence (blue symbols) of nitrate. Calculations performed using thermodynamic data reported in [3, 4].*
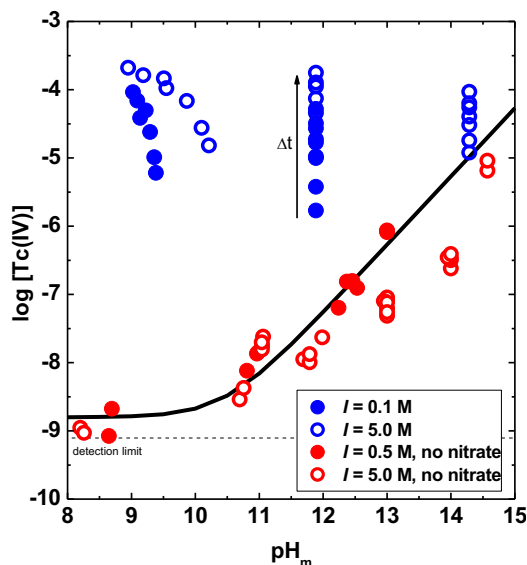

Fig. 2: *Experimental solubility data of Tc(IV) measured in Sn(II) systems in the absence (red symbols) and presence (blue symbols) of nitrate. Solid line corresponds to Tc(IV) solubility calculated using thermodynamic data reported in [4].*

tests were used to determine the presence/absence of nitrite.

Nitrate induces a clear and fast increase of E_h in $SnCl_2$ and $Na_2S_2O_4$ systems with $TcO_2 \cdot 0.6H_2O(am)$ (see Figure 1). After 5-50 days (depending upon reducing system, pH_m and ionic strength), E_h values in these systems fall well above the Tc(VII)/Tc(IV) redox borderline. This observation is correlated with a significant increase of [Tc] compared to nitrate-free

systems (see Figure 2). Solvent extraction and XANES confirm the predominance of Tc(VII) in the supernatant aqueous phase (> 65% Tc(VII)). Colorimetric nitrate/nitrite tests show significant concentrations of nitrite in these samples, thus supporting that the oxidation of Tc(IV) to Tc(VII) takes places through the reduction of NO_3^-. Unexpectedly, Sn(II) and $Na_2S_2O_4$ systems in the absence of $TcO_2 \cdot 0.6H_2O(am)$ show only a minor and very slow increase of E_h. For these systems not containing Tc, colorimetric nitrate/nitrite tests confirm only the presence of (low) nitrite concentration in a limited number of samples. These observations suggest that the solid $TcO_2 \cdot 0.6H_2O(am)$ plays a role in catalyzing the redox processes between nitrate and the reducing agents. Fe(0) containing samples on the other hand show an immediate increase in E_h within the first 24 hours both in the presence and absence of Tc.

As predicted thermodynamically, this work confirms that Tc(IV) is oxidized to Tc(VII) by nitrate in alkaline, dilute to concentrated saline systems. However, the impact of nitrate on the redox potential is strongly dependent on the characteristics of the investigated system, pointing to a kinetically hindered reaction. Complementary experiments in the presence of $ReO_2(s)$ (inactive analogue of $TcO_2(s)$) or ^{137}Cs (soluble β-emitter) were performed to assess the role of $TcO_2 \cdot 0.6H_2O(am)$ as catalyzer in the redox reaction with nitrate.

Solubility of U(VI) in dilute to concentrated KCl solutions

Uranium is expectedly found as U(VI) in aquatic systems under mildly reducing to oxidizing conditions. In the alkaline pH region and in the absence of strong complexing ligands (e.g. carbonate, phosphate, silicate), the solubility of U(VI) is controlled by M-U(VI)-OH (M-uranates, with M = Na, K, Ca, among others). In contrast to Ca- and Na-uranates, very little is known on the solubility of K-U(VI)-OH phases. The latter compounds are expected to control the solubility of U(VI) in the early stages of cement degradation and are therefore in the focus of this work.

All experiments were performed in Ar gloveboxes at $T = (22 \pm 2)$ °C. $K_2U_2O_7 \cdot xH_2O(s)$ was prepared by precipitating a 0.5 m UO_2Cl_2 stock solution in 2.43 M KCl + 0.07 M KOH at $pH_m \approx 13$. The resulting solid was aged for 3 months before starting the solubility studies. Undersaturation solubility experiments with $K_2U_2O_7 \cdot xH_2O(s)$ were performed in 0.1, 0.5, 1.0, 3.0 and 4.0 M KCl-KOH solutions at $8 \leq pH_m \leq 14.5$. The uranium concentration was determined by ICP-MS after phase separation with 10 kD ultrafiltration (2 - 3 nm). [U] and pH_m values were monitored at regular time intervals until attaining equilibrium conditions. The initial $K_2U_2O_7 \cdot xH_2O(s)$ and selected solid phases of samples after completion of the solubility experiments were characterized by XRD, SEM-EDS, chemical analysis and TG-DTA.

Solid phase characterization confirms that $K_2U_2O_7 \cdot 1.5H_2O(cr)$ is the solid phase controlling the
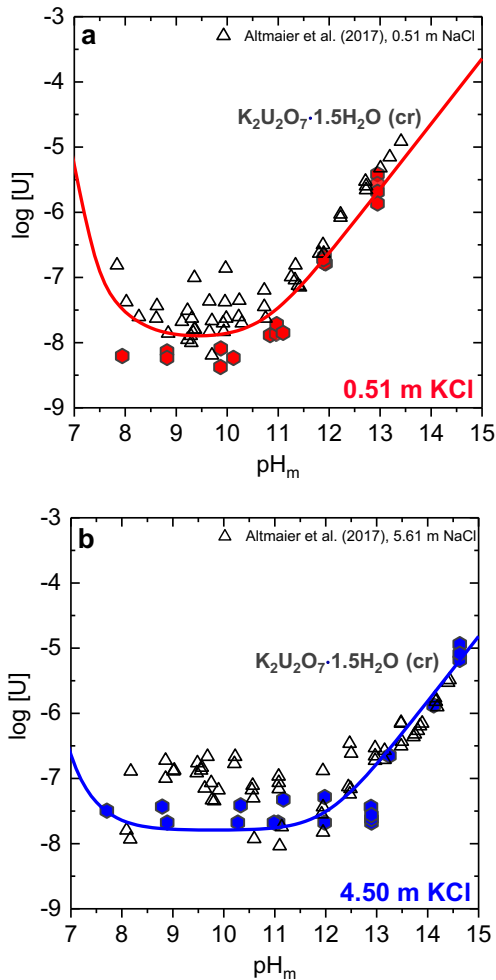
Fig. 3: *Solubility of U(VI) in (a) 0.51; and (b) 4.50 m KCl solutions. Solid lines are calculated with thermodynamic and activity models derived in this work consistently with [5]. Black triangles are appended for comparison and correspond to the solubility of U(VI) in 0.51 and 5.61 m NaCl as reported in [5].*

solubility in all investigated KCl-KOH systems. Experimental solubility data show a pH-independent behavior up to $pH_m \approx 11$ regardless of ionic strength (Figure 3). An increase of the solubility with a well-defined slope of +1 (log [U] *vs.* pH_m) is observed at $pH_m \geq 11$. In this pH region, a decrease of U(VI) solubility was observed with the increase of ionic strength. The combination of solid phase characterization and slope analysis clearly indicate the predominance of $UO_2(OH)_3^-$ and $UO_2(OH)_4^{2-}$ species under near-neutral to hyperalkaline pH conditions and show a solubility behavior very similar to the NaCl case. Solubility data are used to derive new thermodynamic and SIT/Pitzer activity models for the system UO_2^{2+}-H^+-K^+-OH^--Cl^--$H_2O(l)$, which extend the thermodynamic database available for U(VI) and allow more accurate source term calculations under boundary conditions relevant for nuclear waste disposal.

Solubility and speciation of Pu(VI) in alkaline NaCl solutions

In this study, the aqueous chemistry of plutonium(VI) was investigated. In pH neutral to alkaline aqueous solutions, the redox active Pu can exist as Pu(VI) and potentially as Pu(V) under oxidizing conditions, while Pu(III) and Pu(IV) are predominant under redox-neutral to strongly reducing conditions [3, 6]. Although reducing conditions are expected in deep geological repositories in the long-term due to the anoxic corrosion of steel, oxidizing environments may also become relevant at an early period in the post-operational phase or, spatially limited to the container near field, due to radiolysis effects under certain boundary conditions. Oxidizing conditions, and thus Pu(VI), might still be considered in certain scenarios for future repositories with intended measures for reversibility and retrieval of the nuclear waste, *e.g.* due to a non-backfilled shaft, or in accident scenarios for interim storage facilities for nuclear waste located at the surface. As an extension of our previous works on U(VI) [5] and Np(VI) [7], we have investigated the solubility and hydrolysis of Pu(VI) in alkaline NaCl solutions where systematic investigations and reliable thermodynamic data are missing.

All experiments were performed at $T = (22 \pm 2)$ °C under inert Ar atmosphere in a glove box. A radio-chemically well-characterized ^{242}Pu(IV) stock solution in 1.0 M $HClO_4$ containing about 100 mg of ^{242}Pu was electrochemically oxidized at $E_{anode} \approx +1.8$ V vs. SHE. The oxidation state purity of the resulting Pu(VI) stock solution was confirmed by UV-Vis/NIR spectroscopy. The Pu(VI) stock solution was alkalized with NaOH and mildly tempered for several weeks in air tight autoclaves. The resulting brownish Pu solid phase was characterized by conventional and synchrotron based *in-situ* X-ray diffraction (XRD), quantitative chemical analysis of Na and Pu contents, scanning electron microscopy-energy-dispersive spectrometry (SEM-EDS) and X-ray absorption fine structure spectroscopy (XAFS). The solubility of the brownish Pu(VI) solid phase was studied in 0.10-5.0 M NaCl at $pH_m = 9$-14, in some cases using NaOCl as oxidizing agent.

The initial Pu(VI) solid phase showed a similar XRD pattern and a similar platelet-like structure as reported for $Na_2Np_2O_7(cr)$. The chemical analysis revealed a Na:Pu ratio of about 1:1 which corroborates the presence of sodium plutonate, $Na_2Pu_2O_7 \cdot xH_2O(cr)$.

Figure 4 shows the experimental solubility of $Na_2Pu_2O_7 \cdot xH_2O(cr)$ in 5.0 M NaCl in comparison to $Na_2Np_2O_7(cr)$ [7] and $Na_2U_2O_7 \cdot H_2O(cr)$ [5]. Above $pH_m \approx 11$, the Pu(VI) solubility systematically increases with a slope $\approx +1$ (log [Pu(VI)] vs. pH_m), which is in agreement with an equilibrium between sodium plutonate as solubility controlling solid phase and the fourth Pu(VI) hydrolysis complex as predominant Pu(VI) aqueous species, analogous to the Np(VI) and U(VI) cases:
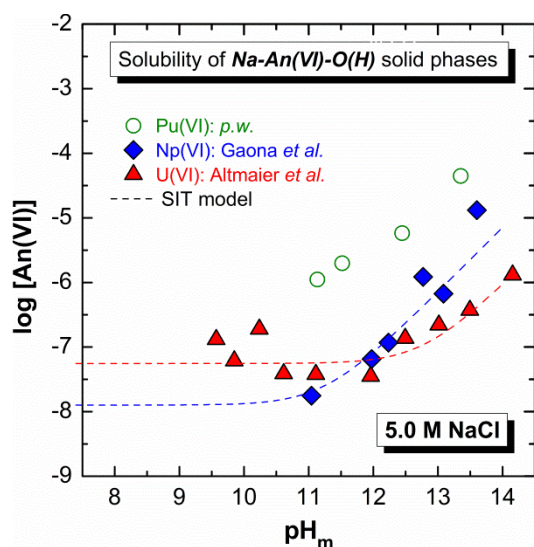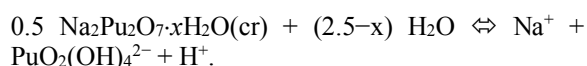
Fig. 4: *Experimental solubility of Na₂Pu₂O₇·xH₂O(cr) (p.w.), Na₂Np₂O₇(cr) [7] and Na₂U₂O₇·H₂O(cr) [5] in alkaline 5.0 M NaCl solutions and the corresponding SIT models (dashed lines).*

$$0.5\ Na_2Pu_2O_7 \cdot xH_2O(cr) + (2.5-x)\ H_2O \Leftrightarrow Na^+ + PuO_2(OH)_4^{2-} + H^+.$$

At lower [NaCl] and lower pH_m values, spontaneous transformation of the initial $Na_2Pu_2O_7 \cdot xH_2O(cr)$ into a substoichiometric Na-Pu(VI)-O(H)(cr) phase with Na:Pu ratio less than 1, and into binary $PuO_2(OH)_2 \cdot xH_2O(cr)$ was observed. Based on the comprehensive solubility and additional spectroscopic data obtained, a reliable assessment of the Pu(VI) behavior in alkaline dilute to concentrated NaCl solutions is possible for the first time. Furthermore, the results allow the evaluation of systematic trends in the An(VI) series with An = U, Np and Pu.

Solubility and hydrolysis of beryllium in dilute to concentrated NaCl, KCl and CaCl₂ systems

Beryllium is an element present in certain waste forms to be disposed of in repositories for radioactive waste. Understanding aquatic Be chemistry is relevant due to the chemotoxic characteristics of Be. The amphoteric behavior of Be(II) is widely accepted in the literature [8, 9], although the number of experimental studies reporting the formation of anionic hydrolysis species ($Be(OH)_3^-$ and $Be(OH)_4^{2-}$) under alkaline to hyperalkaline pH conditions is very scarce [10, 11]. The formation of ternary Na–Be(II)–OH and Ca–Be(II)–OH solid phases under hyperalkaline pH conditions has been described in the literature [12–14]. These solid phases may eventually control Be(II) solubility in cementitious environments, but no thermodynamic data are available so far for these systems. In the context of the EU collaborative project on Cement Based Materials (CEBAMA; www.cebama.eu), one of the research activities on-going at KIT–INE focuses on the aquatic chemistry of Be(II) under alkaline to hyperalkaline pH conditions. In a second stage of the project, the uptake of Be(II) by cement and C–S–H phases with different Ca:Si ratios will be investigated. The main objectives are the development of comprehensive thermodynamic and activity models for the system $Be^{2+}–Na^+–K^+–Ca^{2+}–H^+–Cl^-–HCO_3^-–CO_3^{2-}–OH^-–H_2O(l)$, the determination of robust solubility upper limits for source term estimations and, further, the quantitative assessment of the uptake of Be(II) by cementitious materials.

Solubility experiments were performed from undersaturation conditions using commercial BeO(cr) and synthetic $Be(OH)_2(am)$. The latter phase was prepared at room temperature by precipitating a ~0.35 M $BeSO_4$ stock solution at $pH_m \approx 10.5$, and washed three times with the corresponding background electrolyte solution before use. All sample preparation and handling was performed in an Ar glovebox at $T = (22 \pm 2)$ °C. A total of 120 independent batch samples were prepared by contacting 0.5–5 mg of solid Be phase (per sample) with the following systems: (i) 0.1–5.0 M NaCl–NaOH (5 series, with $5 \leq pH_m \leq 14.5$); (ii) 0.1–4.0 M KCl–KOH (5 series, with $9 \leq pH_m \leq 14.3$); (iii) 0.05–3.5 M CaCl₂ (4 series, with $9 \leq pH_m \leq 12$); (iv) 0.01–4.0 M NaOH; and (v) 0.01–4.0 M KOH (iv and v in the absence of MCl salts). Total concentration of Be(II) in the aqueous phase was quantified by ICP–MS after ultrafiltration with 10 kD filters. [Be(II)] in the clear supernatant (without phase separation) of selected solubility samples was also analysed in order to assess the possible presence of colloidal species. Solid phases in selected solubility experiments were characterized by XRD (see Figure 5), after attaining
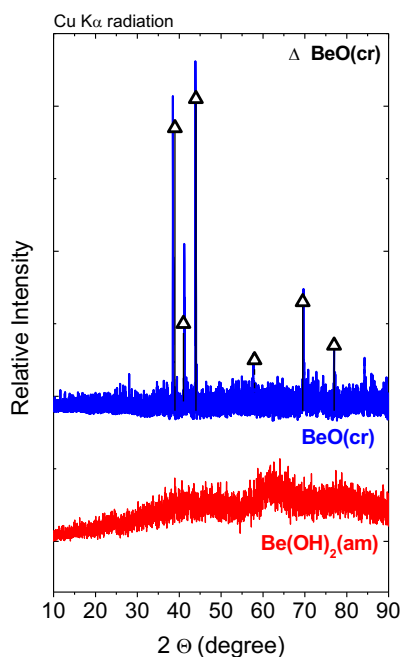

Fig. 5: *XRD patterns of BeO(cr) and Be(OH)₂(am) solid phases used in this study. BeO(cr) reference patterns as reported in JCPDS database.*
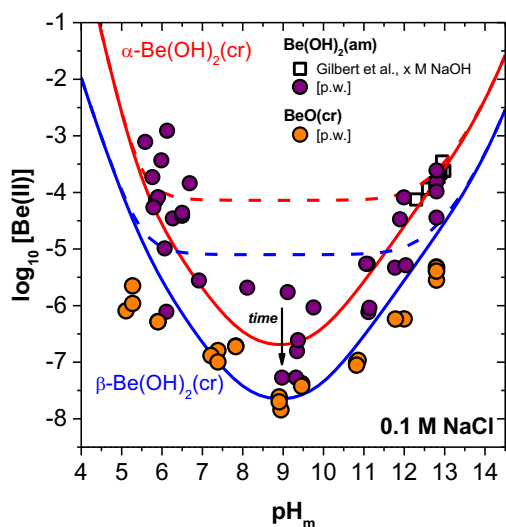
Fig. 6: *Solubility of BeO(cr) and Be(OH)$_2$(am) in 0.1 M NaCl solutions at 5 ≤ pH$_m$ ≤ 13. Squares correspond to Be(II) solubility data reported by Gilbert et al. [10] in NaOH solutions. Calculated solubility appended for comparison: using thermodynamic data based upon "solubility + potentiometric studies" (dashed lines), and based upon "solubility + solvent extraction studies" (solid lines).*

thermodynamic equilibrium (assumed after constant pH$_m$ and [Be(II)] measurements).

Solubility data obtained with BeO(cr) and Be(OH)$_2$(am) confirm the amphoteric character of Be(II), with a solubility minimum at pH$_m$ ≈ 9 (see Figure 6). At this pH$_m$ value, [Be(II)] in equilibrium with BeO(cr) and Be(OH)$_2$(am) is ≈ $10^{-7.5}$ and ≈ 10^{-6} M, respectively. No relevant differences are observed between [Be(II)] quantified in the clear supernatant and after 10 kD ultrafiltration, thus excluding any significant contribution of dissolved colloidal beryllium species to the total Be solubility. The combination of solubility data determined under acidic pH$_m$ conditions and the hydrolysis scheme reported in [14] for cationic hydrolysis species of Be(II) allows the determination of log $*K°_{s,0}${BeO(cr)} and log $*K°_{s,0}${Be(OH)$_2$(am)} for the solid phases used in the present study. Solubility data obtained in weakly alkaline conditions clearly show that the hydrolysis constant previously reported for Be(OH)$_2$(aq) in potentiometric studies is significantly overestimated. The solubility of Be(OH)$_2$(am) determined in strongly alkaline, dilute NaCl systems is in excellent agreement with the single solubility study available to date in this pH region [10]. This work allows deriving chemical, thermodynamic and (SIT) activity models for the system Be^{2+}–Na$^+$–K$^+$–Ca^{2+}–H$^+$–Cl$^-$–OH$^-$–H$_2$O(l).

Thermodynamics of the complexation of NpO$_2$$^+$ with sulfate at elevated temperatures

The early actinides are redox active metals and exist as An(III) to An(VI) within the thermodynamic stability field of water. Within the An(V) series the pentavalent NpO$_2$$^+$ is thermodynamically most stable and

highly soluble in aqueous solution. The complexation of NpO$_2$$^+$ with inorganic ligands in natural ground waters is of high interest. Sulfate is present in natural ground waters, in pore waters of clay rocks and in brines from rock salt formations [15, 16].

In this work, the complexation of NpO$_2$$^+$ with SO$_4$$^{2-}$ is studied as a function of temperature (20 °C – 85 °C) and ionic strength ($I_m = 0.5 - 4.0$ mol·kg^{-1} NaClO$_4$) using near infrared (NIR) absorption spectroscopy. The absorption spectra of NpO$_2$$^+$ with increasing [SO$_4$$^{2-}$]$_{total}$ are displayed in Figure 7 at T = 20 °C and 85 °C.

At 20 °C the hydrated NpO$_2$$^+$ aquo ion shows a single absorption band at λ_{max} = 980.2 nm which is shifted bathochromically with increasing [SO$_4$$^{2-}$]$_{total}$. The red shift is accompanied with a slight increase of the Full Width Half Maximum (FWHM). At 85 °C the bathochromic shift of the absorption band and the broadening of the FWHM are more distinct. These changes clearly indicate the formation of NpO$_2$(SO$_4$)$_n$$^{1-2n}$ complexes, which is favorable at increased temperatures. Evaluation of the spectra by principle component analysis reveals the formation of one complex species with a stoichiometry of NpO$_2$SO$_4$$^-$ [17]. While this (1,1) species is only a minor component at 25 °C, increased temperature results in a distinctively stronger complexation reaction (see Figure 8).

Fig. 7: *Absorption spectra of NpO$_2$$^+$ as function of total sulfate concentration [SO$_4$$^{2-}$]$_{tot}$ at (a) T = 20 °C, and (b) 85 °C, both at I$_m$(NaClO$_4$) = 4.0 mol kg^{-1}.*
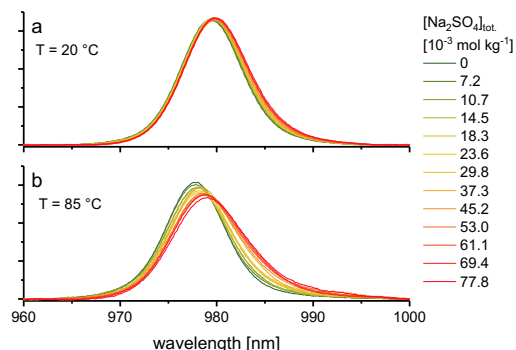
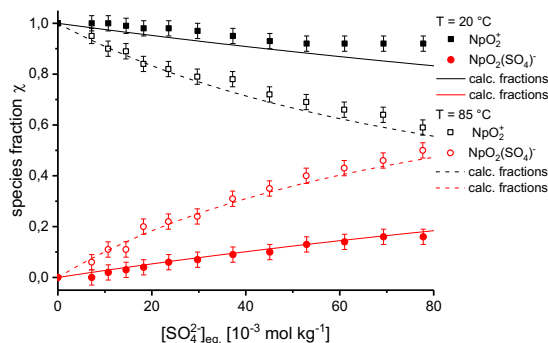**Fig. 8:** *Species distribution of Np(V) as a function of the equilibrium sulfate concentration. (I$_m$ = 4.0 mol kg^{-1} NaClO$_4$); T = 20 °C and 85 °C.*

Tab. 1: *Thermodynamic stability constants log$\beta^0_1(T)$ for the formation of $NpO_2SO_4^-$ in the temperature range of 20 °C to 85 °C [17].*

T [°C]	log $\beta^0_1(T)$	T [°C]	log $\beta^0_1(T)$
20	(0.83 ± 0.09)	60	(1.42 ± 0.03)
30	(0.96 ± 0.15)	70	(1.55 ± 0.10)
40	(1.09 ± 0.04)	80	(1.79 ± 0.10)
50	(1.29 ± 0.02)	85	(1.83 ± 0.08)

Applying the specific ion interaction theory (SIT) and the integrated Van´t Hoff equation the thermodynamic functions (log $\beta^0_j(T)$, $\Delta_rH^0_m$, $\Delta_rS^0_m$) and the binary ion-ion-interaction parameters ($\varepsilon_T(i,k)$) of the complexation reaction are obtained. The log $\beta^0_1(25 \ °C) = (0.92 \pm 0.13)$ increases by 1 order of magnitude within the temperature range of $25 - 85°C$ (see Table 1).

Furthermore, the thermodynamic functions $\Delta_rH^0_m = (30.3 \pm 2.8)$ kJ mol^{-1} and $\Delta_rS^0_m = (119 \pm 9)$ J mol^{-1} K^{-1} show that the complexation reaction is endothermic and driven by the entropy [17]. The $\Delta\varepsilon_{01}$ values of the reaction increase slightly from $-(0.15 \pm 0.04)$ to $-(0.07 \pm 0.02)$ kg·mol^{-1} between $25 - 85 \ °C$. This increase is however within the error range of the data and should not be over-interpreted. Thus, a temperature-independent binary ion-ion interaction coefficient $\varepsilon(Na^+, NpO_2SO_4^-)_{25°C} = (0.02 \pm 0.19)$ kg·mol^{-1} for the $NpO_2SO_4^-$ complex is calculated.

References

[1] Yalcintas, E., et al., Radiochim. Acta, **103**, 57–72, (2015)

[2] Kobayashi, T., Radiochim. Acta, **101**, 323–332, (2013)

[3] Guillaumont, G., et al., *Chemical Thermodynamics Vol. 5*, Elsevier, Amsterdam, (2003).

[4] Yalcintas, E., et al., Dalton Transactions, **45**, 8916–8936, (2016).

[5] Altmaier, M., et al., J. Chem. Thermodynamics, **114**, 2–13, (2017)

[6] Neck, V., et al., C. R. Chimie, **10**, 959-977, (2007)

[7] Gaona, X., et al., Pure Appl. Chem., **85**, 2027-2049, (2013)

[8] Baes, C. F. and Mesmer, R. E., The Hydrolysis of Cations. Wiley, (1976)

[9] Wood, S. A., Ore Geology Reviews, **7**, 249–278, (1992)

[10] Gilbert, R. A. and Garrett, A. B., J. Am. Chem. Soc., **78**, 5501–5505, (1956)

[11] Soboleva, G. I., et al., Geokhimiya, **7**, 1013–1024, (1977) (in Russian)

[12] Everest, D. A., et al., J. Inorg. Nucl. Chem., **24**, 525–534, (1962)

[13] Schmidbaur, H., et al., J. Am. Chem. Soc., **120**, 2967–2968, (1998)

[14] Bruno, J., J. Chem. Soc. Dalton Trans., 2431–2437, (1987).

[15] Gaucher, E., et al., Physics and Chemistry of the Earth, Parts A/B/C, **29**, 55-77, (2004)

[16] Allen, T.R., et al., Comprehensive Nuclear Materials. (2012), Amsterdam, The Netherlands: Elsevier.

[17] Maiwald, M. M., et al., The Journal of Chemical Thermodynamics, **116**, 309-315, (2018)

4.2 Sorption on mineral phases

4.2.1. First electrostatic surface complexation modeling up to 5 M ionic strength

N. Finck, J. Lützenkirchen

In co-operation with:

D. García[a], M. Huguenel[b], L. Camels[b], Vladimir Petrov[c]

[a] Amphos 21, Passeig de Garcia i Fària 49-51, 08019, Barcelona (ES), [b] Ecole européenne de Chimie, Polymères et Matériaux-Strasbourg (ECPM), 25 rue Becquerel, F-67087 Strasbourg Cedex2 (FR), [c] Radiochemistry Division, Chemistry Department, Lomonosov Moscow State University, Moscow, 119991 (RU)

Introduction

Establishing fundamental understanding and modeling of radionuclide retention processes on mineral surfaces at high ionic strength conditions are scientifically challenging. In order to analyze the performance of surface complexation modeling approaches at high ionic strength conditions, well defined lab-systems have been studied in combination with advanced analytical tools.

High salt concentration have been of recent interest in some spectroscopic studies dealing with mineral water interfaces such as the study on silica by Jena et al. [1] at constant pH and up to 5 M NaCl. These interfaces in contact with highly concentrated salt solutions are relevant for the adsorption of radionuclides in the context of nuclear waste repositories where very high salt concentrations are expected. Adsorption of radionuclides up to very high salt levels has been rarely studied. Mostly systematic sets of experimental data have been obtained on clay samples relevant to nuclear waste disposal [2]. These data have been modeled using a non-electrostatic surface complexation model (SCM) with a Pitzer approach to account for activity corrections of aqueous species, which proved quite successful. However, the interfacial electrostatics in these systems cannot be disregarded in more advanced models. Therefore, the combination of an electrostatic model with the Pitzer model to describe charging of and adsorption on an oxide-mineral surface up to high electrolyte concentrations should be tested. Surface titrations of silica have been obtained by Bolt [3] and modelled by Hiemstra et al. [4] up to 4 M NaCl. The model by Hiemstra did not involve electrolyte models that would allow for the accurate calculation of activity coefficients beyond 0.5 M and it is not clear whether all necessary corrections in the experimental work by Bolt [3] were done to obtain accurate experimental results. This uncertainty precludes the use of Bolt's data to test a model up to high electrolyte concentrations. In the present work, a Basic Stern model is instead applied to a set of spectroscopic data by Jena et al. [1] on fused silica. These authors have modeled their results by a Diffuse Layer Model (DLM) for the lower salt concentration, and with a constant capacitance model (CCM) at NaCl concentrations above 0.13 M. The CCM involves a constant surface potential for the latter conditions. The change in model concept with variable ionic strength and the constant potential assumption appear unnecessary, since in principle a well-parameterized SCM like the Stern model not only combines the properties of the DLM and the CCM, but also allows salt variation, while it is not clear whether such a model would be successful up to 5 M NaCl. The purely diffuse layer model (DLM) is known to be a rather bad model for most cases, while for classical silica it may not be as bad as for other oxides. Yet it is of interest to test a comprehensive model framework up to high concentrations of background electrolyte.

Charging and non-linear optics of fused silica in NaCl solutions at near-neutral concentrations

Figure 1 shows the experimental sum frequency generation (SFG) data from the literature and a model prediction by a classical silica model at an assumed pH of 6, which is the pH that the original authors specify for their experiments. Here, $-\log[H^+]/M = 6$ was assumed to be constant, which causes a significant change in the pH over the salt concentration studied. Figure 1a shows the actual data as obtained from the literature (red) and from the SCM output (blue). In the model, the above mentioned variation in pH, a non-monotonic change in the surface charge density is obtained at higher salt level. At low salt levels the typical increase with increasing salt content is predicted, while there is an inversion in the trend at the higher salt levels due to a change in pH. Interestingly, the inversion occurs at the salt levels where the SFG signal remains constant. In Figure 1b it was attempted to scale quantities from the two sources of data in such a way as to obtain overlap. In the lower salt levels, the BSM surface charge density scales very well with the SFG signal. At high salt levels, the surface potential and the diffuse layer potential scale with the SFG signal. The analysis of the non-linear results in terms of surface or diffuse layer potential is still ongoing. While it is generally accepted that the diffuse layer potential is strongly affected by salt concentration, there is contradictory information about the salt dependence of the surface potential. Classical models would predict very small effects in the latter case. This issue will be addressed in future research potentially with direct measurements of changes in the surface potential with variable salt concentrations. For future calculations, a more recent SFG data set in NaCl
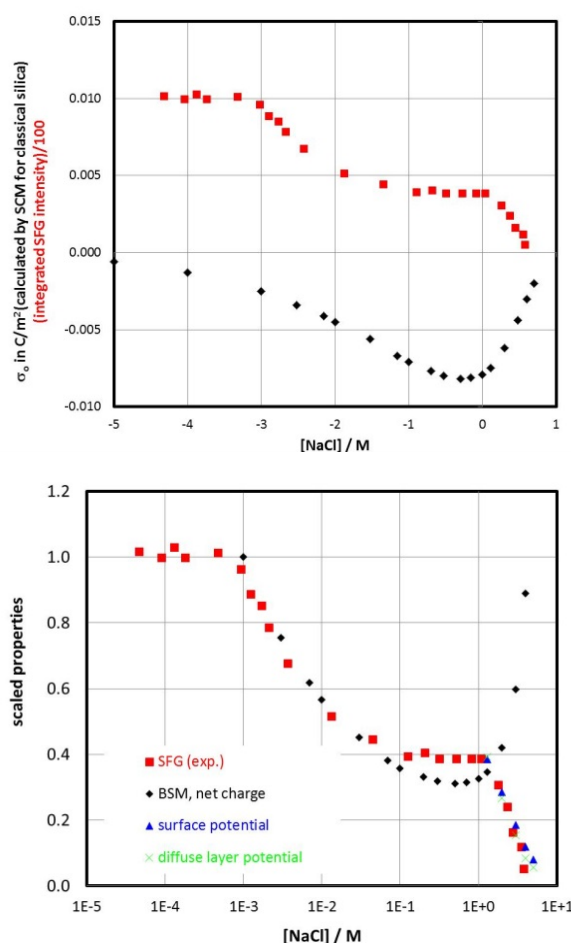
Fig. 1: *(a) Calculated surface charge density (protonable charge) of silica (black) and integrated sum frequency generation signal (from Jena et al. [1] at near-neutral pH as a function of NaCl concentration. (b) Scaled quantities from (a) and (scaled) calculated surface (blue) and diffuse layer potentials (green) for NaCl concentrations above 1 M.*

will be also be considered and an additional set of data in LiCl is also available that can be used to test the inherent ion specific effects. Although the simulations suffer from the ill-posed experimental conditions, the SCM is (for the inevitable assumptions involved) surprisingly successful in mimicking the spectroscopic data.

Adsorption of Sr on goethite up to high NaCl concentration – experiment and modelling

Based on the insight that the SCM is able to describe spectroscopic data up to high salt levels, the following text deals with charging data of and Sr adsorption data on goethite (α-FeOOH). A similarly simple model (Basic Stern model involving one surface site) has been applied to data up to 5 M NaCl. Figure 2 shows the experimental acid-base (charging) data with the obtained model up to 5 M NaCl. The model very well predicts the proton uptake data. It should be noted that the modeling also involved the determined isoelectric point of the goethite (data not shown).

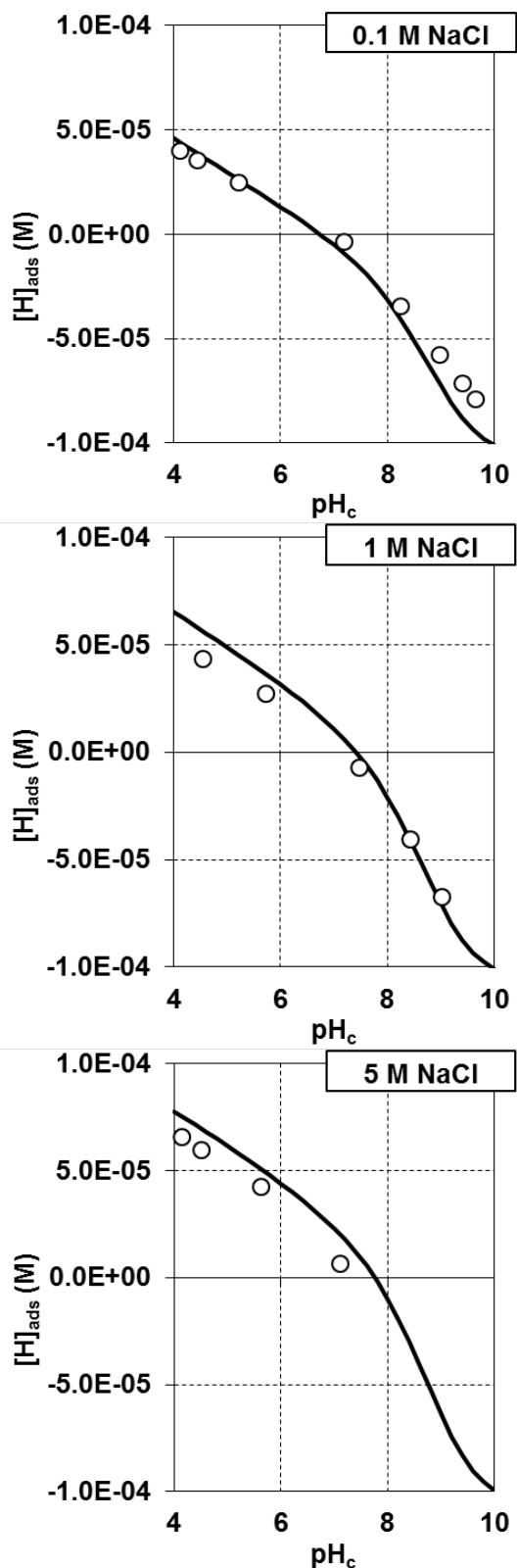**Fig. 2:** *H^+ adsorption (H_{ads}) as a function of pH_c for FeOOH(s) particles at different ionic strengths (0.1-5 M) in NaCl medium. Symbols stand for the experimental results, while lines are the best fit model using parameters within a surface complexation model (Basic Stern approach) for the surface reactions and Pitzer activity coefficients for aqueous solution speciation.*
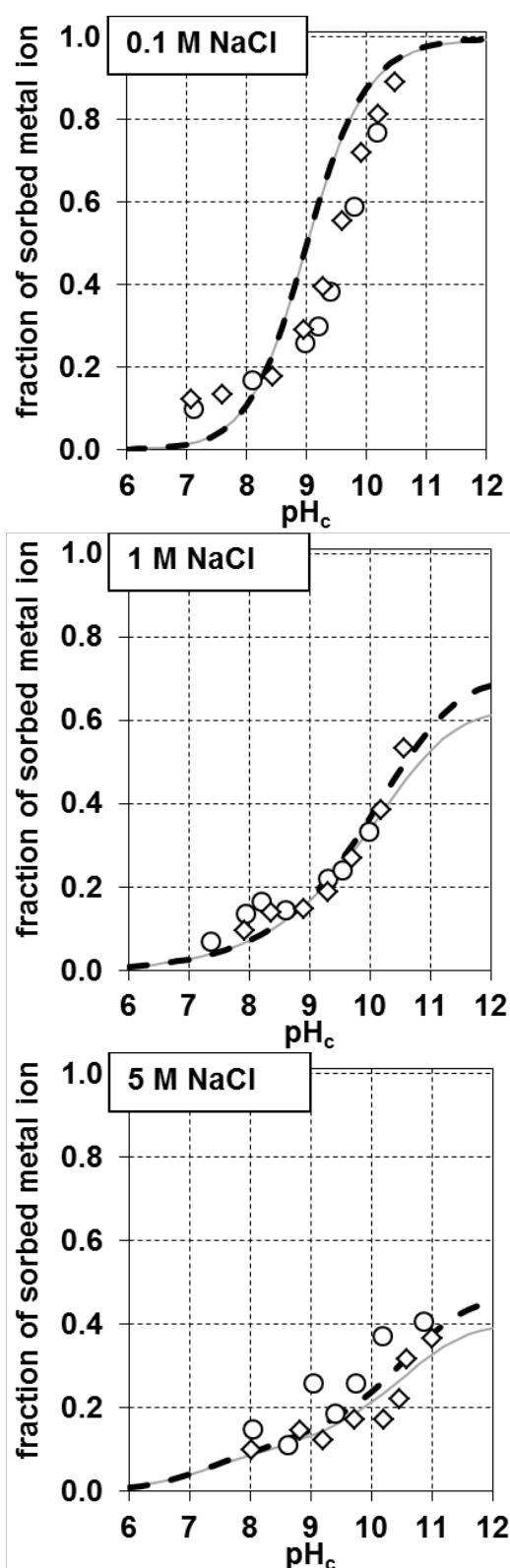
Fig. 3: *Sorption edges for Sr (diamonds $[Sr]_T=1\cdot10^{-5}$ M; circles $[Sr]_T=5\cdot10^{-5}$ M), S:L 9.43 g/L, on FeOOH(s) as a function of pH_c and at different NaCl concentrations. Sorption data (symbols) is presented as percentage uptake. Grey solid line ($[Sr]_T=1\cdot10^{-5}$ M) and black dotted line ($[Sr]_T=5\cdot10^{-5}$ M) stand for SCM predictions obtained with the model used to calculate the charging curves (Figure 2) and one Sr adsorption reaction.*

Figure 3 shows the adsorption data and the concomitant model lines. The model combines the NaCl Pitzer model and the basic Stern charging model from Figure 2 with a Pitzer based solution model for Sr in NaCl solutions and one additional Sr uptake reaction equation. Figure 3 involves Sr data at two slightly different total concentrations. The data at low salt level are not ideally described. This is due to the about 10 % adsorption at low pH for this series, which has been observed elsewhere as well and is difficult to model. The model could be improved by adding additional surface species, but this would not improve the already very good simulations at the higher salt levels. In particular the model is able to describe the much lower adsorption at the higher salt levels surprisingly well. Overall, the previous modelling tests have shown that it is possible to apply traditional electrostatic SCMs when combined with Pitzer formalism for aqueous solutions up to very high salt levels. This supports previous studies involving non-electrostatic models that combined with Pitzer equations well describe radionuclide uptake up to these high salt levels.

References

[1]   K.C. Jena et al., *Phys. Chem. Let.*, **2**: 1056 (2011)
[2]   A. Schnurr et al, *Geochim. Cosmochim. Acta* **151**: 192 (2015)
[3]   G.H. Bolt, *Phys. Chem.*, **61**: 1166 (1957)
[4]   T. Hiemstra et al., *Colloid Interface Sci.* **133**: 105 (1989)

4.2.2. Sorption of europium in presence of gluconate or citrate onto clay minerals

F. Rieder, T. Rabung, H. Geckeis

Introduction

Trivalent actinides generally show a strong interaction with clay mineral surfaces in terms of sorption reactions [1] which is of particular relevance for bentonite barriers or claystone host rocks of nuclear waste repositories. This strong retention was demonstrated recently also for highly saline conditions [2]. A significant decline in sorption is, however, to be expected in presence of organic complexing ligands, either naturally occurring like e.g. humic acids [3] or originating from the waste form or the concrete used as construction material. Among other relevant complexing ligands, gluconate as a representative of α-hydroxo carboxylic acids and an analogue to isosaccharinic acid (main product of cellulose degradation) and an important cement additive, might significantly decrease the sorption of trivalent actinides. Beside gluconate, citrate (another cement additive) is also expected to have an impact on the sorption behavior of trivalent lanthanides and actinides.

In order to assess the radionuclide retention capacity of clay minerals, the potential impact of strong complexing anionic ligands (like gluconate and citrate) on sorption needs to be quantified. For a sound mechanistic understanding and a reliable prediction of the metal ion sorption under relevant conditions a sufficient number of experimental data under variation of sensitive parameters (e.g. pH, ligand concentration, type of background electrolyte and its concentration, composition etc.) is essential. By combining all available information reliable thermodynamic models can be derived and/or validated.

Sorption of europium in presence of gluconate or citrate onto clay minerals

Almost no published data are available dealing with the sorption of trivalent lanthanides and actinides onto clay minerals in presence of gluconate or citrate both for low and high ionic strength conditions. In the present work, batch sorption experiments in presence of gluconate or citrate were performed with Illite du Puy (Na-IdP-2) using a solid to liquid ratio of 1 g/L, different NaCl (0.1, 1, 3 M) and CaCl$_2$ (0.06, 0.6, 2 M) background electrolytes concentrations and a constant ligand concentration of 0.01 M gluconate and 0.001 M citrate. In addition to this first approach with a relatively high gluconate concentration a second batch sorption series at fixed pH-values (pH = 9, 10.5, 12) was setup as a function of decreasing gluconate ligand concentration ([gluconate] = $5·10^{-3}$ - $1·10^{-5}$ M). The total radionuclide concentration in the system was fixed at $2·10^{-8}$ M ^{152}Eu (carrier free) for all batches. All experiments were performed under Ar atmosphere with an equilibration time of 3-4 day. To avoid precipitation

effects (e.g. of Ca-citrate or Ca-gluconate) thermodynamic calculations were performed before the experiments for all experimental conditions using the geochemical code PHREEQC and SIT corrections. To avoid effects of microbial degradation every solution containing organic ligands was freshly prepared and directly used within 4 days.

In presence of gluconate, a significant reduction of Eu (III) retention is observed for pH$_m$ > 7 in NaCl background electrolyte solutions (Figure 1) and the logarithmic distribution coefficient remains between log K_D = 3-4. Compared to the ligand free data of Schnurr *et al.* this corresponds to a decrease of 1-3 orders of magnitude. Experimental data derived from CaCl$_2$ containing systems exhibit a similar behavior between pH$_m$= 7-11 (Figure 2), with a further decrease above pH$_m$= 11. This second decrease might hint at the formation of ternary Ca-Eu(III)-GLU or quaternary Ca-Eu(III)-GLU-OH aqueous complexes. As a remarkable finding, the absence of any dependency on ionic strength in both electrolyte systems can be pointed out.

Figure 1 shows the experimental findings focusing on the influence of different gluconate concentrations on Eu(III) sorption in 0.1 M NaCl solution. Data are compared with experiments in absence (open symbols, black, same ionic strength) and presence of 0.01 M of gluconate (closed symbols, black). By increasing the gluconate concentration from $1·10^{-5}$ M to $1·10^{-4}$ M (yellow, purple and green symbols) no significant influence of gluconate on the sorption of Eu(III) onto illite is observed within the experimental uncertainties.

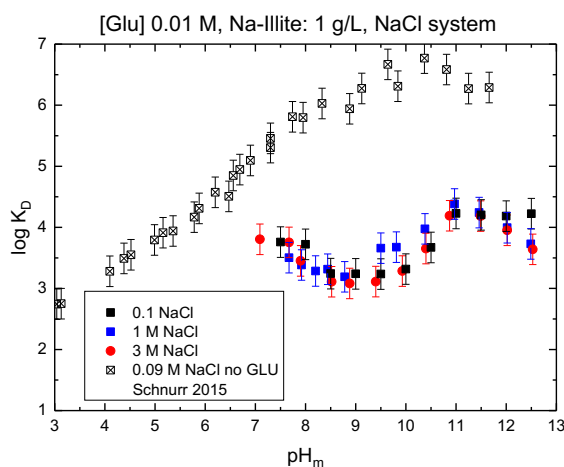**Fig. 1:** *Eu(III) sorption onto Illite du Puy, in presence of 0.01 M Na-Gluconate, in different NaCl electrolytes solutions (0.1 M black, 1 M blue, 3 M red) shown as logarithmic distribution coefficient log K_D vs. pH$_m$. To illustrate the effect of gluconate, experimental data from Schnurr et al. [2] in absence of any competing ligand is shown for comparison (open symbols, 0.09 M NaCl).*
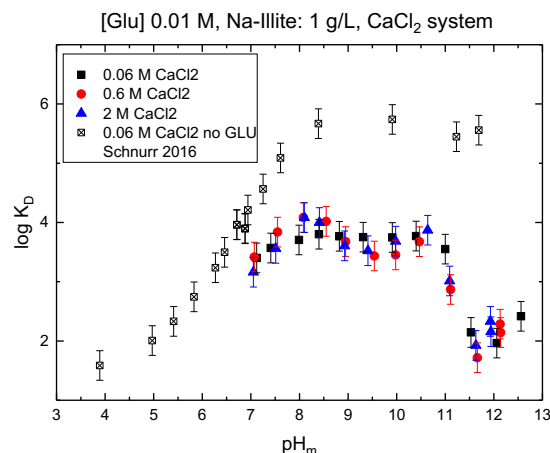
[Glu] 0.01 M, Na-Illite: 1 g/L, CaCl$_2$ system

Fig. 2: *Eu(III) sorption onto Illite du Puy, in presence of 0.01 M Ca-Gluconate, in different CaCl$_2$ electrolytes solutions (0.06 M black, 0,6 M blue, 2 M red) shown as logarithmic distribution coefficient log K$_D$ vs. pH. To illustrate the effect of gluconate, experimental data from Schnurr et al. [4] in absence of any competing ligand are shown (open symbols, 0.06 M CaCl$_2$).*
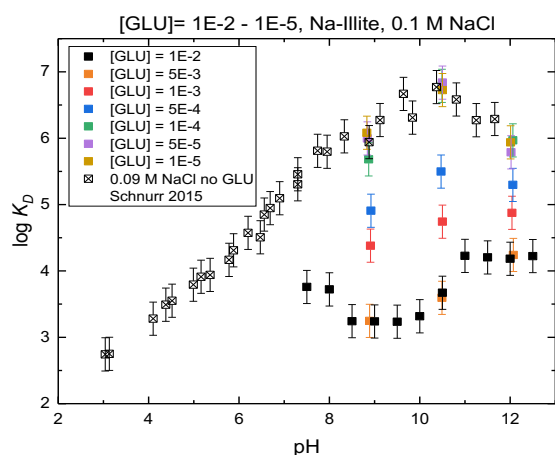

[GLU]= 1E-2 - 1E-5, Na-Illite, 0.1 M NaCl

Fig. 3: *Eu(III) sorption onto Illite du Puy under variation of the gluconate concentration in 0.1 M NaCl. Experimental data from Schnurr et al. [2] in absence of any competing ligand (open symbols, 0.09 M NaCl) and an experimental series in presence of 0.01 M Na-gluconate (black squares, 0.01 M gluconate) are shown for comparison.*

Therefore, the value of $1 \cdot 10^{-4}$ M gluconate may be taken as a lower limiting value for the effect on the sorption of Eu(III) onto Na-Illite (at least for the experimental conditions of the present study, for instance regarding the solid content or Eu(III) concentration). By further increasing gluconate concentration from $1 \cdot 10^{-4}$ M to $5 \cdot 10^{-3}$ M, a significant decrease in retention takes place with similar data observed for $5 \cdot 10^{-3}$ M and $1 \cdot 10^{-2}$ M gluconate. The gluconate concentration of $5 \cdot 10^{-3}$ M can be seen as the concentration limit when the maximum impact on Eu(III) sorption under the chosen experimental conditions of this study is established.

The influence of citrate on the Eu(III) sorption on illite is shown in Figure 4 for 3 different NaCl background electrolyte solutions. In the lower pH-region
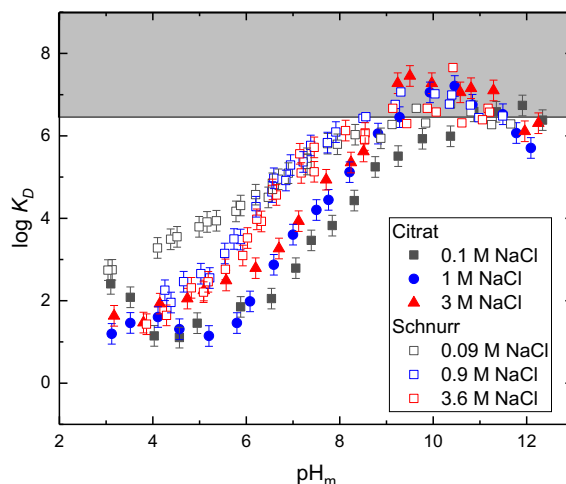

Fig. 4: *Eu(III) sorption onto Illite du Puy, in presence of $1 \cdot 10^{-3}$ M Na-Citrate, in different NaCl electrolytes solutions (0.1 M black, 1 M blue, 3 M red) shown as logarithmic distribution coefficient log K$_D$ vs. pH. To estimate the effect of citrate, experimental data from Schnurr et al. [2] in absence of any competing ligand are shown (open symbols, same color code).*

from pH = 3 to 8 the retention of Eu(III) is remarkably decreased compared to the ligand free system. No pronounced retention is observed for higher pH conditions, however. As in the gluconate system, no drastic impact of ionic strength on sorption is observed.

Conclusions

The presence of complexing ligands like gluconate or citrate can have a major impact on the sorption behavior of trivalent lanthanides and actinides. Batch sorption experiments in presence of gluconate indicate a significantly reduced retention of Eu(III) sorption onto illite over the whole pH-range covered in this study (7<pH<12.5). Sorption experiments in presence of citrate show pronounced reduction of sorption up to pH ~8. In all experimental series for gluconate and citrate, no drastic effect of ionic strength was observed for the same type of background electrolyte solution. Significant effects could be observed when using NaCl instead of CaCl$_2$ solutions in the gluconate system. In the future, time resolved laser fluorescence spectroscopy (TRLFS) will be used to get deeper information on the sorption mechanisms/processes and to establish a thermodynamic model for describing the experimental findings.

References

[1] Bradbury M. et al., *Geochim. Cosmochim. Acta,*. **69**: 5403 (2005)
[2] Schnurr, A., et al., *Geochim. Cosmochim. Acta*, **151**: 192 (2015)
[3] Rabung, T., et al., *Radiochim. Acta*, **82**: 243 (1998)
[4] Schnurr, A., PhD thesis, KIT (2015)

4.3 Retention of radionuclides by secondary phase formation

N. Vozarova, N. Finck, F. Heberling, D. Schild, E. Sobala, S. Kraft, A. Bauer

In Cooperation with:

N. Bogachev[a]

[a] Saint Petersburg State University, Saint Petersburg, Russia.

Introduction

High-level nuclear waste (HLW) is foreseen to be encapsulated in thick-walled steel containers and placed in deep geological repositories where it will be further isolated by additional barriers. During the (geo)chemical evolution of the repository, ground water may migrate through the barriers and contact the waste packages. Secondary phases form as a consequence of alteration or corrosion of materials from the multi-barrier system or from the waste itself. Knowledge of the nature and amount of secondary phase(s) formed, including relevant kinetics, will greatly improve the Safety Case from a geochemical perspective.

Secondary phases can potentially scavenge radionuclides (RNs) released from the waste and significantly retard their migration to the far-field. Various molecular scale retention processes can occur, ranging from surface retention to structural entrapment. Retention of radionuclides by structural incorporation, i.e., by formation of solid solutions, can arguably result in a long-term efficient immobilization mechanism. The formation of solid solutions is common in nature. However, significant efforts are required to establish reliable kinetic and thermodynamic models for use in the specific context of nuclear waste disposal. Such models can be developed by combining information from experiments, i.e. using advanced microscopic, spectroscopic and diffraction techniques, and from complementary computational studies. At KIT-INE, the retention of radionuclides by structural incorporation within the bulk structure of relevant secondary phases is investigated by combing experimental and theory based efforts to develop a thorough molecular scale process understanding. Below are examples of ongoing studies.

Corrosion of iron granules in various brines at elevated temperatures

For safety analysis, knowledge of steel corrosion rates and corrosion mechanisms are important information. On the one hand side, corrosion rates may allow estimating the time frame of the integrity of the waste packages and on the other hand side, corrosion products will provide an additional barrier against radionuclide migration to the far field.

Fe(0) is the main component of various steel types used for canisters and is presently studied in new corrosion experiments under anoxic and saline conditions. The starting materials in the orientative studies presented here were commercial iron granules of 2 mm size, which were cleaned by washing shortly with 5 mM HCl. A surface to brine volume ratio of 1:5 was used. Brines were either NaCl (ionic strength $I = 1$ M and 3 M) or $MgCl_2$ (ionic strength $I = 1$ M and 9 M). Experiments were performed in plastic containers placed in an oven at 60°C. Contact times of 2, 6, 12 and 18 weeks were adopted.

In additional studies, two containers filled with either NaCl at $I = 3$ M or $MgCl_2$ at $I = 3$ M were placed inside an Ar glovebox at 25°C. The preparation of the experiments as well as sampling was done under Ar atmosphere to ensure strict anoxic conditions. pH and E_h were measured after cooling down to room temperature. Sampling of the granules and liquid phase was done in a way so as to keep the surface to volume ratio constant. After sampling, the containers were closed again and placed back into the oven. The same sampling procedure was applied for the samples staying in the Ar box at room temperature. Sampling at several time intervals and at two temperatures allows to constrain the kinetics of the corrosion processes. Various analytical techniques were used to characterize the solid phases. The settled particles in the liquid phase were examined by XRD to identify the formed secondary phases. The iron granules were gently washed to remove adherent dried salt particles and examined by XPS to determine the elemental composition and Fe redox state, and by SEM-(EDX). to see the morphology and perform elemental analysis.

SEM analysis for solid phase in $MgCl_2$ brine at $I = 1$ M shows the presence of hexagonal sheet crystallites of a morphology typical for green rust (GR) or $Fe(OH)_2$ [1] and octahedral crystals typical for magnetite after 6 and 12 weeks. However only GR/$Fe(OH)_2$ is observed after 18 weeks (Figure 1), showing significantly higher coverage of the iron surface by secondary phases as time progresses. This is confirmed by XPS measurements where after 18 weeks, in the narrow O 1s spectrum, no oxide line is present, indicating the absence of magnetite. The narrow Fe 2p spectrum shows almost no Fe(III) peak after 6 and 12 weeks but a significant peak of Fe(III) after 18 weeks. This allows a distinction between GR and $Fe(OH)_2$ as the later does not have any Fe(III) present. The Fe(II) shoulder is very close to the Fe(0) peak in the narrow Fe 2p spectrum but present in all cases. It should be noted that the sample evolution from 12 to 18 weeks is far more evident than the sample evolution from 6 to 12 weeks contact time. EDX measurements also show iron to oxygen ratios which correspond to magnetite (3:4) and GR (1:2) after 6 and 12 weeks, but only GR after 18 weeks. XRD of the settled particles confirms the presence of magnetite after 6, 12 and 18 weeks.
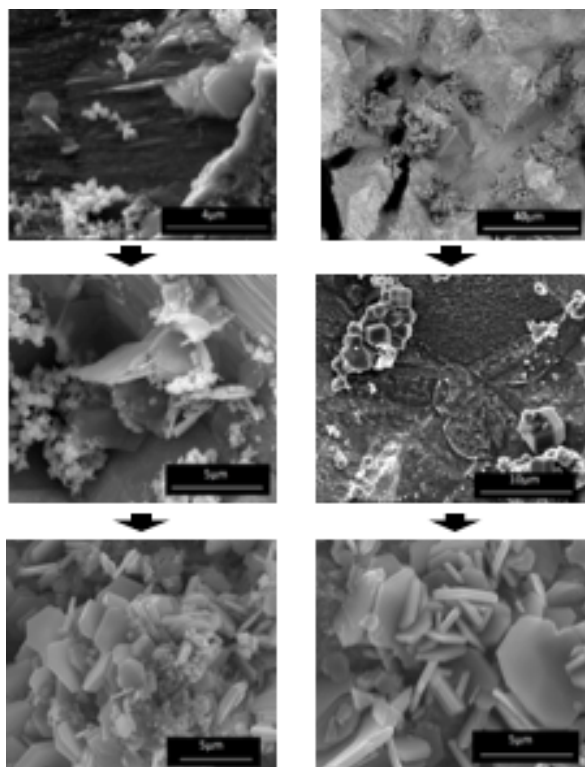
Fig. 1: *SEM pictures of the evolution of the solid phase morphology in the I = 1 M MgCl₂ brine (left) and I = 1 M NaCl brine (right) from 6 weeks (top) to 18 weeks (bottom). Temperature fixed at 60°C.*

Similar studies in $MgCl_2$ brine ($I = 9$ M), SEM reveal no corrosion after 2 weeks and the formation of hexagonal platy crystals suggesting the presence of GR/Fe(OH)₂ only after 6 and 12 weeks with no indication of magnetite. The XPS narrow O 1s spectrum lacks the oxide line after 2, 6 and 12 weeks, which confirms that there is no magnetite present (Figure 2). XPS narrow Fe 2p spectrum shows a similar evolution as in the previous case for $MgCl_2$ brine at $I = 1$ M, indicating the presence of GR after 12 weeks. EDX measurements showed Fe/O ratios corresponding to GR after 12 weeks. XRD rendered inconclusive due to interferences from the high salt content present in the samples.

In the case of NaCl brine at $I = 1$ M, well defined octahedral magnetite crystals are evidenced by SEM after 6 weeks, however in lower amounts after 12 weeks and almost only GR/Fe(OH)₂ platy structures are found after 18 weeks (Figure 1). XPS narrow O 1s spectrum shows the gradual disappearance of the oxide line, reaching almost plateau after 18 weeks. In the narrow Fe 2p spectra, Fe(0) is likewise decreasing whilst Fe(III) gradually increases with time, indicating the presence of GR. EDX measurements confirm the evolution of magnetite into GR. These results could not be confirmed by XRD, again due to interferences from the high salt content.

When increasing the ionic strength for NaCl to 3 M, SEM shows no corrosion after 2 weeks, the coexistence of magnetite crystals and GR/Fe(OH)₂ platelets after 6 weeks, and only GR/Fe(OH)₂ after 12 weeks. These findings are corroborated by EDX spectroscopy. XPS

narrow O 1s and Fe 2p spectra show hydroxide and oxide contributions after 6 weeks, no oxide line after 12 weeks, and increase in Fe(III) with time (Figure 3), confirming SEM and EDX results, and, as in the previous cases, the presence of GR.

Regarding pH_m evolution, in case of $MgCl_2$ brine at $I = 1$ M, the pH_m shifted from slightly acidic range to neutral, from pH_m 5.8 to 6.8 after 18 weeks. For the remaining 3 cases, the pH shift was within 1 unit after 18 weeks. E_h increased slightly for all cases, possibly suggesting incomplete tightness of the vessels and eventually intrusion of oxygen. pH_m and E_h were not measured at elevated temperature but at room temperature, which may have caused a shift in equilibrium and thus a shift in absolute values observed. All pH_m values reported here account for ionic strength correction factors and are plotted as molal proton concentrations. All E_h values are reported vs. SHE.

The experiments at room temperatures reveal slower and less aggressive corrosion processes, as expected, with no changes observed on the iron solid phase or liquid phase after 6 and 12 weeks for NaCl at $I = 3$M and no changes after 6 weeks for $MgCl_2$ at $I = 3$M. The sample from $MgCl_2$ brine shows the presence of GR/Fe(OH)₂ platelets on spots in SEM after 12 and 18 weeks. XPS and EDX confirms SEM findings, while XPS also shows a large Fe(0) peak in addition to a small Fe(III) peak, highlighting the presence of a major un-corroded surface and indicating the presence of green rust. Samples in NaCl brines yield very similar results with SEM showing corroded spots covered with GR/Fe(OH)₂ platelets after 18 weeks. XPS shows the

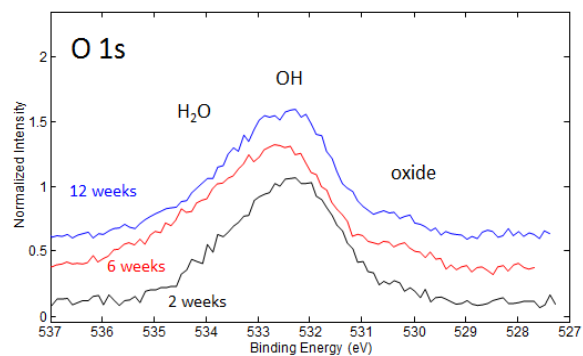**Fig. 2:** *XPS narrow O 1s spectrum comparison for experiments in MgCl₂ I = 9 M (T = 60°C).*

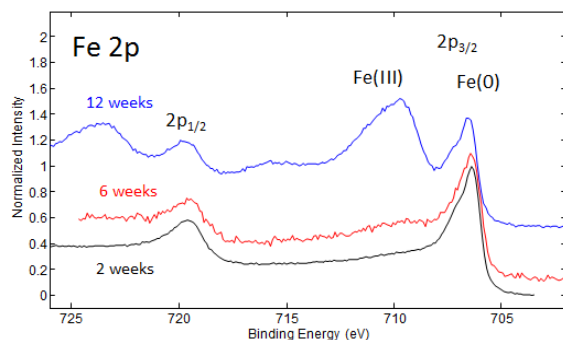**Fig. 3:** *XPS Fe 2p narrow spectrum comparison for NaCl brine I = 3 M (T = 60°C as function of time).*

same results as in the case of MgCl₂, also confirming the presence of GR, while EDX measurements show mainly iron. The E_h remains constant and the intrusion of oxygen can be excluded in these experiments. pH_m shows an initial increase from 7 to 8 for MgCl₂ and to 9.5 for NaCl after 6 weeks. A further increase by 0.5 units is observed for NaCl after 18 weeks. This pH_m increase can be linked to the volumetric replacement of iron between the non-corroded surface and the formed secondary phases [2].

It is challenging to quantify the dependence on temperature, as the corrosion rate was not measured. A significant effect of temperature on the corrosion of iron was previously reported by Foley [3]. The comparison of SEM pictures between two granules in brines with identical ionic strength ($I = 3$ M) at 25°C and 60°C after 12 weeks of exposure, respectively show that while at 60°C the surface coverage by secondary phases is distributed evenly and covers approximately half of the surface, while at 25°C the only coverage is seen at grain boundaries or at uneven structures of the surface.

Overall, considering the time evolution, Mg-rich brines seem to favor GR as a major corrosion product particularly at high ionic strength ($I = 9$ M), though magnetite is present at low ionic strength ($I = 1$ M) at early stages. Na-rich brines also seem to favor GR as a major corrosion product at both intermediate ionic strength ($I = 3$ M) and low ionic strength ($I = 1$ M) but in both cases, the magnetite is present at early stages and is gradually substituted/covered by GR. It seems from the time evolution that higher ionic strength accelerates this transformation. High ionic strength hinders growth of magnetite and likely favors nucleation of Fe(OH)₂ and hence the GR forms faster and thus covers the surface completely [4].

At $I = 1$ M, both Mg- and Na-rich brines show similar behavior regarding the development of secondary phases at elevated temperature. Like observed at room temperature, both brines with $I = 3$ M showed similar behavior, independent of the salt type, but lacking magnetite. This indicates that the cations do not play a significant role as long as identical ionic strength is given, pointing to a key effect of chloride [3].

Referring to the Pourbaix diagram by Refait and Génin [5], the green rust is stable under similar pH and E_h conditions as magnetite [6] with the E_h varying from -0.5 V to 0.0 V and pH varying from 6.5 to 12 [5]. The magnetite stability field is slightly smaller in terms of E_h and also shifting towards the basic range with increasing ionic strength. Considering the pH and E_h values in the experiments, the conditions are at the border of the stability field of magnetite. It was found that even though on the solid phase only GR is present, there is magnetite present in the precipitate. Since formation of green rust and magnetite are competing processes, and magnetite was present at early stages as observed in SEM, it appears to have precipitated. Since during the experiment the conditions remained within the stability field of magnetite, the measured magnetite by XRD was likely from early stages. There was no direct indication that new magnetite was formed, and, if it has formed, it has been covered by GR.

Transformation of magnetite to green rust is not likely as GR usually transforms towards magnetite and not vice versa [7].

This experiment serves as a prerequisite for the currently ongoing comprehensive steel corrosion experiments at elevated temperature (90°C) under defined conditions in tightly closed vessels (autoclaves). With this optimized experimental setup, the gas phase evolution can be observed and the polished sample surface allows for better morphological evaluation. Application of complementary analytical techniques (e.g., TEM or Raman) and weight loss measurements are planned. Most importantly, the corrosion rate will be evaluated, which was not feasible with granular Fe(0).

Spectroscopic signature of iron in natural and synthetic saponite

Over extended periods of time, the integrity of steel canisters may be lost and groundwater can reach the waste. Glass alteration experiments under repository relevant geochemical conditions have evidenced the formation of trioctahedral smectites. In recent studies (e.g., [8]), the mineralogy of these newly formed secondary phases has been reported. The octahedral sheet contains predominantly Mg along with some Al while the tetrahedral sheet is made of Si tetrahedra with some substitution by Al tetrahedra. Consequently, saponite forms during glass alteration. This mineral is also able to contain structural Fe, for example by substituting for Al. Structural iron within clay minerals can undergo oxidation and reduction cycles when located at octahedral position, and thereby promote the reductive immobilization of radionuclide released by the waste matrix. In contrast, such oxidation/reduction cycles may be much less likely for Fe located in the tetrahedral sheet. Below are preliminary results on characterization of structural iron within a natural saponite and a synthetic saponite, with iron expected to be located at tetrahedral lattice sites in the synthetic material.

The saponite SapCa-2 was purchased from the Source Clay Repository, purified and the fraction <0.1 µm separated. The second saponite (sample SapoFe) was synthesized using a hydrothermal protocol, provided by J.-L. Robert (Université Pierre et Marie Curie, Paris, France) and used without further purification. For both samples, Fe K-edge powder X-ray absorption spectra were collected at the INE beamline [9] at the synchrotron light source ANKA (Karlsruhe, Germany).

The XANES of both samples significantly differ, meaning that the Fe local chemical environments are different (Figure 4). The pre-edge centered at ~7114 eV is weak for SapCa-2 and substantial for SapoFe. This feature originates predominantly from a dipolar $1s \rightarrow 3d$ transition, which is forbidden in O_h symmetry [10], but allowed in T_d symmetry. Pre-edge spectra may thus hint at Fe located in the octahedral sheet in SapCa-2 and very likely in the tetrahedral sheet in SapoFe. The maximum of the edge is of lower intensity and contains a high amplitude shoulder at higher energies in SapoFe. Finally, the first resonance centered at
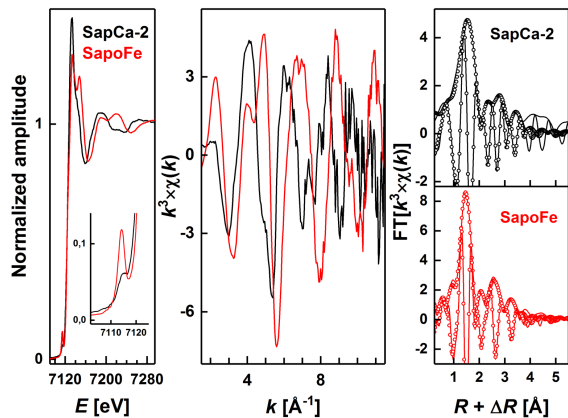
Fig. 4: *X-ray absorption spectroscopy data for structural Fe within SapCa-2 and SapoFe. Experimental XANES (left) and EXAFS spectra (middle), and experimental and modeled Fourier transforms (right).*

around 7200 eV also significantly differs. However, the edge is located at similar energy position, typical of Fe(III), in both samples, implying that both contain Fe(III). These observations indicate that the Fe(III) local environment, and thus the location within the structure, differs.

The EXAFS spectra of both compounds differ in amplitude and in frequency of the oscillation (Figure 4). These differences in spectral features originate from differences in the type of neighboring atoms and their distance to the absorber. Accordingly, the FT contain contributions of different amplitude at different distances.

Preliminary fits to the experimental data indicate that Fe in SapCa-2 is surrounded by a first O shell containing ~6 atoms at 2.01(2) Å whereas in SapoFe it is surrounded by only ~4 O atoms at 1.86(2) Å. This is a clear evidence that Fe(III) is located in the octahedral sheet in the former and in the tetrahedral sheet in the later, in agreement with conclusions from XANES spectra. Higher distances shells in SapCa-2 consist of octahedral Mg (at 3.05 Å) and tetrahedral Si (at 3.28 Å) shells. In contrast, neighboring Si and Mg shells were detected at 3.18 Å and 3.33 Å in SapoFe that can only correspond to tetrahedral and octahedral neighbors, respectively.

Data show that Fe can be located at tetrahedral position within smectites, despite the difference in size ($^{IV}Fe(III) = 0.49$ Å) with Si ($^{IV}Si(IV) = 0.26$ Å) [11]. Consequently, it is reasonable to assume that Fe can be incorporated at tetrahedral sites in smectites formed as secondary phases in a deep underground repository, given that favorable geochemical conditions prevail during their formation.

Potential interaction of Eu^{3+} and Cm^{3+} with $CaCO_3$ pre-nucleation clusters

As a supplement to the investigation on trivalent actinide and lanthanide (An/Ln(III)) uptake by calcite, reported in last year's annual report of KIT-INE [12], we present here a study on the potential interaction of

An/Ln(III) with aqueous precursors of calcite formation, i.e. $CaCO_3$ pre-nucleation clusters [13,14]. First results indicate a possible interaction. This may be a key towards a mechanistic understanding of An/Ln(III) co-precipitation with calcite.

Guided by the first studies on $CaCO_3$ pre-nucleation clusters (PNCs) [13] we chose experimental conditions, where, starting from pure An/Ln(III)-cabonato complexes, we may expect increasing amounts of PNCs to be present in solution. These conditions are: 10 mM NaCl, 10 mM Na_2CO_3, and either 1 μM Eu^{3+} or 50 nM Cm^{3+}. Experiments are performed at fixed pH values, 7.8 and 9.4 in the Eu-system and 7.0 and 8.95 in the Cm-System. For lack of space, only the pH 7.8/7.0 results will be presented here. At these pH conditions we expect the respective mono-carbonato complexes to dominate the aqueous An/Ln(III) speciation. Increasing amounts of $CaCl_2$ were added to the solutions in order to sequentially increase the concentration of $CaCO_3^0{}_{(aq)}$ (calculated with PhreeqC 2.18 [15] and the NaPSI database [16]), which is expected to be directly correlated with the concentration of PNCs in solution.

Time resolved laser luminescence spectroscopy is performed on aqueous solutions in quartz cuvettes at room temperature. We excite Eu^{3+} at 394 nm and record the $^5D_0 \rightarrow {}^7F_j$ (j = 0, 1, 2) transitions in a range from
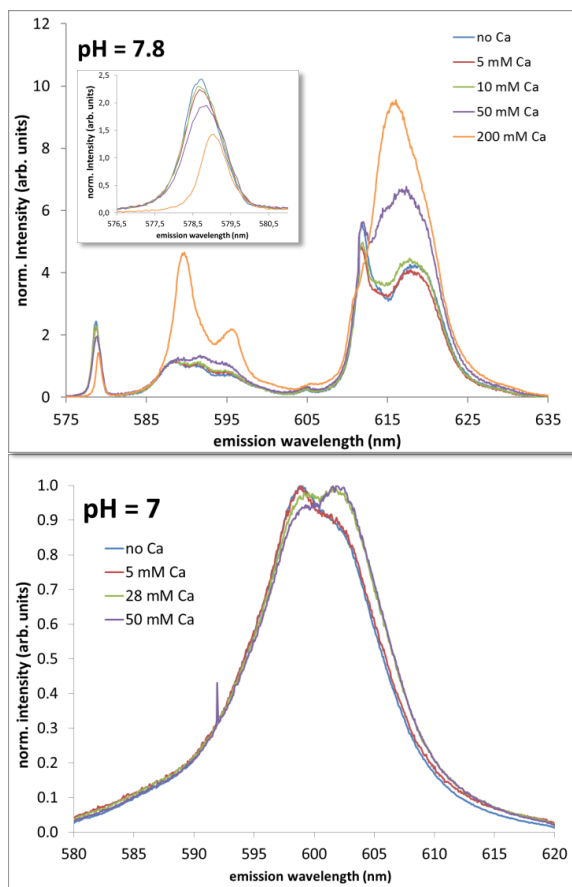

Fig. 5: *Emission spectra of Eu^{3+} (upper graph) and Cm^{3+} (lower graph) recorded at increasing Ca^{2+} concentration in solution. The insert in the upper graph highlights details in the Eu $^7F_0$ band.*

575 nm to 635 nm. We excite Cm^{3+} at 396.6 nm and record the $^6D_{7/2} \rightarrow {}^8S_{7/2}$ transition in a range between 580 nm and 620 nm.

Spectroscopic results are presented in Figure 5. Up to 50 mM Ca, we observe a sequential small redshift in the Eu $^7F_0$-band and a pronounced redshift in the Cm spectra, as well as subtle but reproducible changes in the Eu $^7F_1$- and $^7F_2$ bands. If we further increase the Ca concentration, as shown for Eu, we observe sudden, spontaneous precipitation of calcite, accompanied by a pronounced change in all Eu-spectral features. The changes up to 50 mM Ca indicate an increasing carbonate complexation [17]. This happens at constant total C concentration. Considering Ca-CO_3 complexes in solution, the free CO_3^{2-} concentration in solution even decreases.

PNCs are expected to form under the conditions chosen for our study [13]. They are expected to consist of up to ~70 $CaCO_3$ moieties [18], have sizes of 0.5-1.2 nm [14], and are expected to consist of strongly hydrated chain-, branch-, and ring-like structures [19]. Thus, we think the results would be in line with an incorporation of An/Ln(III) into PNC-chains. Nevertheless, we can to date not exclude the possibility that the spectral changes just reflect the formation of a yet unknown type of solution complex.

References

[1] Ruby, C. et al., *Applied Clay Sci.* **2009**, *48*, 195-202.

[2] Schlegel, M.L. et al., *Applied Geochem.* **2008**, *23*, 2613-2633.

[3] Foley, R., *Corrosion* **1970**, *26* (2), 58-70.

[4] Vayssières, L. et al., *J. Colloid Interface Sci.* **1998**, *205* (2), 205-212

[5] Refait, P. and Génin, J., *Corrosion Sci.* **1993**, *34* (5), 797-819.

[6] Eisele, T. and Gabby, K. *Min. Process. Extr. Metall. Rev.* **2014**, *35* (2), 75-105.

[7] Miot, J. et al., *Geochim. Cosmochim. Acta* **2014**, *139*, 327-343.

[8] Debure, M. et al., *J. Nucl. Mater.* **2016**, *475*, 255-265.

[9] Rothe, J. et al., *Rev. Sci. Instrum.* **2012,** *83* (4), 043105.

[10] Westre, T.E. et al., *J. Am. Chem. Soc.* **1997**, *119*, 6297-6314.

[11] Shannon, R.D., *Acta Cryst.* **1976**, *A32*, 751-767.

[12] F. Heberling et al., in H. Geckeis et al. (ed.) INE-Annual Report 2016, *KIT-Scientific Reports* (2017).

[13] Gebauer, D. et al., *Science* **2008**, *322*, 1819-1822.

[14] Pouget, M. et al., *Science* **2009**, *323*, 1455-1458.

[15] D. L. Parkhurst and C. A. J. Appelo, *USGS Report* **99** (1999).

[16] Hummel, W. et al., *Radiochim. Acta* **2002**, *90*, 805-813.

[17] Kim, J.I. et al., *J. Alloys Compds.* **1994**, *213-214*, 333-340.

[18] Gebauer, D. et al., *Chem. Soc. Rev.* **2014**, *43*, 2348-2371.

[19] Demichelis, R. et al., *Nat. Comm.* **2011**, *2*, 590.

5. Applied studies: radionuclide retention in the multi-barrier system

Long-term safety of a deep geological repository for nuclear waste depends on a multi-barrier system which consists of technical and geo-technical barriers such as the waste form, the canister, backfilling and sealing of the mined openings as well as on the natural barrier function of the host rock. A series of applied studies on subsystems of various multi-barrier systems are performed, which cover a variety of components with specific characteristics and properties. Investigations presented in the first sub-chapter cover the quantification of actinides, fission and activation products in Zircaloy of a spent nuclear fuel rod segment. In the following, a review paper on microbial effects in the context of disposal of non-heat producing waste forms is summarized. The third subchapter deals with the occurrence and stability of colloids, and their impact on radionuclide migration. These research activities comprise studies on the characterization of natural organic matter derived from the Boom Clay formation and their interaction with radionuclide, experiments on compacted bentonite erosion and colloid formation at the bentonite pore water interface, and further experimental studies on clay colloid stability, colloid / mineral surface interaction and radionuclide sorption. Experimental studies on diffusion of with HTO, Cl-36 and Sr-85 in compacted natural and reduced-charge dioctahedral smectites are described in the fourth subchapter. In addition to these mainly experimental studies, modelling studies of multi-barrier systems are conducted, which are described in the final sub-chapter.

5.1 Highly radioactive waste forms

E. González-Robles, M. Herm, N. Müller, M. Böttle, E. Bohnert, V. Metz

In collaboration with:

R. Dagan[a], D. Papaioannou[b]

[a] Karlsruhe Institute of Technology, Institute for Neutron Physics and Reactor Technology, Karlsruhe, Germany; [b] European Commission, Joint Research Centre, Directorate G – Nuclear Safety and Security, Karlsruhe, Germany

Introduction

In Germany as well as many other countries, spent nuclear fuel (SNF) assemblies, after being discharged from a nuclear power reactor, are cooled in spent fuel pools for several years, and eventually sent for dry cask storage. Dual-purpose casks (CASTOR®, GNS) are used for transport and dry interim storage of SNF assemblies [1].

In the German waste management concept, SNF is designated for direct disposal in a deep geological repository available by 2050 at the best [1]. However, considering the delay in the site selection process so far as well as the time needed for exploration, construction, and commissioning of a repository for high-level waste, start of waste emplacement is expected by the end of this century/beginning of next century [1].

Thus, a prolonged dry interim storage of SNF assemblies is inevitable [1]. Moreover, dry interim storage of SNF assemblies was intended to last only a few decades, and hence licenses for storing of CASTOR® casks in the interim storage facilities expires already in the years 2034 to 2047 [1]. Therefore, a thorough revaluation of all safety relevant aspects is required, taking into account the extended dry cask storage of SNF assemblies.

Integrity of the irradiated Zircaloy cladding after 50 years or considerably longer periods of dry interim storage is of importance e.g. to ensure a safe reloading of the fuel assemblies from the CASTOR® to the final disposal canister.

However, the cladding is affected during reactor operation by various processes such as elongation of the fuel rods due to creep behavior and oxidation with the water coolant causing a reduction of the Zircaloy wall thickness, respectively. Further, dissolution and precipitation of hydrogen within the Zr-alloy matrix, during reactor operation, possibly leads to hydrogen embrittlement and delayed hydride cracking of the cladding. Swelling of the fuel pellets during irradiation due to fission products build-up eventually leads to the contact of the fuel pellets with the cladding. The so-called pellet/cladding interaction (PCI) induces tensile stress on the cladding, especially during power ramps. In presence of (volatile) fission (and activation) products released from the pellets stress-corrosion-cracking can occur.

Using experimental and modelling methods, the radionuclide inventory of an irradiated Zircaloy-4 plenum section is analyzed in this study. The results and findings of this study is prerequisite work for studies involving Zircaloy-4 cladding in contact with fuel pellets.

Materials and irradiation characteristics

The studied Zircaloy-4 plenum cladding was sampled from fuel rod segment N0204 of fuel rod SBS1108. The fuel rod was irradiated during four cycles in the pressurize water reactor Gösgen (KKG, Switzerland) and discharged in May 1989 after 1226 effective full power days. During reactor operation, an average burn-up of 50.4 GWd/t$_{HM}$ as well as average linear power of 260 W/cm was achieved.

Experimental and analytical methods

Subsamples of the Zircaloy-4 plenum section (see figure 1a) were dry cut using an IsoMet® Low Speed Saw (11-1180, Buehler Ltd.) equipped with an IsoMet® diamond wafering blade (11-4254, Buehler Ltd.). Cutting was performed very slow (about one hour per sample) to prevent overheating of the material. In total six subsamples (see figure 1b) with masses ranging from 119.7 ± 0.2 mg to 189.0 ± 0.2 mg were prepared by remote handling in a shielded box for dissolution experiments. Masses and dose rates were measured using an analytical balance (MS304S, Mettler-Toledo International Inc.) and a dose rate meter (6150AD6, automess – Automation und Messtechnik GmbH). Dose rate of the subsamples was typically less than 0.3 mSv/h.

The specimens were digested within 30 minutes in a dilute H_2SO_4/HF mixture at room temperature and anoxic conditions using a flask or autoclave. Radionuclides present in the digestion liquor (and gas phase) were analyzed using various analytical and separation methods.

α-spectroscopy was used to quantify $^{235,238}U$, ^{237}Np, $^{238,239,240,242}Pu$, $^{241,243}Am$, and $^{243,244}Cm$ (ion implanted Si semiconductor detector, MXR Model 1520, MCA System 100, ASP data evaluation software, Canberra Industries Inc.). Drops of a diluted (1:100) aliquot of the digestion liquor were placed on a metal disk (target) and dried for the measurements.

α-spectroscopy was also performed from Pu isotopes after separation from other α-emitting radionuclides. Fission products and minor actinides with characteristic γ-rays e.g. $^{134,137}Cs$, $^{241,243}Am$, ^{154}Eu, and ^{125}Sb were quantified in digestion liquors obtained from dissolution experiments performed with irradiated Zircaloy-4 using γ-spectroscopy. Measurements in this study were performed by means of an extended range coaxial Ge detector (GX3018, Canberra Industries Inc.) with a relative efficiency of $\geq$ 30%. Energy and efficiency calibration of the detector was performed using a certified multi-nuclide standard solution (Mixed Gamma 7600, Eckert & Ziegler Strahlen- und Medizintechnik AG). Data evaluation was performed using the Genie 2000 software (Canberra Industries Inc.). Aliquots of one milliliter from the digestion liquors were measured using APEX® screw-cap microcentrifuge tubes (2 mL, polypropylene, PP, Alpha Laboratories Ltd.).

Minor actinides, activation and fission products such as ^{14}C, ^{55}Fe, and ^{241}Pu were measured, after separation from other radionuclides, in digestion liquor or gas phase obtained from dissolution experiments performed with irradiated Zircaloy-4 using liquid scintillation counting (LSC). LSC measurements were performed using an ultra-low level spectrometer (Quantulus 1220, Wallac Oy, PerkinElmer). Up to 3 mL of sample solution were mixed with scintillation cocktail (Hionic Fluor™ or Ultima Gold™ LLT/XR, PerkinElmer) and measuring time was 3×30 minutes. Polyvials (HDPE, Zinsser Analytic) were used for liquid scintillation counting.

In addition, actinides/isotopes such as $^{235,238}U$, ^{237}Np, $^{238,239,240,241,242}Pu$, $^{241,243}Am$, and ^{244}Cm present in digestion liquors from Zircaloy-4 dissolution were also quantified using mass spectrometry. Measurements were performed using an ICP-SF-MS (inductively coupled plasma – sector field – mass spectrometer, ELEMENT XR™ ICP-MS, Thermo Scientific), which combines a dual mode secondary electron multiplier with a Faraday detector.

Samples were diluted to a volume of 5 mL using 2% HNO_3 for the measurements. Dilution ratios used in this study were 1:10, 1:100, and 1:1000. Separation techniques used in this study include extraction chromatography e.g. ^{55}Fe [2], extraction of ^{14}C by conversion into $^{14}CO_2$ and absorption in NaOH [3] as well as separation of Pu isotopes by liquid-liquid extraction [4].

Inventory calculations

The activation of the Zircaloy-4 plenum cladding, under investigation, was calculated using the Monte Carlo N-particle code (MCNP 2.7), which simulates the neutron flux of the subassembly and the CINDER program which calculates the activation [5, 6]. The ENDF/B-VII cross-section library was used for the simulation [7]. The burn-up simulation of the subassembly was optimized to five steps. At the end of the 1226 effective full power days in the reactor, a decay period of 9600 days was considered, which corresponds to the period between the end of the irradiation in 1989 and the measurement of the radionuclides in the samples, performed in this study.

The properties of the Zircaloy-4 plenum cladding such as geometrical shape, dimensions, alloying constituents and impurities, irradiation time, burn-up level, and linear power rate were accounted for in such a way that it included as much as possible all heterogeneity effects around the fuel rod segment. Thereby, the local neutron flux within the plenum could be simulated more accurately.

Inventory calculation of minor actinides and fission products present in the Zircaloy-4 plenum cladding is based on 3.5 ppm natural uranium impurity found in Zircaloy-4 [8]. The inventory of activation products is based on the respective precursor elements (e.g. ^{14}N, ^{54}Fe, ^{124}Sn) present as alloying constituent or impurity in Zircaloy-4.

Simulation of PWR Gösgen fuel assembly

Fuel rod SBS1108 was a test fuel rod and consisted of five segments containing nuclear fuel and two dummy segments to make it a full length PWR Gösgen fuel rod.
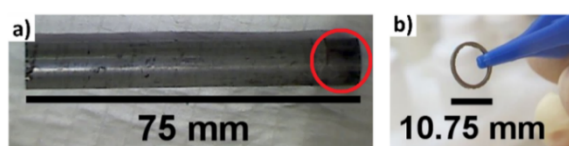

Fig. 1: Pictures of the irradiated plenum Zircaloy-4 cladding: (a) dimensions, the red circle indicates the welded end-plug; (b) a subsample prepared for a dissolution experiment.
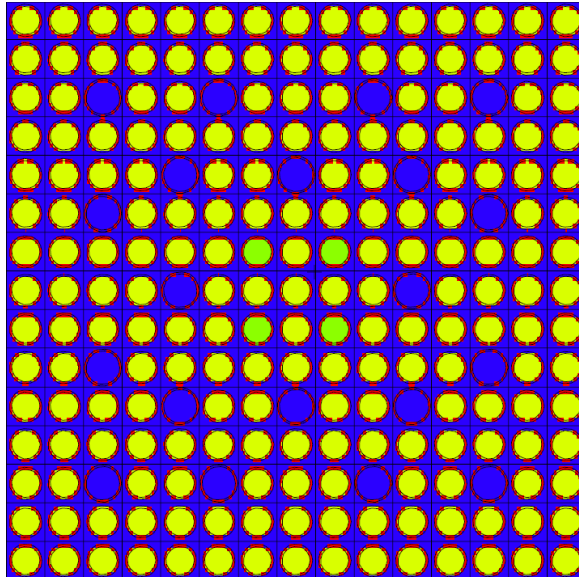
Fig. 2: *Simulated PWR Gösgen 15×15 fuel assembly. Consisting of 205 fuel rods (green and yellow pins) and 20 guide tubes (red circles). Water of primary cooling circuit is colored in blue.*

Segment N0204, where the investigated plenum was obtained from, was in the active zone of the reactor. The test fuel rod was inserted into a 15×15 PWR Gösgen fuel assembly and irradiated to the aforementioned burn-up conditions.

For the numerical simulation and in order to avoid statistical errors as well as due to symmetry reasons, four equivalent fuel rods were simulated in the center of the fuel assembly (green fuel pins in figure 2). The yellow fuel pins in figure 2 generate the power and thus the flux however, without getting activated. The 20 positions of the guide tubes of the fuel assembly are shown as red circles in figure 2. They are filled with water of the primary cooling circuit (dark blue color) since the control rods are considered fully extracted for the simulation.

Neutron flux was simulated in such a way, that average burn-up, effective full power days and average linear power rate were met.

Results and Discussion
In table 1 the experimentally determined inventories of various activation products are shown and compared to calculated inventories. A very good agreement between experimental and calculated data can be seen and the ratio experimental/calculated (E/C) is almost one.

In case of minor actinides, again a reasonable agreement of E/C ratios is seen (see table 2). However, the experimental values exceed the calculated by a factor of about 57 ± 9. The excess inventory of minor actinides is due to fission of uranium adherences on the inner surface of the plenum not taken into account in the neutronic calculations. These uranium remnants on the inner Zircaloy surface originate from loading of fuel pellets into the cladding tube during the fuel rod fabrication process.

Table 3 shows the comparison of experimentally obtained data with calculated values for (non-)volatile fission products. In case of the non-volatile fission product ^{154}Eu the E/C ratio of 56 ± 6 is very similar to that of the minor actinides (57 ± 9). In case of the volatile fission product ^{137}Cs, the experimental data exceeds the calculation by a factor of about 114 ± 11. An E/C ratio similar to that of the minor actinides or ^{154}Eu would be expected if ^{137}Cs originates only from fission of uranium present in the plenum (U impurity in Zircaloy + U remnants on inner surface). However, the massive excess of cesium found in the plenum is due to migration of cesium released from fuel pellets during reactor operation to the plenum ($T_{\text{pellets}} \gg T_{\text{plenum}}$).

Summary and conclusion
In general, good agreement between experimental and calculated inventories are seen for activation products. The experimental inventory of minor actinides as well as non-volatile fission products exceeds the calculated values by a factor of about 57 ± 9 due to nuclear fuel adhering on the inner plenum cladding surface.

Three sources contribute to the massive excess of the volatile fission product ^{137}Cs in the plenum:

1. Fission of U impurity present in Zircaloy-4 (3.5 ppm).
2. Fission of nuclear fuel/U remnants present on the inner surface of the plenum cladding.
3. Cs volatilized from subjacent fuel pellets during reactor operation.

Tab. 1: *Comparison of experimental and calculated inventories of various activation products.*

	^{14}C [Bq/g]	^{55}Fe [Bq/g]	^{125}Sb [Bq/g]
experimental	3.7(±0.4)×10^4	1.5(±0.1)×10^5	2.4(±0.2)×10^5
calculated	3.5×10^4	1.3×10^5	2.6×10^5
ratio (E/C)	1.06 ± 0.11	1.15 ± 0.12	0.92 ± 0.09

Tab. 2: *Comparison of experimental and calculated inventories of various minor actinides.*

	^{239}Pu [Bq/g]	^{242}Pu [Bq/g]	^{241}Am [Bq/g]	^{243}Am [Bq/g]	^{244}Cm [Bq/g]
experimental	1.2(±0.1)×10^4	2.3(±0.2)×10^2	1.7(±0.2)×10^5	3.3(±0.3)×10^3	3.1(±0.3)×10^5
calculated	2.4×10^2	4.1×10^0	3.6×10^3	4.9×10^1	4.7×10^3
ratio (E/C)	50 ± 5	56 ± 6	47 ± 5	67 ± 7	66 ± 7

Tab. 3: *Comparison of experimental and calculated inventories of various fission products.*

	^{154}Eu [Bq/g]	^{137}Cs [Bq/g]
experimental	$3.5(\pm0.3)\times10^4$	$3.3(\pm0.3)\times10^6$
calculated	6.3×10^2	2.9×10^4
ratio (E/C)	56 ± 6	114 ± 11

References

[1] Abschlussbericht der Kommission Lagerung hoch radioaktiver Abfallstoffe. K-Drs. 268, Berlin, Germany (2016).

[2] Grahek, Z., Rozmaric Macefat, M.: Extraction chromatographic separation of iron from complex liquid samples and the determination of ^{55}Fe. J. Radioanal. Nucl. Chem. **267**, 131 (2006).

[3] Herm, M.: Study on the effect of speciation on radionuclide mobilization – C-14 speciation in irradiated Zircaloy-4 cladding and nitrate/chloride interaction with An(III)/Ln(III). PhD thesis, Karlsruhe Institute of Technology (KIT) Karlsruhe (2015).

[4] Geckeis, H., Degering, D., Goertzen, A., Geyer, F. W., Dressler, P.: Langzeitsicherheit nuklearer Endlager: Radiochemische Analytik von Proben aus Brennstoffauslaugungsexperimenten. FZKA 5650, Forschungszentrum Karlsruhe (FZK), Karlsruhe, Germany (1995).

[5] Pelowitz, D. B.: MCNPX Users Manual Version 2.7.0. LA-CP-11-00438, Los Alamos National Laboratories (2011).

[6] Wilson, W. B., Cowell, S. T., England, T. R., Hayes, A. C., Moller, P.: A Manual for CINDER'90 Version 07.4 Codes and Data. LA-UR-07-8412, Los Alamos National Laboratory (2008).

[7] Chadwick, M. B., Herman, M., Oblozinsky, P., Dunn, M. E., Danon, Y., Kahler, A. C., Smith, D. L., Pritychenko, B., Arbanas, G., Arcilla, R., Brewer, R., Brown, D. A., Capote, R., Carlson, A. D., Cho, Y. S., Derrien, H., Guber, K., Hale, G. M., Hoblit, S., Holloway, S., Johnson, T. D., Kawano, T., Kiedrowski, B. C., Kim, H., Kunieda, S., Larson, N. M., Leal, L., Lestone, J. P., Little, R. C., McCutchan, E. A., MacFarlane, R. E., MacInnes, M., Mattoon, C. M., McKnight, R. D., Mughabghab, S. F., Nobre, G. P. A., Palmiotti, G., Palumbo, A., Pigni, M. T., Pronyaev, V. G., Sayer, R. O., Sonzogni, A. A., Summers, N. C., Talou, P., Thompson, I. J., Trkov, A., Vogt, R. L., van der Marck, S. C., Wallner, A., White, M. C., Wiarda, D., Young, P. G.: ENDF/B-VII.1 Nuclear Data for Science and Technology: Cross Sections, Covariances, Fission Product Yields and Decay Data. Nucl. Data Sheets **112**, 2887 (2011).

[8] Rudling, P., Strasser, A., Garzarolli, F.: Welding of Zirconium Alloys. A.N.T. International, (2007).

5.2 Microbial effects in the context of disposal of non-heat producing waste forms

B. Kienzler

Background

Numerous public funded research projects have been carried out in the past and most of the data and information gained in these projects have been published. However, these publications are distributed across different reports, journals, conferences, and sometimes gray literature. Therefore, it is not easy to get an overview especially for newcomers in the various fields. At INE, a series of summary reports on different research topics were prepared, which allow to get a quick overview on previous research efforts, skills and experiences.

Relevance of microbial effects for safety assessment of nuclear waste disposal

As an example, the microbial effects in the context of past German Safety Cases are presented [1]. Current Safety Assessment concepts either ignore microbial processes, or adopt a simplified approach. In December 2016, an article was published in the German journal "Spektrum der Wissenschaften" raising the question if microbes can live in a nuclear waste repository and if they could cause problems in the disposal safety or if they could increase disposal safety [2]. The article dealt with microbes under aerobic conditions prevailing in the Swedish Äspö underground research laboratory and in the former Königstein uranium mining facility in Germany. Other investigations on microbial effects in repositories were not reported.

A variety of anthropogenic polymers and organic wastes (including plastic, textile materials, paper and ion exchange materials among others) might be present in nuclear waste repositories especially considering LLW/ILW disposal. In addition, bitumen is/was used in several European countries as an encapsulant for nuclear waste and organic additives are present in cement used in the different barriers. These organic materials provide an energy and carbon source that has the potential to fuel microbiological processes in a repository. In Germany, the effects of microorganisms on disposal safety has not yet been profoundly considered [4].

The available information on organics in radioactive waste materials in German waste disposals are summarized including a literature overview on the typical degradation processes and some investigations performed in Germany. This overview considers mainly low-level or intermediate-level wastes, as they may contain organics which can be substrates for microorganisms, metallic components, which can undergo corrosion processes caused by microorganisms, and the presence of cemented waste forms, which increase the pH. The realization that microbes could exist in the environment of a nuclear waste repository posed a series of questions [4]:

1. Do microorganisms occur naturally in deep geological formations?
2. Can introduced microorganisms survive after repository closure? If the answer to these is yes,
3. What effect have the environmental conditions of a nuclear waste repository on resident or introduced microorganisms?
4. What effect will microorganisms have on a repository in terms of structural integrity of the engineered barriers, or radionuclide release and subsequent migration?

For bituminized waste forms microbial degradation studies were performed and the results are published specifically in regard to the Waste Isolation Pilot Plant (WIPP). A summary of some reports on microbial degradation of bitumen is given in this study. Other topics covered by this summary are attributed to the microbial degradation of paper, plastics and textiles which is an important issue for the Asse II safety case. For the Konrad low/intermediate level waste disposal site in Germany, studies on the microbial degradation of compacted mixed wastes were performed. These studies were not published but presented in the minutes of the panel dealing with low- and intermediate waste forms ("Arbeitskreis LAW/MAW-Produkte").

Further grey literature information is provided for microbial attack of cement, investigation of the microbiological populations in the cap rocks above the Gorleben salt dome as well as the analyses of microbial effects on mobilization of radionuclides. Considerations concerning the sulfate reduction processes are described, which were a topic of the preliminary safety analysis of the disposal in the Gorleben salt dome.

References

[1] B. Kienzler and Juliet S. Swanson, "Microbial Effects in the Context of Past German Safety Cases", KIT SR 7744, 2017.
[2] R. Knauer, "MIKROBEN: Gut leben im Endlager." *Spektrum der Wissenschaft,* 2016.
[3] J. West, "A review of progress in the geomicrobiology of radioactive waste disposal." *Radioactive Waste Management and Environmental Restoration,* Vol. 19, pp. 263-283, 1995.
[4] J. M. West and I. G. McKinley, "The Geomicrobiology of Nuclear Waste Disposal." *MRS Proceedings,* Vol. 26, 1983.

5.3 Colloid impact on radionuclide migration

M. Bouby, F. Geyer, U. Kaplan, S. Kraft, S. Kuschel, F. Quinto, Th. Rabung,, Th. Schäfer, D. Schild, M. Stoll

In co-operation with:

S. Brassines[a]

[a]ONDRAF/NIRAS, Belgian Agency for Radioactive Waste and Enriched Fissile materials, Geological Disposal, R&D, Avenue des Arts, 14, 1210 Bruxelles, Belgium

Introduction

Nanoscopic solids / compounds (from ~1 nm up to ~1 µm) of organic or inorganic nature are continuously generated by multiple physico-chemical processes (inter alia erosion, nucleation / precipitation, …) [1, 2]. These naturally occurring nano suspended material (organic detritus, iron and aluminosilicate oxi/hydroxide…), residues and transformation products of alteration and corrosion processes of the multi barrier system (i.e. waste matrix, geotechnical and geological barriers) may potentially contribute to the migration of radioactive waste material towards the biosphere [3-5]. To state if this is a parameter to be considered in a safety assessment and to define thus the boundary conditions for its relevance are our objective. What are the species to be considered (detection, identification, stability)? How do they interact with the radioelements (kinetics)? Under which conditions will they be able to migrate (interaction with various natural mineral surfaces)? Those are the key questions to be answered from the near-field to the far-field.

Laboratory and in-situ migration experiments are required which need the use and development of highly sensitive and sophisticated analytical techniques. The present work is conducted with the support and in close collaboration with Belgian and Swiss nuclear waste management agencies (ONDRAF / NIRAS, Belgium; NAGRA, Switzerland), in the framework of collaborative projects like the BMWi project KOLLORADO-e2 closely related to the international Colloid Formation and Migration (CFM) project performed in the Grimsel Test Site (GTS) in the frame of the investigation Phase VI.

Over the past, the following general statements have been formulated. The colloid-borne radionuclides (RNs) transport is more relevant in presence of advective flow, high pH, low salinity, large geochemical gradients, organics (Humic-/Fulvic acids) and strongly sorbing / incorporated RNs.

In clay formation, transport is diffusion limited. Only very small sized matter entities can circulate and migrate like for example the natural organic matter (NOM) known to be present in clay formations like the Belgian Boom Clay (BC), swiss Opalinus clay or French callovo-oxfordian. All those formations are presently under studies as potential deep geological repositories hosts.

In crystalline rock formation, the presence of open fractures results in advective transport of small matter entities, which might thus act as potential RN vectors. It is thus mandatory to understand and quantify the erosion processes occurring, to define the stability and the transport properties of the nanoparticles (NPs) present and to define the (ir)reversible character of their interactions (sorption/incorporation) with the radionuclides.

This year, in the present report we highlight some specific results related to these questions.

Characterization of NOM derived from different layers within the Boom Clay formation and their radionuclide interaction

In Belgium, deep geological disposal of nuclear waste is envisaged by ONDRAF/NIRAS, the Belgian Agency for Radioactive Waste and enriched Fissile Material, in poorly indurated clay formations like the Boom Clay (BC) or Ypresian clays (http://www.ondraf-plandechets.be). These host rocks have favourable intrinsic properties promoting the retention of radionuclides (low hydraulic conductivity, reducing redox capacity, slightly alkaline character, high specific surface area, cationic exchange capacity and plasticity). Organic material (OM) is nevertheless present in 1 to 5% wt in BC [6].

The conceptualisation of the role of OM in RN transport was found questionable by NEA (2003) during the review of the Belgian SAFIR 2 report (www.oecd-nea.org/rwm/reports/2003/nea4431-safir2.pdf). To refine the model on OM-facilitated transport, complementary results were necessary aiming at i) to determine the mobile size fraction of DOM (including geochemical evolution of the environment) and ii) to test the reversibility of RN complexation on DOM. More specifically, the research requested at KIT-INE aimed at 1) characterising the DOM size within BC pore waters currently present and to be expected within the lifespan of the repository (i.e., taking into account the possible geochemical evolution), 2) investigating the RN-DOM/kerogen interactions, 3) identifying the origin of DOM (tentatively interpreted as deriving from kerogen) and this, in complement of what has been done so far at the Belgian Nuclear Research Centre (SCK–CEN) [6-9] thanks to the use of other analytical techniques available at INE.

The pore waters and solid clay samples presentlyinvestigated comes from the HADES underground research laboratory (Mol, Belgium), see [6, 7] for details, and are representative of different
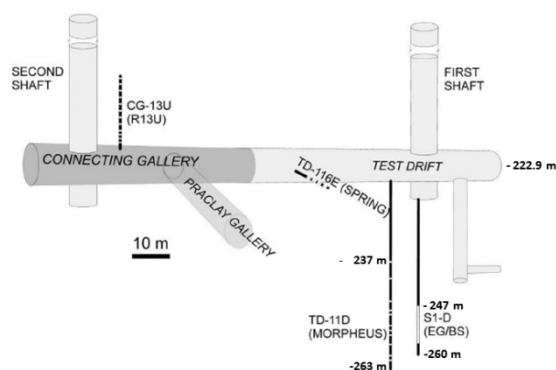
Fig. 1: Location of the piezometers considered in this work, in the HADES underground facility, dimensions are not to scale, see [6,7] for details. Depth in BSL (Below Surface Level).

horizons of the Boom Clay formation under present-day conditions (i.e., 15 mM NaHCO₃). BC pore waters (BCPW) samples were obtained from three piezometers: Spring (Filter 1), Morpheus (Filter –F4, -F8, -F12, F20) and EG/BS. Solid BC samples originated from the Praclay gallery (see Figure 1). It is assumed that the piezometers installed in the Boom formation around the HADES underground research facility collect mobile DOM. The use of various piezometers, installed vertically or horizontally, allows to evaluate the variation of the characteristics (size, functionalities, complexation properties) of the mobile DOM in the formation.

The Boom formation can be subdivided into four main stratigraphic units which are from the basis to the top: the Belsele-Waas Member, the Terhagen member, the Putte Member and the Boeretang Member. All the BCPW are sampled from filters located in the Putte Member except the Morpheus-F4 sample representative of the Terhagen Member. To note is the position of the filter Morpheus-F8, located at the level of the so-called Double Band (DB). The DB correspond to two thin, very silty layers at the bottom of the Putte Member which displays significantly higher hydraulic conductivity compared to the surrounding layers. The pore water collected via the EG/BS filter encompasses the silty DB and thus the water collected is influenced by the characteristics of the DB [6].

The aim of our work [10] was to complement what has been done so far at SCK-CEN [6,7,7a] thanks to the use of other analytical techniques available at INE like the asymmetric flow field-flow fractionation (AsFlFFF) coupled to UV-Vis./ICPMS for the size distribution and elemental content association determination, the time resolved laser induced fluorescence spectroscopy (TRLFS) for complexation studies or the use of X-ray photoelectron spectroscopy (XPS, see chapter 8.3 for the details on that study), Nuclear magnetic resonance (NMR) or Scanning Transmission X-Ray Microscopy (STXM) to identify the main DOM functionalities and its origin.

AsFlFFF/UV-Vis show that all BCPW samples contain small sized DOM consisting mainly of materials < 60 - 70 kDa (or < 11 - 12 nm, i.e.

hydrodynamic diameter (hyd. diam.)) while the dominating size fraction is centered at 0.9 - 1 kDa (or 1.5 – 1.6 nm hyd. diam.) by reference to a calibration of the system made with polystyrene sulfonate salt standard (PSS). Those results are in agreement with our SEC/UV-Vis. measurements and as well with the results obtained at SCK-CEN by SEC-UV-Vis. even if different chromatographic columns were used [8]. The OM extracted/leached from solid clay samples consist of several size fractions, the dominant one is > 100 kDa and represents 75 % of the detected part. The size of the smallest OM fraction extracted/leached is again at 0.9 kDa (~ 1.5 nm hyd. diam.). Again, these results are in line with those obtained by SCK-CEN [8]. UV-Vis spectrophotometry (E3/E4 ratio determination) and EEM (fluorescence yield) reveal the dominance of fulvic acid-like material or a mixed humic and fulvic acid type in the BCPW from the piezometers Spring and Morpheus-F4, -F12 and -F20. In the bulk BCPW from the piezometer EGBS and Morpheus-F8, the dominance of a humic acid-like material (E3/E4 ratio < 3.3) is shown, while after size fractionation, fulvic acid type material is evidenced in addition. Durce et al. [8] already indicated that the mobile DOM concentration in the BCPW is scattered over the Boom formation. While it remains constant at the same level (as seen from the analysis of the BCPW from the various filters of the horizontal Spring piezometer, 7 m covered), it varies widely along the BC layer from 43 to 270 mgC.L⁻¹ [8]. The highest value is reported for the BCPW sampled close to the silty DB (i.e., Morpheus-F8 and EG/BS). The present results, as already mentioned by Durce et al., suggest that filtration occurs (promoted by clay minerals) which might preferentially retain larger organic species against smaller ones which are the most mobile ones. This is evidenced from the analysis of the Morpheus-F4, -F20 and Spring BCPW presenting all a thinner (UV-Visible) OM size distribution (AsFlFFF-UV-Vis data) and a more fulvic-acid-like character (UV-Vis/ EEM data). In comparison, the OM size distribution are broader and present a more humic-acid-like character for the BCPW originating from the EG/BS, Morpheus-F8 and –F12 piezometers, located close to silty layers, as might be expected from layers presenting higher porosity and permeability and thus less filtration.

The present data support the previous ones [6-8] and might be taken as an indication that the exchange of pore water and of DOM between different layers seems to be rather limited.

Investigations have been carried out to get more insight into the effect of IS on DOM concentration, conformation and size. The influence of NaCl, CaCl₂ and MgCl₂ content has been examined by SEC/UV-Vis. for both institutes [9]. Two main mechanisms which are OM-size dependent, can be identified the compaction /decomposition and the aggregation of the DOM molecules. The largest OM size fractions tend to coagulate under high IS with a more pronounced effect of the divalent cations (Mg²⁺ and Ca²⁺) compared to the monovalent cation (Na⁺). On the opposite, small OM

size fraction tends to become even smaller, a process which calls for further investigations.

The distribution of the inorganic elements between the different colloidal size fractions give a first hint on their potential mobility. A consistent picture is obtained from AsFlFFF-ICPMS and UF-ICPMS results. The alkaline elements (Mg-Ba) and the transition metals (Mn-Hf) recovered are mainly found in the smaller size fractions < 3 nm. The light REE (Sc, La, Ce, Pr, Nd, Pm, Sm, Eu, and Gd) are enriched in the largest size fraction, 3-15 nm, whereas the heavy REE (Y, Tb, Dy, Ho, Er, Tm, Yb, and Lu) are enriched in the smaller size fractions < 3 nm. For the actinides presently analyzed (Th, U) the proportion in the smaller size fraction < 3 nm decreases for decreasing DOC content in favor of the 3-15 nm fraction, the nature of which remains to be identified.

For a comparison with the natural inorganic element distribution, complexation properties have been examined by using the time resolved laser induced fluorescence spectroscopy (TRLFS) applied to Cm(III) ions as representative of trivalent actinides. The two pore waters investigated (Morpheus-F20 and EG/BS) contain two types of strongly complexing ligands: DOM and carbonates. Indirect excitation measurements allow to elucidate the Cm(III) speciation. It is concluded that the Cm(III)-DOM complexes are the dominant species and no ternary complexes (e.g. Cm(III)-carbonato-DOM) are formed. In addition, the binding properties of specific DOM size fractions isolated by ultrafiltration for one of the BCPW investigated (EG/BS) are very similar. Nevertheless, in presence of the complete OM size distribution, the Cm(III) repartition is not homogenous but size fraction dependent, in-line with AsFlFFF/ and UF/ICPMS. This first investigations have now to be completed with reversibility studies.

Finally, to state on the DOM origin, preliminary STXM investigations have been carried out. They showed a good correlation between the BCPW DOM and the solid organic matter (SOM). This agree with previous results [8] showing that the amount of leachable OM is controlled by the TOC of the solid which suggests that the SOM is the source of leachable OM and most likely of mobile DOM. Kerogen is thought to be involved in the production of the leachable OM pool [8]. All our results are compiled in a report which will be available soon [10].

Experiments on compacted bentonite erosion and colloid formation at the bentonite pore water interface.

The presence of nanoparticles/colloids might be a key in Safety Assessment of a high level nuclear waste repository in crystalline rock. The mechanisms of bentonite erosion from the compacted bentonite barrier leading to the generation of (colloidal) particles detaching from the clay have to be deeply investigated and understood for two main reasons: 1) the long term integrity of the clay barrier could be compromised if a significant clay loss occurs; 2) the clay colloids may play a role in the radionuclide (RN) migration.

Erosion processes have been simulated under dynamic but rather stagnant flow conditions simulating repository post-closure conditions. To better understand the FEBEX [12] and MX-80 [13] bentonite erosion behavior, variation of the compaction density, chemistry of the contact water (ionic strength (IS), pH value, cation composition), contact surface and angle, and type of bentonite (raw material or homo-ionic Na/Ca form) was performed. Results were compared with modeling approaches.

Our data are consistent with those obtained in parallel by other institutes and summarized notably at the end of Deliverable D2.11 of the European FP7 CP-Belbar project [14]. The main conclusions are presented in the following with some of our more specific results.

The erosion of bentonite depends first on its hydration state which should be high enough to allow the gel formation and on its physico-chemical characteristics (its main composition, if trace minerals are present, the quantity and the type of smectite). The swelling pressure is the driving force causing the gel intruding the fracture and/or the pores of the rock. The water flow (in dispersive systems) and thus the chemical forces via the groundwater chemistry are the driving forces for (clay) particle detachment. Nevertheless even if the water can reach and hydrate the bentonite, the particles cannot move and thus no mass loss will be possible without an appropriate transport path. The dimensions of the pore sizes/fractures have thus to be considered in the normalization processes of the erosion data.

The conditions that favor colloid stability favor the bentonite erosion but a threshold electrolyte concentration exists above which erosion does not occur. Accordingly erosion only takes place under highly dilute solution conditions. The maximum mass loss is measured under dynamic conditions for the Na-exchanged bentonite and deionized water. This value can thus be considered as the upper limit for performance assessment. The mass loss rates are dependent of the ionic strength and are typically about one order of magnitude lower for the as-received clay than for the Na-exchanged one. Contrary to what is generally admitted, even if considerably lower than for the raw or Na-clay (~ resp.1 or 2 orders of magnitude), in our work, the detection and quantification of intrinsic Th as clay colloid fingerprint allowed us to calculate an erosion rate for the Ca-clay [13].

Salt/mineral dissolution from the natural clay is observed accompanied by cation exchange, like Ca [13,14]. This long term progressive Ca enrichment might inhibit the erosion of the gel as it was shown that 1 mM of Ca in solution is enough to hinder the erosion process. This has thus to be considered in modeling exercise. Nevertheless, in the presence of a significant amount of Na (above 20 %), the Na-Ca-exchanged-clay dispersion remains still possible [13,14] and rather similar to the one observed for a pure Na-exchanged clay system.

Clay colloid dispersions collected during experiments remain stable for months. As tested for Eu(III), they can

strongly bind cations with respective logK$_d$ values equal to ~ 4-5 [13]. Therefore they need to be considered as potential RN carriers.

Studies on clay colloid stability, colloid / mineral surface interaction and RN sorption

In complement to the bentonite erosion activities, a systematic clay colloid stability study has been started in the frame of the European FP7 CP-Belbar project to complement the knowledge acquired so far. While numerous studies have been conducted over a rather short time period (fast coagulation) only few are reported over period of more than 1 year [15]. In that case, agglomeration has been reported even under geochemical conditions where colloids are supposed to be highly stabilized. To confirm this observation, a systematic study has been initiated in the frame of the BelBar project. Clay colloid suspensions have been prepared at different concentrations, at two pHs (~ 6 and ~ 8.4), in various electrolytes at fixed ionic strength (10^{-3}M), in presence or not of organic matter (i.e. fulvic acids (FA)). After 4,5 years aging, the samples are now under investigations.

Experiments devoted to the study of the colloid interaction with mineral surface [16,17] are as well carried on. Recently the impact on colloid retention of the residence time, of the gravity, of the collector surface roughness and of the fracture orientation has been tested in an artificial fracture using atomic force microscopy (AFM). The experiments are modeled using COMSOL Multiphysics® (2-D numerical simulations). Large colloids (polystyrene particles, 1 μm Ø) undergo sedimentation and deposition on the surface. Contrariwise, the smaller colloids (polystyrene, 25 nm Ø) does not sediment but are influenced by surface inhomogeneities such as surface roughness (see [16] for details). Under similar physico-chemical conditions (setup and elution conditions), the transport of Na-illite clay colloids have been investigated by using the very sensitive Laser-Induced Breakdown Detection (LIBD) technique. Despite their higher solid density, the Na-illite colloids present a higher mobility compared to the polystyrene spheres without significant impact of surface roughness or gravity. In conclusion, polystyrene spheres are no ideal analogue to predict the mobility and transport behavior of a polydisperse clay colloid suspension [17].

Finally RNs sorption and reversibility studies are still on-going (PhD work of F. Rinderknecht [12], Kollorado-e and BelBar projects), under realistic conditions (pore water and glacial melt water) and long contact time periods (more than 5 years). In addition to those laboratory studies, in-situ measurements are performed at the GTS [12] and the application of Accelerator Mass Spectrometry (AMS) [18] is a very efficient tool (see chapter 8.5). AMS does not provide direct information on the association of actinides with colloids and neither on their speciation, however due to its extreme sensitivity, it has enabled to study the long term release and retention of the actinide tracers within the system of groundwater – bentonite colloids – fault gouge minerals at the GTS [18,19].

References

[1] Honeyman, B.D., *Nature*, **397**, 23-24, (1999)
[2] Stumm, W. et al., Aquatic Chemistry: chemical equilibria and rates in natural waters, 3rd. Ed., John Wiley & Sons, USA, 1996.
[3] Kim, J.I., *Radiochim. Acta*, **52/53**, 71-81 (1991)
[4] Geckeis, H. Geological Society Special Publication, **236**, 529-543, 2004
[5] Schäfer, Th. et al., *Appl.Geochem*, **27**, 390-403, (2012)
[6] De Craen et al., Geochemistry of BC pore water at the mol site. SCK.CEN-ER206, Scientific report, (2004)
[7] Bruggeman, C. et al., Boom clay natural organic matter. External report 2011, SCK.CEN-ER206, External report, 2012
[8] Durce, D. et al. App. Geochem. **63**, 169-181, (2015)
[9] Durce, D. et al., J. Cont. Hydrology, **185-186**, 14-27, (2016)
[10] Kaplan, U. et al. KIT-Report, 20004085, under prep., 2018
[11] Huber, F. et al. Project Kollorado-e final report, DOI: 10.5445/IR/1000059756
[12] Rinderknecht, F. PhD Thesis, (2017) https://publikationen.bibliothek.kit.edu/1000076660
[13] Bouby, M. et al., under prep., (2018)
[14] Missana, T. Deliverable D2.11, BelBar Project, 01/2016
[15] Bouby, M. et al., *Geochim. Cosmochim. Acta*, **75**, 3866-3880, (2011)
[16] Stoll, M. et al., *J. Coll. Int. Sci*, **475**, 171-183, (2016)
[17] Stoll, M. et al. *Coll. Surf. A: Physicochem. Eng. Aspects*, **529**, 222-230, (2017)
[18] Quinto, F. et al., *Anal. Chem*, **87**, 5766-5773, (2015)
[19] Quinto, F. et al.; *Anal. Chem,* **89**, 7182-7189, (2017)

5.4 Diffusion

M. Fuss, C. Joseph, S. Moisei-Rabung, V. Montoya, M. Trumm, T. Schäfer

In co-operation with:

L. Delavernhe[a], K. Emmerich[a], M. Glaus[b], T. Kupcik[c], R. Schuhmann[a]

[a] Competence Center for Material Moisture (CMM), Karlsruhe Institute of Technology, Eggenstein-Leopoldshafen, Germany; [b] Laboratory for Waste Management, Paul Scherrer Institute, Villigen PSI, Switzerland; [c] Hessian Ministry of the Environment, Climate Protection, Agriculture and Consumer Protection, Wiesbaden, Germany

Introduction

In the context of the safe disposal of nuclear waste in deep geological formations, the scenario of the migration of waste-released radionuclides through the multiple barrier system is an important research topic for safety assessment. Potential geotechnical or geological barriers, which should hinder or retard the transport, can consist of compacted porous minerals, sedimentary rocks, or manufactured concretes. In such materials in the absence of fractures and cracks, molecular diffusion is the main transport process for contaminants.

At INE, laboratory experiments with radiotracers and compacted clay minerals, natural clay rock, sea sand, and cement mixtures are conducted. One of the main objectives is the determination of diffusion parameters of repository-relevant radionuclides under a wide range of conditions. In particular we study experimentally the change of transport parameters due to chemical reactions and the fundamental processes underlying the interaction of ions with the porous material during diffusion. For instance, the description of the influence of secondary mineral formation on the diffusion process of neutral and ionic species or the accessibility of interlayer space for anions during the diffusion process remain open questions.

Multitracer (HTO, ^{36}Cl, ^{85}Sr) diffusion in compacted natural and reduced-charge dioctahedral smectites

Internationally, a few reference bentonites are studied for their function as backfill material in nuclear waste repositories. Smectite represents their main mineral fraction. It is characterized by a three layer structure. One octahedral sheet (O), composed of O^{2-} or OH^- octahedra with mostly Al^{3+} as central cation, is enclosed by two tetrahedral (T) mostly SiO_4^{4-} sheets (TOT). The space between two T sheets is called interlayer. Resulting from isomorphic substitutions within the O and T sheets, e.g., Al^{3+} by Mg^{2+}, the negative charge of the layers is in excess. This charge is compensated by weakly bound cations located in the interlayers, which can be exchanged by other cations of the surrounding solution (cation exchange capacity, CEC).

The focus of the present study was to investigate the influence of layer charge and particle size distribution of smectites on the diffusion behavior of neutral, positively, and negatively charged species. In addition, the study was aimed to clarify to which extent interlayer and interparticle porosities participate in the diffusion process.

Purified Na-saturated < 0.2 μm-fractions of dioctahedral smectites separated from four different bulk bentonites were investigated. Their characteristics are listed in table 1.

Tab. 1: *Characteristics of the smectites and their reduced-charge material (RCM) analogues investigated in this study [1]. (Sm: smectite; Ms: muscovite; I(9%)-Sm: interstratified illite(9%)-smectite; Qz: quartz; f.u.: formula units)*

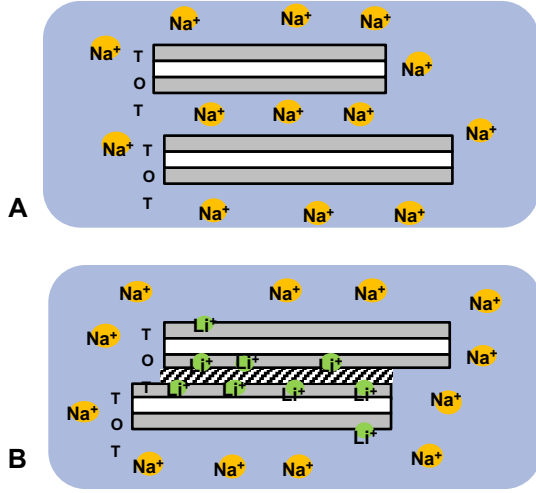|	Bentonite	Calcigel® (Bavaria, Germany)	FEBEX (Almeria, Spain)	Bentonite P	Volclay® (Wyoming, USA)
Smec-tites	Mineralogical composition	95% Sm 5% Ms	100% I(9%)-Sm	100% Sm	98% Sm 2% Qz
	Layer charge [eq. per f.u.]	0.30 ± 0.01	0.37 ± 0.01	0.32 ± 0.01	0.26 ± 0.01
	CEC at pH 5.5 [cmol(+) kg^{-1}]	85 ± 2	100 ± 2	110 ± 2	85 ± 2
	Equivalent diameter [nm]	118 ± 50	107 ± 50	101 ± 50	241 ± 100
RCM	CEC at pH 5.5 [cmol(+) kg^{-1}]	15 ± 2	15 ± 2	9 ± 2	7 ± 2
	Layers per stack	7 ± 1	7 ± 1	7 ± 1	14 ± 3

Fig. 1: *Schematic structure of Na-saturated smectites (A) and the reduced-charge material (B).*

Additionally, from each of these smectite fractions a Na-saturated reduced-charge material (RCM) was prepared using the Hofmann-Klemen effect [2]. The samples were Li-saturated and heated at 300°C for 24 h. Their interlayers collapse and are no longer accessible for water (Figure 1). More details about the samples can be found in [1].

With these materials through- and out-diffusion experiments were performed with HTO, $^{36}Cl^-$, and $^{85}Sr^{2+}$ as tracers. Each smectite or RCM was compacted in PEEK diffusion cells to a dry density, ρ_d, of about 1700 kg m^{-3}, a thickness of about 1 cm, and a diameter of about 2.54 cm. Each cell was connected to a high (HCR) and a low concentration reservoir (LCR) containing 0.3 mol/L NaClO$_4$ at pH 5.5 ± 0.5. To each HCR, the tracers [HTO] ≈ $9.0 \cdot 10^{-9}$ mol/L, [$^{36}Cl^-$] ≈ $2.3 \cdot 10^{-5}$ mol/L, and [$^{85}Sr^{2+}$] ≈ $3.4 \cdot 10^{-12}$ mol/L were added. Each LCR was initially tracer-free. The full setup is described in detail in literature [3].

At distinct time steps, the LCR was exchanged and the activity and diffusive flux, J [mol m^{-2} s^{-1}], were determined. Based on the experimental data and Fick's laws, a 1-dimensional single porosity model was set up using COMSOL Multiphysics® [4]. Fick's first law describes the diffusion process in porous media as follows:

$$J = -D_e \cdot \frac{\partial c}{\partial x} \quad (1)$$

where D_e [m^2 s^{-1}] is the effective diffusion coefficient, c [mol m^{-3}] is the tracer concentration in the mobile phase, and x [m] is the spatial coordinate. D_e is correlated to the diffusion coefficient of a species in water, D_w [m^2 s^{-1}], by:

$$D_e = \frac{\varepsilon_{acc}}{G} \cdot D_w \quad (2)$$

with ε_{acc} [–] as accessible porosity and G [–] as pore network geometric factor considering the tortuosity and constrictivity of the diffusion path. In addition, the diffusion is influenced by the potential sorption of the diffusing species on the material surface expressed here as sorption distribution coefficient, R_d [m^3 kg^{-1}].

This diffusion retarding effect is considered in the rock capacity factor α [–].

$$\alpha = \varepsilon_{acc} + \rho_d \cdot R_d \quad (3)$$

For non-sorbing tracers such as HTO with $R_d = 0$, it is assumed that α is equal to ε_{acc}. The inclusion of α in Fick's law leads to the apparent diffusion coefficient D_a [m^2 s^{-1}]:

$$D_a = \frac{D_e}{\alpha} \quad (4)$$

Fick's second law, where the change of concentration with time, t [s], is considered, is then expressed by:

$$\frac{\partial c}{\partial t} = D_a \cdot \frac{\partial^2 c}{\partial x^2} \quad (5)$$

Based on the model set up in COMSOL and coupled with the parameter estimation program PEST [5], diffusion and sorption parameters (D_e; ε_{acc}; R_d) were determined for each tracer in each material. For comparison of R_d values, batch sorption experiments were conducted with $^{85}Sr^{2+}$ (solid-to-liquid ratio = 40 g L^{-1}) under the same conditions as used in the diffusion experiment.

The obtained D_e and ε_{acc} values of HTO and $^{36}Cl^-$ are depicted in Figure 2. The data points from the Volclay® bentonite represent outliers. In addition, there was no diffusion but advection observed in the experiment with the RCM of Volclay®. This can be attributed to the relatively large particle size and large G (not shown) of Volclay® compared to the other bentonites. The widespread use of Volclay® as reference material could lead to some uncertainties.

The data for the HTO diffusion through the bentonites is in very good agreement with literature values obtained for Na-montmorillonite [6]. It can be seen, that the D_e values of RCM are slightly higher than the ones of smectites. It seems, that the diffusive flux of HTO through interlayer space is slower than through interparticle space. This is in agreement with observations described in [7,8]. However, in contrast to the D_e values of RCM the D_e values of illite are even higher. Although structurally, illite does not differ much from RCM. Illite also has a TOT structure, is
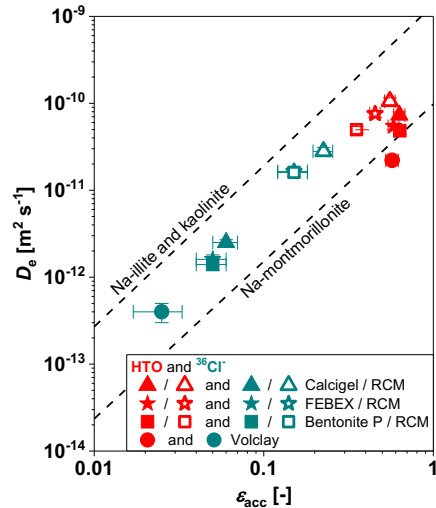

Fig. 2: *D_e as a function of ε_{acc} for HTO and $^{36}Cl^-$. (Reference lines taken from [6].)*

non-expandable, and has a low CEC. Its interlayers are occupied with K^+ ions which lost their bound water. Compared to smectite, the layer charge of illite is higher (~ 0.75 eq./f.u.).

In the case of the $^{36}Cl^-$ diffusion, the influence of interlayers is expressed significantly. For Na-bentonite, it is known, that the fraction of interlayer nanopores amounts to 0.96 ± 0.04 at a dry density of 1700 kg m^3 [9]. There should be only space for two water layers in each interlayer [10]. Recently, [11] showed using molecular dynamics simulations that under these conditions $^{36}Cl^-$ has no access to the interlayers. These findings are reflected by the diffusion experiments of this study, $\varepsilon_{acc}(^{36}Cl^-)$ of smectites decreased by 91-96% compared to $\varepsilon_{acc}(HTO)$ of smectites. In the case of the RCM, due to the blocking of interlayers, $\varepsilon_{acc}(^{36}Cl^-)$ is significantly larger (~ 0.2) than $\varepsilon_{acc}(^{36}Cl^-)$ of smectites (~ 0.05). However, compared to $\varepsilon_{acc}(HTO)$ of RCM, a reduction by 60% was observed showing that also after the blocking of the interlayers, the electrical double layers on the edge and basal surfaces of the solids exclude the diffusing anion.

The results of the $^{85}Sr^{2+}$ diffusion and batch sorption experiments are summarized in Table 2. In the model, it was assumed, that $\varepsilon_{acc}(HTO)$ equals $\varepsilon_{acc}(^{85}Sr^{2+})$. The D_a values for each smectite and its respective RCM are comparable. That means, although there is a stronger sorption of $^{85}Sr^{2+}$ onto smectites than onto RCM, and consequently, a more pronounced retardation, there is also a faster diffusive flux of the cation through the interlayers of smectite than through the interparticle space of RCM. Both effects compensate each other leading to a similar tracer breakthrough. Using the formula given in [12], the Sr surface mobility, μ_s [−], was calculated. For the smectites an average value of 0.38 ± 0.13 and for the RCM samples a value of 0.30 ± 0.06 was obtained. Both values are in reasonable good agreement with the reference value of 0.39 ± 0.02 [12]. This shows that the Sr surface mobility is not influenced by the presence of interlayers. The surface properties remain intact in the RCM samples.

The comparison of the R_d values shows that the data obtained by diffusion and batch sorption experiments are consistent, except for Volclay®. Here, differences in the accessible sites could be the reason. It is known, that under the present experimental conditions, the main Sr uptake mechanism is cation exchange. The

lower the CEC the lower the R_d value (cf. Table 1 and Table 2). Based on the reaction for the cation exchange:

$$2\ Na\text{-clay} + Sr^{2+} \rightleftharpoons Sr\text{-clay} + 2\ Na^+ \qquad (6)$$
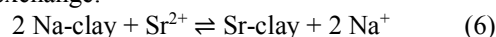
as well as the CEC and R_d values, the selectivity coefficients $^{Sr}_{Na}K_{SEL}$ could be calculated for each material investigated.

$$^{Sr}_{Na}K_{SEL} = \frac{2 \cdot R_d}{CEC} \cdot [Na^+]^2 \quad (7)$$

The mean log $^{Sr}_{Na}K_{SEL}$ value for the smectites amounted to 0.7 ± 0.1, which is comparable to the literature value for FEBEX of 0.66 ± 0.06 [13]. For RCM a value of 1.1 ± 0.1 was obtained, which is in agreement with the value of illite with 1.4 ± 0.4 [13].

At next, the total and anion porosity profiles will be determined experimentally following the procedure described in [14]. Concerning modelling, a new approach will be tested which considers the surface charge of the materials.

References

[1] L. Delavernhe et al., *Colloids Surf., A*, **481**, 591-599, (2015).

[2] U. Hofmann and R. Klemen, *Z. Anorg. Chem.*, **262**, 95-99, (1950).

[3] L.R. Van Loon et al., *Appl. Geochem.*, **22**, 11, 2536-2552, (2007).

[4] *COMSOL Multiphysics®*, **5.2a**, COMSOL AB, Stockholm, (2016).

[5] *PEST*, J. Doherty, Brisbane, (2003).

[6] M.A. Glaus et al., *Geochim. Cosmochim. Acta*, **74**, 7, 1999-2010, (2010).

[7] R.M. Tinnacher et al., *Geochim. Cosmochim. Acta*, **177**, 130-149, (2016).

[8] F. González Sánchez et al., *J. Chem. Phys.*, **129**, 17 (174706), 1-11, (2008).

[9] I.C. Bourg et al., *Clays Clay Miner.*, **54**, 3, 363-374, (2006).

[10] T. Kozaki et al., *Nucl. Technol.*, **121**, 1, 63-69, (1998).

[11] C. Tournassat et al., *Clays Clay Miner.*, **64**, 4, 374-388, (2016).

[12] T. Gimmi and G. Kosakowski, *Environ. Sci. Technol.*, **45**, 4, 1443-1449, (2011).

[13] T. Missana et al., *Phys. Chem. Earth.*, **33**, S156-S162, (2008).

[14] M.A. Glaus et al., *J. Contam. Hydrol.*, **123**, 1-2, 1-10, (2011).

Tab. 2: *Best-fit parameter values for $^{85}Sr^{2+}$ from diffusion experiments and R_d values from batch sorption experiments.*

	Bentonite	D_e [10^{-11} m^2 s^{-1}]	R_d diffusion [10^{-2} m^3 kg^{-1}]	R_d sorption [10^{-2} m^3 kg^{-1}]	D_a [10^{-11} m^2 s^{-1}]
Smectites	Calcigel®	29 ± 2	2.5 ± 0.3	2.2 ± 0.1	0.7 ± 0.3
	FEBEX	36 ± 4	4.0 ± 0.3	3.5 ± 0.2	0.5 ± 0.1
	Bentonite P	54 ± 4	4.3 ± 0.3	3.8 ± 0.1	0.7 ± 0.2
	Volclay®	52 ± 8	7 ± 1	1.8 ± 0.1	0.4 ± 0.2
RCM	Calcigel®	23 ± 4	0.88 ± 0.08	0.80 ± 0.01	1.5 ± 0.5
	FEBEX	11 ± 1	0.86 ± 0.08	0.80 ± 0.01	0.7 ± 0.2
	Bentonite P	5 ± 1	0.58 ± 0.04	not determined	0.5 ± 0.1

5.5 Geochemical modeling and modeling of coupled processes

V. Montoya, N. Ait Mouheb, T. Schäfer

In co-operation with:

B. Baeyens[a], M.A. Glaus[a], T. Kupcik[c], M. Marques Fernandes[a], L. Van Laer[b], C. Bruggeman[b], N. Maes[b]
[a]Paul Scherrer Institut (PSI-LES), Villigen, Switzerland; [b]SCK CEN, Mol, Belgium; [c]KIT-INE, Karlsruhe, Germany

Introduction

At INE, the main research activities in the field of geochemical modeling and modeling of coupled processes are focused on development and application of conceptual and numerical models on:

- Radionuclides and contaminants migration in porous and fractured media in repository and laboratory scale.

- Temporal hydro-geochemical evolution of the multi-barrier system of a repository, i.e. alteration / degradation of (geo-)technical and geological barriers (waste form dissolution, Fe-canister corrosion, interactions at interfaces of backfilling material / concrete / adjacent host rock).

The understanding of the evolution of a repository system over long geological time scales requires a detailed knowledge of a series of highly complex coupled processes. By using small-scale laboratory experiments, under well-defined boundary conditions, numerical modelling can provide information to help in the repository design and predict future radionuclide migration in case of an accident.

Research activities during 2017 have been mainly focused on coupled diffusive transport processes with different chemical reactions solved with

Fig. 1. *3D representation of the diffusion cell used to study processes between clay / low pH cement materials. [HTO]$_0$ = 1x10^{-6} M. Model implemented in COMSOL.*

1000 years

Fig. 2. *2D Evolution of pH vs time in the interface bentonite/cement. Model implemented in the interface COMSOL-PHREEQC (iCP [1])*

thermodynamic and kinetics laws (i.e. sorption, precipitation/dissolution and aqueous speciation).

Presently there are different systems under study in a laboratory scale were reactive transport modelling is applied:

- Diffusion of HTO, Cl-36 and Sr-85 in compacted natural and reduced-charge dioctahedral smectites (see chapter 5.4).

- Diffusion in the interface low pH cement / clay system (EU Horizon2020 CEBAMA project (www.cebama.eu) and study of the change in the pore structure where Naila Ait Mouheb is performing her Ph.D. thesis (see Figure 1)

- Diffusion and sorption of Sr, Co and Zn in compacted illite.

This kind of calculations in the laboratory scale can provide the scientific basis for the safety assessment of various repository design options. Additionally, within the ENTRIA project (www.entria.de) reactive transport modelling tools have also been used to predict the geochemical evolution in the near field of a generic repository in a clay formation (see Figure 2).

The reactive transport simulations described previously, have been conducted with different codes depending on the studied system: PHREEQC v. 3 [2] and COMSOL Multiphysics ® 5.2 [3]. Additionally, the interface iCP [1] has been used and tested taking advantage that KIT-INE is part of the Consortium where this tool has been developed. One of the advantages of using these codes is that all of them are in continuous development. This interface provides a numerical platform that can efficiently simulate a wide number of multiphysics problems coupled to geochemistry (i.e. liquid flow, solute and heat transport, elastic and plastic mechanical deformations and geochemical reactions).

In the following subsection is explained in more detail one of the recent results obtained in collaboration with PSI (Switzerland) and SCK CEN (Belgium) which has been recently published [4].

Sorption of Sr, Co and Zn on illite: Batch experiments and modelling including Co in-diffusion measurements on compacted samples.

Argillaceous formations are investigated in several European countries as potential host rocks for the deep geological disposal of high-level radioactive waste.
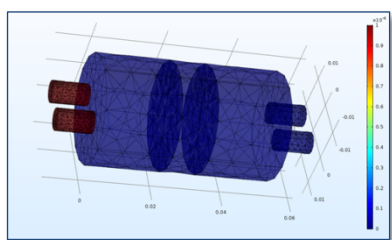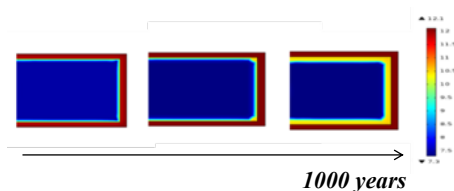
Due to their remarkable chemical and physical properties (i.e. low hydraulic conductivity, high radionuclide retention, high swelling capacity, low lateral variability and permeability) transport processes in such media are largely controlled by diffusion and characterized by strong retardation for many elements. Is for this reason that an adequate mechanistic understanding of transport and sorption processes of radiotracers under a wide range of geochemical conditions is thus required to reliably predict the long-term evolution of a deep-geological repository and the dose rates emanated from it.

Various experiments and modelling works described in the literature [5, 6, 7] have shown that alkali and earth alkaline cations bound to the surface by cation exchange processes may retain a certain mobility describing higher diffusive fluxes than anions and neutral species under the same conditions. This behavior has been attributed to an enrichment of these cations at the planar sites of the clays. Whether this behavior can also be observed for cations interacting with edge surface sites by specific sorption, e.g. divalent transition metals such as Co or Zn, is a remaining open question. In addition sorption models of strongly sorbing species such as transition metals and lanthanides/actinides are based on experimental measurements of Rd values by batch sorption
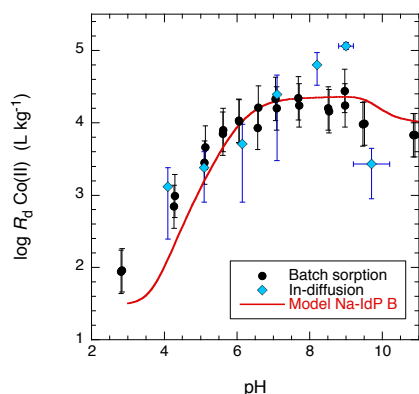

Fig. 3. *Comparison of sorption values measured by batch sorption and in-diffusion experiments using ^{57}Co tracer as a function of pH (I = 0.1 M NaClO$_4$).*
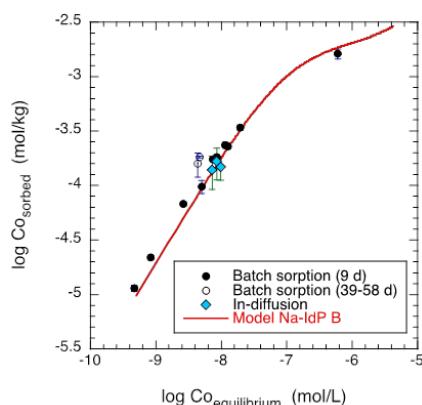

Fig. 4. *Comparison of sorption values measured by batch sorption and in-diffusion experiments using ^{57}Co tracer as a function of stable Co concentration at pH = 7.1 (I = 0.1 M NaClO$_4$).*

technique restricted to dilute homogeneous clay suspensions because of experimental constraints. Thus, it is also not clear if the sorption models obtained in diluted system are transferable to compact clay media studies.

It is for this reason that the present study aims to provide the sorption equilibrium data for three different divalent metal cations, namely Sr, Co and Zn on the single mineral phase Na-illite and to validate the applicability of sorption data parametrized by experiments obtained in dilute clay suspensions to compacted clays. Additionally, important gaps in the literature data related to possible ambiguities in surface speciation are filled with the present measurements. The dependence of solid-liquid distribution ratios (R$_d$ values) on pH at trace metal conditions (sorption edges) and on the metal ion concentration (sorption isotherms) was determined in dilute suspensions of homo-ionic Na-illite under controlled N$_2$ atmosphere. The experimental results were modelled using the 2 Site Protolysis Non Electrostatic Surface Complexation and Cation Exchange (2SPNE SC/CE) sorption model [8].

For Sr, the experimental data showed a strong ionic strength dependency, and rather weak pH dependence in the range 3 to 11. The data were modelled with cation exchange reactions, taking into account competition with H$^+$, K$^+$, Ca^{2+}, Mg^{2+} and Al^{3+}. A surface complex involving weak edge sites was required to model the Sr uptake at higher pH values.

The sorption of Co on Na-illite, however, was strongly pH dependent. The results summarized in Fig. 3 show that R$_d$ values increased between pH 4 to 7 from 2 to 4 at a logarithmic scale (L kg^{-1}) and levelled off at log R$_d$ ~4 (L kg^{-1}) for pH 7 to 9.

Cation exchange at the planar sites and surface complexation on strong and weak edge sites were used to quantitatively reproduce the Co sorption data (continuous line in Fig. 3). R$_d$ values for trace Co between pH 5 and 9 (0.1 M NaClO$_4$) deduced from diffusion experiments on compacted Na-illite samples (bulk-dry density of 1700 kg m^{-3}) were in a good agreement with the data from the batch sorption experiments, see Fig. 3 and Fig. 4. The equivalence of the two different approaches to measure sorption was thus confirmed for the present system. In addition the results highlighted again the importance of both major and minor surface species for the diffusive transport behavior of strongly sorbing metal cations. While surface complexes at the edge sites determine largely the solid-solution equilibrium distribution, the diffusive flux may be governed by those species bound to the planar sites, even at low fractional occupancies. The sorption edge determined for Zn showed high R$_d$ values (log R$_d$ up to ~5.5 at the L kg^{-1} scale) across the entire pH range with almost no dependence on the background electrolyte concentration. The data obtained independently by the three groups (INE, PSI and SCK-CEN) unambiguously showed that at Zn trace concentration, cation exchange is almost negligible, suggesting that another mechanism is ruling the Zn uptake. Additional experiments on Zn^{2+}-Na$^+$

exchange at higher Zn loadings, confirmed that this unusually high uptake is restricted to Zn trace concentration and allowed to determine a selectivity coefficient (K_c) for Zn^{2+}-Na^+ exchange on the planar sites of illite.

References

[1] Nardi A., et al. (2014) *Computers & Geosciences,* **69,** 10-21.

[2] Parkhurst and Appelo (2013) C. A. J. U.S. Geological Survey Techniques and Methods, 2013, book 6, chap. A43, 497 p.

[3] COMSOL (2014) COMSOL-Multiphysics. Version 5.2, www.comsol.com

[4] Montoya V. et al. (2018). *Geochimica et Cosmochimica Acta* **223**, 1-20.

[5] Glaus M. et al. (2007). *Environ. Sci. Technol.,* **41,** 478-485.

[6] Gimmi T. and Kosakowski (2011) *Environ. Sci. Technol.* **45**, 1443- 1449

[7] Glaus M et al. (2010) *Geochimica et Cosmochimica Acta* **74**, 1999- 2010

[8] Bradbuty and Baeyens (2009) *Geochimica et Cosmochimica Acta* **73**, 990- 1003

6 Coordination chemistry

We perform coordination chemistry studies related to actinide separations by solvent extraction. These studies aim at understanding the interactions and the speciation between actinide ions (and other ions) and ligands potentially useful for separating actinides. The focus is on nitrogen donor ligands and on the subtle differences in their interactions between actinide and lanthanide ions of the same charge. Further to BT(B)P ligands,[1] we study nitrogen donor ligands based on ethylenediamine such as TPAEN (see 6.3) and diethylenetriamine such as DTPA-amino acid conjugates (see 6.2). Furthermore, oxygen donor ligands such as TODGA[2] and DMDOHEMA (see 6.1) are studied; these co-extract actinide and lanthanide ions, separating them from other fission products. By combining an extracting agent such as TODGA and a water soluble complexing agent such as TPAEN, sufficient selectivity between Am(III) and Cm(III) is obtained (see 6.3).

Our studies are performed in the framework of past and present EURATOM projects, SACSESS, TALISMAN and GENIORS, and in cooperation with CEA, CIEMAT, Heidelberg University, HZDR, INL, Jülich, Manchester University, NNL, ORNL, Politecnico di Milano, among others.

Close in-house cooperation with the NMR, X-ray spectroscopy and theoretical chemistry groups is indispensable to our work, as is the support of the analytics and infrastructure department.

6.1 TRLFS study on the complexation of Cm(III) with DMDOHEMA

P. Weßling, P. J. Panak, A. Geist

Background

N,N'-dimethyl-*N,N'*-dioctyl-2-(2-hexyloxy-ethyl)-malon-amide (DMDOHEMA, figure 1) is an extracting agent for An(III) and Ln(III) used in actinide separations processes such as the EURO-GANEX process[3-5] developed in European projects.

An equilibrium model for the extraction of HNO_3 and Am(III) by DMDOHEMA was established earlier.[6] This model is solely based on the evaluation of distribution data; no spectroscopic data are considered. It postulates the formation of the following Am(III) complexes,

- $Am(NO_3)_3(DMDOHEMA)_4$
- $Am(NO_3)_3(HNO_3)(DMDOHEMA)_3$
- $Am(NO_3)_3(HNO_3)_2(DMDOHEMA)_2$

with increasing aqueous HNO_3 concentration.

To underpin this model, the complexation of Cm(III) (as an analogue for Am(III)) with DMDOHEMA is studied by TRLFS. First, Cm(III) in water saturated octanol is titrated with DMDOHEMA to characterise the Cm(III)-DMDOHEMA complexes that form as a function of the DMDOHEMA concentration. Next, Cm(III) is extracted from nitrate solutions with varied proton concentrations and the organic phase is probed by TRLFS. Comparing their emission spectra with those obtained from the titration experiment allows identifying the number of DMDOHEMA molecules present in the extracted complexes. The results are compared to the equilibrium model.[6]
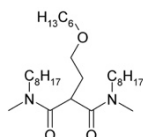

Fig. 1: *DMDOHEMA.*

Results

Figure 2 shows the single component spectra of the $[Cm(DMDOHEMA)_n]^{3+}$ complexes *(n = 0–3)* in water saturated octanol. These exhibit emission bands at 596.5 nm *(n = 1)*, 598.5 nm *(n = 2)* and 601.9 nm *(n = 3)*. The Cm(III) speciation as a function of the free DMODHEMA concentration is shown in Figure 3. The speciation is described with lg β'_1 = 2.63 ± 0.33, lg β'_2 = 3.99 ± 0.48 and lg β'_3 = 4.34 ± 0.52 The formation of a 1:4 complex is not observed. Nevertheless, lifetime measurements indicate the existence of a 1:4 complex for *[DMDO-HEMA]* > 0.13 mol/L.

Figure 4 shows the fluorescence spectra of organic phase samples from the extraction of Cm(III) from aqueous phases containing a constant nitrate concentration (6.04 mol/L) and varying proton concentrations (10^{-3}–6.04 mol/L).

Two different species are observed, depending on the proton concentration. At low proton concentrations (10^{-3}–0.3 mol/L), a species with an emission
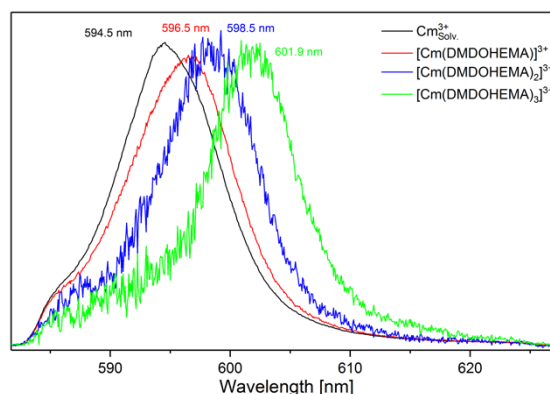

Fig. 2: *Single component spectra of the [Cm(DMDO-HEMA)$_n$]$^{3+}$ complexes (n = 0–3) in water saturated octanol. [Cm(III)] $_{ini}$ = 10^{-7} mol/L.*
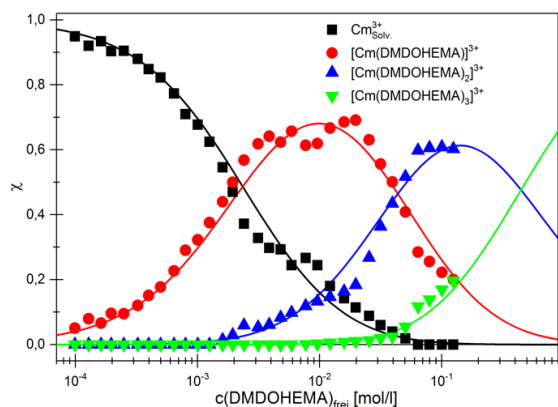
Fig. 3: *Speciation of [Cm(DMDOHEMA)$_n$]$^{3+}$ complexes (n = 0–3) in water saturated octanol. [Cm(III)]$_{ini}$ = 10^{-7} mol/L. Symbols, experimental data. Lines, calculated with lg β'$_1$ = 2.63 ± 0.33, lg β'$_2$ = 3.99 ± 0.48, lg β'$_3$ = 4.34 ± 0.52.*
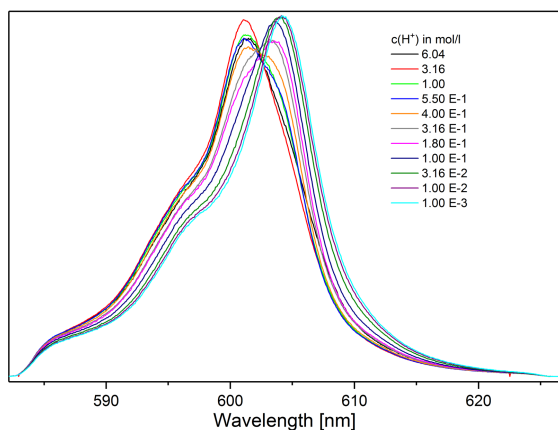

Fig. 4: *Emission spectra of organic phase samples from the extraction of Cm(III) into DMDOHEMA at varied proton concentration. [Cm(III)]$_{ini}$ = 10^{-7} mol/L, [NO$_3^-$] = 6.04 mol/L, [DMODHEMA]$_{ini}$ = 0.4 mol/L,*

band at 604.2 nm is found (species I). At high proton concentrations (0.4–3.16 mol/L), a Cm(III) species having an emission band at 601.3 nm is prominent (species II). The spectrum obtained from the sample containing a proton concentration of 6.04 mol/L differs somewhat from those observed for species II, having a lower intensity and being broader. This may indicate the presence of yet another species at this proton concentration.

Lifetime measurements confirm the existence of one molecule of water in the first coordination sphere. Hence, eight coordination sites are available for further ligands. Comparison of the spectrum of the 1:3 Cm(III) complex in octanol (figure 1) with the spectrum from the extraction at high proton concentrations indicates that species II (601.3 nm) is [Cm(DMDOHEMA)$_3$(NO$_3$)(H$_2$O)]$^{2+}$, the 1:3 complex. Consequently, species I (604.2 nm), present at lower acidity, is expected to be the 1:4 complex, [Cm(DMDOHEMA)$_4$(H$_2$O)]$^{3+}$.

Conclusions

Emission spectra from monophasic titrations of Cm(III) with DMDOHEMA are compared to those from Cm(III) extracted into DMDOHEMA organic phases. A 1:4 complex (at low acidity) and a 1:3 complex (at higher acidity) are identified in the extraction experiments; a third species may be present at even higher acidity.

These results support the equilibrium model for the extraction of Am(III) from HNO$_3$ into DMDO-HEMA[6] which is derived from distribution measurements.

6.2 Trivalent actinide-lanthanide discrimination using DTPA-amino acid conjugates

C. Adam, U. Müllich, A. Geist

In co-operation with:

Jennifer E. Jones,[a] Peter Kaden,[b] Leigh R. Martin,[c,d] Louise S. Natrajan,[a] Clint A. Sharrad[a]

[a]The University of Manchester, United Kingdom, [b]Helmholtz-Zentrum Dresden-Rossendorf, Germany, [c]Idaho National Laboratory, Idaho Falls, ID, USA [d]Oak Ridge National Laboratory, Oak Ridge, TN, USA

Introduction

The TALSPEAK process[7] was developed to separate trivalent actinide ions, An(III), from chemically similar lanthanide ions, Ln(III) by solvent extraction. The idea was using an extracting agent unselective for An(III) over Ln(III) and adding a complexing agent to the aqueous phase to mask An(III), thus keeping them from being extracted.[8] The original TALSPEAK system, consisting of HDEHP (bis-2-ethylhexyl phosphoric acid) as the extracting agent, DTPA (diethylenetriamine pentaacetic acid) as the

Fig. 5: *DTPA-His-P (top) and DTPA-Ala-D (bottom).*

Fig. 6: *Extraction of Am(III) and Ln(III) in the DTPA-His-P/HDEHP system. Distribution ratios as a function of pH. Organic phase, 0.2 mol/L HDEHP in kerosene; aqueous phase, 50 mmol/L DTPA- His-P, Am(III) and Ln(III). pH adjusted by adding HNO$_3$ or NaOH.*

An(III)-selective complexing agent and lactic acid as buffering agent, has constantly been improved by substituting the components of the original system.[9-11]

In the framework of a TALISMAN project, University of Manchester have pursued a concept which differs in two aspects, (a) using amino acids (AA) as buffering agent[12] and (b) linking them to the complexing agent, DTPA. This way, only a single molecule is added to the aqueous phase and the system is expected to behave more simply. Several DTPA-AA conjugates (AA = Arg, His, Ser and Ala) were synthesised. The most promising results are achieved with DTPA-His-P and DTPA-Ala-D, figure 5.
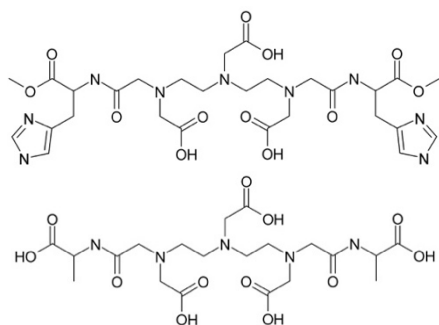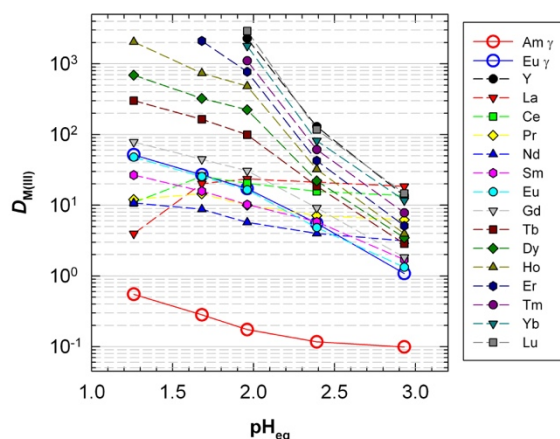
Solvent Extraction

DTPA-AA are tested in solvent extraction experiments, determining Am(III) and Ln(III) distribution ratios as a function of pH.

Results of DTPA-His-P are shown in figure 6. The lowest pH at which separation is achieved (i.e., Am(III) distribution ratio < 1 and all Ln(III) distribution ratios > 1) is < 1.2. Separation factors for Eu(III) over Am(III) are > 90 and the minimum separation factors between Am(III) and the least extracted Ln(III) being Nd(III), are 30–40.

Coordination Chemistry

The DTPA-AA coordination chemistry is studied by luminescence and NMR. Luminescence studies of the Eu(III)-DTPA-AA complexes demonstrate consistent coordination in the pH range 2–4. The luminescence lifetime indicates the presence of one water molecule in the first coordination sphere, consistent with 1:1 coordination by three amine nitrogens, three deprotonated carboxylates and two amidic oxygens. ^{1}H NMR studies performed with Am(III) confirm the 1:1 complexation.

Conclusion

In conclusion, an improved TALSPEAK system is reported which compares favourably to known TALSPEAK systems as it extends the usable acidity range to lower pH values while maintaining the good selectivity of the original system.

6.3 TPAEN coordination chemistry

C. Wagner, A. Geist, P. J. Panak

In co-operation with:

N. Boubals,[a] T. Dumas,[a] L. Chanèac,[a] G. Manie,[a] P. Kaufholz,[b] C. Marie,[a] G. Modolo,[b] P. Guilbaud[a]

[a]CEA Marcoule, DMRC/SPDS/LILA, France, [b]Forschungszentrum Jülich GmbH, IEK-6, Nukleare Entsorgung und Reaktorsicherheit, Jülich, Germany

Introduction

Two solvent extraction systems for separating Am(III) from Cm(III) were developed in the SACSESS project. Both systems combine TODGA's slightly stronger affinity for Cm(III) vs. Am(III)[2] with the inverse selectivity of a water-soluble masking agent, SO₃-Ph-BTBP[13, 14] or TPAEN *(N,N,N',N'*-tetrakis[(6-carboxypyridin-2-yl)methyl]ethylenediamine, figure 7).[15]

In collaboration with CEA and Jülich, the coordination chemistry and speciation of TPAEN with Am(III), Cm(III) and Ln(III) ions is studied by EX-AFS, TRLFS, UV-vis and micro-calorimetry.[16]

Results

EXAFS demonstrates 1:1 coordination of Am(III) by TPAEN in solution, with a coordination number of 10 (four carboxylate oxygens, four pyridine nitrogens and two amine nitrogens), in agreement with the solid-state structure of the respective Eu(III) complex. The ten-fold coordination results in significantly longer bond distances compared to those observed for nine-fold coordination.

Conditional stability constants (in 0.1 mol/L HNO₃) for the complexation of Am(III), Cm(III) and

Fig. 7: *TPAEN.*

Tab. 1*: Conditional stability constants of the M(III)-TPAEN complexes in 0.1 mol/L HNO₃. T = 298 K.*

M(III)	lg β	Method
Am	4.5 ± 0.2	UV-vis
Cm	4.3 ± 0.2	TRLFS
La	2.8 ± 0.1	μc
Ce	2.6 ± 0.1	μc
Pr	3.2 ± 0.1	μc
Nd	3.3 ± 0.1	μc
	3.1 ± 0.4	UV-vis
Sm	3.0 ± 0.1	μc
Eu	2.8 ± 0.1	μc
	2.4 ± 0.3	TRLFS
Dy	2.3 ± 0.1	μc

several Ln(III) determined by means of micro-calorimetry, TRLFS and UV-vis are reported in table 1

Stability constants for the An(III) complexes are 1–2 orders of magnitude higher than those for the Ln(III) complexes. TPAEN forms slightly stronger complexes with Am(III) compared to Cm(III). Within the Ln(III) studied, stability constants increase from La(III) to Nd(III), followed by a decrease to Dy(III).

These results, combined with TODGA's selectivity, explain the trends observed in solvent extraction experiments:[17] Adding TPAEN to the aqueous phase has almost no effect on La(III) extraction; Pr(III) and Nd(III) extraction is slightly suppressed; the effect diminishes with increasing Ln(III) atomic number. Extraction of Cm(III) and Am(III) is suppressed by approximately one order of magnitude, with a stronger effect on Am(III) than on Cm(III). Finally, the TODGA/TPAEN system allows separating Am(III) from Cm(III) and Ln(III).

References

[1] Panak, P. J.; Geist, A., *Chem. Rev.* **2013,** *113*, 1199–1236.

[2] Sasaki, Y.; Sugo, Y.; Suzuki, S.; Tachimori, S., *Solvent Extr. Ion Exch.* **2001,** *19*, 91–103.

[3] Carrott, M.; Geist, A.; Hérès, X.; Lange, S.; Malmbeck, R.; Miguirditchian, M.; Modolo, G.; Wilden, A.; Taylor, R., *Hydrometallurgy* **2015,** *152*, 139–148.

[4] Carrott, M.; Bell, K.; Brown, J.; Geist, A.; Gregson, C.; Hérès, X.; Maher, C.; Malmbeck, R.; Mason, C.; Modolo, G.; Müllich, U.; Sarsfield, M.; Wilden, A.; Taylor, R., *Solvent Extr. Ion Exch.* **2014,** *32*, 447–467.

[5] Malmbeck, R.; Magnusson, D.; Carrott, M.; Geist, A.; Hérès, X.; Miguirditchian, M.; Modolo, G.; Müllich, U.; Sorel, C.; Taylor, R.; Wilden, A., *Radiochim. Acta* **2017**.

[6] Geist, A., Equilibrium model for the extraction of Am(III), Eu(III), and HNO3 into DMDOHEMA in TPH. In *Proc. Internat. Conf. ATALANTE 2008 (Nuclear Fuel Cycles for a Sustainable Future)*, Montpellier, France, 19–23 May, 2008.

[7] Weaver, B.; Kappelmann, F. A., *J. Inorg. Nucl. Chem.* **1968,** *30*, 263–272.

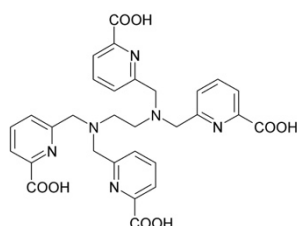[8] Nilsson, M.; Nash, K. L., *Solvent Extr. Ion Exch.* **2007,** *25*, 665–701.

[9] Gelis, A. V.; Lumetta, G. J., *Ind. Eng. Chem. Res.* **2014,** *53*, 1624–1631.

[10] Braley, J. C.; Grimes, T. S.; Nash, K. L., *Ind. Eng. Chem. Res.* **2012,** *51*, 629–638.

[11] Lumetta, G. J.; Casella, A. J.; Rapko, B. M.; Levitskaia, T. G.; Pence, N. K.; Carter, J. C.; Niver, C. M.; Smoot, M. R., *Solvent Extr. Ion Exch.* **2015,** *33*, 211–223.

[12] Grimes, T. S.; Tillotson, R. D.; Martin, L. R., *Solvent Extr. Ion Exch.* **2014,** *32*, 378–390.

[13] Wagner, C.; Müllich, U.; Geist, A.; Panak, P. J., *Solvent Extr. Ion Exch.* **2016,** *34*, 103–113.

[14] Wagner, C.; Müllich, U.; Geist, A.; Panak, P. J., *Dalton Trans.* **2015,** *44*, 17143–17151.

[15] Gracia, S.; Arrachart, G.; Marie, C.; Chapron, S.; Miguirditchian, M.; Pellet-Rostaing, S., *Tetrahedron* **2015,** *71*, 5321–5336.

[16] Boubals, N.; Wagner, C.; Dumas, T.; Chanèac, L.; Manie, G.; Kaufholz, P.; Marie, C.; Panak, P. J.; Modolo, G.; Geist, A.; Guilbaud, P., *Inorg. Chem.* **2017,** *56*, 7861–7869.

[17] Vanel, V.; Marie, C.; Kaufholz, P.; Montuir, M.; Boubals, N.; Wilden, A.; Modolo, G.; Geist, A.; Sorel, C., *Proc. Chem.* **2016,** *21*, 223–230.

7 Department of Decommissioning of Nuclear Facilities

M. Brandauer, E. Zellmann, S. Kaiser, S. Gentes [a]

[a] Department of Deconstruction and Decommissioning of Conventional and Nuclear Buildings, Institute for Technology and Management in Construction (TMB), Karlsruhe Institute of Technology (KIT)

Overview

After the integration of the decommissioning of nuclear facilities subject to the program-oriented funding research of the Helmholtz Association (HGF) in 2015, the former report year was a further important step for establishing the decommissioning competences in the HGF program.

The year started with the first meeting of the five partners of the "Decommissioning Cluster" established in February 2016. The partners, namely the Duale Hochschule Baden-Württemberg (DHBW), the Paul Scherrer Institut (PSI), the University of Stuttgart (including the Materials Testing Institute), the Joint Research Center (JRC) of the European Commission (EC), and the KIT, met in Karlsruhe from the 15th to the 16th of February 2017 at KIT (see Fig. 1). The following main topics have been addressed [1]:

- Harmonization of E&T (including lectures on decommissioning at PSI/ETH and KIT, the Summer Schools at JRC and KIT, possible integrations in Stuttgart and the DHBW as well as establishing the connection to the ELINDER program of the EC;
- Cooperative working on defined research topics (i.e. radiological characterization, long-term storage of radioactive waste, automatization of decommissioning techniques);
- Possible extension of the cluster to further partners;

In March the biggest German conference for nuclear decommissioning (KONTEC) took place in Dresden, where the group was strongly represented with three plenary presentations [2]–[4]. With the efforts taken by Prof. Gentes, the students of the current semester where given the possibility to attend the conference as well. The conference ended with a surprising highlight, where the paper of C. Krauß et al. [3] was awarded best paper of the KONTEC 2017.

Starting 2017, Martin Brandauer accepted to be chair of the decommissioning session at the "Annual Meeting on Nuclear Technology" (AMNT), which was held

Fig. 1: *Participants at the "Decommissioning Cluster" meeting in 2017 [1].*

in Berlin. Three technical presentations and one presentation in the young scientist's workshop were held by the department at the same conference [5]–[8]. Further activities where the organization of the decommissioning working group of the "Kerntechnische Gesellschaft e.V. (KTG)" which in this year was held in Krefeld at the site of Siempelkamp GmbH & Co. KG.

In Mai 2017 Dr.-Ing. Ahmed Stifi defended his doctoral thesis related to the development of an anti-corruption toolkit for the lean construction concept, while working in the decommissioning department [9]. In October of the same year, Dr.-Ing. Martin Brandauer defended his doctoral thesis related to magnetic separation of granular mixtures for the treatment of radioactive waste mixtures [10]. Background for these analysis are contaminated mixtures of silicate and grenade abrasives with activated steel chips after the usage in the water abrasive suspension cutting of activated components, such as a reactor pressure vessel and core internals. The investigations showed, that using a strong rod magnet filter, with proper filtration parameters, a reduction of 90% of the contamination within the abrasive mixtures can be achieved, even if containing weak diamagnetic stainless steel alloy chips. The simple set-up allows a reliable and cost-effective treatment of this abrasive mixtures, as an important first approach for the significant reduction of secondary waste caused by the water abrasive suspension cutting. With this principle, further significant waste reduction methods are currently being investigated by the ongoing BMBF project 15S 9225A&B. This has been extensively covered in the last years report. The project allowed the detailed analysis of the experimental investigations carried out by Dr.-Ing. M. Brandauer, where the results have been submitted for publication in the beginning of 2018. Within the last year of the project, new representative abrasive mixtures using both stainless and ferritic steel alloys have been generated in cooperation with ANT GmbH, the cutting technique developing company. These will be required for the extensive experimental investigations planed within the project. With the help of new findings made during the year, an improved separation system is currently being built which will be able to treat real activated secondary waste within a controlled area [3], while furthermore substantially reducing the secondary waste with a further novel treatment approach. This new approach is currently being submitted to a patent.

In the last year the group has also been very successful in acquiring new third party funded projects. In May a two and a half year project sponsored by the BMWi for the development of an automated wet sandblasting

system with pneumatic discharge for removing asbestos-containing putties in concrete structures in cooperation with OFTEC GmbH was acquired [11]. Later in the year, a new three year project in cooperation with the university of Kassel and Kraftanlagen Heidelberg GmbH, sponsored by the BMBF, with two doctoral positions at KIT was obtained [12]. By usage of state of the art digital planning tools, a safe and cost-effective dismantling of nuclear facilities with a real project application is pursued. Further intensive efforts have been placed in the acquiring of funds for the groundbreaking development of robotic systems for the decommissioning of nuclear facilities. These lead to two new promising projects, one starting in January 2018 [13] and the other possibly starting in April 2018. With the settled joint venture with many leading German actors in the robotic field, a major contribution in the robotic sector for the decommissioning of nuclear sites is planned.

Further two major research topics in the last year will be addressed in more detail below.

Implementation of a Nuclear Decommissioning Knowledge Database

With the implementation of a comprehensive decommissioning knowledge database in 2017 a powerful evaluation basis of previously and ongoing nuclear decommissioning projects in Germany, with an extension possibility for Europe, is pursued. Therefore, in 2016, an applicable database software based on a team collaboration platform by Atlassian Inc., *Confluence,* has been chosen and implemented.

Following the acquisition and setup, relevant information has been gathered in the last year, which covers following topics:

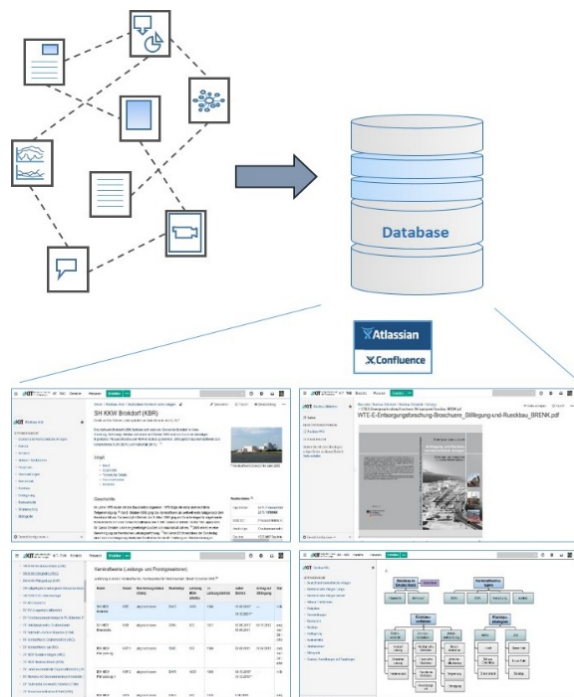- existing and former nuclear facilities,

Fig. 2: The decommissioning database system.

- status of actual conducted decommissioning projects,
- involved authorities, operators and conducting companies (stakeholders),
- licensing process management and related licensing steps,
- decommissioning procedures and techniques,
- nuclear waste management and storage know-how,
- public participation structures and actions,
- required knowledge in the field of nuclear physics and energy, radiation measurement and protection.

Furthermore, the chosen specific software tool allows the gathering of information of different source types e.g. scientific papers, articles, other databases, datafiles, books and news (as illustrated in the following Fig. 2).

The integration of tables, documents, and links leads to a tool for combining management aspects with technical procedures and provides an overview and interconnection of information needed for the planned R&D in decommissioning of nuclear facilities.

By 2018, besides a further acquisition of data, the creation of evaluation tools for the analysis and processing of recent, ongoing and completed decommissioning procedures will move into the main focus of the research activities. Planned tools will further allow the illustration of the current decommissioning status of nuclear facilities, decommissioning knowledge and technologies. They will help to identify relevant characteristic values for nuclear decommissioning procedures and the necessity of development of required technologies. This, therefore, leads to the overall project goal, which is the creation of a basis for future research and development and allow considerations for the possible standardization and optimization of procedures and technologies.

Development of a system for the in depth decontamination of reinforced concrete structures

One of the decontamination challenges of concrete structures is the deep decontamination of cracks, fractures, and the removal of steel fixtures (e.g. anchor plates, dowels, etc.). This procedure requires the application of a tool, which can not only remove a deep layer of concrete but also deal with the reinforcement within the structure while generating a smooth enough surface to allow the subsequent measurement of contamination. The different properties of the materials (i.e. concrete and steel) make it very challenging to design a tool that can deal with a ductile and a brittle material at the same time. State-of-the-art decontamination tools for this application usually rely on the usage of two different set of tools for each of the components.

In a joint effort, a novel patented tool is being tested by the Karlsruhe Institute of Technology (including this working group and the chair of mobile machinery), the Institute of Production Engineering and Machine

Tools (IFW) at Leibniz University Hanover, Kraftanlagen Heidelberg GmbH, and Herrenknecht AG. The system allows the removal of highly reinforced concrete, the removal and transportation of debris, as well as suitable storage and packaging of the debris for the nuclear repository. These efforts are being sponsored by the Federal Ministry of Education and Research (BMBF) through the project 15S9093A „Definierter Abtrag hocharmierter Stahlbetonstrukturen (DefAhS)".

In the year 2017 numerous tests had been run on the test rig at the institute. It allowed to figure out the best possible operating points for the removal of concrete. The possible variables being investigated are the feed, the infeed and the cutting speed. During the experimental investigations, the machining forces were measured. The resulting force by milling concrete is significant smaller compared with the required force for the machining of steel. The required forces have been determined as follows:

- F_{max} = 300N for the machining of concrete by applying the following parameters: infeed=3,5mm; cutting speed=600m/min; feed=0,12 and 0,2mm
- F_{max} = 5300N for the machining of steel by applying the following parameters: infeed=3,5mm; cutting speed=600-1100m/min; feed= 0,08 and 0,04mm)

All detailed measurements, diagrams and results have been documented in a project internal test report (report No. 3, October 2017).

During the tests, several problems were faced, making the following modifications necessary:
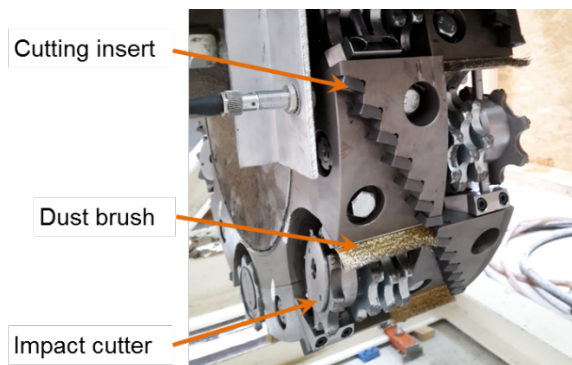

Fig. 3: Inclined outer impact cutters.

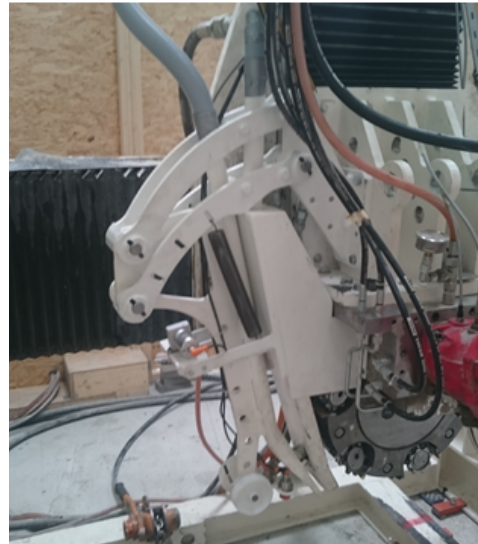*Fig. 4: Uneven concrete removal between two reinforcement rods.*

Fig. 5: Local suction system.

1. Narrow cut width with increasing infeet

The deeper the cut, the narrower became the groove created by the milling drum. This led to the fact, that the outer cutting inserts get in direct contact with the groove concrete walls at a certain depth and therefore get destroyed. Several ideas were tested so solve this problem and the best solution was to introduce an inclined outer impact cutter (see Fig. 3). On each side of the drum now two sets of impact cutters with an angle of 10° and two sets with 20° have been designed and installed.

2. Uneven exposure of the reinforcement rods

Between two reinforcement rods, the concrete removal is uneven (see Fig. 4). This uneven exposure of the steel inserts causes the destruction of the cutting inserts. To solve the problem, the control software had to be modified, so that the tool head can spin and work in both directions. The new software has been implemented in November 2017.

3. Vibrations within the test rig

The high induced forces by machining steel fixtures induces speed dependent vibrations within the test rig. The rig needed to be stiffened by additional structures in the test rig frame. The stiffening was carried out in October of the last year.

4. Local suction device

The first parts for the local suction device were destroyed by wedging. In addition, there was a strong dust formation while immersing in the concrete. Fig. 5 shows the new suction system, which does not wedge any more. There are, however, still issues to fully contain the strong dust formation during the milling process.

The project was supposed to end in September 2017. All project partners applied for a 6 month extension until March 31, 2018, which was approved by the BMBF. This allows the time to do more tests with the following focus:

- Evaluate the new software with both tool spinning directions
- Measurements to figure out the best possible operating points for working steel
- Evaluate all functions on a new test piece with steel fixtures

References

[1] W. Tromm and M. Brandauer, "Aufbau eines Cluster Rückbau für den Rückbau kerntechnischer Anlagen," Annual Meeting on Nuclear Technology (AMNT), Berlin, 2017.

[2] S. Müller and S. Gentes, "Untersuchungen zum Geometrieeinfluss auf Hartmetalllamellen beim Betonfräsen," KONTEC, Dresden, Germany, 2017.

[3] D. C. Krauß, D. M. Brandauer, P. H. Geckeis, P. S. Gentes, A. Heneka, M. Plaschke, D. Schild, and W. Tobie, "Verbesserung eines Separationsverfahrens zur Behandlung des Sekundärabfalls der Wasser-Abrasiv-Suspensions-Schneidtechnik," Dresden, KONTEC 2017, 2017.

[4] U. Hess, M. Weber, S. Gentes, D. Engelmann, F. Cousseau, and M. Kisling, "Entwicklung eines Werkzeugsystems für die Oberflächendekontamination von Stahlbetonstrukturen," KONTEC, Dresden, Germany, 2017.

[5] S. Kaiser, Gentes, Engelmann, Geimer, Hess, Dekena, Braun, Kisling, and Cousseau, "Definierter Abtrag hochbewehrter Stahlbetonstrukturen (DefAhS)," AMNT, Berlin, 2017.

[6] C. Krauß and Gentes, "Untersuchung der Strömungsverläufe in einem Magnetfilter zur Minimierung von Sekundärabfll der WASS-Schneidtechnik," AMNT, Berlin, 2017.

[7] S. Müller and S. Gentes, "Untersuchungen zum Geometrieeinfluss auf Hartmetalllamellen beim Betonfräsen," AMNT, Berlin, 2017.

[8] Y. Yakubov, M. Brandauer, and S. Gentes, "Alternative Methods for Decomissioning and Decontamination of pipes with small diameter," AMNT, Young Generation Workshop, Berlin, 2017.

[9] A. Stifi, "Development of an Anti-Corruption Toolkit with Components from Lean Construction," Dissertation Thesis, 2017.

[10] M. Brandauer, "Experimentelle Unter-suchungen zur Separation von Korngemischen in einem Stabmagnetfilter," Dissertation Thesis, 2017.

[11] S. Müller, "Entwicklung eines automatisierten Feucht-Sandstrahlsystems mit pneumatischer Abförderung zum Abtrag asbesthaltiger Spachtelmassen auf Beton (FeSS)." [Online]. https://www.tmb.kit.edu/Forschung_3743.php

[12] M. Brandauer, "Sicherer und kosteneffektiver Rückbau (SiKoR)." [Online]. https://www.tmb.kit.edu/Forschung_3940.php

[13] M. Brandauer, "Autonomous Robotic Networks to Help Modern Societies (ARCHES)." [Online]. https://www.tmb.kit.edu/Forschung_3950.php

8 Development of radionuclide speciation methods

Maintaining a state-of-the-art portfolio of advanced surface science and spectroscopy methods at INE is an important R&D activity, as these methods are crucial tools for advancing our understanding of actinide and radionuclide (geo)chemistry or the behavior of nuclear waste forms during interim storage. Radionuclide speciation methods available at INE controlled area laboratories and the nearby KIT synchrotron source are continuously adapted to serve the requirements of the INE in house and the HGF R&D programs. Access to this unique instrumentation is as well provided to INE's national and international partners in the frame of cooperation agreements or joint research projects. The multi analyzer-crystal X-ray emission spectrometer, core instrument at the ACT experimental station of the new CAT-ACT beamline commissioned in 2016, has provided unprecedented insight into electronic and bonding characteristics of actinides, as shown by a combined HR-XANES/RIXS/computational chemistry study revealing the role of the 5f valence orbitals of the early actinides U, Np, Pu in the chemical bonding of their trans-dioxo (actinyl) species. The portfolio of laser based speciation techniques at INE currently comprises TRLFS, LIBD and LIBS. An ambitious program to upgrade all existing systems and to improve their performance was finished in 2017. The refurbished cryo-TRLFS setup has been successfully used to reinvestigate the incorporation of Cm(III) in calcite, allowing for a new assignment of spectral signatures depending on the charge compensation mechanism. Prolonged interim storage of spent nuclear fuel at surface facilities during several decades is envisaged considering the expected time frame for site selection and construction of a suitable deep underground repository. Attempts to study mechanisms possibly limiting the integrity of fuel pins (e.g., fission product induced corrosion) have been recently started at INE. The inner surfaces of irradiated Zircaloy-4 cladding fragments (from the plenum and a section, where the hull had been in contact with a fuel pellet) are investigated by combining SEM-EDX, XPS and synchrotron based methods (XANES, XRF). NMR spectroscopy gives direct insight into metal-ligand bonding phenomena relevant, e.g., in the field of actinide/lanthanide separation chemistry. NMR investigations of the metal cation binding sites of the blood serum protein HSA upon titration with trivalent actinides or lanthanides revealed the involvement of a histidine group in the binding as previously observed for Cu^{2+}. These early results show that NMR can be as well successfully applied to study metal ion complexation by highly complex protein macromolecules. A method more recently established at INE is accelerator mass spectrometry (AMS). AMS is presently one of the most sensitive analytical techniques with an overall sensitivity of $\sim 10^4$ atoms in a sample. The analytical capability to determine concentrations of actinides and long-lived fission products (like ^{99}Tc) in natural samples at ultra-trace levels (fg/g and ag/g) is of great relevance both for environmental studies and for in situ tracer tests or diffusion experiments as, e.g., in the frame of the CFM project at the Grimsel test site. Many of the in-house research activities at INE benefit from strong support by quantum chemical calculations, providing molecular structures or thermodynamic data. In the past year the systems under investigation comprised the incorporation of selenite into the calcite ($10\bar{1}4$) surface - corroborating a recently proposed entrapment model for selenium(IV) co-precipitation with calcite, a study of the covalence of the triple bonds in UO_2^{2+}, NpO_2^{2+} and PuO_2^{2+} using localized molecular orbitals, the role of induced dipole and quadrupole interactions in trivalent lanthanide and actinide complexes or a molecular modelling/force field study of the intrusion of methanol molecules in the first hydration shell of Cm(III) in binary H_2O/MeOH mixtures.

8.1 R&D projects conducted at the INE-Beamline and at CAT-ACT at the KIT synchrotron source

S. Bahl, E. Bohnert, K. Dardenne, D. Fellhauer, E. González-Robles, M. Herm, V. Krepper, Ch. Marquardt, V. Metz, I. Pidchenko, J. Rothe, T. Vitova

In co-operation with

[a]*J.-D. Grunwaldt,* [a]*H. Lichtenberg,* [b]*T. Prüßmann,* [b]*A. Zimina*

Karlsruhe Institute of Technology, [a]Institute for Chemical Technology and Polymer Chemistry (ITCP), [b]Institute for Catalysis Research and Technology (IKFT)

[c]*S. Bagus,* [d,e]*Y. Joly*

[c]Department of Chemistry, University of North Texas, Denton, TX 76203-5017, USA; [d]Univ. Grenoble Alpes, Inst NEEL, F-38042 Grenoble, France; [e]CNRS, Inst NEEL, F-38042 Grenoble, France

[f]*A. L. Smith*

[f]Delft University of Technology, Radiation, Science & Technology Department, 2629 JB Delft, The Netherlands

Introduction

Synchrotron radiation (SR) based speciation techniques have become key methods in basic and applied radionuclide research. This development is primarily driven by the need to secure molecular-scale understanding for (geo-)chemical processes determining the mobility of long-lived radionuclides possibly released from a projected disposal site for highly active, heat producing nuclear waste (HAW). Presently, final disposal in deep bedrock repositories is deemed as the preferred option for the management of spent nuclear fuel (SNF) and high-level waste (HLW) glass used for conditioning of highly radioactive residues from nuclear fuel reprocessing. Solving the nuclear disposal safety case requires the assessment of an envisaged disposal site on geological time scales, where speciation techniques like XAS (X-ray Absorption Spectroscopy) and XES (X-ray Emission Spectroscopy) provide necessary input parameters to model the geochemical behavior of radionuclides. More recently, as well attempts to directly characterize HAW matrices by XAFS techniques came into focus, mainly due to the necessity to assess effects of an extended interim storage period before final disposal.

The INE-Beamline for radionuclide science [1] at the KIT synchrotron facility became fully operational in 2005 as a flexible experimental station for X-ray based radionuclide speciation investigations. About one decade later, commissioning of the new hard X-ray beamline 'CAT-ACT' for CATalysis and ACTinide research at an adjacent beam port has been completed [2] and the ACT lab for synchrotron based radionuclide speciation studies fully equipped and licensed to handle radioisotopes with activities up to one million times the (isotope specific) exemption limits. The multi analyzer-crystal (MAC) X-ray emission spectrometer originally installed at INE-Beamline serves as core component of the experimental infrastructure at the ACT lab. The INE-Beamline and the ACT experimental station are the only facilities of their kind in Europe offering direct access to radiochemistry laboratories operating a shielded box-line in close proximity to the synchrotron light source on the same research campus.

INE- and CAT-ACT beamline operation in 2017

After conversion of the former ANKA LK-II facility from a national user facility to a KIT internal research infrastructure in 2015, beamline operation had to be rearranged in 2016 to suit new boundary conditions, first of all a markedly reduced availability of beamtime shifts allowing for extended storage ring operation (now the KArlsruhe Research Accelerator KARA, cf. www.ibpt.kit.edu) as test facility for the development of accelerator technology - including insertion devices, electron beam sources and beam diagnostic tools. As a consequence of ANKA restructuring, beamtime distribution is no longer based on a peer review proposal process, but on in-house needs within the KIT and HGF research programs and individual agreements between beamline operators and external cooperation partners.

For 2017 a total of 101 days of standard SR operation had been initially scheduled (compared to 73 days in 2016), 12 of which were lost due to storage ring failure or insufficient beam quality. At INE-Beamline a further beam loss (16 days) had to be faced due to a failing double crystal monochromator (DCM) actuator, which had to be manufactured on customer request. The remaining beamtime was spent for INE in-house research (33%), beamline development and maintenance (8%) and external projects (34%). A total of 30 in-house and external projects were finally successfully carried out at the beamline. At CAT-ACT, beamtime at two in-line experimental stations is shared between CATalysis (KIT-IKFT/ITCP) and ACTinide/radionuclide research groups (KIT-INE). In 2017 a total of 26 beamtime days were available at ACT for INE in-house research, 16 days were given to external users and 6 days were required for beamline setup and maintenance, development and pilot experiments. A total of 16 in-house and external projects were hosted at the ACT station during this period.

After full commissioning of the CAT-ACT beamline optics and experimental infrastructure in 2016 – a major milestone of the NUSAFE program within the HGF program oriented funding period 2015-19 – remaining open issues covered in 2017 were related to the control system (e.g., automation of alignment procedures) and the DCM fine tuning. Parallel alignment of the DCM crystals at the rocking curve maximum may now be detuned to achieve constant I_0/I_{ring} flux conditions during energy scans (where I_0 denotes the intensity signal of the first ionization chamber at the individual experimental station or – alternatively – the photocurrent delivered by a retractable tungsten mesh placed in the monochromatic beam downstream from the optic section, and I_{ring} the storage ring current), applying a closed-loop feedback system developed by KIT-IPS based on a NI Compact RIO controller. The same system has been as well implemented at INE-Beamline and enables efficient suppression of spectral distortions caused by higher harmonic radiation in the incoming beam such as 'crystal glitches'.

As in previous years, INE in-house projects in 2017 covered the investigation of a broad range of materials containing actinides (*An*), fission products or their chemical homologues in the context of nuclear waste disposal safety research or basic actinide and radionuclide science. These studies comprised the investigation of Gd(III) complexation by sulphate, Np(V) complexation by succinate, oxalate and other carboxylic ligands, a combined XAFS + XRD study on the coordination of Am(III) by thiocyanate in a La(III) host lattice, the investigation of rhenium oxidation states and local chemical environments of rhenium and cesium within solid glass matrices, Yb(III) incorporation into $CaMoO_4$, XANES measurements to identify the redox-state and speciation of antimony, arsenic and lead in scaling samples from a geothermal

power plant, the solubility and carbonate complexation of Tc(IV) in Na_2CO_3 and $NaNO_3$, the redox behavior of U(VI/IV) under acidic to hyper-alkaline conditions and the solubility of U(IV) under reducing conditions in the absence and presence of carbonate, the solid phase transformation of Np(V) at elevated temperature in $NaCl/CaCl_2/MgCl_2$ solutions, XAFS, XRF and µ-XRF investigations of irradiated Zircaloy cladding segments in contact with SNF, the characterization of uranium oxidation states in natural granites, XAFS + XRD of Lu(III) incorporated in aged ferrihydrite, XAFS investigations of adsorbed Pu(III/IV) species on hardened ordinary Portland cement pastes in the absence and presence of isosaccharinic acid, a RIXS study of non-stoichiometric magnetite or speciation of chlorine in low pH cement pastes.

Some of these studies are presented in more detail elsewhere in this annual report. A study focusing on the advanced high-resolution X-ray emission techniques (HRXES) in the tender X-ray regime (actinide M-edges) is highlighted in the last section below.

HGF external scientists from the German and international research institutions listed below conducted research at the INE-Beamline in 2017:

- HZ Dresden-Rossendorf, Germany
- FZ Jülich, IEK-6, Germany
- Heidelberg University, Germany
- Mainz University, Germany
- CEA Cadarache, France
- JRC Karlsruhe, European Commission
- Delft Technical University, The Netherlands

As in the preceding years, a considerable share of INE in-house beamtime was spent for experiments conducted by master and graduate students in the frame of their thesis projects.

XAS, µ-XAS and µ-XRF investigation of irradiated Zircaloy-4 cladding fragments

In the light of a yet unclear timeframe for the necessary site selection, construction and licensing procedure before a final HLW repository becomes operational in Germany, a significant prolongation of SNF interim storage above surface has to be considered (see chapter 5.1). In this context, the possibly limited integrity of fuel pins - affecting SNF transportability and conditioning prior to final disposal - is of major concern. Hence, a better understanding of the effects of thermal, mechanical and radiological stress on fuel pin claddings is mandatory. Research at INE focuses on Zircaloy-4 - a cladding material commonly used in PWR fuel rod assemblies - both with respect to the formation of activation nuclides (cf. chapter 5.1) during reactor operation and the possible hull material corrosion. In 2017 Zircaloy-4 cladding ring segments for investigation by SR-based methods were sampled from a central fuel pin section (irradiated in the Swiss PWR Gösgen, average burn-up: 50.4 GWd/tHM), where the hull material had been in contact with a fuel pellet (cf. section 8.3

and Annual Report 2016 for investigation of corresponding fuel pin plenum material). Two mm-sized cladding fragments cut from a hull material ring (contact dose rate ~300 µSv/h) were sealed in acryl glass sample holders, allowing for exposure of the inner surface or the cross section towards the incident beam. Fig. 1 depicts µ-fluorescence maps of the inner cladding surface (top row) and a cross section (bottom row) recorded by a silicon drift Vortex detector at the U Lα and the Zr Kα emission energy (beam spot size ~20 µm FWHM), the left and right-hand side graphs in Fig. 2 depict XAFS spectra recorded from a U rich area in Fig. 1 (top row, left image) in fluorescence detection mode in the vicinity of the U L_3 and the Pu L_3 absorption edges, respectively. Contrast inversion (the highest fluorescence intensity is depicted in red) in the Fig. 1 top row images (scan area 1.5 mm(v) × 3 mm(h)) indicates that residues of high burnup SNF material are still adhering to the inner hull surface, partially blocking Zr Kα fluorescence excitation from the underlying Zr-rich alloy. This fact enabled recording of Pu L_3-XAFS spectra (E_0 Pu(2p$_{3/2}$) = 18.057 keV) without detector saturation by Zr Kα fluorescence emission (E_0 Zr(1s) = 17.998 keV). The U L_3- and Pu L_3-XAFS spectra depicted in Fig. 2 indicate that both U and Pu are predominantly present in tetravalent oxidation state. The weak Zr K absorption signal in the rising edge of the Pu L_3 spectrum originates most likely from Zr as fission product in the
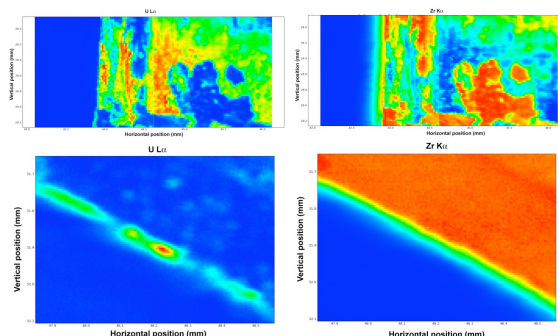

Fig. 1: *(top) µ-XRF map of the inner surface and (bottom)-cross-section of an irradiated cladding ring segment cut from a fuel rod section where the Zircaloy-4 hull had been in contact with a fuel pellet – left: U Lα fluorescence, right: Zr Kα fluorescence. The dotted line in the upper images marks the rim of the hull fragment.*
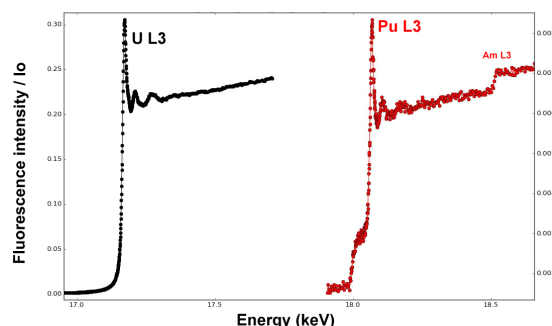

Fig. 2: *XAFS spectra obtained from the SNF (high burnup) material adhering to the inner hull surface after decladding – left: in the vicinity of the U L_3-edge, right: in the vicinity of the Pu L_3-edge.*
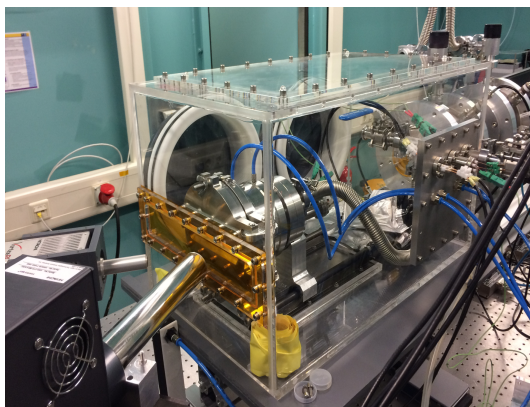
Fig. 3: *Oven setup inside glove box on the experimental table at INE-Beamline. The incident SR beam enters through the KAPTON® window on the left-hand side – the X-ray fluorescence signal is collected by two Vortex detectors in backwards geometry.*
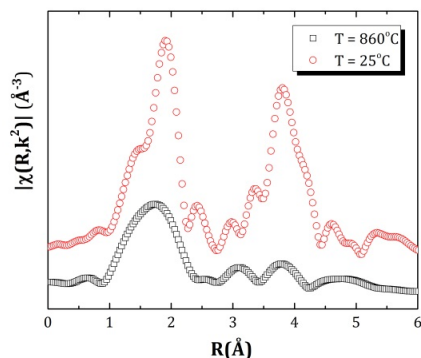

Fig. 4: *Experimental FT modulus of the (LiF:ThF₄)= (0.9:0.1) sample measured at T=860°C and room temperature after melting and re-solidification.*

SNF matrix, as this signal has been previously observed for SNF fragments not in contact with cladding.

Commissioning of a high-T in situ setup for the investigation of radionuclides in molten salts

An experimental setup adapted for high temperature in-situ XAFS measurements of radioactive, air sensitive and corrosive fluoride molten salts has been developed at the Delft University of Technology (TU Delft, The Netherlands) and successfully tested at the INE-Beamline. A dedicated furnace design allowing simultaneous measurements in transmission and fluorescence geometry has been developed (Fig. 3), as well as a specific sample containment cell (airtight, leak tight, compatible with the corrosive salts) made of boron nitride (BN). The suitability of the sample containment cell has been checked by mapping of the thorium concentration over the entire sample area after melting and re-solidification. The resulting thorium concentration shows a homogeneous distribution, and gamma spectroscopy measurements have confirmed the absence of contamination on the outside of the BN containment. First results have been obtained on selected salt mixtures in the LiF-ThF₄ and

NaF-ThF₄ systems. Fig. 4 shows the Fourier Transform (FT) of the k^2-weighted Th L_3-EXAFS of the (LiF:ThF₄)=(0.9:0.1) mixture collected in the molten state at T=860°C, and at room temperature after cooling. One single coordination shell is observed in the FT signal in the liquid, against two coordination shells at room temperature, as well as a clear decrease in amplitude caused by the disorder in the liquid and the occurrence of inharmonic atomic vibrations [3,4]. These features confirm the liquid state of the sample during the high temperature measurements. This set-up will be used in future studies to investigate coordination numbers and bond distances of molecular complexes formed in the molten salts at high temperatures.

HR-XANES/RIXS studies: The role of the 5*f* valence orbitals of early actinides in chemical bonding

Measurements performed at the new HRXES spectrometer have provided insights into one of the most controversial questions in actinide chemistry: What is the role of the 5*f* valence orbitals in the covalence of the chemical bonding of the actinide elements? High energy resolution X-ray absorption near edge structure (HR-XANES) and resonant inelastic X-ray scattering (RIXS) at the $M_{4,5}$ absorption edges of the early actinide elements (U, Np, Pu) probe the 5*f* unoccupied density of states of the actinides with superior energy resolution. The experiments have been performed at the INE-Beamline and the ACT station. These advanced spectroscopy tools allow to distinguish between the increase of covalence due to building up of electronic charge between the atoms, classical overlap of orbitals, and due to better energy match between metal and ligand valence orbitals as illustrated for U(VI)O₂²⁺, Np(VI)O₂²⁺ and Pu(VI)O₂²⁺. It is demonstrated that the 5*f* orbitals are more localized for Pu compared to U and Np and their energies are not influenced by changes in bonding environments. A broad set of data obtained from different actinide compounds is compared - including spectra for aqueous and solid-state species as well as highly radioactive materials like spent nuclear fuel. Spectroscopic results are corroborated by state of the art quantum-chemical calculations [5]. Part of the obtain results are summarized here.

Actinide 3*d*4*f* RIXS maps. The RIXS maps of UO₂²⁺, NpO₂²⁺ and PuO₂²⁺ are shown in Fig. 5a-c. When recording a HR-XANES spectrum the analyzer crystals of an X-ray emission spectrometer are typically positioned at the energy position of the maximum of the normal emission line and the energy of the incident beam is scanned across the absorption edge. Then the HR-XANES spectrum corresponds to a cross section of the RIXS map marked with line B in Fig. 5a-c. The HR-XANES spectrum can exhibit different features compared to the conventional XANES spectrum when the core-hole potential in the intermediate ($3d^9 5f^{N+1}$) state is significantly different
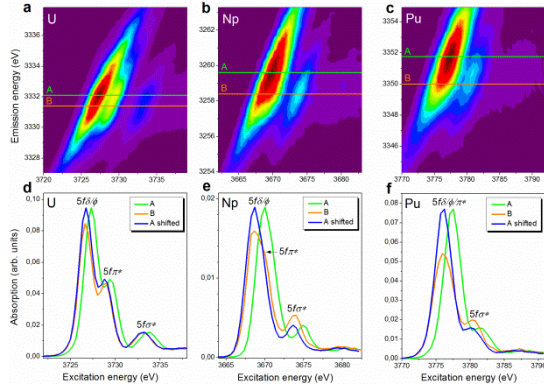
Fig. 5: *RIXS maps and extracted HR-XANES spectra.*

than that for the final state $(4f^{13}5f^{N+1})$. This effect is well visible in Fig. 5, where line B marking the normal emission maximum is shifted with respect to the most intense resonant peak, line A. The HR-XANES spectra extracted at emission energy marked with line A are also shown in Fig. 5d-f. Three peaks at about 3726.7, 3728.8 and 3732.9 eV are resolved in the UO_2^{2+} RIXS map, which are also visible in the HR-XANES spectra. We have previously been able to assign these peaks to transitions of 3d electrons to $5f\delta/\phi$, $5f\pi^*$ and $5f\sigma^*$ orbitals, respectively (cf. Ref. 17 in [5]). The energy difference or shift between lines A and B (RIXS maps a-c in Fig. 5) is 0.6, 1.3 and 1.6 eV for UO_2^{2+}, NpO_2^{2+} and PuO_2^{2+} in 1M $HClO_4$, respectively. These values are compared to those measured for these actinides with different speciation [5]. The size of this shift varies between 0 - 0.85 eV (U) and 0.5 - 1.3 eV (Np) for the various materials, whereas it remains constant for Pu(III)/Pu(IV)/PuO_2^{2+} in 1M $HClO_4$ and solid PuO_2. Emission energy shifts of the resonant peaks with respect to the normal emission was previously reported for 3d and 4f elements and was attributed to the strong interaction between the excited electron in the lowest unoccupied bound electronic states and the created core-hole, which differs from the ionized case, i.e. excitation into continuum. The energy shift between lines A and B, therefore, probes the localization of those lowest unoccupied 5f states on the absorbing atom. The experimentally observed increase in energy shift going from U to Pu in our actinyl system shows that the 5f orbitals undergo stronger localization in this order, i.e. from UO_2^{2+} to NpO_2^{2+} and from NpO_2^{2+} to PuO_2^{2+}. Observed invariance of the Pu energy shifts indicates that the localization of the Pu 5f orbitals is not influenced by changes in oxidation state and appears to be the same for molecular and solid-state species. This is not the case for U and Np, as significant variations are observed for these elements.

Actinide $M_{4,5}$ absorption edge HR-XANES.

In Fig. 6 the HR-XANES spectra of UO_2^{2+}, NpO_2^{2+} and PuO_2^{2+} are aligned so that the $5f\sigma^*$ peaks coincide at 0 eV. Comparison of the HR-XANES reveals differences in intensity and energy position of resonant features. The seven empty or partially occupied 5f

orbitals of the AnO_2^{2+} cation are split by spin-orbit coupling and the ligand field of the axial and equatorial ligands (ax. field and eq. field). When there is more than one electron in the 5f shell, Coulomb repulsion between the electrons becomes important and affects the covalent mixing. The spin-orbit splitting of the 5f electrons is ~1 eV while their ligand field splitting can be as large as 7 eV for actinyls. S. Matsika et al. pointed out that the influence of these effects can be ordered as follows: ax. field ($5f\sigma^*$, $5f\pi^*$) > spin-orbit > ax. field ($5f\delta$, $5f\phi$) + eq. field (cf. Ref. 40 in [5]). The ax. field exerts the strongest effect caused by the strong covalent nature of the An-O_{ax} bond. As a result, the $5f\sigma^*$ and $5f\pi^*$ states are shifted with respect to the $5f\delta$ and the $5f\phi$ orbitals ($5f\delta \approx 5f\phi < 5f\pi^* \ll 5f\sigma^*$). The shift is stronger for the $5f\sigma^*$ than the $5f\pi^*$ states due to interaction of the filled An-O σ_υ orbital and the semi-core $6p_z$ orbital with the same σ_υ symmetry ("pushing from below", cf. Refs. 1,41-44 in [5]). It is the formation of a σ_υ hybrid orbital from An 5f and pseudocore 6p, mixed with O_{ax} 2p valence orbitals, that is the source of high covalence of the U-O_{ax} bond. The mixing coefficient $(t_{ij}^{(1)})$ of a metal (ϕ_i) with ligand (ϕ_j) orbitals is associated with the covalency of the bond; it can be large due to their strong overlap or near degeneracy as described to the first order by perturbation theory: $t_{ij}^{(1)} \propto \frac{-S_{ij}}{\varepsilon_i - \varepsilon_j}$, where S_{ij} and $\varepsilon_i - \varepsilon_j$ are the overlap and energy difference of the orbitals, respectively (cf. Refs. 2, 12 in [5]). The change of these two parameters, S_{ij} and $\varepsilon_i - \varepsilon_j$, can lead to increase of $t_{ij}^{(1)}$ and thereby to increase of overlap or energy-driven covalence (cf. Refs. 2, 45 in [5]). R. Denning pointed out that the strong overlap of the 6p with 2p orbitals plays a substantial role for the covalence of the UO_2^{2+} bond (cf. Ref. 3 in [5]). Changes in this overlap lead to variations in the filled-filled interaction and is manifested in the HR-XANES spectra as the observed changing peak energy differences, most substantially between the $5f\delta/\phi$ and $5f\sigma^*$ peaks. In Fig. 6 the energy difference between the main $5f\delta/\phi$ peak and the $5f\pi^*/5f\sigma^*$ peaks for Np is significantly smaller (Δ $5f\delta/\phi$ - $5f\pi^*$ = 1.6 eV, Δ $5f\delta/\phi$ - $5f\sigma^*$ = 5.4 eV) compared to that for U (Δ $5f\delta/\phi$ - $5f\pi^*$= 2.3 eV, Δ $5f\delta/\phi$ - $5f\sigma^*$ = 6.4 eV). The trend is preserved for Pu but difficult to quantify since the
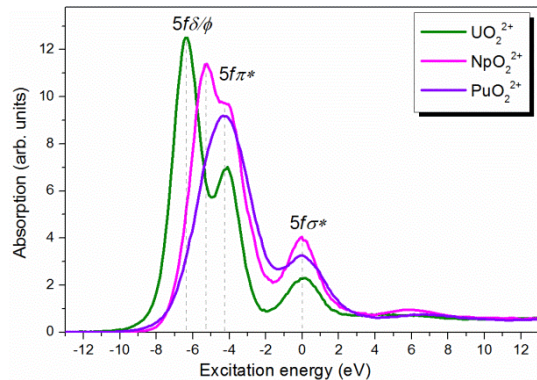

Fig. 6: *U M_4 and Np/Pu M_5 absorption edge HR-XANES.*

$5f\delta/\phi$ and $5f\pi^*$ peaks are not resolved in the HR-XANES spectrum. We propose to use the relative energy difference between the $5f\delta/\phi$ and the $5f\pi^*/5f\sigma^*$ HR-XANES spectral peaks as a qualitative measure of relative changes in the overlap driven covalence of the actinyl bond (cf. Ref. 2 in [5]). Recent experiments and calculations for $AnO_2^{+/2+}$ support the concept that the covalence of the An increases with the Z number across the actinide series (cf. Refs. 45,50-51 in [5]). One strong argument is the less favorable oxo-exchange of $AnO_2^{+/2+}$ with methanol and water going from U to Pu. The theoretical results are inconclusive but the notion prevails that this is an energy-driven covalence. This hypothesis is underpinned by the observed trends for the $5f$ orbitals in our RIXS maps. The stronger localization of the $5f$ orbitals likely leads to a better energy match with the O $2p$ orbitals for Pu, a less optimal energy match for U.

In summary, we illustrated the unique utility that An $3d4f$ RIXS offers in characterizing actinide electronic structures - it allows direct determination and comparison of the level of $5f$ orbital localization and participation of these orbitals in the chemical bonding for any type of materials, under static or dynamic conditions, not possible with other methods. We have applied this technique to U, Np and Pu in the actinide series and find that the localization of the U and Np $5f$ orbitals varies for different materials, but does not change for Pu, although studied in several different oxidation states (III, IV, VI) and states of matter (solid, solution). This result indicates that the $5f$ states in Pu are less active in the chemical bonding, compared to U and Np, and contrasts the general notion that the $5f$ orbitals are widely responsible for the ability of Pu to co-exist in several different oxidation states. Investigations of additional An materials and quantum chemical calculations of An $3d4f$ RIXS maps will be very beneficial for verification of these conclusions. Further, changes in the relative energy differences between the $5f\delta/\phi$ and the $5f\pi^*/5f\sigma^*$ orbitals, determined from their RIXS and HR-XANES, provide a direct qualitative measure for the level of overlap driven covalence in the actinyl bond. The observed trends in these energy differences indicate that U(VI)-O_{ax} is more covalent compared to the Np(VI)-O_{ax} and Pu(VI)-O_{ax} bonds due to stronger orbital overlap of U $5f/6p$ and O $2p$ orbitals. The An $M_{4,5}$ absorption edge HR-XANES and $3d4f$ RIXS can help to distinguish between the classical notion of overlap driven covalence and energy-driven covalence. Apparently, the overlap-driven covalent character of the An-O binding in the actinyl cations decrease within the U-Pu series, while the energy-driven covalent character increases without increasing the electron density of the binding. Taking into account the results on oxygen isotope exchange of Lucena et al. (cf. Ref. 51 in [5]) and the computational results of Kaltsoyannis (cf. Ref. 12 in [5]), the energy-driven covalence might have a higher impact on chemical binding stability/strength than the overlap-driven covalence.

References
[1] Rothe, J. et al., *Rev. Sci. Instrum.*, **83**: 043105 (2012).

[2] Zimina, A. et al., *Rev. Sci. Instrum.*, **88**: 113113 (2017).

[3] Bessada, C. et al., *J. Nucl. Mater.*, **494**: 192-199 (2017).

[4] Pauvert, O. et al., *J. Phys. Chem. B*, **114**: 6472-6479 (2010).

[5] Vitova, T. et al., Nature Comm., **8**: 16053 (2017).

8.2 Laser spectroscopy

C. Garcia, T. Hippel, R. Götz, F. Holl, F. Heberling, F. Endrizzi, X. Gaona

In co-operation with:

Z. Nie[a]

[a]College of Chemistry and Molecular Engineering at the Beijing University, Beijing, China

Introduction

The development of laser based spectroscopy methods and their application in studies carried out for the characterization of materials associated to the nuclear waste repository has been for many years a central aspect of the research at KIT-INE. Currently efforts are focused on broadening the speciation capabilities offered by Time Resolved Laser Fluorescence Spectroscopy (TRLFS) and the automatization and optimization of the home-made instrumentation used for Laser Induced Breakdown Detection (LIBD) of colloids and nanoparticles. In order to broaden the characterization possibilities for solid samples, a LIBS (Laser Induced Breakdown Spectroscopy) set-up for the determination of deposition or corrosion layers with high spatial and spectral resolution has been installed during this report period. Possibilities of isotopic LIBS are under evaluation.

In this chapter, some recent applications of TRLFS at INE will be shortly described. We have used cryo-TRLFS to reinvestigate the incorporation species of Cm(III) in calcite. High resolution spectra of Cm(III) in calcite - synthesized (1) in the presence of NaCl and (2) in the presence of KCl - reveal differences in the crystal-field splitting of the Cm(III) ground state and allow for a new assignment of the Cm(III) incorporation species. Additionally, a recently built system for uranyl speciation has been used to characterize U(VI) solid phases after equilibration in NaCl solutions.

Crystal field splitting in Cm(III):calcite

Similar to the investigation of Eu(III) in calcite reported in the 2016 annual report [1] and the approach in [2], we have prepared Cm(III) doped calcite, starting from 100 mg vaterite. As vaterite is metastable at standard conditions, it transforms within a few days to stable calcite. This transformation is performed in 100 mL solution containing (1) 4 nM Cm(III) and 100 mM NaCl and (2) 4 nM Cm(III) and 100 mM KCl. In the following the resulting calcite samples will be denoted (1) Cm,Na:calcite and (2) Cm,K:calcite.

TRLFS spectra are measured in a He-cryostat (CryoVac) at 4-6 K and ca. 10^{-8} mbar. The excitation wavelength, 396.6 nm, is produced by a Radiant Dyes laser, using an Exalite398 dye, pumped by the third harmonic of a Nd:YAG laser (Continuum) at 355 nm. Luminescence is collected with a fiber optic. The output of this fiber optic is coupled to the variable entrance slit of a 0.3 focal length Czerny-Turner spectrometer (Shamrock SR 303i, Andor Technology)

with a triple grating turret with 400, 1200 and 2400 l/mm gratings, where the dispersed light is detected by a time-gated intensified CCD camera (iStar 734, Andor Technology). For this experiment, the 1200 lines/mm or the 2400 lines/mm grating were used according to spectral resolution requirements.

Spectra recorded on the two samples at various delay times are depicted in Figure 1 a) and b). Both spectra show three species. The short-lived (680 µs) species A may be related to a surface species as already stated by Schmidt et al. [3]. Species B (1.1 ms) and C (> 4 ms) are incorporation species. Differences in species B between the two samples are already obvious in spectra recorded using the 1200 lines/mm grating. The spectra indicate that species B is related to a coupled substitution mechanism where Na^+ + Cm^{3+} (or K^+ + Cm^{3+}) replace two Ca^{2+} ions in order to assure charge compensation upon substitution. Species C is not affected by the synthesis in different ionic media. This observation is in contradiction to a previous study [3], which assigned species C to the coupled substitution mechanism based on fluorescence lifetime measurements in analogy to Eu(III) incorporation species. The differences in species B and the equality of species C are even more evident in
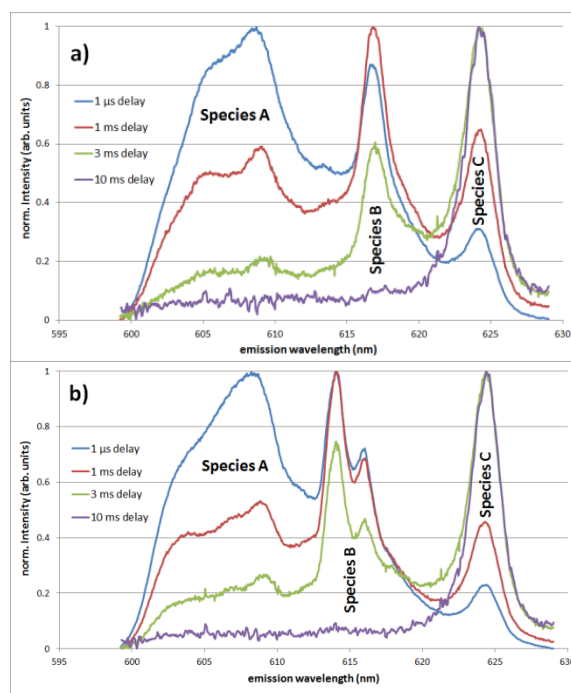

Fig. 1: *Emission spectra of Cm,Na:calcite (a) and Cm,K:calcite (b) measured at various delay times with the 1200 lines/mm grating.*
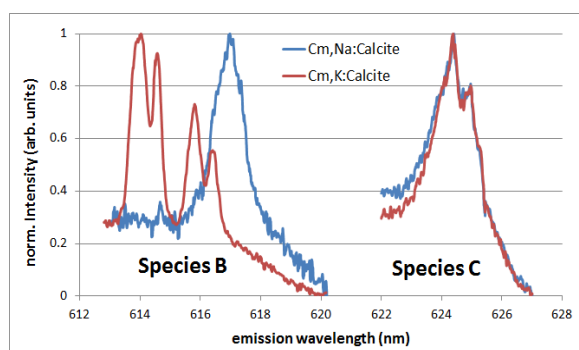
Fig. 2: *High resolution emission spectra of Cm,Na:calcite (blue) and Cm,K:calcite (red) measured with the 2400 lines/mm grating.*

the high-resolution spectra depicted in Figure 2. The pronounced ground-state splitting of Species B in Cm,K:calcite indicates a well-defined, but low-symmetry structural environment of Cm(III). This may be explained by the large ionic radius of K^+ (138 pm) as compared to the host cation Ca^{2+} (100 pm). Cm^{3+} (97 pm) and Na^+ (102 pm) instead match well with the host cation size. Correspondingly, the absence of a significant crystal-field splitting for species B in Cm,Na:calcite indicates a high-symmetry structural environment [4] as it would be expected for nearly undisturbed calcite (D_{3d}). The ground-state splitting in species C is intermediate between that of Species B in Cm,Na:calcite and that of Species B in Cm,K:calcite, but it is certainly not affected by the choice of the charge compensating ion. This indicates that species C corresponds to a different, not yet specified substitution mechanism (e.g., if 2 Cm^{3+} are exchanged for 3 Ca^{2+} the substitution is not affected by additional ions).

Luminescence of transformed U(VI) solid phases following solubility and hydrolysis studies

Understanding uranium mobility under geochemical conditions relevant for underground nuclear waste disposal sites is of high relevance when assessing the future performance of such repositories. In recent years comprehensive investigations have been carried out at KIT-INE in order to establish a reliable geochemical model predicting the solubility and aqueous speciation of U(VI) in dilute to concentrated NaCl brines [5,6]. The experiments covered the entire pH range in dilute to concentrated NaCl solutions as well as different temperatures. In the current study metashoepite, $UO_3 \cdot 2H_2O(cr)$, and sodium uranate, $Na_2U_2O_7 \cdot H_2O(cr)$, have been used as initial solid phases to determine the solubility and hydrolysis equilibria of U(VI) in $0.1 - 5$ M NaCl solutions at T = 25, 55, 80 °C in the pH_m range 4 to 14.3 ($pH_m = -\log [H^+]$). Batch experiments were conducted in an Ar atmosphere in the absence of CO_2. The metashoepite phase, after a preliminary aging in solution at 80°C, was equilibrated in solutions with $4 \leq pH_m \leq 6$. The solid phases isolated at the end of the solubility exper-

iments were washed, dried and characterized by means of different techniques including TRLFS. In this section, we will only describe the luminescence results obtained for the transformation product and the crystalline metashoepite reference.

TRLFS analyses were performed by using the 4th harmonic of a Nd:YAG laser (SpitLight Compact 100, InnoLas Laser) at 266 nm with 7 ns pulse duration as excitation source described in [7]. A pulse energy of 0.6 mJ and 10 Hz repetition rate were used for these experiments. Simultaneous control of the laser stability was possible by placing a beam splitter in the optic path and sending a part of the beam to a thermopile sensor (Newport Corporation). Depending on the ligand system, uranyl luminescence emission at room temperature can be very weak, e.g., for pure uranyl carbonate complexes, but easier to detect at liquid helium temperature [8-10]. Therefore, samples were prepared in small cupper holders with sapphire windows and introduced in the customized vacuum chamber of a He cryostat (CryVac), reaching temperatures down to 5.5 ± 1 K. In this instrument, the sample holder with a capacity for two samples is directly attached to the cold finger of the cryostat. Once the laser beam reaches the sample, the emitted luminescence is collected at 90° by a customized bundle-type fibre optic. The output of this fibre optic is coupled to the variable entrance slit of the Czerny-Turner spectrometer and recorded by the time-gated CCD camera mentioned in the previous section. During the experiments, a long-pass filter (10CGA-295, Newport) was inserted into the spectrometer to avoid the second-order diffraction of the laser stray light at 532 nm.

Figure 3 shows the emission spectra of the metashoepite and transformed metashoepite solid phases at 6 K. Luminescence bands of most solid or dissolved uranyl salts/minerals are found in the blue-green part of the spectrum; however, in many cases those bands are only clearly resolved at very low temperatures [11,12]. In the case of oxy/hydroxide minerals, e.g. metashoepite, broadening of the emis-
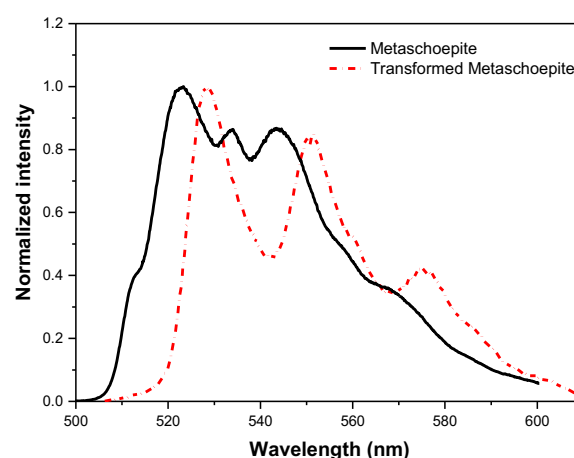

Fig. 3: *Luminescence spectra of metaschoepite (solid line), just after equilibration at 80°C, and transformed metaschoepite (short dash dot line) (T = 80°C, NaCl 5.6 M, pH_m 5, 1 year). Spectra measured at ~6 K, 1 µs delay, 1 ms gate width, 500 accumulations, $\lambda_{exc} = 266$ nm; 600 µJ/pulse.*

sion peaks due to quenching by OH⁻ groups and water molecules can be reduced at low temperature, improving the spectral resolution and increasing the spectral intensity. These improvements are also due to the reduction of the emission from thermally populated vibrational levels in the excited electronic state and the diminishing of energy losses due to the suppressed vibrations [10].

The acquisition shown in Figure 3 was performed with a 400 lines/mm diffraction grating. Spectral features typical for uranyl compounds can be observed in both spectra, including vibronic bands with specific peak spacing or peak maxima. In both cases the position of the spectral bands are red-shifted as compared to those from carbonate or phosphate uranyl minerals [13,14]. The spacing between vibronic bands corresponds to the symmetric stretching frequency of the O=U=O moiety [11]. This frequency is inversely correlated to the strength of the coordination of U(VI) with ligands in the equatorial plane. The ν_1 values measured here in both metaschoepite phases are between 720 and 780 cm^{-1}. Usually low symmetric stretching frequency values are associated with uranyl silicate and oxy/hydroxide minerals. This fact can be explained by the stronger ionic interaction of uranyl (hard acid) with anions with stronger basicity (larger pKa values) [14]. In addition, a bathochromic shift of ~5 nm of the position of the first-peak maximum is observed for the transformed metaschoepite. According to Gorobets et al. [15] an increase of the basicity of the molecules in the uranyl solvation or coordination sphere could induce a shift of the luminescence spectrum to low frequencies. The reason is a stronger chemical bond of the uranium atom with the ligand and a weakening of the U=O bond.

Luminescence lifetimes were also determined for the analyzed metaschoepite phases, obtaining in both cases a bi-exponential decay. In the case of the pristine metaschoepite the two decay components have lifetimes of (15.4 ± 0.3) µs and (81.8 ± 0.6) µs. For the transformed metaschoepite both lifetimes are shorter, (5.6 ± 0.8) µs and (63.2 ± 35.2) µs. This bi-exponential decay has been already observed for uranyl minerals at low temperature [13,14,16,17]. In the paper by Volodko et al. [16] the bi-exponential decay is explained as a redistribution of energy after excitation. Perry and Brittain [17] explain this observation by proposing two geometrically similar uranyl coor-

dination environments. Shorter lifetimes as observed for the transformation sample can be an indication for increased quenching in this phase.

These results together with complementary information obtained by XRD, quantitative chemical analysis and SEM-EDX suggest that a partial solid phase transformation of metashoepite occurred, leading to a solid phase different from metashoepite and characterized by a non-stoichiometric Na:U ratio.

References

[1] F. Heberling et al., in H. Geckeis et al. (eds.), INE Annual Report 2016, *KIT-Scientific Publishing KIT-SR 7743* (2017).

[2] M. Schmidt et al., *JCIS* **351 (1)**, 50 (2010).

[3] M. Schmidt et al., *Angew. Chem. Int. Ed.* **47**, 5846 (2008).

[4] P. Lindqvist-Reis et al., *Phys. Rev. B* **110**, 5279 (2006).

[5] M. Altmaier et al., *J. Chem. Thermodynamics* **114**, 2 (2017).

[6] F. Endrizzi et al., *J. Chem. Thermodynamics* 2018 (accepted).

[7] C. Garcia et al., in H. Geckeis et al. (eds.), INE-Annual Report 2016, *KIT Scientific Publishing KIT-SR 7743* (2017).

[8] R. N. Collins et al., *J. Environ. Qual.* **40**, 731 (2011).

[9] G. Geipel, *Coord. Chem. Rev.* **250**, 844 (2006).

[10] Z. Wang et al. *Environ. Sci. Technol.* **38**, 5591 (2004).

[11] E. Rabinowitch et al., International Series of Monographs on Nuclear Energy, Chemistry Division. Vol. 1. Spectroscopy and Photochemistry of Uranyl Compounds; New York Macmillan (1964).

[12] B. S. Gorobets et al., *At. Energiya* **36**, 6 (1974).

[13] Z. Wang et al., *Geochim. Cosmochim. Acta* **69** 1391 (2005).

[14] Z. Wang et. al, *Radiochim. Acta* **96**, 591 (2008).

[15] B. S. Gorobets et al., *At. Energiya* **42**, 177 (1977).

[16] L. V. Volod'ko et al., *J. Lumin.* **8**, 198 (1974).

[17] H. G. Brittain et al., *J. Phys. Chem.* **84**, 2630 (1980).

8.3 Microscopy and surface analytics

D. Schild, E. Soballa, M. Bouby, U. Kaplan, E. González-Robles, M. Herm

In co-operation with:

S. Brassines

ONDRAF/NIRAS, Belgian Agency for Radioactive Waste and Enriched Fissile materials, Geological Disposal, R&D, Avenue des Arts, 14, 1210 Bruxelles, Belgium

Introduction

Prolonged interim storage of spent nuclear fuel at surface facilities during decades is presently envisaged due to the search for a suitable site accepted by the public and construction of a qualified deep underground nuclear repository in Germany (cf. chapter 5.1). Integrity of fuel pins is essential until they are moved from casks for storage and transport (CASTOR®) to disposal casks. Fission gas and helium from alpha decay increase the pressure inside fuel pins. In addition, inner surfaces of Zircaloy claddings are exposed to volatile fission products causing corrosion during reactor operation and beyond. Pressure increase and degradation of Zircaloy by corrosion and irradiation damage may impact fuel pin integrity. A possible cladding attack at the inner surface is analyzed by scanning electron microscopy and energy dispersive X-ray spectroscopy (SEM-EDX) as well as X-ray photoelectron spectroscopy (XPS).

In addition to studies on Zircaloy-4 cladding material, dissolved organic matter (DOM) of a potential host rock is investigated. The Boom Clay formation in Belgium is investigated by ONDRAF/NIRAS for its potentiality of a deep underground nuclear waste repository. Dissolved organic matter may facilitate migration of radionuclides by complexation. DOM analyses by various techniques are described in chapter 5.3 of this annual report. In this chapter, size fractions of DOM were characterized by XPS.

Post-irradiation examination of the plenum section of a Zircaloy-4 fuel rod segment

In this study, the inner surface of a Zircaloy-4 ring segment of about 2×2 mm^2 from the plenum section was analyzed by XPS and SEM-EDX. At the plenum, where a spring holds the pellets in position, the compounds originating from the interaction between the

volatile fission products, which are released from subjacent nuclear fuel pellets, and the Zircaloy-4 cladding can be studied. The fuel pin was discharged in May 1989 after 1226 days of operation (1985-1989) in a commercial pressurized-water reactor (cf. chapter 5.1) [1]. The pin was stored gas tight until 2012.

XPS was performed by a ULVAC-PHI VersaProbe II spectrometer to characterize composition and chemical bonding of elements at the outermost atomic layers of the surface. Besides Zr of the cladding, C, N, O, Rb, Cs, Ba, Hg, and U were detected by survey spectra. Carbon (51-58 at%) is present due to adventitious hydrocarbon. Hg observed at a concentration up to 4.5 at% presumably originates from contamination inside the hot cells where the samples were prepared. Subsample preparation under oxic condition may have influenced the chemical state of alkaline and earth-alkaline elements or compounds. Rb up to about 7 at% is the most abundant fission product detected at the inner surface of the cladding at the plenum section. Narrow scans of elemental lines were recorded
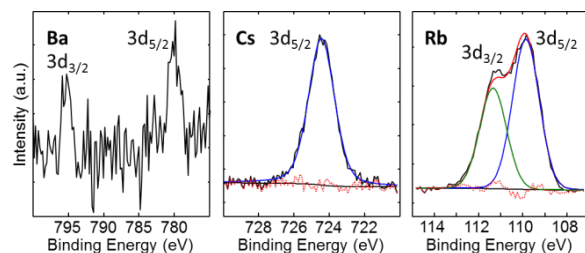

Fig. 1: *Narrow scans of elemental lines of the fission products Cs, Ba, and Rb. Binding energies are charge referenced to C 1s (C$_x$H$_y$) at 284.8 eV.*
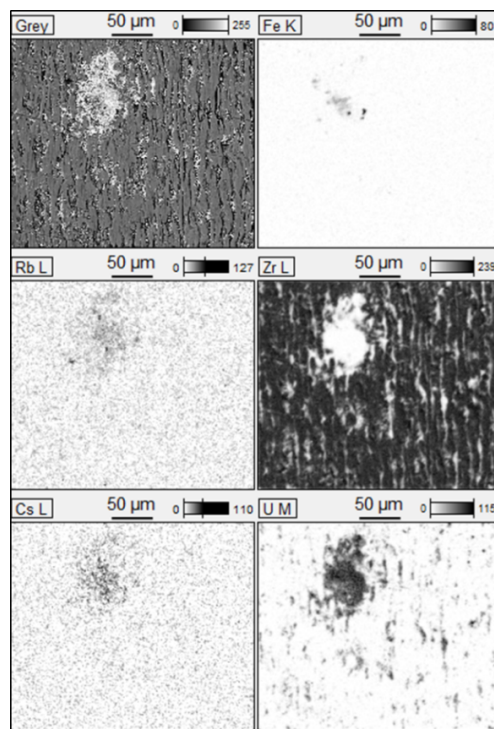

Fig. 2: *SEM backscattered electron image (Grey) of the inner surface at the gas plenum section of the cladding in combination with SEM-EDX elemental maps of Fe, Rb, Zr, Cs, U. Accelerating voltage 30 kV.*
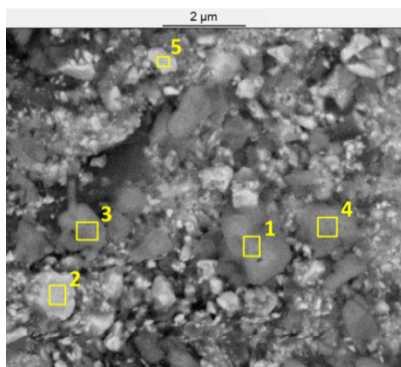
Fig. 3: *Backscattered electron image of an area at the inner surface of the gas plenum section covered by particles. Areas of SEM-EDX analyses are indicated by numbered boxes. Accelerating voltage: 10 kV.*
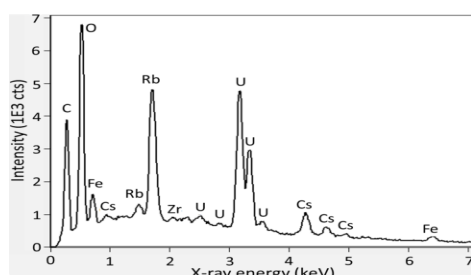

Fig. 4: *SEM-EDX spectrum of area #1, Figure 3.*

to characterize the chemical bonding and corrected for surface charging. The binding energy of the Rb $3d_{5/2}$ elemental line at 109.8 eV is assigned to Rb-O bonding (Figure 1). Rb metal in contact with humid air forms RbOH. The binding energy of Cs $3d_{5/2}$ at 724.4 eV is similar to the reported binding energy of CsOH (724.5 eV [2]). Alkali metal zirconates expected as corrosion products [3] could not be identified by XPS. The Ba $3d_{5/2}$ elemental line at 780.1 eV is close to the reference value 779.9 eV of BaO and $BaCO_3$ [2]. Narrow scans of the Zr 3d spectrum show the $3d_{5/2}$ elemental line at 182.4 eV binding energy, characteristic of ZrO_2 (ref. 182.2 eV [2]). U 4f spectra are composed of two components assigned to U(IV) and U(VI). The Hg $4f_{7/2}$ spectrum is fitted by two Gaussian functions at 99.6 eV and 101.3 eV assigned to Hg(0) and Hg(II), presumably HgO.

To increase lateral resolution, SEM-EDX was performed by a FEI Quanta 650 FEG instrument. The Zircaloy cladding sample was coated by a conductive carbon film to avoid surface charging during the analyses in high vacuum.

SEM-EDX elemental maps of Fe, Rb, Zr, Cs, and U are compiled in Figure 2 in combination with a backscattered electron image depicting material contrast. Bright areas at the backscattered electron image correspond to high *Z* elements. No contact with nuclear fuel was expected at the inner surface of the plenum section. However, individual fuel particles and particle agglomerations are observed at the oxidized cladding surface. The fuel particles are presumably remnants of filling UO_2 pellets into the Zircaloy-4 cladding during production. The elemental maps

exhibit enhanced concentrations of Rb and Cs at the fuel particle agglomerate. In addition, Fe is present at the area of the particle agglomerate but shows a different pattern. A potential source of iron may be wear debris from the austenitic steel spring located at the plenum gas section.

Analyses of individual particles were performed at accelerating voltage of 10 kV to minimize the excitation volume of characteristic X-rays (Figure 3). Particles of U-oxide (analysis areas #2, #5) and of Fe-(Cs,Rb)U-oxide (analysis areas #1, #3, #4) are observed. For example, a SEM-EDX spectrum of analysis area #1 is depicted in Figure 4. Since Rb is detected by XPS at higher concentrations than U and Zr at some analysis areas, a part of the Rb located in the plenum section is not bound to U-oxide or Zircaloy.

Hg was detected as a trace element by SEM-EDX which approves Hg as a surface contaminant.

Natural organic matter derived from Boom-Clay by XPS

In this study, XPS was used to characterize size fractions of dissolved organic matter derived from Boom Clay pore water [4] by ultrafiltration under anoxic condition: (1-10) kDa, (10-100) kDa, and > 100 kDa corresponding to a Stokes radius of about (0.8-2) nm, (2-7) nm, and > 7 nm, respectively. Filter cakes were rinsed with few µL of water to remove $NaHCO_3$. About 2 µL of resuspended filter cake was deposited and dried on aluminum foil for XPS analyses. In addition, a drop of dried Boom Clay pore water (EG/BS bulk) was analyzed by XPS for comparison.

Survey spectra and narrow scans of elemental lines were acquired by use of monochromatic Al K$_\alpha$ X-ray excitation (1486.7 eV) for determination of atomic concentrations and functional groups. In Figure 5,
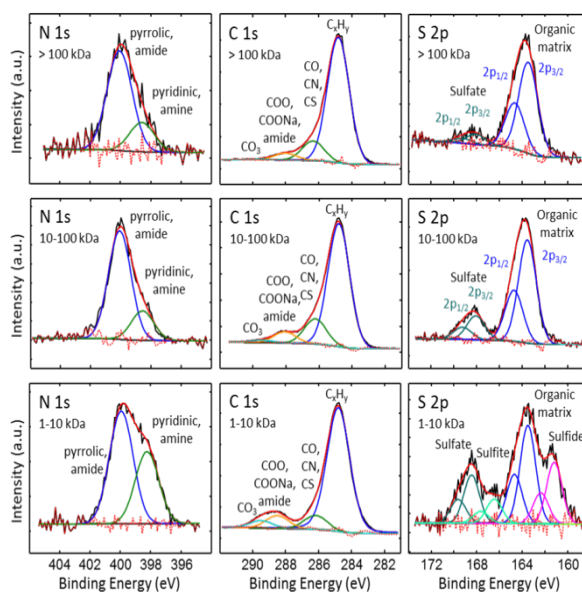

Fig. 5: *XPS narrow scans of N 1s, C 1s, and S 2p elemental lines, size fractions of > 100 kDa, (10-100) kDa, and (1-10) kDa (top to bottom) of EG/BS samples prepared under anoxic condition. Binding energies are charge referenced to C 1s (C_xH_y) at 284.8 eV.*

narrow scans of N 1s, C 1s, and S 2p elemental lines of the three size fractions are depicted with results of curve fits.

DOM of all size fractions is composed mostly of C and O. Elements at lower concentration are N (2-4 at%), Na (1-12 at%), and S (< 1 at%). The O/C ratio of atomic concentrations is about 0.34 ± 0.03 at the small size fraction (1-10) kDa and 0.2 ± 0.03 for size > 10 kDa. The higher value of O/C is assigned to a higher carboxyl concentration, as well indicated by the relative intensity of COO at the C 1s elemental line (Figure 5). Even if the O/C ratio of DOM is influenced by oxygen bound at inorganic compounds, it remains useful in case of purified DOM. An alternative to determine O/C ratios is determination of the ratio of carbon bound as carboxyls to total carbon, since the carboxylic line at the C 1s spectrum is superposed by possible amide only, at low concentration. The [COO]/[C_{tot}] ratio, i.e. percentage of COO area by curve fit of C 1s, does not take into account oxygen bound at inorganic compounds, CO bonds, and hydrate. The [COO]/[C_{tot}] ratio can serve as indicator of the oxidation state in case of natural DOM since alcohols oxidize to carboxyls. In case of the > 100 kDa size fraction this ratio is 4.3 %, at the mean size fraction (10-100 kDa) 6.7 %, and at the small size fraction (1-10 kDa) 7.7 %. Slow oxidation of organic colloids in deep underground pore water results in hydrophilic carboxyls which may be preferably located at the surface of colloids. Since XPS has an information depth comparable to the size of small colloids, the different ratios may be explained by the higher surface-to-volume ratio for smaller colloids compared to larger ones. The small size fraction may have a higher portion of carboxyls per volume available for radionuclide complexation and thus, in combination with the small size of the colloids, possess a higher potential for radionuclide migration. However, migration is additionally influenced by electrical charges at surfaces of colloids and pore volumes.

Actinide ions can be complexed either by carboxyls or N-donor ligands. The nitrogen N 1s elemental line is composed of at least two components. A component at 398.3 eV binding energy is assigned to pyridine and amine, and another one at 400.0 eV is assigned to pyrrole and amide (Figure 5). A potential nitrate N 1s elemental line in the range of (407-408) eV was not detected. In the small size fraction, the relative amount of pyridine and amine at the N 1s elemental line appears enhanced. However, the molar concentrations of pyrrole and amide are diminished while pyridine and amine concentrations are slightly enhanced.

The concentrations of sulfur in the samples are low, representing less than 1 at%. The S 2p spectrum consists of two components; each component was fitted by a doublet according to the spin-orbit splitting of S 2p into $2p_{1/2}$ and $2p_{3/2}$, Δ 1.18 eV, and spin-orbit splitting ratio 1:2 (Figure 5). The S $2p_{3/2}$ elemental line of the main component at about 163.4 eV is assigned to sulfur bound to the organic matrix. The less intense component with S $2p_{3/2}$ at about 168.1 eV is
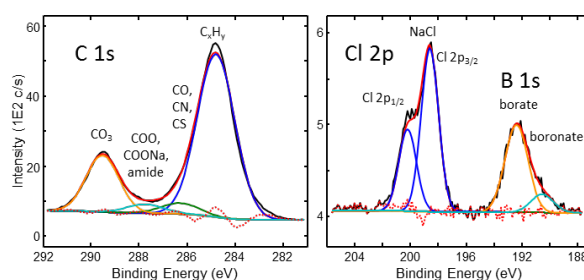

Fig. 6: *Narrow scans of C 1s, Cl 2p, and B 1s elemental lines of dried EG/BS bulk with the result of curve fits.*

assigned to sulfates. In the small size fraction, (1-10 kDa), two additional components with S $2p_{3/2}$ at around 166.5 eV characteristic of sulfites, and at 161.3 eV assigned to sulfides are observed. DOM may decompose under anaerobic conditions in presence of sulfate-reducing bacteria [5] which use the sulfates present to oxidize the DOM, producing hydrogen sulfide as by-product. This hydrogen sulfide can react with metal ions present to produce metal sulfides, such as Fe(II)-sulfide, which is one of the redox sensitive species that could interact with redox sensitive radionuclides but also be directly incorporated in DOM [6].

The dried Boom Clay pore water (EG/BS bulk) sample contained a high concentration of carbonate, i.e. $NaHCO_3$ (Figure 6). In addition, boron at low concentration is detected. The Cl 2p spectrum is shown in Figure 6 to verify B 1s assignment since Cl 2p can have similar binding energy values as B 1s for certain compounds, but in this case, also the Cl 2p doublet signature must be present which is not observed. On the other hand, P 2s may have similar binding energy like B 1s, but P 2p was not detected. The B 1s spectrum consists of two components, the first at 190.6 eV binding energy (area 17%, 0.2 mol%) characteristic of boronate, and a second at 192.4 eV (area 83 %, 0.9 mol%) typical for borate, e.g. borax ($Na_2B_4O_7*10H_2O$). Total boron concentration in EG/BS bulk is (6-9)E-4 M [7]. If inorganic boron concentration is higher than 0.04 M, trivalent actinides may become immobilized by formation of borate-bearing solid phases with low solubility [8].

References

[1] Metz, V. et al., *KIT-SR 7639*, KIT Scientific Publishing, Karlsruhe, 117 (2013).

[2] Moulder, J.F. et al., *Handbook of X-ray Photoelectron spectroscopy*, ULVAC-PHI, Inc., Japan, (1995).

[3] Kohli, R.; *Thermochim. Acta* **65**, 285 (1983).

[4] Bruggeman, C. et al., *SCK•CEN-ER-206*, Mol, Belgium, (2012).

[5] Aerts, S.; *SCK•CEN-ER-75, Mol, Belgium, (2009).*

[6] Einsiedl, F.; *Environ. Sci. Technol.* **42**, 2439 (2008).

[7] De Craen, M. et al., *SCK•CEN-BLG-990*, Mol, Belgium, (2004).

[8] Hinz, K. et al., *New J. Chem.* **39**, 849 (2015).

8.4 Structural investigations on radioactive materials in solution by NMR-Spectroscopy

C. Adam, N. Adam, P. J. Panak

In co-operation with:

J. Pfeuffer-Rooschüz[a], A.-L. Ditter[a], M. Keskitalo[b]

[a] Heidelberg University, Heidelberg, Germany; [b] Faculty of Chemistry, University of Helsinki, Helsinki, Finland

Introduction

In case of the accidental release of radionuclides into the environment, incorporation into the human organism is one of the main risks. Due to their long half-lives, inherent radiotoxicity and chemical toxicity, transuranium elements are of particular concern. Knowledge of the overall toxicokinetics of actinide (An) ions in the human body and the exact mechanisms of the distribution throughout the body is very scarce. Especially the interaction of actinide ions with blood serum proteins is relevant here, as many metal ions as well as other substances are transported by transport proteins [1-2].

Proteins are not only responsible for the distribution of substances through blood vessels, but are also active in transporting substances into cells. Transport proteins such as transferrin and human serum albumin (HSA) form complexes with a variety of different metal ions. HSA is the most abundant protein in human blood [3], and thus the elucidation of binding mechanisms with An(III) ions is of high relevance for a general understanding of An(III) transport in humans as well as tailored decorporation agents.

Human Serum Albumin

In the human body, HSA is the main contributor to the colloid-osmotic pressure in blood, together with different globulines. It is a water-soluble protein that consists of 585 amino acids and has a molecular weight of 66.5 kDa. The protein is divided in three identical homogeneous subunits (I-III), each consisting of two sub-units A and B, overall, 67% of the tertiary structure is an α-helix [5-7]. Most coordination sites are located in sub-units IIA and IIIA. This includes seven different coordination sites for fatty acids, in addition to binding sites for billirubin and haem in sub-unit IB. Binding sites for the transport of metal ions have been identified by spectroscopic and crystallographic methods. HSA has a high affinity for Cu^{2+}, Zn^{2+}, Cd^{2+}, Co^{2+} and Ni^{2+} [4, 8-12]. These metals have different affinities to three identified binding sites that have been visualized in table 1. Cu^{2+} binds most strongly to the N-terminal binding site (NTS), also referred to as ATCUN-site (Amino-Terminal Cu and Ni Binding Site). This site includes the final amino acids at the N-terminus of the protein. The Multi-metal Binding Site (MBS) is a very versatile binding site for many different metal ions. The exact position of the third binding site, Site B, in the protein structure has so far not been identified.

In our earlier studies, we examined the complexation of Cm(III) and Eu(III) with HSA using time-resolved laser fluorescence spectroscopy (TRLFS) [13]. Results from competition experiments with Cu^{2+} and Cm^{3+} suggest that the ATCUN-site is the preferred binding site for An(III) in HSA.

To study the complexation of metal ions by HSA, two sets of experiments were performed: Firstly, the complexation of native HSA with different metal ions was studied. Secondly, we used the tripeptide (DAH, abbreviation for aspartic acid, alanine and histidine) that is crucial for the binding at the N-terminal site as a surrogate for the intact protein.

NMR on protein molecules is a very demanding task due to the overlap of the multitude of signals. However, previous work on HSA by Bos and Labro includes a partial assignment on signals from the N-terminal site, especially of the signals from histidine residues that bind directly to the metal ions (Figure 2) [14-15].

Fig. 1: *Structure of HSA.*

Tab. 1: *Affinity of the three binding sites in HSA for different ions. Darker shades of green represent higher affinities (from [4]).*

Ion	NTS	MBS	Site B
Cu(II)			
Zn(II)			
Co(II)			
Ni(II)			
Cd(II)			
V(IV)			

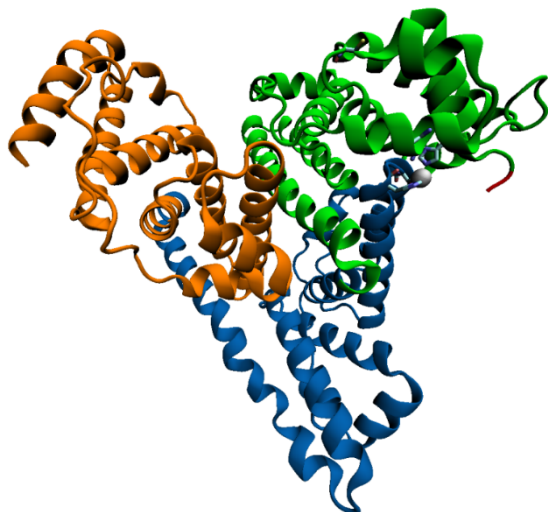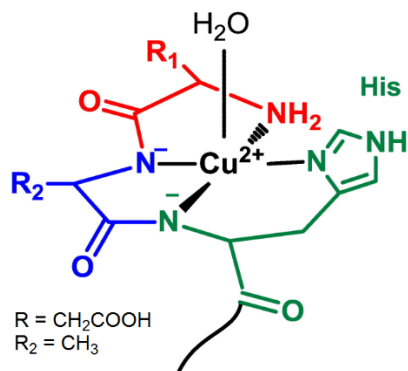**Fig. 2:** *Structure of the ATCUN binding site with coordinated Cu^{2+} in HSA.*

In NMR spectroscopy, deuterated solvents are used to minimize the solvent signal in proton spectra. However, this will lead to the exchange of protons e.g. from amide positions and rapidly exchanging proton positions in the side chains of amino acids. This phenomenon can only be overcome by the use of non-deuterated water. To provide a deuterium signal for the internal field lock of the spectrometer, 10% D_2O was added to the TRIS or HEPES buffer solutions that are used to stabilize the pH. As this will lead to a strong solvent signal and thus decreased resolution and intensity of the protein signals due to the limited dynamic range of the spectrometer, solvent suppression was essential for the measurement of the spectra. We achieved this by use of the WATERGATE pulse sequence [16-18].

In a first step, we reproduced the work of Bos and Labro to identify the relevant histidine signal in our spectra. This assignment was confirmed by pH titrations showing that the chemical shift dependence of the NMR signal we identified as the histidine signal corresponds to the reported values [14-15].

After that, we performed NMR titrations of the HSA

with Eu^{3+} and Am^{3+}.

NMR titrations of HSA

Bos and Labro identified a signal at 7.5 ppm (at pH 7.7) as the C-H signal of the histidine side chain at the N-terminal binding site (*cf.* Figure 2), which we also found in our spectra [14-15]. Upon titration with Cu^{2+}, which has a high affinity for the NTS, this signal disappears, as would be expected: Both paramagnetic relaxation enhancement and chemical shifts resulting of the change in electronic structure contribute to the so-called "bleaching" of the ^{1}H NMR signal.

In titrations of native HSA with solutions containing Eu^{3+} and Am^{3+} the same disappearance of the histidine proton signal was observed. This result indicates an involvement of the histidine group in the binding of lanthanide and actinide ions.

However, in titrations with Co^{2+} and Ni^{2+}, which have lower affinities for the NTS, the histidine signal is bleached. An explanation for this is that both ions have a non-zero affinity for the NTS and coordination takes place at the MBS as well as at the NTS. Still, even with Cd^{2+}, which according to literature does not bind at the NTS, the signal at 7.5 ppm decreases. A viable explanation for this is that in the crowded ^{1}H spectrum the resonance signals of more than one histidine residue from different bindings sites overlap.

While this last finding admittedly impedes the interpretation of the results, it does show that both actinide and lanthanide ions are coordinated by HSA. This is a first prerequisite for the involvement in a relevant transport pathway in the human organism and encourages further research on this complicated system.

NMR titrations of DAH

To overcome the crowded spectra of the HSA, we used the tripeptide DAH as a surrogate for the ATCUN binding site. We performed titrations of DAH
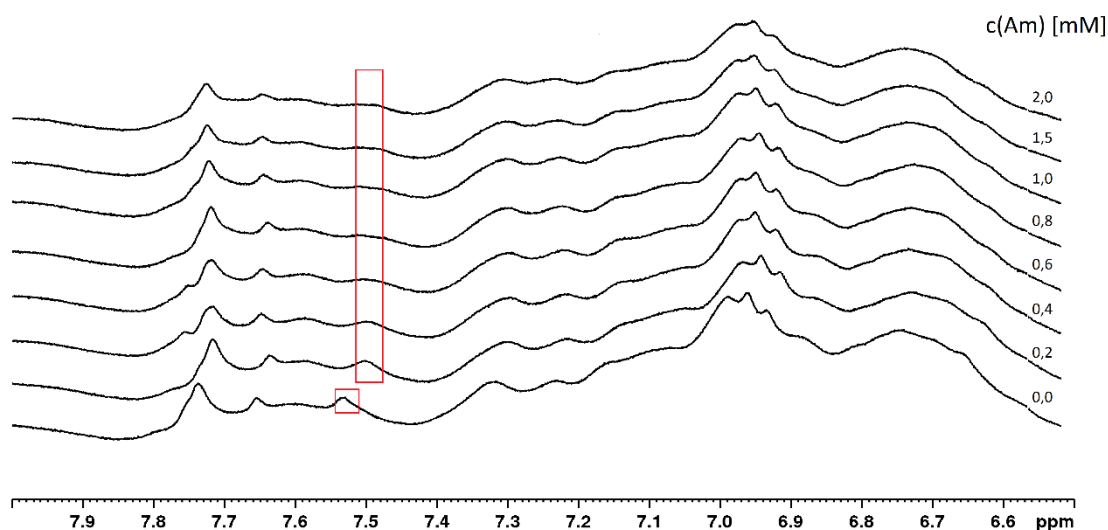

Fig. 3: *Histidine region of the ^{1}H WATERGATE spectra of HSA during the titration with Am(III) at pH 8.0 and T = 298 K. HSA concentration was 0.1 mM, the buffer solution contained 10 % D_2O. The histidine signal marked in red disappears during the titration, indicating coordination of Am(III) in the protein. The chemical shift difference in the first titration step is due to very slight pH inconsistencies.*
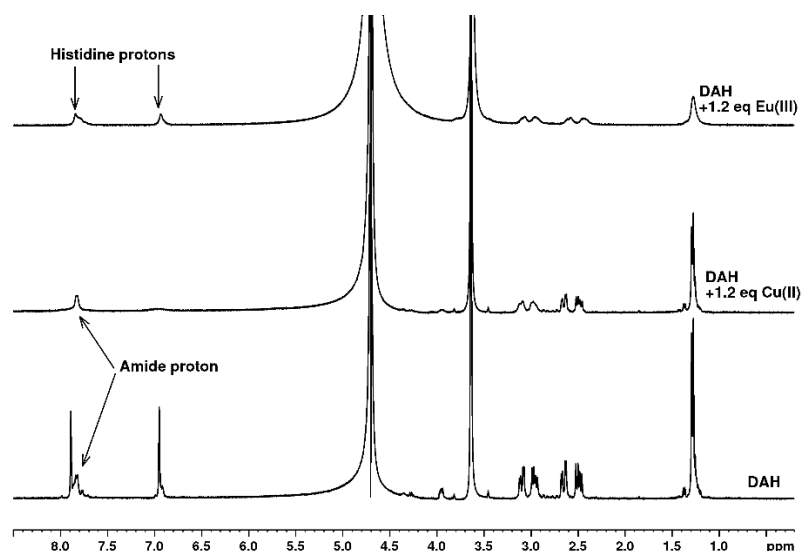
Fig. 4: *Comparison of the ^1H WATERGATE spectra of free DAH (bottom), and after addition of 1.2 eq. Cu(II) (middle) or Eu(III) (top) at pH 7.7. While Cu(II) complexation influences the histidine protons stronger than the rest of the protons in HSA, the effect of Eu(III) addition is uniform.*

with Eu^{3+} and Cu^{2+} to compare the influence of metal ion coordination on the NMR spectra (Figure 4).

The spectra of HSA with equal metal concentrations show differences between Cu^{2+} and Eu^{3+}. In the Cu^{2+} complex both histidine protons disappear due to strong paramagnetic relaxation enhancement. In contrast, in the Eu^{3+} titration all signals are broadened uniformly, *i.e.* the integral ratio of signals from different parts of the molecule does not change. This difference indicates that Cu^{2+} is complexed by the tripeptide while Eu^{3+} seemingly does not coordinate to the tripeptide at all.

However, it is still unclear if DAH is a good model substance for the ATCUN site. Probably, the next amino acid, lysine (K), also takes part in metal coordination at this specific site as already suggested in the literature [19]. Furthermore, the strong influence of the bulk protein is neglected by this model approach.

This work shows that NMR can be used to study metal ion complexation even in systems as complex as proteins. The approach to combine NMR measurements, that offer insight into the observed system from the ligand or protein molecule, and TRLFS with its outward view from the metal ion, shows encouraging results even for highly complicated systems.

In a next step, we will study the metal coordination by a modified (recombinant) HSA that does not have the aspartic acid residue at the N-terminal site.

References

[1] E. Ansoborlo, et al., *Biochimie, 88:* 1605-1618 (2006).

[2] J. Duffield, et al., in *Handbook on the Physics and Chemistry of the Actinides* (Eds.: A. J. Freeman, C. Keller), Elsevier Science, Amsterdam, **1991**.

[3] *Pschyrembel Klinisches Wörterbuch*, 266 ed., De Gruyter, **2014**.

[4] W. Bal, et al., *Bba-Gen Subjects, 1830:* 5444-5455 (2013).

[5] D. C. Carter, et al., *Science, 249:* 302-303 (1990).

[6] X. M. He, et al., *Nature, 358:* 209-215 (1992).

[7] S. Sugio, et al., *Protein Eng, 12:* 439-446 (1999).

[8] D. Bar-Or, et al., *Eur J Biochem, 268:* 42-47 (2001).

[9] J. P. Laussac, et al., *Biochemistry-Us, 23:* 2832-2838 (1984).

[10] J. Lu, et al., *Biochem Soc T, 36:* 1317-1321 (2008).

[11] M. Rozga, et al., *J Biol Inorg Chem, 12:* 913-918 (2007).

[12] A. J. Stewart, et al., *P Natl Acad Sci USA, 100:* 3701-3706 (2003).

[13] Adam, N. et al., in preparation

[14] O. J. M. Bos, et al., *J Biol Chem, 264:* 953-959 (1989).

[15] J. F. A. Labro, et al., *Biochim Biophys Acta, 873:* 267-278 (1986).

[16] R. T. McKay, *Annu. Rep. NMR Spectrosc., 66:* 33-76 (2009).

[17] M. Piotto, et al., *J. Biomol. NMR, 2:* 661-665 (1992).

[18] V. Sklenar, et al., *J. Magn. Reson., Ser A, 102:* 241-245 (1993).

[19] P. J. Sadler, et al., *Eur J Biochem, 220:* 193-200 (1994).

8.5 Accelerator mass spectrometry (AMS)

F. Quinto, M. Plaschke, Th. Schäfer, H. Geckeis

In co-operation with:

[a]*Th. Faestermann,* [a]*G. Korschinek,* [a]*P. Ludwig*

[a]Physics Department, Technical University of Munich, James-Franck-Straße 1, D-85748 Garching, Germany.

[b]*K. Hain,* [b]*P. Steier*

[b]VERA Laboratory, Faculty of Physics, University of Vienna, Währinger Straße 17, A-1090 Vienna, Austria.

Introduction

In situ tracer tests allow to study the partitioning of radionuclides (RNs) among environmental compartments in real and complex natural conditions. The Grimsel Test Site (GTS) in Switzerland offers geochemical conditions representing a possible scenario of glacial meltwater intrusion into a repository for high-level radioactive waste in granitic host rock. At the GTS, four *in situ* tracer tests (CRR run 1 and 2 and CFM 12-02 and 13-05) were performed in the last 15 years, involving the injection of RNs and bentonite colloids in a groundwater (GW) conductive fracture. A further experiment (LIT) focused of the diffusion of actinide (An) nuclides and ^{99}Tc through a bentonite cylinder placed in a fracture. Because of obvious radiation protection constrains, only low activities of RN tracers could be employed. As a consequence of that, the RN tracers could be initially determined only in GW samples in which their concentration was above the detection limits (DL) of the employed analytical technique, Sector Field - Inductively Coupled Plasma Mass Spectrometry (SF-ICPMS). Such samples were confined to a period of one month from the starting of the experiment and did not allow, therefore, the analysis of a long-term (years and decades) migration or retention of the RNs [1].

The difficulty in determining low levels of long-lived RNs in the environment translates into the difficulty to determine their long-term behavior in *in situ* experiments. The sensitivity of a mass spectrometric technique towards a certain nuclide is greatly affected by its capability of background suppression. In the analysis of the An, the detection of ^{239}Pu and ^{237}Np is hindered by the tailing from the strong directly neighboring peak of ^{238}U. At the same time, the molecular isobaric background from ^{238}UH and ^{235}UH hampers the determination of ^{239}Pu and ^{236}U. In the analysis of ^{99}Tc, not only the background from the molecular isobar ^{98}MoH must be taken into account, but also the one from the atomic isobar ^{99}Ru. Accelerator mass spectrometry (AMS) is characterized by the acceleration of the ions to MeV energies and the stripping process, providing both the destruction of molecular isobaric background, and a strong reduction of tailing interferences. Atomic isobaric background in the mass range of ^{99}Tc can be suppressed with the use of a Gas-Filled Analyzing Magnet System (GAMS) placed

before the ionization chamber detector at the 14 MV Tandem AMS facility of TUM (Garching) [2]. With such features, AMS is presently one of the most sensitive analytical techniques for the determination of An and ^{99}Tc in environmental samples. In fact, AMS can achieve abundance sensitivities for ^{236}U, ^{237}Np and ^{239}Pu relative to ^{238}U at levels $\leq 10^{-15}$ and DL for An nuclides at a value of ca. 10^4 atoms per sample (corresponding to ca. 4 ag) [1]. The sensitivity for ^{99}Tc is at the level of ca. 3×10^6 atoms per sample (corresponding to ca. 0.5 fg). In the following paragraph, we discuss the recent findings obtained with AMS in the study of the long-term behavior of the An and ^{99}Tc in *in situ* tracer tests, and we describe the new ongoing experiments motivated from those findings.

Study of the long-term behavior of actinides and ^{99}Tc in *in situ* radionuclide tracer experiments

The analytical procedure for the determination of ^{99}Tc with AMS was validated with the analysis of aliquots of a ^{99}Tc standard solution (GE Healthcare Limited Product code: TCZ44) and aliquots of the reference material IAEA 443, as depicted in Fig. 1.

^{99}Tc was chemically separated from the IAEA 443 samples by using TEVA® resin and the obtained results were in agreement with the literature value.

The long-term diffusion of An and ^{99}Tc through a bentonite barrier is being studied in the frame of the in situ LIT experiment. In Fig. 2, the number of atoms of ^{99}Tc determined in four GW samples, 1.5 ml each, are depicted as a function of the time from the starting of
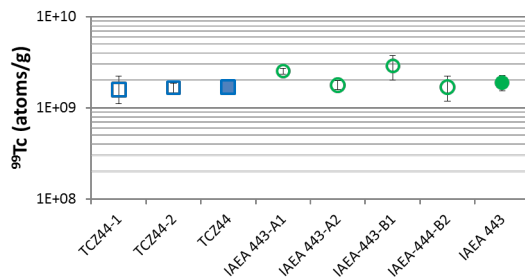
Fig. 1: *Concentration of ^{99}Tc in two samples of a reference ^{99}Tc solution (blue empty squares) and in four aliquots of the Reference Material IAEA 443 (green empty circles). The corresponding nominal values are represented with a full blue square and a full green circle, respectively.*
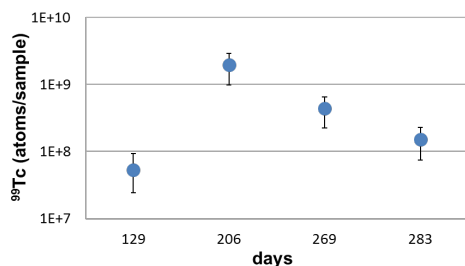
Fig. 2: *Concentration of ^{99}Tc in four samples of the LIT experiment.*

Fig. 3: *Concentrations of ^{233}U (yellow), ^{237}Np (red), ^{242}Pu (grey), ^{244}Pu (violet), ^{243}Am (blue) and ^{241}Am (green) in the Grimsel groundwater samples of CFM run 13-05 at the peak of the breakthrough curves (a) and along the entire duration of the experiment (b) measured with AMS.*

the experiment. Levels of ^{99}Tc from ca. 5×10^7 to 3×10^9 atoms/ml can be determined in the analyzed samples, accounting for an experiment duration from ca. 4.3 to 9.4 months.

In the frame of the *in situ* test CFM run 13-05, we have demonstrated the possibility for long-term *in situ* studies over a time span of more than a decade. In addition to the employed tracers, ^{233}U, ^{237}Np, ^{242}Pu and ^{243}Am, also An with masses 241 and 244 u were detected and we proved that they can be attributed to a release of ^{241}Am and ^{244}Pu from the fracture injected 11 years before within the previous *in situ* tests CRR run 2 [3]. The six An nuclides were determined with AMS over eight orders of magnitudes in sample sizes of 0.1 to 250 g. A concentration maximum of $(3.71 \pm 0.04) \times 10^{10}$ atoms/g (ca. 15 pg/g) of ^{242}Pu was found after 1.5 days from the starting of the experiment, while a concentration minimum of $(3 \pm 1) \times 10^2$ atoms/g (ca. 0.8 ag/g) of ^{241}Am was determined at the sampling time of 518 days. While ^{241}Am and ^{244}Pu were exclusively employed in CRR run 2, ^{233}U, ^{237}Np, ^{242}Pu and ^{243}Am were used in more than one test before CFM 13-05. The concentration of the An nuclides before the arrival of the GW containing the injection cocktail of CFM 13-05 originate from the previous *in situ* tests [3]. Even though AMS does not provide any speciation analysis of the An, the results depicted in Fig. 3 allow some considerations on their geochemical behavior. The concentrations of ^{237}Np, ^{242}Pu and ^{243}Am in the samples after the peaks (Fig. 3b) are lower than those preceding it (Fig. 3a). The opposite trend is observed for ^{233}U. We hypothesize that this difference reflects a stripping of Pu and Am from the fracture via binding to bentonite colloids. Np(V) and U(VI) preferentially exist as aquo species. However, Np could undergo a partial reduction to Np(IV), followed by adsorption/precipitation in the shear zone and onto the bentonite colloids [3].

In order to verify such hypothesis, a new *in situ* test has been carried out at the GTS, in which GW containing bentonite colloids but no RNs was injected into the fracture. The observation of a maximum in the concentrations of ^{242}Pu, ^{244}Pu, ^{241}Am, ^{243}Am and, possibly ^{237}Np, in correspondence to the arrival of the colloid peak would support the hypothesis of a stripping of these An through sorption onto benton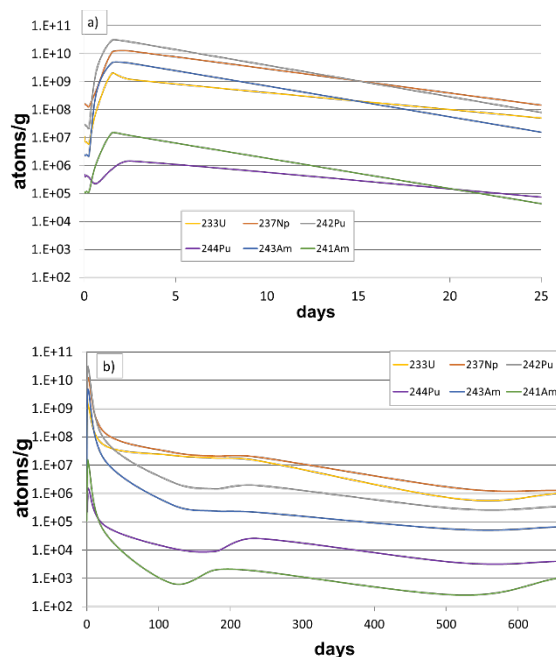ite colloids after they were retained several years in the granodiorite fracture. The analysis of samples from this remobilization experiment is presently ongoing.

In the frame of another project carried out in collaboration with the Institute for Geological Science of the University of Bern, the An nuclides released by the atmospheric testing of thermonuclear devices (1951 – 1980 CE) are analyzed in GW samples from the GTS. GW shows in various locations of the GTS different percolation and retention patterns. The age of such GW can be determined with the measurements of its tritium, ^{3}H, activity ($T_{1/2}$ = 12.32 y). In this way, GW samples older than the nuclear age as well as contemporary or subsequent to the period of the atmospheric nuclear weapon tests can be selected. The detection of global fallout derived An in the recent GW samples would testify their mobility over several decades through the environmental and geological system of the GTS.

Knowledge of the environmental behavior of long-lived An and fission products is prerequisite for a safe management and final disposal of nuclear waste. In this context, the analytical capability of AMS allows the direct study of such RNs at ultra-trace levels in long-term *in situ* tests as well as in the general environment.

References

[1] Quinto, F. et al., *Anal. Chem.*, **87**, 5766-5773, (2015).

[2] Koll, D. et al., submitted to Nucl. Instrum. Methods Phys. Res., Sect. B.

[3] Quinto, F. et al., *Anal. Chem.*, **89**, 7182-7189 (2017).

8.6 Computational chemistry

B. Schimmelpfennig, M. Trumm, R. Polly

Introduction

Computational Chemistry using ab initio, first principle and classical mechanics methods at KIT-INE provides valuable insights on a molecular scale, greatly assisting and complementing experimental investigations in the field of nuclear waste disposal. There is a wide range of applications for Computational Chemistry at INE: from providing detailed structures of complex chemical systems including actinides in solution, at surfaces or incorporated in solid phases, thermodynamic data, spectroscopic information for TRLFS or reproducing actual experimental XAFS spectra, to performing simulations and visualization of complex chemical reactions. Hence, the considered systems vary from molecular species in the gas phase over small complexes in solution to bulk phases or mineral/liquid interfaces at ambient conditions.

New theoretical methods and the constantly improving hardware allow a steadily increasing precision of the description of actinide systems at the electronic structure level. These improvements also increase the accuracy and reliability of quantum chemistry as a predictive tool.

Quantum chemical investigation of the Selenite incorporation into the calcite $(10\bar{1}4)$ surface

Selenium is a common pollutant in soils and aquifers. The radioisotope ^{79}Se, an abundant fission product of ^{235}U, is of particular concern in the context of nuclear waste disposal safety due to its long half-life and its expected high mobility in the multi-barrier system around potential nuclear waste disposal sites. Oxidized selenium species are relatively soluble and show only weak adsorption at common mineral surfaces. However, a possible sorption mechanism for selenium in the geosphere is the structural incorporation of selenium(IV) (selenite, SeO_3^{2-}) into calcite ($CaCO_3$).
We carried out a detailed quantum chemical study of the incorporation of SeO_3^{2-} into the calcite surface and the subsurface layers.
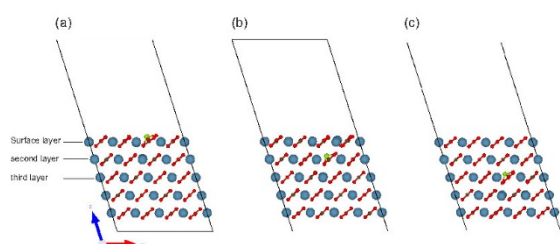
As the main result [1] we present the structural changes upon incorporation of selenite (SeO_3^{2-}) into the dry and hydrated calcite $(10\bar{1}4)$ surface. For the dry surface, we add results for the incorporation into the subsurface layers. These results are complemented by energetic considerations and in turn used to estimate the thermodynamic partition coefficient **D** for SeO_3^{2-} incorporation into the surface and subsurface layers. The results corroborate the recently proposed entrapment model for selenium(IV) coprecipitation with calcite [2] and show that equilibrium incorporation of selenite into calcite may occur in the surface layer, but is practically impossible in subsurface layers or the bulk.

The incorporation energies calculated accordingly may be transformed into excess free energies [2] (see eq. (10) to (16) therein) and allow to approximate for each layer a thermodynamic partition coefficient **D**. **D** relates the selenite/carbonate ratio in the solid to the selenite/carbonate ratio in the aqueous contact solution, and thus provides a good basis to discuss the practical implication of the layer by layer increase of the incorporation energy. First of all, the theoretical partition coefficient for the hydrated surface (**D**=0.005, Fig. 2) is in fair agreement with the experimentally determined value (**D** = 0.02±0.01) [2]. The subsequent layer by layer increase of the incorporation energy may seem as a smooth transition from the surface towards the bulk. However, looking at the values in terms of partition coefficients, it becomes clear that, while at the surface considerable selenite incorporation is possible (**D**$_{1st\ layer}$~10^{-2}), from the first to the second layer there is a jump in the partition coefficient about seven orders of magnitude (**D**$_{2nd\ layer}$~10^{-9}), which means that already in the 2nd layer

Fig. 1: *Incorporation of selenite SeO_3^{2-} into the dry $(10\bar{1}4)$ surface and subsurface layers of calcite. (a), (b) and (c) show the incorporation into the surface, the second and the third layer, respectively (Ca: blue, O: red, C: brown, Se: green).*
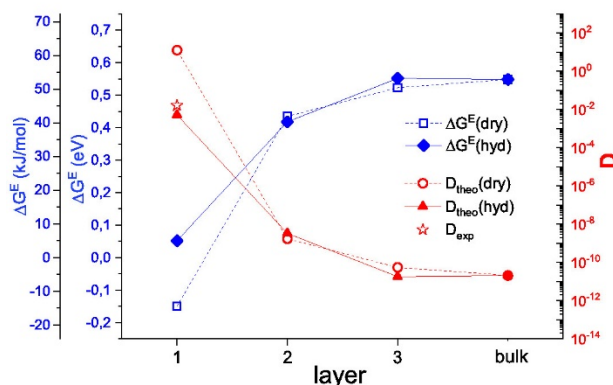

Fig. 2: *Relative incorporation energies ΔG_{incorp} and thermodynamic partition coefficient **D** of selenite SeO_3^{2-} into the dry and hydrated $(10\bar{1}4)$ surface and subsurface layers and the bulk phase of calcite*

Tab. 1: *Internuclear distances and charges of the AnO_2^{2+} species.*

	UO_2^{2+}	NpO_2^{2+}	PuO_2^{2+}
R	173.4 pm	172.6 pm	170.0 pm
charge An	3.41	3.36	3.28
charge O	-0.70	-0.68	-0.64

Tab. 2: *Contributions of atomic orbitals to the bonding σ- and $\pi_{x,y}$-orbitals in AnO_2^{2+}.*

	UO_2^{2+}		NpO_2^{2+}		PuO_2^2	
	c_u	c_o	c_u	c_o	c_u	c_o
σ	0.53	0.70	0.55	0.68	0.57	0.67
$\pi_{x,y}$	0.38	0.80	0.38	0.81	0.38	0.81

there is practically no more selenite incorporation possible at thermodynamic equilibrium. The further decrease in partition coefficient from 10^{-9} to 10^{-11} in layer three and bulk is hardly of practical relevance. The sudden drop in the partition coefficient from the first to the second layer, however, is the key to corroborate the previously proposed entrapment mechanism [2]. Especially the interpretation in terms of entrapment energy, previously used to estimate the supersaturation level necessary to drive entrapment, gains now relevance as it is demonstrated that the free energy related to a certain surface composition rises abruptly when this surface is buried under an additional layer of calcite.

Covalence in UO_2^{2+}, NpO_2^{2+} and PuO_2^{2+}

We studied the covalence of the triple bonds in UO_2^{2+}, NpO_2^{2+} and PuO_2^{2+} using localized molecular orbitals. Orbitals are by no means defined uniquely and localized molecular orbitals in theoretical chemistry match best to orbitals as understood by experimental chemists. Therefore, we rely on localized molecular orbitals in this study.

In Tab. 1 we show the structural parameters R (determined with CASPT2/ANO-RCC-DZ) and the corresponding charges of the AnO_2^{2+} ions. The decrease of the charges at the An and O ions show that the An-O bonds are getting more covalent when moving from U to Pu, although the An 5f orbitals are supposed to shrink with increasing nuclear charge.

In Tab. 2 we show the sum of the MO coefficients at the An and O atoms, which give a direct measure of the contribution of the An and Oxygen to the molecular orbital. As can be seen from the data in Tab. 2 the covalence of the σ-bonds increase when going from U to Pu whereas the $\pi_{x,y}$-bonds remain virtually unchanged. With this we find that the reason for the increasing covalence is the change of the bonding in the σ-orbitals formed by the $5f_\sigma$ and $2p_z$ orbitals of the An and xygen, respectively.

Chemistry and thermodynamics of actinides and fission products in aqueous solution

Higher order multipole interactions

Polarization effects have been proven to play an important role in the theoretical description of chemical processes. Commonly the inclusion of polarization into atomic models is accomplished by a point-multipole development on the atom centers. The multipole expansion of the energy function offers important insights in the electrostatic interaction of a system. Induced dipoles are commonly considered when analyzing classical interactions. This study focused on the anisotropic part of induced dipoles as well as on induced quadrupole interactions in trivalent lanthanide and actinide complexes [3,4].

Dipole polarizabilities are often computed as numerical second derivative of the energy for ions with a mostly single-reference ground state. Throughout the Ln(III) and An(III) series, however, multi-configurational effects often dominate the ground state and appropriate methods should be applied. Due to the computational demands of sophisticated wave-function based methods, literature values for most heavy ions have been obtained on the Hartree-Fock or Dirac-Fock level of theory. To properly account for multi-configurational and relativistic effects as well as correlation, we have performed CASPT2 calculations using a second order Douglas-Kroll-Hess (DKH) Hamiltonian. The CASPT2 dipole and quadrupole polarizabilities are collected in figures 4 and 5. All determined An(III) dipole and quadrupole polarizabilities proved to be larger compared to their Ln(III) counterparts. Especially within lighter elements following La and Ac, the ratio between the polarizabilities is significant. Determined dipole polarizabilities agree well with values found in literature. Dipole-quadrupole polarizabilities are negligibly small and close to zero within the uncertainty of the method
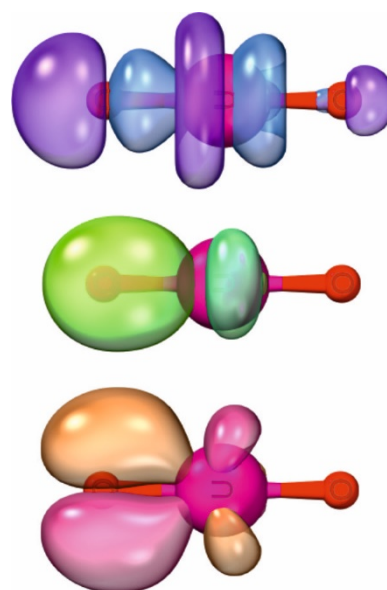

Fig. 3: *Bonding localized σ- and $\pi_{x,y}$-orbitals in UO_2^{2+}*

employed. Quadrupole polarizabilities show the same trend as the dipole polarizabilities with Th(III) being the most polarizable (1.34 $Å^5$), comparable to a value of 1.56 $Å^5$ obtained for Cs(I). Determination of the induced multipole moments for various An(III) and Ln(III) complexes revealed anisotropic contributions of up to 50% in some cases, whereas quadrupolar interactions are mostly negligible. In some asymmetric structures, however, we find the quadrupoles to account for as much as 30 kJ/mol of the total binding energy (cf. Fig. 6).
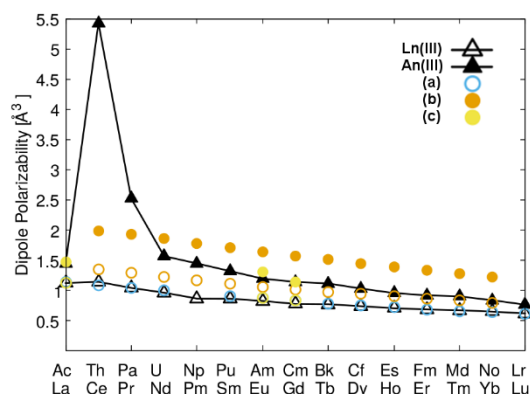

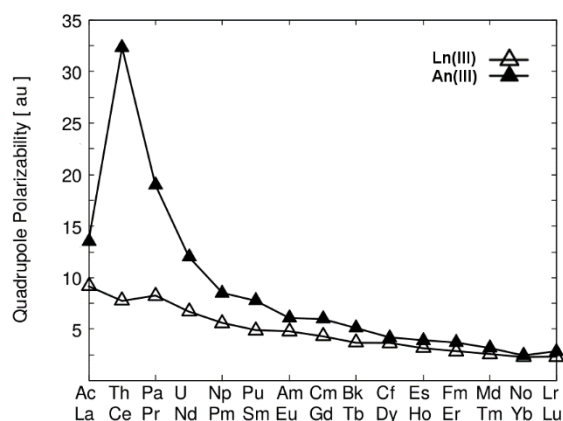**Fig. 4:** *CASPT2 dipole polarizabilities of trivalent lanthanides and actinides*

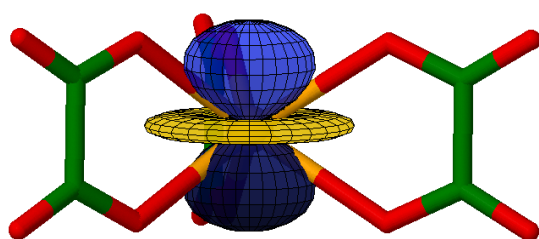**Fig. 5:** *CASPT2 quadrupole polarizabilities of trivalent lanthanides and actinides*

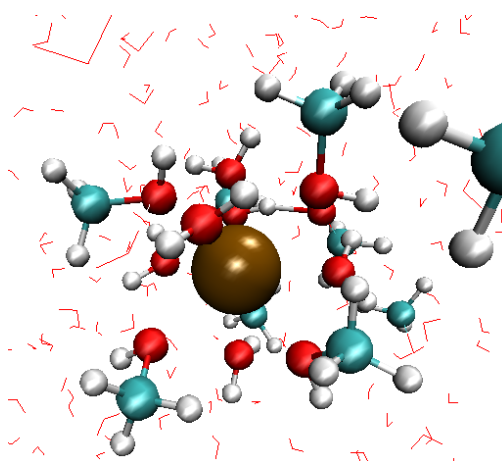**Fig. 6:** *Electronic quadrupole moment in the [Cm(oxalate)_3]^{3-} complex.*

Fig. 7: *Snapshot of the first Cm(III) hydration shell from the MD simulation*

Cm(III) in binary H_2O/MeOH mixtures

The aqueous solutions of repository relevant ions is of great importance not only for a fundamental understanding of the ions' chemistry. Hence, the Cm(III) aquo ion (amoung others) has been the center of interest of earlier studies at INE [5,6]. Bremer et al. [6] presented TRLFS measurements in different H_2O/MeOH ratios observing a shift of the main emission band from 594.3 nm at 50% water content to 599.1 nm at 1.5% water content. In this study the intrusion of methanol molecules in the first hydration shell of Cm(III) was suggested as possible explanantion.

In order to investigate this system closer, an MD force field to describe H_2O/MeOH mixtures has been created [7]. Remaining parameters for the Cm/MeOH interaction have been adjusted to reproduce the quantum chemical reference energies. Subsequent MD simulations based on the force field suggest that even at 50% water content 4-5 MeOH molecules are present in the first hydration shell (see Fig. 7). By increasing the MeOH concentration the computed coordination number of Cm(III) drops from 9 to 8. Hence, we attribute the shift in the TRLFS to a drop in coordination number rather than the intrusion of methanol based on the findings of Lindqvist-Reis et al. [8] who determined a TRLFS shift of about 4 nm between the 9- and 8-fold coordinated Cm(III) aquo ions.

UV-Vis and core-excitation spectroscopy of actinide compounds

The number of unpaired electrons and their electromagnetic interaction including spin-orbit coupling are computationally demanding for actinides and their compounds. In a two-step procedure with quasi-degenerate perturbation theory of spin-orbit coupling as the second step the number of states to be treated can reach several hundreds. In the employed MOL-CAS software package the extended Multistate CASPT2 method (XMS-CASPT2) was recently implemented and allows to treat such complicated sys-

tems as the actinides without artificial symmetry broken solutions where artificial energy splitings may be of the order of ligand field effects. The approximate treatment of post-Hartree Fock contributions leads to deviations from experiment in the order of up to 0.1 eV. Further benchmark studies and likely even modifications of the employed atomic mean-field spin-orbit approach are needed to reliably extend the approach to electronic states with core holes. Including a first coordination shell is computationally still demanding and current approximate schemes are tested on actinide model systems for applicability in order to reduce required CPU-time without significant loss of accuracy.

References

[1] Polly, R, Hebeling, F., Schimmelpfennig, B., Geckeis, H., *J. Phys. Chem.* 121 (37), 20217 (2017)

[2] Heberling, F., Vinograd, V.L., Polly, R., Gale, J.D., Heck, S., Rothe, J., Bosbach, D., Geckeis, H., Winkler, B., *Geochimica et Cosmochimica Acta* 134, 16-38 (2014).

[3] M. Trumm, *J. Comp. Chem.*, accepted (2017).

[4] A. Holt et al., *J. Comp. Chem.* 31, 1583-1591 (2010).

[5] F. Réal et al., J. Comp. Chem., 34, 707-719 (2013)

[6] A. Bremer et al., *New J. Chem.* 39, 1330-1338 (2015)

[7] M. Trumm et al., *Mol. Phys.*, accepted (2017)

[8] Lindqvist-Reis et al., *J. Phys. Chem.* 109, 3077-3083 (2005)

9 (Radio-)chemical analysis

The radio-analytical unit provides competences in radio-analytical procedures, well-trained personal and state-of-the-art analytical techniques for the INE R&D projects and third parties collaborations. Routine and advanced instrumentation is available both in radioactive and cold labs. Our special skills are in handling of radioactive material, separation procedures for element and isotope analysis, as well as operation and maintenance of glove box adapted instrumentation. These capabilities are also beneficial for external clients, e.g., in the fields of decommissioning of nuclear installations, nuclear waste declaration or nuclear pharmacy. Analytical techniques are adapted and improved with a special focus on mass spectrometry for trace element analysis and speciation studies of actinides and fission products. Hyphenated techniques, like Sector Field (SF)-ICP-MS or Collision Cell Quadrupole (CC-Q)-ICP-MS coupled to species sensitive methods, e.g., to capillary electrophoresis (CE) or ion chromatography (IC), enables redox speciation and solubility studies of actinides and fission products. We develop new methods in Accelerator Mass Spectrometry (AMS) for the supersensitive determination of actinides below ppq levels and ^{99}Tc at the ppq levels in ground-, surface and seawater in collaboration with external AMS facilities (see chapter 8.5 for further details). Method development is also integrated in research projects, e.g. in the context of decommissioning or large-scale field experiments. In addition, the analytical unit supports the INE infrastructure, is involved in various teaching activities and is responsible for education of chemical laboratory assistants.

M. Plaschke, A. Bauer, M. Böttle, M. Bouby, M. Brandauer, N. Cevirim-Papaioannou, N. Finck, D. Fellhauer, M. Fuss, J. Gaona Martinez, A. Geist, F. W. Geyer, F. Heberling, F. Huber, A. Kaufmann, T. Kisely, S. Kraft, S. Kuschel, J. Lützenkirchen, C. M. Marquardt, S. Moisei-Rabung, U. Müllich, F. Quinto, F. Rinderknecht, E. Rolgejzer, P. Salee, T. Schäfer, D. Schild, A. Seither, W. Tobie, C. Walschburger, and H. Geckeis

In co-operation with:

Z. Nie[a], K. Hanna[b], R. Marsac[c], C.-O. Krauß[d], A. Heneka[d], S. Gentes[d] and P. Steier[e]

[a] College of Chemistry and Molecular Engineering at the Beijing University, Beijing, China; [b] ENSCR – ISCR UMP CNRS 6226, Rennes France; [c] Géosciences Rennes – UMR CNRS 6118, Rennes, France, [d]Department of Deconstruction and Decommissioning of Conventional and Nuclear Buildings, Institute for Technology and Management in Construction (TMB), Karlsruhe Institute of Technology (KIT), [e]VERA Laboratory, Faculty of Physics, University of Vienna, Währinger Straße 17, A-1090 Vienna, Austria

Instrumentation

In Table 1 the wide spectrum of analytical techniques available at INE is listed. Many of the techniques are operated both in cold and radioactive labs. The amount of routinely analyzed samples is growing year after year with over twenty thousand samples in the reporting period. We provide the data mainly for the INE R&D projects but also for commercial analytical services. Our routine instrumentation is continuously modernized, e.g., in 2017 our technicians have designed the adaptation of a new Q-ICP-MS (Perkin Elmer NEXION 2000) to a glove box for handling of radioactive material. Such new analytical instrument will start operation in 2018.

Inter-laboratory comparison

The use of Certified Reference Materials (CRMs) is necessary in order to control the performance of analysis techniques, to answer to quality systems and accreditation tests as well as to validate new analysis methods and equipment. The first CRM for ^{243}Am is jointly produced by EC-JRC and CEA and named ^{243}Am-CRM or IRMM-0243; its certification process is under course and the first inter-laboratory comparison (ILC) exercise concluded in July 2017. The INE radio-analytic group is part of the array of international laboratories participating in the certification process. In the frame of the first ILC, the determination of the following measurands was required: ^{243}Am, ^{241}Am and total Am content (mol/kg), $n(^{241}Am)/n(^{243}Am)$ and $n(^{242m}Am)/n(^{243}Am)$ ratio (mol/mol). As the results of our lab cannot be presented before the final ILC report is published, we describe here the two analytical methods chosen for the determination of the total Am content by using SF-ICP-MS. With method 1, ^{241}Am and ^{243}Am contents were obtained with a standard addition of a ^{243}Am reference solution (Eckert und Ziegler) to the ^{243}Am-CRM (5 replicate samples). With method 2, ^{243}Am and ^{241}Am contents were directly measured by an external calibration with ^{238}U Standard Material SLRS-6. In both methods, the total Am (mol/kg) was obtained summing up ^{241}Am and ^{243}Am. It is important to note that in method 2, the estimate of the total Am is independent from the ^{241}Am/^{243}Am of the pure ^{243}Am-CRM. The deviation of the replicate samples determined with method 1 and 2 is depicted in Fig. 1. It can be seen how the measurement results of method 1 are more sparsely distributed than those of method 2 with a maximum deviation of ca. 1.7%. However, the average values of the total Am content and of the ^{241}Am/^{243}Am amount ratio obtained with the two methods are, within their statistical uncertainties, consisted with each other and differ by only the 0.54% and 0.48%, respectively, revealing a high degree of precision.
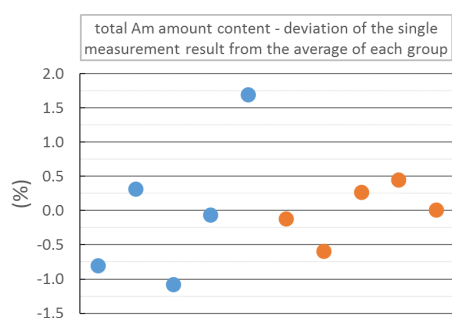
Fig. 1: *Deviation [%] of total Am of the replicate samples from the average values. Blue and orange circles indicate the replicate samples analyzed by SF-ICP-MS with methods 1 and 2, respectively (see text).*

Tab. 1: *Analytical techniques available at INE*

Elemental and Isotope Analysis
Quadrupole Inductively Coupled Mass Spectrometry (Q-ICP-MS)
Collision Cell Q-ICP-MS (CC-Q-ICP-MS)
Sector Field ICP-MS (SF-ICP-MS)
Inductively Coupled Optical Emission Spectrometry (ICP-OES)

Nuclear Spectroscopic Methods
Alphaspectrometry
Liquid Scintillation Counting (LSC, conventional/high sensitivity)
Gammaspectrometry (with auto-sampler)

Other Methods
Ion Chromatography (IC) for cations and anions
Gas Chromatography (GC)
Carbon Analysis (TOC, DOC, TIC, NPOC)
Specific Surface Area Analysis (BET)
Differential Thermal Analysis (DTA)
Dilatometry
Fusion and Microwave Digestions
Gravimetry and Titrations

Analytical service for external clients

Analytical service is offered to external clients on the basis of formal contract agreements, e.g. in the fields of nuclear waste declaration or nuclear pharmacy.

Nuclear pharmacy

A ^{223}Ra containing alpha-radiopharmaceutical (Xofigo®) is routinely analyzed since more than four years for *Bayer* (www.pharma.bayer.com) with regard to toxic heavy metal trace impurities. In 2017/2018 a new co-operation in this field with the Norwegian company *Oncoinvent AS* (www.oncoinvent.com) is envisaged. The ^{224}Ra containing radiopharmaceutical Radspherin® is a novel alpha-emitting microsphere designed for treatment of metastatic cancers in body cavities. The first clinical studies will be in the treatment of ovarian cancer [1].

Nuclear waste treatment and decommissioning of nuclear facilities (KTE-HDB)

We analyze routinely since more than 20 years radio-active waste and decommissioning samples from the KTE-HDB (since 2017 Kerntechnische Entsorgung Karlsruhe GmbH, Hauptabteilung Dekontaminationsbetriebe, HDB) to obtain isotope concentrations

and nuclide vectors, mainly for waste declaration. Samples are obtained from different facilities, namely ashes (incineration facility), LAW liquid concentrates (evaporation plant), annually averaged samples (different waste treatment facilities), samples from decommissioning of nuclear facilities (e.g., demolition waste) and others (e.g., wipe tests). The analyzed nuclides include neutron activation and fission products (^{55}Fe, ^{63}Ni, ^{90}Sr), as well as actinides (^{233,234,235,236,238}U, ^{238,239,240,241,242}Pu and $^{242,243+244}$Cm). In 2017 our activities in this area were successfully audited.

Analysis for INE R&D

In the following, selected INE R&D topics are highlighted from the analytical perspective.

Uranium(IV) solubility studies

Uranium is the main actinide (An) element present in nuclear fuel and accordingly contributes with the largest inventory to the nuclear waste. U(IV) prevails under strongly reducing conditions, forming the sparingly soluble UO_2(am, hyd) that defines [U] $< 10^{-8}$ M above pH $\approx$ 5. In the context of the BMWi project EDUKEM, the present work focusses on the solubility and hydrolysis of U(IV) in dilute to concentrated saline systems and pH-E_h conditions relevant for nuclear waste disposal. A U(IV) stock solution was prepared by electrochemical reduction of U(VI) in 1.0 M HCl, and precipitated as UO_2(am, hyd) at pH $\approx$ 12 under reducing conditions. Undersaturation solubility experiments with UO_2(am, hyd) were performed in 0.1 M–5.0 M NaCl, 0.25–4.5 M $MgCl_2$ and $CaCl_2$ solutions with (pH$_m$ + pe) $\approx$ 2 and $1 \leq$ pH$_m \leq$ 14.5. Concentration of uranium, pH$_m$ and E_h were measured at regular time intervals until attaining equilibrium conditions. Because of the very low concentrations of U (under weakly acidic to hyperalkaline pH conditions) and the high salt content, both standard and micro-flow-injection (μFI)-ICP–MS were used for the quantification of [U]$_{tot}$ in solution after 10 kD ultrafiltration. Figure 2 exemplarily shows UO_2(am, hyd) solubility data in 0.1 M NaCl solutions within with $2 \leq$ pH$_m \leq$ 13, as quantified using standard and μFI-ICP–MS. Red line in figure 2 is calculated with the preliminary thermodynamic model derived in the present work. Using μFI-ICP–MS sample dilution factors can be reduced and, therefore, markedly lower detection limits (DL) are achieved compared with standard sample injection (Fig. 2). Attaining lower U concentration ranges improves our understanding of the U(IV) solution chemistry and allows the development of more reliable source terms for U(IV) under conditions relevant for nuclear waste disposal.

Selenium migration experiments

In order to test a newly developed adsorption model for SeO_3^{2-} and Sr^{2+} co-adsorption on goethite [4], Se migration experiments in goethite coated sand filled columns were performed. Columns were filled with 15 g sand providing $0.7 - 1.7$ m^2/g reactive surface area, a total column volume of 9 mL and a porosity in
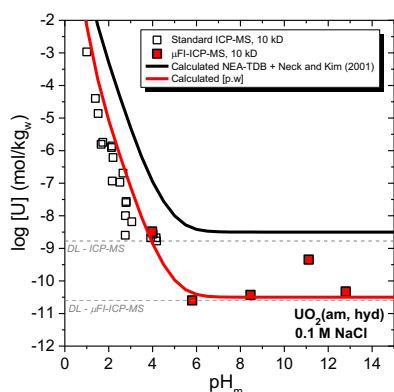
Fig. 2: *Solubility of UO$_2$(am, hyd) in 0.1 M NaCl as quantified by standard and µFI-ICP–MS. Red and black lines calculated with thermodynamic data derived in this work and reported in references [2] and [3], respectively (see text).*
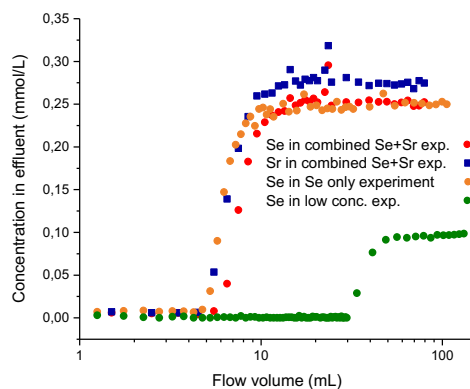

Fig. 3: *Se and Sr breakthrough curves as determined by CC-Q-ICP-MS, from migration experiments with goethite coated sand filled columns (see text).*
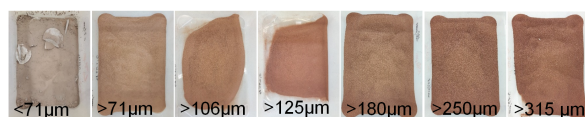

Fig. 4: *Optical images of the sieved abrasive grain fractions (red-brown and grey color represent abrasive and steel grains, respectively).*

the filled column of 42%. In the combined Se+Sr experiments (red dots and blue squares in Fig. 3), the inflow solution (0.5 mmol/L NaCl, pH 6) contained 0.25 mmol/L SeO$_3^{2-}$ and Sr^{2+}. In the Se-only experiment (orange dots) conditions were equivalent, but no Sr was added. In the low concentration experiment (green dots) the inflow solution (10 mmol/L NaCl, pH 4) contained only 0.1 mmol/L Se. The results in figure 3 show that the presence of Sr slightly retards the Se transport through the column (orange and red dots), as expected due to the electrostatic adsorption amplification [4]. At lower pH (and lower Se concentration, green dots), the Se dwelling time in the column strongly increases. Se is determined on mass 78 by CC-Q-ICP-MS with a He/H$_2$ mixture as collision cell gas allowing an efficient suppression of the mass

interference caused by the Ar plasma gas and DL in the range of 1 µg/L.

Extraction chemistry

The coordination chemistry group performs solvent extraction studies, mainly in support of the EURATOM GENIORS program. These studies require determining concentrations of both radionuclides (RN) and inactive metallic species in organic and aqueous phase samples. Analyses are typically performed by gamma and alpha spectrometry and by ICP-MS. Recently, approximately 600 µg ^{248}Cm were recuperated from waste solutions from TRLFS experiments collected over many years. The huge separation and purification efforts were constantly monitored by combining the analytical methods ICP-MS, LSC and alpha spectrometry.

Bio-ligands and -surfactants in remediation studies

We are presently investigating the RN and lanthanides (Ln) sorption properties of a naturally abundant nanomaterial compound extracted from wood. We investigate in parallel the RN/Ln de-complexation/extraction properties of bio-macromolecules known as metallophores [5] to solid waste matrices and we compare the results with those obtained by using a recently newly developed bio-surfactant. The challenge of the analytical measurement lies in the complexity of the investigated organic matrices, i.e. the bio-surfactant, which is a concentrated, viscous and highly foaming substance. A measurement protocol considering the complex matrices and suppression of relevant mass interferences in ICP-MS was developed and applied to large sample series in the frame of a kinetic study.

Large-scale field experiments

In the course of the Colloid formation and Migration experiment (CFM) at the Grimsel Test Site (GTS) two experimental foci were followed in 2017. The first one consists in the monitoring of a bentonite source including the isotopes ^{45}Ca, ^{75}Se, ^{99}Tc, ^{137}Cs, ^{233}U, ^{237}Np, ^{241}Am and ^{242}Pu and the conservative tracer Amino-G. The source was emplaced in the shear zone in May 2014 for the better understanding of real *in-situ* conditions in a bentonite-based geotechnical barrier (so-called **L**ong term **I**n situ **T**est, LIT). The second focus is on the investigation of the migration/retention behavior of colloid-associated RN under hydraulically well controlled advective flow conditions thanks to the CFM mega-packer.

In the previous migration experiments with bentonite derived clay nanoparticles, a sorption reversibility kinetics (see, e.g., [6] and references therein) and a significant colloid filtration were observed. In particular, a colloid/nanoparticle recovery of only 38 ± 3% in Run 13-05 was determined with ICP-MS of Ni-labelled montmorillonite and LIBD nanoparticle detection. Therefore, a moderate reverse circulation test was performed applying hydraulic "shocks" which are

expected to remobilize colloids and associated RN immobilized at the fracture walls (REMO-I test). An extraction flow in the former injection borehole BO-MI 87.010-i2 with 5 ml/min was established and two short hydraulic shocks/stimuli with 58 ml/min and 192 ml/min were performed. Higher or longer shocks were avoided to prevent any hydraulic disturbance in the LIT experiment, which was monitored by measuring hydraulic gradients across the LIT boreholes. The analytical results show very low colloid remobilization with a maximum concentration of 30 ppb and average size of 212 nm under the highest stimulus. A second remobilization test was performed injecting Grimsel groundwater with bentonite colloids into the fracture. In the frame of this test, named REMO-II, the bentonite colloids would provide a new surface for the fractions of RN not recovered in previous *in situ* tests, determining in this way their desorption from the fracture. However, first results of REMO-II revealed that direct recovery by extraction was not feasible and the colloid plume was sampled from the Pinkel surface packer. The two remobilization tests are presently under evaluation and additional AMS ultra-trace analysis of An and ^{99}Tc are in progress (cf. chapter 8.5 and [7]).

Decommissioning projects

The project MASK aims at the development and optimization of a separation technique for the reduction of the amount of activated secondary waste produced by waterjet cutting during the deconstruction of nuclear facilities (for more details cf. chapter 7 and [8]). In 2017 a technical-scale separation device has been designed and partially mounted, especially in view of a future operation in radioactive conditions. Inactive abrasive/steel grain mixtures were produced by cutting various steel alloys commonly used in nuclear reactors. The steel content of several grain size fractions (obtained by sieving) was quantified by ICP-OES measuring the alloying component Ni as tracer. It was found that the < 125 μm grain size fractions contain > 95% of the total steel in the grain mixture (Fig. 4). Knowledge of the grain mixtures is indispensable in order to adapt the separation process and to develop new strategies to further reduce the remaining steel content in the abrasive fraction.

References

[1] Westrøm, S. et al., *Nucl. Med. Biol.*, **51**, 1 (2017).

[2] Guillaumont, R. et al, Update on the Chemical Thermodynamics of Uranium, Neptunium, Plutonium, Americium and Technetium, Vol. 5 of Chemical Thermodynamics. Elsevier Science Publishers, Amsterdam, 2003.

[3] Neck, V. et al, *Radiochim. Acta*, **89**, 1 (2001).

[4] Nie, Z. et al., *ES&T*, **51**, 3751 (2017).

[5] Kraemer, S.M. et al., *Aquatic Geochemistry*, **21(2-4),** 159 (2015).

[6] Huber, F.M. et al., *Geochim. Cosmochim. Acta*, **148,** 426 (2015).

[7] Quinto, F. et al., *Anal. Chem.*, **89**, 7182 (2017).

[8] Krauß, C.-O. et al., *Best Paper Award*, KONTEC Dresden, 22.-24. März 2017.

10 Radiation protection research

Radiation Protection Research at KIT-INE deals with assessing radiation exposures by estimation of doses from external radiation fields and with effects of ionizing radiation on materials. The basis for research is the recording and evaluation of radiation exposures by sources of natural and artificial origin. In particular, mixed photon, beta and / or neutron radiation fields are investigated, with simulations contributing to a deeper understanding of the radiation fields. During 2017, research activities have been focused on experimental and numerical simulations of shielding / transmission properties of concrete in the context of interim storage of high-level waste and on the performance of a High Purity Ge detector. Close collaborations are established with national and internationals partners in networks such as the expert group "Dosimetry" (AKD) from the German-Swiss Fachverband für Strahlenschutz e.V. and the European Radiation Dosimetry Group (EURADOS).

10.1 Investigation of shielding/transmission properties of concrete and influence of structural inhomogeneity

F. Becker
in co-operation with:

D. Köhnke[a], M. Reichardt[a], H. Budelmann[a]
[a]*Technische Universität Braunschweig, Institut für Baustoffe, Massivbau und Brandschutz, Materialprüfanstalt für das Bauwesen (iBMB), Braunschweig*

Introduction

For reinforced concrete shielded buildings a few cases occurred where an underestimation of the shielding effect has been observed. In these cases, the observations were in contradiction to structural engineering predictions i.e. they were not consistent with the shielding properties expected from theoretical calculations. In addition, some publications on shielding investigations also report discrepancies between (theoretical) literature values and measurement results. Since concrete is a building material which is designable for specific requirements like for radiation protection in interim storage facilities for high-level waste and in surface facilities of deep geologic repositories, different concretes were investigated with respect to radiation shielding and mechanical/structural properties in an interdisciplinary approach.

At iBMB different concrete samples were prepared consisting of the following concrete types: normal concrete (Ordinary Concrete), hematite concrete, and baryte concrete, as well as a micro-reinforced and self-compacting high-performance concrete. Several samples were investigated with computer tomography (CT). At KIT experiments and simulations concerning gamma ray transmission were realized. The present report focuses on the first results obtained for normal concrete ("N concrete") and hematite concrete ("H concrete").

Experiments

At iBMB four different types of concrete plates each with a width and height of about 8 cm with a thickness of 16 mm were prepared. In addition to normal and hematite concrete samples, denoted as "N" and "H", respectively, normal and hematite concrete samples were synthesized with certain imperfections during the concrete production process. Normal and hematite

concrete samples with imperfections were denoted as "NF" and "HF", respectively. Artificial imperfections in these plates were realized through poking little rods in the freshly poured concrete without sufficient compaction afterwards. In consequence several defects remained in the hardened NF and HF samples.

Independent of the particular type of aggregates each concrete mixture was designed in order to achieve comparable volumetric amounts of water, cement and aggregates. Therefore, the target volume fraction of the hydrated cement including pores was 30 % and the aggregates should take 70 % of volume by design. The maximum aggregate size of gravel was 16 mm, in contrast to the smaller hematite crystal diameter of 5.6 mm. The measurement of each aggregate size distribution showed good agreement with the grading curves according to DIN EN 206-1 [1].

Gamma-ray transmission measurements were performed with a set-up of three plates of the same concrete type for the four concrete types (i.e. triples of N, NF, H and HF plates). Collimated gamma ray beams from a Cs-137 source were directed onto different positions of the concrete plates by means of a lead collimator (8 mm diameter hole in a 48 mm thick lead brick). The transmission of mono-energetic gamma radiation (Cs-137, $E_\gamma = 662$ keV) was determined from spectra recorded by a high-purity Germanium detector. In each case, five measuring points were determined on the N, NF, H, and HF concrete plates. The measuring points on the concrete plates are indicated in figure 1. The measuring points 1 to 4 are located each 2 cm from their two nearest edges of the plate and point 5 is in the center.

For detecting the exact positions of local imperfections, the samples were scanned at iBMB using cone beam microcomputer tomography (µCT) with 200 kV, 350 µA and a focus object distance of about 420 mm resulting in a voxel size of 103 µm for the
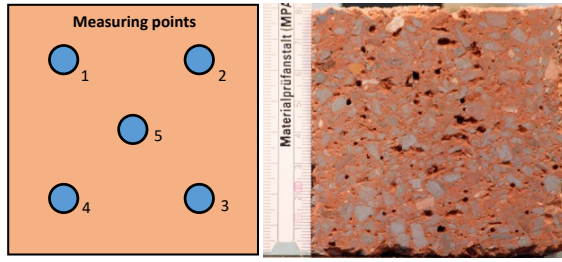
Fig. 1: *Front view of a concrete plate with the position of the different measuring points and a corresponding photo of a hematite concrete plate.*
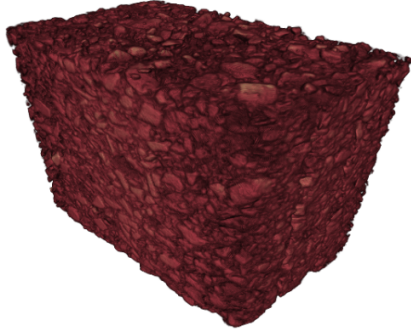

Fig. 2: *Three dimensional projection of the data from µCT for hematite concrete (sample H4-6).*

reconstructed image data. Every scan was done with three plates to reduce the total µCT-scan-time. To ensure the comparability of the data all concrete types were scanned and reconstructed with the same parameters. Figure 2 shows the visualized image data of one of the scans with hematite concrete.

For the comparison of the inner structure of the different concretes with the gamma ray transmission measurements, five Regions of Interest (ROI) with respect to the size of the collimator were extracted at the positions of the measurement points.

For a comparison with Geant4 simulations [2] further transmission experiments were performed in order to determine transmission curves. For this purpose, concrete plates made of the same material were lined up and measured with the same measuring setup as before. For the Geant4 simulations, a suitable model of the measurement setup, consisting of gamma radiation source, corresponding concrete plates and germanium detector, was generated. The material composition of the concrete and density was provided by iBMB. As in literature a wide range of densities is given e.g. in reference [3] and the density is supposed to be one of the crucial parameters, the densities were determined experimentally by means of underwater weighing at iBMB.

The gamma spectra produced by the Monte Carlo simulations were evaluated in the same way as the measured spectra.

Results

Figure 3 shows the resulting position-dependent transmission values for triple concrete plates of the composition N, NF, H, and HF. The measurement results, at a first look, indicate that concrete plates with defects
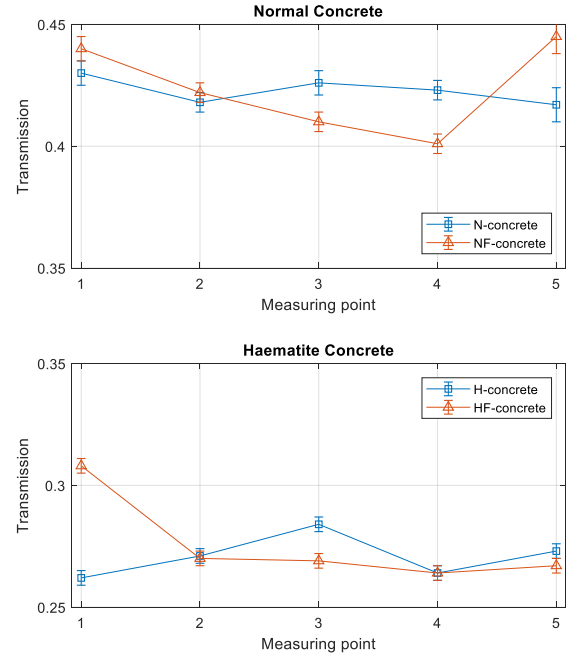
Fig. 3: *Results for transmission measurements at the different measuring points with and without defects for the different concrete compositions.*

Fig. 4: *Histograms of the ROI at the measurement points 4 and 5 for NF (top) and at the measurement points 1 and 2 for HF (bottom).*

do not generally show a relatively high deviation from the mean value, but all samples show strong variations depending on the measurement point. These variations are larger than the measurement errors. They can be

explained by analyzing the ROI of the µCT-scans for the different measurement points of the concrete samples. Figure 4 shows some histograms of the reconstructed image data. Although it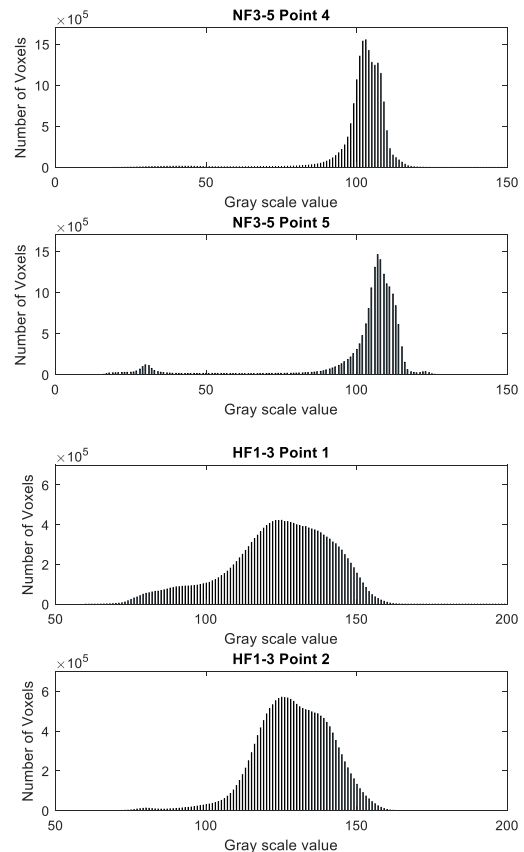 is not possible to calculate an attenuation coefficient from these data, the histograms give an indication for it. The lower the grey scale value, the lower the density of the material is. Consequently, air voids and void defects are on the left side of the histograms, while the solid phases are on the right side.

By segmenting the histogram into two parts using a simple threshold technique [4], semi-quantitative values for the amount of porosity (defects and air voids) can be calculated. Figure 5 shows the results of such segmentation.

Picking out the ROI at point 1 and 2 of the hematite concrete with defects (HF) we find that the macro porosity is much higher at point 1 than at point 2, which is also qualitatively visible on a slice of the image data and the corresponding segmented and binarized image in figure 6. The black areas represent the air voids.

However, the results show that porosity is not the only valuable criteria for evaluating the shielding properties of the different concretes. Especially for heavy weight concrete, it is also necessary to segment the heavy weight aggregates. The aggregates in normal concrete typically have similar attenuation coefficients
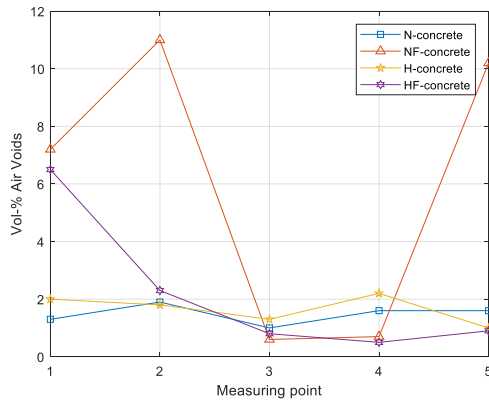

Fig. 5: *Results of the air void segmentation of the µCT scans for N, NF, H, and HF.*
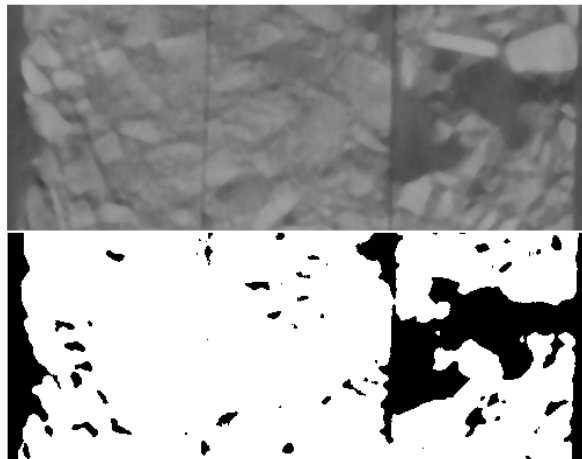

Fig. 6: *Grey scale image (top) and binarized image (bottom) of HF at point 1*
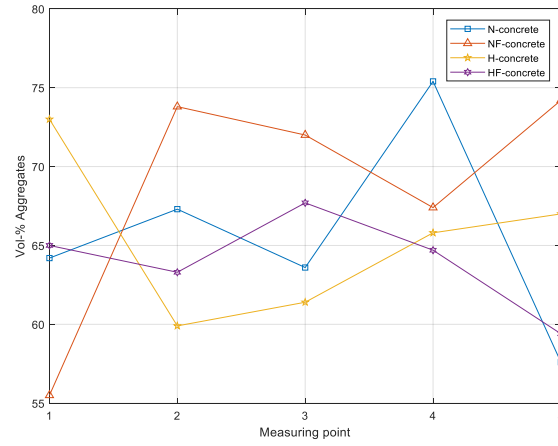

Fig. 7: *Results of the aggregate segmentation of the µCT scans for N, NF, H, and HF.*
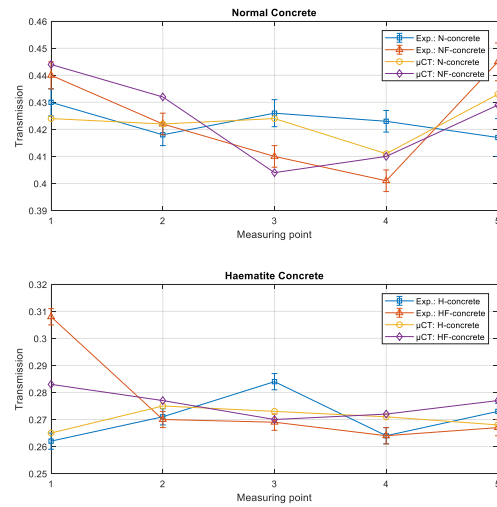
Fig. 8: *Comparison of experimental transmission data with calculated data derived from the results of the µCT scans.*

like the cement matrix and could therefore be treated like the same material in a first approximation. Heavy weight concrete should be segmented in three parts, because the amount of heavy weight aggregates influences the attenuation coefficients more than the amount of macro-porosity. For segmenting the aggregates from grayscale data more extensive image processing steps need to be done. Here it was done with MATLAB® by first using the 3-d boxfilter and histogram equalization function and the multithresh method afterwards. Figure 7 shows the results of this segmentation.

Figure 8 shows a comparison of experimental transmission data with calculated data derived from the analysis of the Gray scale value spectra. Here, in a first approximation the attenuation coefficient was supposed to be proportional to a linear combination of the intensity obtained in different regions in the Gray scale value spectra. The results of the simple approach already show analogies with respect to the curve progressions.

In order to benchmark related Geant4 simulations, transmission curves were measured and simulated.

Fig. 9: *Comparison of the transmission curves of the measurements (Experiment) with the Geant4 simulations for H concrete.*

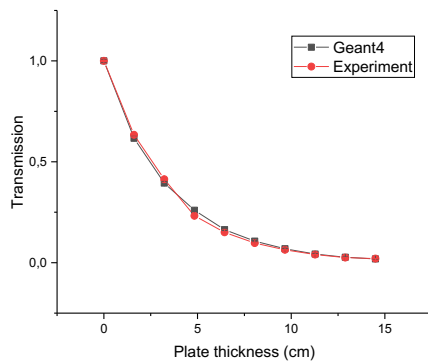Figure 9 shows representative results of the transmission curves for hematite concrete with stacks of up to 9 plates. The Geant4 simulations are based on a model of the measurement setup including material compositions of the concrete and densities provided by iBMB. As a result the simulation data are in accord with the experimental data.

Summary and conclusions

The interdisciplinary approach between civil engineering and physics in this work showed the benefit of this co-operation for a deeper understanding of concrete composition and structures with respect to radiation protection properties. The application of μCT scans supports the concrete design process by giving a first indication for the shielding properties and the distribution of the different components.

A good agreement between Geant4 simulations and measurements show that appropriate Monte Carlo calculations can be performed. However an accurate specification of the concrete composition is very important as literature or databases show in general a wide range of values. Moreover structural details as observed by μCT scans should be considered too.

References

[1] DIN EN 206:2017-01: Beton – Festlegung, Eigenschaften, Herstellung und Konformität; Deutsche Fassung EN 206:2013+A1:2016

[2] Geant4 - a toolkit for the simulation of the passage of particles through matter, http://www.geant4.org/geant4/ (2017)

[3] Zement-Merkblatt. Betontechnik. B 10 1.2002 https://www.vdz-online.de/fileadmin/gruppen/vdz/3LiteraturRecherche/Zementmerkblaetter/B10.pdf

[4] Otsu, N.: A Threshold Selection Method from Gray-Level Histograms. In: IEEE Transactions on Systems, Man, and Cybernetics, Vol. SMC-9, No. 1, January 1979

10.2 Investigation of a simplified approach for HPGe well detector modeling for Monte Carlo simulations

F. Becker
in co-operation with:

H. Li[a], Y. Zhang[a]
[a]*Northwest Institute of Nuclear Technology (NINT), China*

Introduction

Numerical simulations are a modern approach to predict the detector behavior in radiation fields. To employ simulations for e.g. detector calibration and efficiency determination required for quantitative analyses in the field of spectra recording and dose determination, the knowledge of the detector response is important. Modelling of Ge detectors and simulating spectra is a concern even if the detailed manufacturer's information is taken into account. Several approaches show that a focus on the determination of the different deadlayer thicknesses of the crystal is necessary. However this determination is very elaborative and requires a lot of precise measurements e.g. considering 25 reference thickness elements in a crystal half (Ref. [1]). In this investigation we propose a less complex method which also includes the electric potential profile in the Ge detector crystal.

Modelling and simulations

A HPGe well detector used for gamma-spectroscopic investigations with available engineering drawings was employed. In a first step a simulation detector model was constructed based on the dimensions according to the manufacturer's information (structures and materials of engineering drawings, crystal, holding structure, cooling finger, and aluminum cap as well as deadlayer dimensions). The model was included in the Monte Carlo code Geant4 [2]; figure 1 shows the Geant4 model of the active part of the detector crystal. It can be seen that the detector type is a coaxial one open end
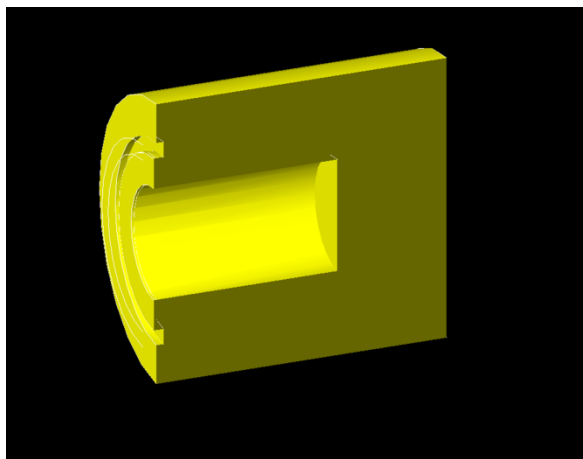
detector. The crystal is mounted in the detector housing with the open end facing the radiation entrance window. On the entrance side the circular groove is visible. Measurements with sources and respective simulations were performed. However, the agreement between experimental and simulated spectra in this approach was not satisfying. According to other investigations e.g. Courtine et al.[1] or Bosin et al. [3], the lower efficiency observed in the measurements compared to the simulations is most likely due to a dead layer thicker than stated by the manufacturer. Hence a new approach for the simulation model was investigated. First the origin of the differences was attributed to different deadlayer thicknesses as stated by Courtine et al. [1]. Moreover the question arises, if the electric field in the crystal and in turn the charge collecting property could play a role too. Therefore simulations with the code QuickField [4] were performed.

The electric potential distribution in the crystal revealed an ellipsoid or barrel like shape (Fig. 2). Moreover detailed scanning results of the deadlayer distribution of a Ge crystal [1] also points to such kind of shape. As a result, two different ellipsoid models were constructed which allow for a more simple determination of the detector's deadlayer including a possible influence of the charge collection as given by the electric potential profile. In the model "ellipsoid model 1", a barrel type crystal was chosen, so that the shape of the crystal has equal pieces (circles) cut from the ends (Fig. 3, top). The diameter of both circles is determined by the position of the groove of the crystal. In the other model "ellipsoid model 2" (Fig. 3, bottom), the diameter of the circle at the cooling finger side is changed to the borehole's diameter. The parameters of the ellipsoid/barrel models were determined by the manufacturer's specifications and results of measurements with a collimated Cs-137 source revealing an effective

Fig. 1: *Cross section of the active part of the crystal region of the investigated HPGe detector model*
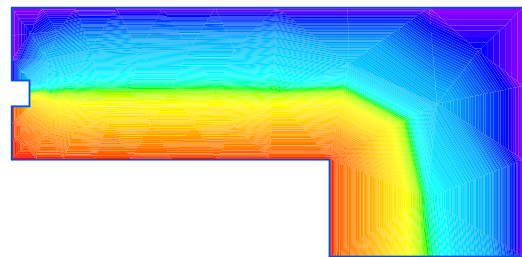
Fig. 2: *Distribution of the electric potential in the half cross-section of the crystal. The colour scale indicates the progression from high (red) to low (violet) potential.*
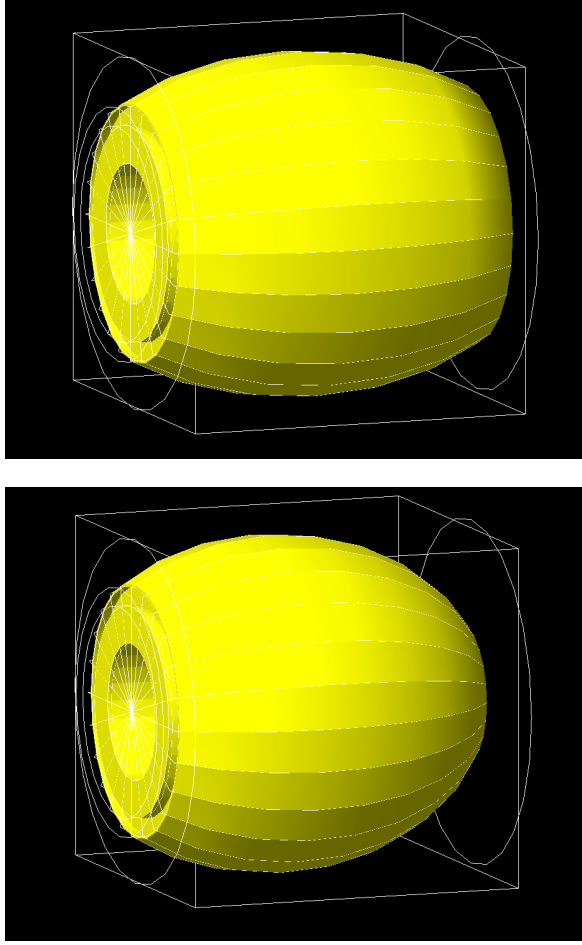
Fig.3: *The two different models "Ellipsoid model 1" (top) and "ellipsoid model 2" (bottom) for the approximation of the effective active crystal region.*

deadlayer thickness at a position of the crystal's side and in turn the curvature of the barrel. It is obvious that the effort is much less than for the detailed scanning of the Ge crystal with more than 20 measuring points as suggested by reference [1].

A series of measurements were performed with a Eu-152 source placed at 40 cm distance from the entrance window of the detector. Experimental results were compared to Geant4 simulations.

Results

A comparison of selected experimental and simulation results is presented in figs. 4 to 7.

The measurement results are indicated by black squares, the simulation results according to the manufacturer's specifications with red pentagons, the ellipsoid models 1 and 2 with blue squares with a cross inside and red triangles, respectively. The simulation results according to the manufacture's specifications show always too high intensities in the gamma-ray
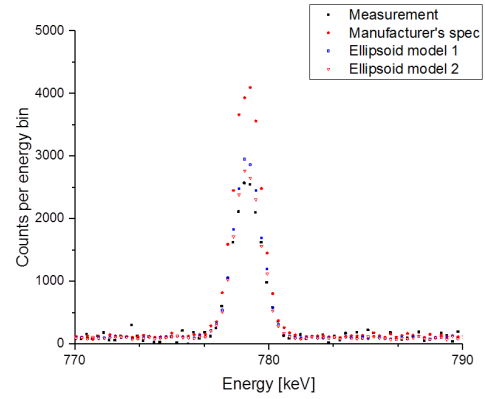
Fig. 5: *Section of the measured and simulated Eu-152 spectra around 780 keV.*
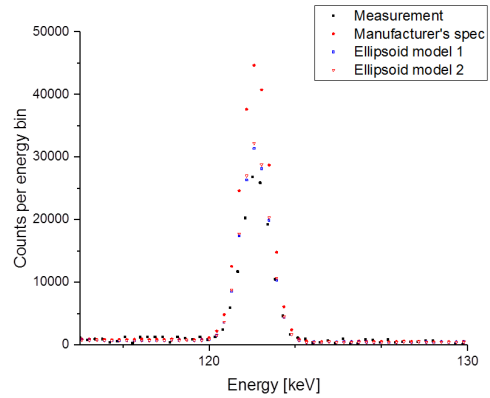
Fig. 6: *Section of the measured and simulated Eu-152 spectra around 120 keV.*

Fig. 4: *Section of the measured and simulated Eu-152 spectra around 1,4 MeV.*
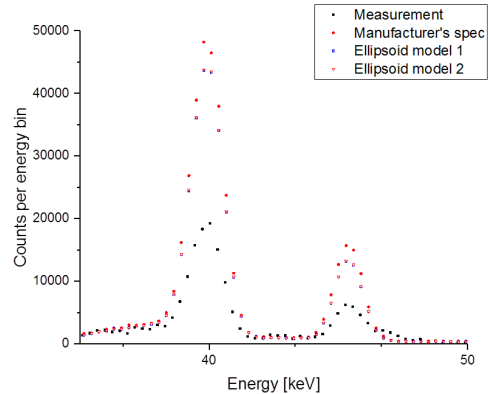
Fig.7: *Section of the measured and simulated Eu-152 spectra around 40 keV.*

peaks in the whole investigated energy range from 40 keV to 1.4 MeV. In contrast, the results for the two ellipsoid/barrel models show a quite good agreement in the energy range of 120 keV to 1.4 MeV with a slightly better agreement at 1.4 MeV for ellipsoid model 2. For the low energy range around 40 keV still a large discrepancy to the experimental data is observed.

Summary

In the present investigation a simplified approach for HPGe well detector modelling was developed. It is less laborious than other approaches as it is based on simple source measurements, which can be realized within a short time frame. A quite good agreement of the experimental data with the simulation results could be achieved in the energy range from 100 to 1400 keV.

References

[1] F. Courtine et al., *Nucl. Instr. and Meth.*, **A 596**, 229-234 (2008)

[2] Geant4 - a toolkit for the simulation of the passage of particles through matter, http://www.geant4.org/geant4/ (2017)

[3] J. Boson et al., *Nucl. Instr. and Meth.*, **A 587**, 304-314 (2008)

[4] Code QuickField 6.3, http://www.quickfield.com (2017)

11 Geoenergy

The Karlsruhe Institute of Technology has defined a broad research program on Enhanced Geothermal Systems (EGS) technology development. Research activities cover the whole process chain of geothermal exploration, engineering and production including system integration and social acceptance and span from fundamental to applied research across scales [1]. Compared to a nuclear waste disposal research, the conditions at a geothermal site are characterized by elevated temperature, flow rate and pressure conditions. Therefore, the influence of hydraulic processes extends even further: not only the direct hydraulic observables like flow / pressure fields or tracer propagation is affected by the petrophysical setting, but the changes in the system setting due to mechanical and chemical interaction becomes important. In this context, the geoenergy research at INE concerns mainly physical and chemical processes in the thermal water circuit and in fractured reservoir systems. The technical feasibility of EGS in fractured crystalline basement was demonstrated first at the Soultz-sous Forêts project, France [2]. Major conclusion from this project are that effective enhancement of hydraulic yield under environmentally friendly condition, e.g., reducing induced seismicity, are technically feasible during reservoir engineering and operation. However, both was achieved by reducing the injection wellhead pressure at the expense of economic viability. In the surface facilities, scaling and corrosion remains an issue.

For the further development of EGS, this learning curve needs to be continued by applying controlled high-flowrate injection and inhibition of scaling and corrosion. Against this background, the research at INE in 2017 focused on (1) the application of new methods to assess subsurface circulation systems [3]. This includes fractionation of oxygen isotopes of the SO_4-H_2O system to estimate reservoir temperatures and the investigation of chlorofluorocarbons contents in the geothermal water to quantify dilution. (2) Scaling characterization was advanced to proof the efficiency of inhibitors as well as demonstrate the subsequent prominence of secondary scaling [4]. (3) For injection at high flow rate, effects from fluid dynamics need to be carefully evaluated. In a heterogeneous network with tube-like structures at the interface of fractures, apparent transmissivity decreases with higher flowrate. Therefore, at Reynold's numbers > 10, Navier-Stokes solvers need to be applied to describe the flow in fractured rock. There are ample theoretical and numerical considerations of the flow behavior in fractured rock, however, little was done to quantify these effects in laboratories or under real field conditions. In this respect, solute tracer experiments at lab-scale have been used to approximate the effect of rough surfaces on the flow in fractures [5]. (4) Geothermal fluid driven transport is a dynamic process, in which parameters may change with time. Injection in fractured reservoirs can include a high variety of thermal, hydraulic, mechanical, and chemical interactions. The insight in these interactions is especially a demanding task for process identification, test design and forecast of reservoir behavior by numerical models. As an experimental infrastructure, the *Geothermal Laboratory in the Crystalline Basement, GeoLaB*, will allow for modification and calibration of new theoretical concepts on the scale relevant for reservoir management. Until now, these models are based mostly on laboratory measurements quantifying the interaction between single fracture(s) and the matrix, fully neglecting complexity of fracture networks or alteration in matrix and effects from the difference in scale. In this context, the feasibility study for GeoLaB has been extended to a description of the existing fault and fracture network at the potential sites in the Southern Black Forest [6] and the Odenwald. Remote sensing techniques and lineament mapping were applied to describe the spatial arrangement of faults and fractures. Reactivation potential was localized using the critical stress concept. (5) Finally, the issue of social acceptability was addressed by establishing a geoethical concept for GeoLaB [7].

Y. Abdelfettah, L. Eggeling, N. Haaf, F. Heberling, F.M. Huber, M. Pavez, Y. Qin, T. Schäfer, E. Schill, M. Stoll

In co-operation with:

R. Haas Nüesch[a], S. Held[a], T. Kohl[a], J. Meixner[a], C. Meller[a]

[a] AGW, Karlsruhe Institute of Technology, Germany

Introduction

In central Europe, major geothermal resources are contained within deep fractured crystalline rock at high differential stresses. Economic viable projects require about 50 L s⁻¹ of flow at temperature > 130 °C. There are a number of scientific challenges along with an environmentally friendly development of deep geothermal energy in these geothermal fields. Key issues relate mainly to perceptible seismicity during enhancement of the reservoir performance and operation, as well as radioactive scaling. These technical issues led to a controversial discussion in the German society: 95% of the Germans support renewable energies (Agentur für Erneuerbare Energien, 2017), but locally concerned action groups of citizens express their preoccupations related to technical challenges (Fig. 1). The geothermal research at INE has taken up this discussion and extended its research fields in 2017 from purely geoscientific to socioscientific in close collaboration with our

Fig. 1: *"No geothermal power plant at Steinweiler"-manifestation including negative impacts related to geothermal energy development on the community expected by the citizen's action group of Steinweiler (Germany, photo: H. Geckeis, 4.12.2016).*

Helmholtz partners, the Institute for Advanced Sustainability Studies at Potsdam and the Université de Strasbourg.

This goes along with the embedding of the geothermal research at INE into Helmholtz Portfolio project *Environmentally friendly provision of local energy from georesources – Geoenergy* and the Helmholtz program *Renewable Energies*. In the view of economically viable condition and low environmental impact, fundamental and applied research is carried out in particular on the relations between chemical and hydrogeological aspects of fluid circulation, as well as hydromechanics. Related phenomena are investigated at reservoir and laboratory scale. This concerns the investigation of hydrogeological condition in natural geothermal systems and based on this, the understanding of flow in fractures and mineral precipitation in the surface installations. Continuous preparation of the large-scale infrastructure project GeoLaB add regional and socioscientific components to this research program. The Helmholtz research in these fields is completed among others in two EC H2020 projects:

1) Deployment of deep enhanced geothermal systems for sustainable energy business (DEEPEGS, www.deepegs.eu/)
2) Cooperation in Geothermal energy research Europe-Mexico for development of Enhanced Geothermal Systems and Superhot Geothermal Systems (GEMex, www.gemex-h2020.eu/)

Reservoir temperature and dilution of geothermal fluids

Besides mineralogy of the reservoir rock, temperature and dilution are crucial for water-rock interaction intensity and thus influence, e.g., the scaling potential in the surface installations of a geothermal plant. Reservoir temperatures are typically estimated from solute geothermometers. Their application, especially in low temperature environment, often leads to a broad range and inconsistent temperature values, with a variation of partly up to 200 K for one fluid. Given its temperature dependence, for the assessment of reservoir temperatures of thermal springs around the Villarrica volcano,
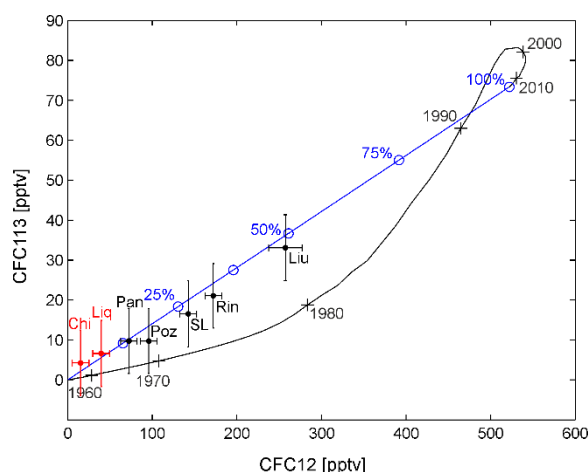

Fig. 2: *Tracer plots comparing CFC-12 vs. CFC-113 for the southern hemisphere atmospheric input concentrations. Black line represents the piston flow approach with selected infiltration ages (+). The blue line depicts binary mixing of modern water with pre-modern, CFC-free water with different mixing ratios. Red/black dots show measured CFC concentrations of selected thermal fluids with no dilution/dilution inferred from oxygen isotope fractionation.*

Southern Chile, oxygen isotope fractionation between H_2O and SO_4, is used [3]. Geothermometer equations and, hence, equilibrium conditions have to be selected according to the sulfate species and physicochemical parameter prevailing in the reservoir. Temperatures between 80-90°C (no dilution) and 125-140°C (dilution) are in accordance with re-evaluated temperature estimations from SiO_2 and Na/K geothermometers.

Dilution of the geothermal fluids by shallow groundwater is quantified using different chlorofluorocarbons (CFC). CFC-11, -12 to -113 analyses were performed, using purge and trap gas chromatography with an electron capture detector. The ratio between the different CFC is investigated for piston flow and binary (or higher) mixing (Fig. 2). The obtained mixing ratios correspond to the observation from oxygen isotope fractionation between H_2O and SO_4. On the basis of the analysis, a conceptual reservoir model was derived [3].

Characterization of scaling in geothermal sites in the Upper Rhine graben

Besides a negative impact on the performance of geothermal plants, scale formation concerns the acceptability processes (Fig. 1) because scales formed within the geothermal water circuit frequently accumulate natural radionuclides. Moreover, scale formation may lead to radiation dose rates, which are of radiological concern, and deposits, which may have to be disposed as radioactive waste. In order to minimize these problems and to foster geothermal power plant availability, it is of major interest to understand scale formation processes and to develop methods for their inhibition. One important pre-requisite towards this goal is a sound mineralogical and geochemical characterization of the formed material.

Geothermal brines at sites in the Upper Rhine Graben exhibit salinities in the order of 100 g/L and become,
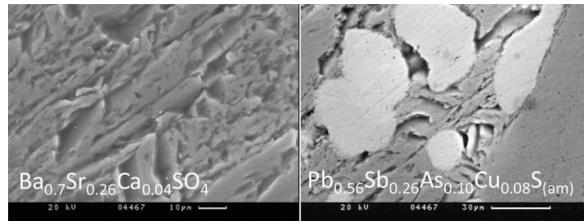
Fig. 3: *SEM images recoded on scale A. The left image shows the lamellar morphology of the barite type solid solution. SEM-EDX reveals a composition of $Ba_{0.70}Sr_{0.26}Ca_{0.04}SO_4$. The right image shows, embedded into the lamellar barite-type minerals, an amorphous mixed sulfide phase (Pb, Sb, As, Cu)$S_{(am)}$ with a cation composition: 56 % Pb, 26 % Sb, 10 % As, and 7 % Cu.*

Fig. 4: *Comparison of the tracer break through curves with numerical models including different approaches of addressing fracture aperture for the altered and unaltered fracture.*

upon cooling in the heat exchanger, supersaturated with respect to sulfate solid-solutions, e.g. (Ba,Sr)SO_4, and other mineral phases.

The mineralogy of solid scale samples from geothermal power plants in the Upper Rhine Valley in absence and presence of sulfate scaling inhibitors is investigated by wet-chemistry (after digestion), XRPD, SEM-EDX, XPS, EA-IRMS, Raman spectroscopy, and XANES [4]. Samples of scales deposited in the absence of a sulfate scaling inhibitor mainly consist of two phases. The largest part is made up of a barite type (Ba,Sr,Ca)SO_4 solid-solution (Fig. 3). Traces of Ra occurring in the scaling are assumed to be incorporated in the barite type solid solution. Further minor phases are sulfide phases, either an X-ray amorphous nano-particulate phase or galena (PbS).

After application of the sulfate inhibitor, sulfate minerals are no longer detectable in the scale samples. Subsequent scalings are Pb-dominated and consist mainly of galena (PbS), elemental lead (Pb), arsenic (As) and antimony (Sb). As and Sb are likely present as a nano-crystalline intermetallic mixed compound ((Sb, As) or $Pb_3(Sb,As)_2S_3$). The absence of barite-type minerals demonstrates the success of the application of the sulfate inhibitor. The precipitation of elemental Pb, As, and Sb, which are more noble than iron, may enhance the corrosion of mild steel pipes in the geothermal water circuit. Elution tests and oxidation of the scalings upon storage at atmospheric conditions demonstrate that proper disposal of the toxic heavy metal and metalloid containing scalings may be challenging.

Flow in natural fracture with rough surfaces

At high flow rates, in particular, the roughness of fractures reduces its transmissivity. In order to predict and investigate solute and mass transport, numerous analytical and numerical approaches were postulated for both single fractures and fracture networks. The parallel-plate approach with its cubic law is applicable for fractures with smooth and wide apertures. However, a model of such reduced geometry cannot describe the flow dynamics, because the cubic law approach does not include rough or irregular fracture surfaces and tortuous flow paths created by asperities and asperity contacts. Other modelling approaches, like e.g. the Stokes equation, show to be valid under very low Reynold's
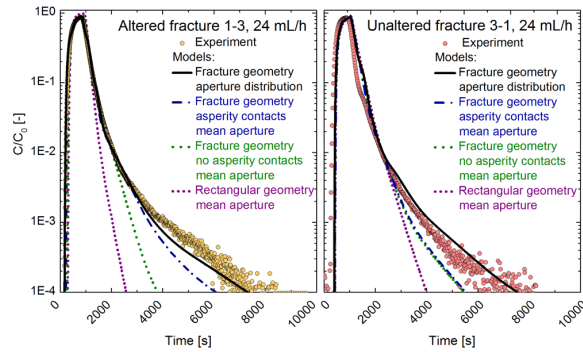
numbers. In complex geometries like natural fractures the Navier-Stokes equation needs to be used to simulate precisely the fluid flow.

There are, however, only a few studies comparing such numerical simulations with experimentally obtained data. Here, we present transport experiments in fracture flow cells of two rock samples from the geothermal reservoir at Soultz [5]. The samples contain natural single fractures over their whole length parallel to the drilling direction. One rock core shows a distinct mineralogical alteration while the other rock core is macroscopically unaltered. Three in- and outlets were placed at the rim of the fractures. The residence time of a conservative solute tracer, 10 ppb UV-fluorescent 7-amino-1.3-naphthalene injected at flow rates of 12 and 24 mL/h, is measured continuously by fluorescence spectroscopy. Based on the μ-CT data sets of both drill cores, 3-D digital models of both fractures are generated. Fluid flow and tracer transport are simulated in 2.5-Dusing COMSOL Multiphysics®. The Navier-Stokes equations are solved for laminar flow.

The tracer recovery (Fig. 4) reveals comparable breakthrough curves for the two cores with a small-time shift in the maximum. The tailing is slightly more prominent in the altered fracture. Comparison with the models including different complexity of surface asperities and fracture aperture distribution reveals that it can be explained to a large extend by the complexity of the fracture surface.

Although carried out at comparatively low flow rates with respect to geothermal fluid production, these results provide a good example for the importance of experimental data on flow in fractures as targeted in *GeoLaB*.

GeoLaB - feasibility

GeoLaB is aimed as the first geothermal reservoir simulator for reservoir technology and borehole safety. It is designed as a generic underground research laboratory in the crystalline rock adjacent to the Rhine Graben, one of the most prominent geothermal hotspots in Germany including the Campus North of KIT. Furthermore, it is an analogue site representative of the world's most widespread geothermal reservoir rock, the crystalline basement. Among others, the GeoLaB

will address specific objectives such as to perform controlled high flow rate experiments, CHFE, in fractured rock, to integrate multi-disciplinary research to solve key questions related to flow regime under high flow rates, or higher efficiency in reservoir engineering, risk mitigation by developing and calibrating smart stimulation technologies without creating seismic hazard, and to develop save and efficient borehole installations using innovative monitoring concepts.

In an initial phase, the suitability of a site for *GeoLaB* located in the Black Forest-Odenwald crystalline complex for a two-km long gallery will be excavated, tapping individual caverns, from which controlled, high flow rate experiments will be conducted at depths of 400 m must be proven by geological, geophysical, and geochemical drilling exploration.

With respect to the necessary control on the existing fracture zones regarding its re-activation potential, a statistical assessment of the orientation, average length, and the total length of lineaments occurring in the southern Black Forest has been carried out using two digital elevation models (ASTER, LIDAR) and satellite imagery data sets [6]. First, the analyses reveal an impact of the different resolutions of the data sets that allow to define maximum (censoring bias) and minimum (truncation bias) observable lineament length for each data set. The increase of the spatial resolution of the digital elevation model from 30 m x 30 m to 5 m x 5 m results in a decrease of total lineament length by about 40% whereby the average lineament lengths decrease by about 60%. Lineament length distributions of both data sets follow a power law distribution as documented elsewhere for fault and fracture systems. Predominant NE-, N-, NNW-, and NW directions of the lineaments are observed in all data sets and correlate with well-known, large-scale structures in the southern Black Forest. Therefore, mapped lineaments can be correlated with faults and hence display geological significance. Lineament density in the granite-dominated areas is apparently higher than in the gneiss-dominated areas. Application of a slip- and dilation tendency analysis on the fault pattern (Fig. 5) reveals largest reactivation potentials for WNW-ESE and N-S striking faults as strike-slip faults at the potential *GeoLaB* site, whereas normal faulting may occur along NW-striking faults within the ambient stress field. Remote sensing techniques in combination with highly resolved digital elevation models and a slip- and dilation tendency analysis thus can be used to quickly get first order results of the spatial arrangement of critically stressed faults.

GeoLaB – social acceptance

With the *GeoLaB* initiative, research at INE takes up societal concerns and responds to socially relevant issues by carrying out projects on technical solutions. In this respect, the new research on social acceptance of geothermal energy shall reveal public opinion to overcome unidirectional communication strategies and information flow [7].

Geoethical concepts emphasize that geoscientific knowledge may assist society in decision making as well as in dealing with risks, user conflicts and environmental threats on local, regional and global scale in order to support more sustainable practices at the intersection of human beings and the geosphere.

We analyzed the social response to recent geothermal development and identified the precondition for public
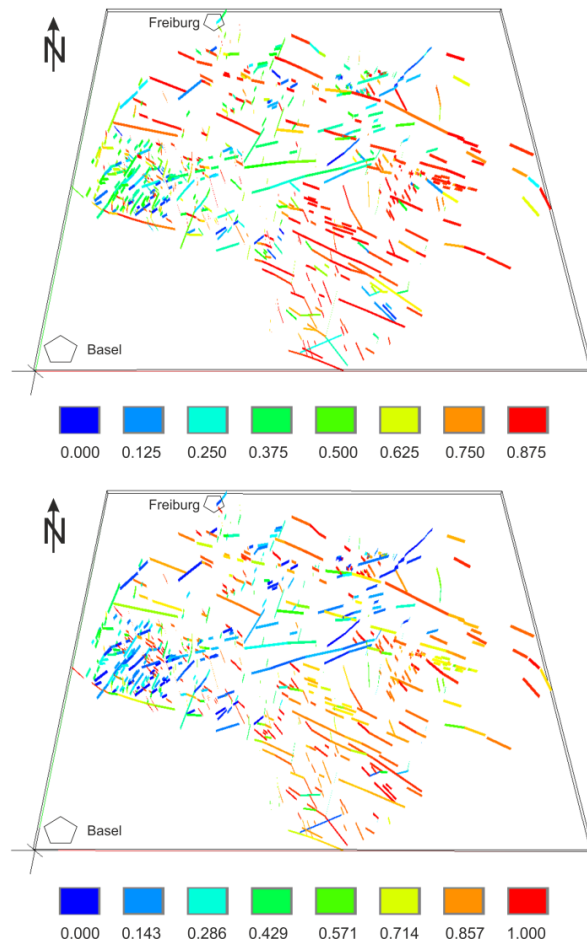
Fig. 5: *Apparent resistivities versus period obtained from robust processing including remote referencing of RITT station from representative three days for production from GRT2.*
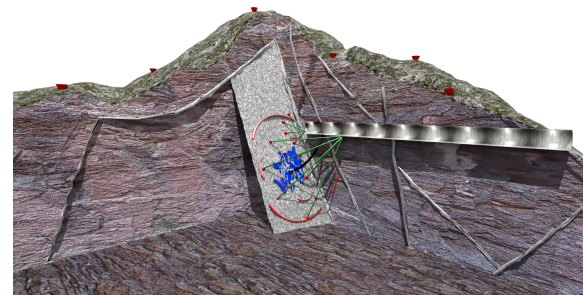
Fig. 6: *Possible layout of GeoLaB (not to scale) with an access tunnel to a fracture zone, observation wells (green) from the tunnel into the fracture zone. In addition to the monitoring stations (red cones), the main injection well (black) for controlled high-flow experiments (CHFE) targets the fracture zones. Possible CHFE with high flow rate injection from the surface into a fracture zone (blue volume) and related mechanical deformation indicated by red ring segments.*

acceptability of geothermal projects. On this basis, the potential contribution of GeoLaB to a geoethic approach in geothermal research and technology development was discussed. The underground research laboratory is planned as an infrastructure to answer scientific challenges and to offer the necessary transparency to interact with the public. The GeoLaB approach aims on transparent, tangible science and can serve to enhance mutual understanding of stakeholder groups. It may increase public awareness on geothermal research and potentially enhance the opportunity for public approval of planned activities. As a generic site, GeoLaB can develop scientific-technological solutions for a responsible exploitation of geothermal energy accompanied by sociological studies. The underground research laboratory will serve as a platform for science communication, participation and dialog of stakeholders from industry, politics, administration and society.

This complies with the comprehension of responsible research in a geoethical sense.

References
[1] Meller, C., et al., *Energy Technology* 10.1002/ente.201600579 (2016)
[2] Schill, E., et al., *Geothermics* **70**, 110-124 (2017).
[3] Held, S., et al., *Geothermics* (subm.)
[4] Haas Nüesch, R., et al., *Geothermics* (in press).
[5] Stoll, M. et al., *Water Resource Research* (subm.).
[6] Meixner, J., et al., *Journal of Structural Geology* 10.1016/j.jsg.2017.11.006 (in press).
[7] Meller, C., *Geothermics* 10.1016/j.geothermics.2017.07.008 (in press).

12 Publications

ISI/SCOPUS

1. Afsar, A.; Edwards, A. C.; Geist, A.; Harwood, L. M.; Hudson, M. J.; Westwood, J.; Whitehead, R. C., Effective Separation of Am(III) from Cm(III) Using Modified BTPhen Ligands. *Heterocycles* **2017,** *95* (1), 575-586.

2. Altmaier, M.; Yalçintaş, E.; Gaona, X.; Neck, V.; Müller, R.; Schlieker, M.; Fanghänel, T., Solubility of U(VI) in chloride solutions. I. The stable oxides/hydroxides in NaCl systems, solubility products, hydrolysis constants and SIT coefficients. *The journal of chemical thermodynamics* **2017,** *114*, 2-13.

3. Alyn, C. E.; Mocilac, P.; Geist, A.; Harwood, L. M.; Sharrad, C. A.; Burton, N. A.; Whitehead, R. C.; Denecke, M. A., Hydrophilic 2,9-bis-triazolyl-1,10-phenanthroline ligands enable selective Am(III) separation: a step further towards sustainable nuclear energy. *Chemical communications* **2017,** *53* (36), 5001-5004.

4. Amgarou, K.; Paradiso, V.; Patoz, A.; Bonnet, F.; Handley, J.; Couturier, P.; Becker, F.; Menaa, N., Erratum, A comprehensive experimental characterization of the iPIX gamma imager. *Journal of Instrumentation* **2017,** *12* (1), Art.-Nr.

5. Bae, S.; Gim, S.; Kim, H.; Dorcet, V.; Pasturel, M.; Greneche, J.-M.; Darbha, G. K.; Hanna, K., New Features and Uncovered Benefits of Polycrystalline Magnetite as Reusable Catalyst in Reductive Chemical Conversion. *The journal of physical chemistry <Washington, DC> / C* **2017,** *121* (45), 25195-25205.

6. Bahl, S.; Peuget, S.; Pidchenko, I.; Pruessmann, T.; Rothe, J.; Dardenne, K.; Delrieu, J.; Fellhauer, D.; Jégou, C.; Geckeis, H.; Vitova, T., Pu Coexists in Three Oxidation States in a Borosilicate Glass: Implications for Pu Solubility. *Inorganic chemistry* **2017,** *56* (22), 13982-13990.

7. Banik, N. L.; Marsac, R.; Lützenkirchen, J.; Marquardt, C. M.; Dardenne, K.; Rothe, J.; Bender, K.; Geckeis, H., Neptunium sorption and redox speciation at the illite surface under highly saline conditions. *Geochimica et cosmochimica acta* **2017,** *215*, 421-431.

8. Baumann, A.; Yalçintaş, E.; Gaona, X.; Altmaier, M.; Geckeis, H., Solubility and hydrolysis of Tc(IV) in dilute to concentrated KCl solutions: An extended thermodynamic model for Tc^{4+}-H^+-K^+-Na^+-Mg^{2+}-Ca^{2+}-OH^--Cl^--$H_2O(l)$ mixed systems. *New journal of chemistry* **2017,** *41* (17), 9077-9086.

9. Börsig, N.; Scheinost, A. C.; Shaw, S.; Schild, D.; Neumann, T., Uptake mechanisms of selenium oxyanions during the ferrihydrite-hematite recrystallization. *Geochimica et cosmochimica acta* **2017,** *206*, 236-253.

10. Boubals, N.; Wagner, C.; Dumas, T.; Chanèac, L.; Manie, G.; Kaufholz, P.; Marie, C.; Panak, P. J.; Modolo, G.; Geist, A.; Guilbaud, P., Complexation of Actinide(III) and Lanthanide(III) with H_4TPAEN for a Separation of Americium from Curium and Lanthanides. *Inorganic chemistry* **2017,** *56* (14), 7861-7869.

11. Bracco, J. N.; Lee, S. S.; Stubbs, J. E.; Eng, P. J.; Heberling, F.; Fenter, P.; Stack, A. G., Hydration Structure of the Barite (001)-Water Interface: Comparison of X-ray Reflectivity with Molecular Dynamics Simulations. *The journal of physical chemistry <Washington, DC> / C* **2017,** *121* (22), 12236-12248.

12. Choi, S.; Lee, J.-Y.; Yun, J.-I., Stability Constants and Spectroscopic Properties of Thorium(IV)–Arsenazo III Complexes in Aqueous Hydrochloric Medium. *Journal of solution chemistry* **2017,** *46* (6), 1272-1283.

13. Dietrich, C.; Schild, D.; Wang, W.; Kübel, C.; Behrens, S., Bimetallic Pt/Sn-based Nanoparticles in Ionic Liquids as Nanocatalysts for the Selective Hydrogenation of Cinnamaldehyde. *Zeitschrift für anorganische und allgemeine Chemie* **2017,** *643* (1), 120-129.

14. Edwards, A. C.; Geist, A.; Müllich, U.; Sharrad, C. A.; Pritchard, R. G.; Whitehead, R. C.; Harwood, L. M., Transition metal-free, visible-light mediated synthesis of 1,10-phenanthroline derived ligand systems. *Chemical communications* **2017,** *53* (58), 8160-8163.

15. Edwards, A. C.; Mocilac, P.; Geist, A.; Harwood, L. M.; Sharrad, C. A.; Burton, N. A.; Whitehead, R. C.; Denecke, M. A., Hydrophilic 2,9-bis-triazolyl-1,10-phenanthroline ligands enable selective Am(III) separation: a step further towards sustainable nuclear energy. *Chemical communications* **2017,** *53* (36), 5001-5004.

16. Endrizzi, F.; Di Bernardo, P.; Zanonato, P. L.; Tisato, F.; Porchia, M.; Ahmed Isse, A.; Melchior, A.; Tolazzi, M., Cu(i) and Ag(i) complex formation with the hydrophilic phosphine 1,3,5-triaza-7-phosphadamantane in different ionic media. How to estimate the effect of a complexing medium. *Dalton transactions* **2017,** *46* (5), 1455-1466.

17. Fellhauer, D.; Gaona, X.; Rothe, J.; Altmaier, M.; Fanghänel, T., Neptunium(VI) solubility in alkaline $CaCl_2$ solutions: evidence for the formation of calcium neptunates Ca_xNpO_{3+x}(s,hyd). *Monatsh. Chem.* **2017**.

18. Fieser, M. E.; Ferrier, M. G.; Su, J.; Batista, E.; Cary, S. K.; Engle, J. W.; Evans, W. J.; Lezama Pacheco, J. S.; Kozimor, S. A.; Olson, A. C.; Ryan, A. J.; Stein, B. W.; Wagner, G. L.; Woen, D. H.; Vitova, T.; Yang, P., Evaluating the electronic structure of formal LnII ions in LnII$(C_5H_4SiMe_3)^{31-}$ using XANES spectroscopy and DFT calculations. *Chemical science* **2017**, *8* (9), 6076-6091.

19. Finck, N.; Bouby, M.; Dardenne, K.; Yokosawa, T., Yttrium co-precipitation with smectite: A polarized XAS and AsFlFFF study. *Applied clay science* **2017**, *137*, 11-21.

20. Fröhlich, D. R.; Kremleva, A.; Rossberg, A.; Skerencak-Frech, A.; Koke, C.; Krüger, S.; Rösch, N.; Panak, P. J., Combined EXAFS Spectroscopic and Quantum Chemical Study on the Complex Formation of Am(III) with Formate. *Inorganic chemistry* **2017**, *56* (12), 6820-6829.

21. Fröhlich, D. R.; Maiwald, M. M.; Taube, F.; Plank, J.; Panak, P. J., A thermodynamical and structural study on the complexation of trivalent lanthanides with a polycarboxylate based concrete superplasticizer. *Dalton transactions* **2017**, *46* (12), 4093-4100.

22. González-Robles, E.; Herm, M.; Montoya, V.; Müller, N.; Kienzler, B.; Gens, R.; Metz, V., Dissolution of spent nuclear fuel fragments at high alkaline conditions under H_2 overpressure. *MRS Advances* **2017**, *1* (62), 4163-4168.

23. Gorbunov, A. O.; Lindqvist-Reis, P.; Mereshchenko, A. S.; Skripkin, M. Y., Solvation and complexation of europium(III) ions in triflate and chloride aqueous-organic solutions by TRLF spectroscopy. *Journal of molecular liquids* **2017**, *240*, 25-34.

24. Heberling, F.; Schild, D.; Degering, D.; Schäfer, T., How well suited are current thermodynamic models to predict or interpret the composition of $(Ba,Sr)SO_4$ solid-solutions in geothermal scalings? *Geothermal Energy* **2017**, *5* (9), 16-S.

25. Huber, F. M.; Totskiy, Y.; Marsac, R.; Schild, D.; Pidchenko, I.; Vitova, T.; Kalmykov, S.; Geckeis, H.; Schäfer, T., Tc interaction with crystalline rock from Äspö (Sweden): Effect of in-situ rock redox capacity. *Applied geochemistry* **2017**, *80*, 90-101.

26. Kaufhold, S.; Stucki, J. W.; Finck, N.; Steininger, R.; Zimina, A.; Dohrmann, R.; Ufer, K.; Pentrák, M.; Pentráková, L., Tetrahedral charge and Fe content in dioctahedral smectites. *Clay minerals* **2017**, *52* (1), 51-65.

27. Kerry, T.; Banford, A. W.; Thompson, O. R.; Carey, T.; Schild, D.; Geist, A.; Sharrad, C. A., Transuranic contamination of stainless steel in nitric acid. *Journal of nuclear materials* **2017**, *493*, 436-441.

28. Kienzler, B., Corrosion of Canister Materials for Radioactive Waste Disposal. *Atw* **2017**, *62* (8-9), 542-549.

29. Kienzler, B.; Duro, L.; Lemmens, K.; Metz, V.; De Pablo, J.; Valls, A.; Wegen, D. H.; Johnson, L.; Spahiu, K., Summary of the Euratom collaborative project FIRST-nuclides and conclusion for the safety case. *Nuclear technology* **2017**, *198* (3), 260-276.

30. Kotz, F.; Arnold, K.; Bauer, W.; Schild, D.; Keller, N.; Sachsenheimer, K.; Nargang, T. M.; Richter, C.; Helmer, D.; Rapp, B. E., Three-dimensional printing of transparent fused silica glass. *Nature <London>* **2017**, *544* (7650), 337-339.

31. Krauter, C. M.; Schimmelpfennig, B.; Pernpointner, M.; Dreuw, A., Algebraic diagrammatic construction for the polarization propagator with spin-orbit coupling. *Chemical physics* **2017**, *482*, 286-293.

32. Lee, J.-Y.; Oh, J. Y.; Putri, K. Y.; Baik, M. H.; Yun, J.-I., Redox behaviors of Fe(II/III) and U(IV/VI) studied in synthetic water and KURT groundwater by potentiometry and spectroscopy. *Journal of radioanalytical and nuclear chemistry* **2017**, *312* (2), 221-231.

33. Lee, J.-Y.; Vespa, M.; Gaona, X.; Dardenne, K.; Rothe, J.; Rabung, T.; Altmaier, M.; Yun, J.-I., Formation, stability and structural characterization of ternary $MgUO_2(CO_3)_3{}^{2-}$ and $Mg_2UO_2(CO_3)_3$(aq) complexes. *Radiochimica acta* **2017**, *105* (3), 171-185.

34. Lemmens, K.; González-Robles, E.; Kienzler, B.; Curti, E.; Serrano-Purroy, D.; Sureda, R.; Martínez-Torrents, A.; Roth, O.; Slonszki, E.; Mennecart, T.; Günther-Leopold, I.; Hózer, Z., Instant release of fission products in leaching experiments with high burn-up nuclear fuels in the framework of the Euratom project FIRST- Nuclides. *Journal of nuclear materials* **2017**, *484*, 307-323.

35. Maiwald, M. M.; Wagner, A. T.; Kratsch, J.; Skerencak-Frech, A.; Trumm, M.; Geist, A.; Roesky, P. W.; Panak, P. J., 4,4′-Di-tert-butyl-6-(1H-tetrazol-5-yl)-2,2′-bipyridine : modification of a highly selective N-donor ligand for the separation of trivalent actinides from lanthanides. *Dalton transactions* **2017,** *46* (30), 9981-9994.

36. Malmbeck, R.; Magnusson, D.; Geist, A., Modified diglycolamides for grouped actinide separation. *Journal of radioanalytical and nuclear chemistry* **2017,** *314* (3), 2531-2538.

37. Marsac, R.; Banik, N. L.; Lützenkirchen, J.; Catrouillet, C.; Marquardt, C. M.; Johannesson, K. H., Modeling metal ion-humic substances complexation in highly saline conditions. *Applied geochemistry* **2017,** *79*, 52-64.

38. Marsac, R.; Banik, N. L.; Lützenkirchen, J.; Diascorn, A.; Bender, K.; Marquardt, C. M.; Geckeis, H., Sorption and redox speciation of plutonium at the illite surface under highly saline conditions. *Journal of colloid and interface science* **2017,** *485*, 59-64.

39. Meller, C.; Bremer, J.; Ankit, K.; Baur, S.; Bergfeldt, T.; Blum, P.; Canic, T.; Eiche, E.; Gaucher, E.; Hagenmeyer, V.; Heberling, F.; Held, S.; Herfurth, S.; Isele, J.; Kling, T.; Kuhn, D.; Mayer, D.; Müller, B.; Nestler, B.; Neumann, T.; Nitschke, F.; Nothstein, A.; Nusiaputra, Y.; Orywall, P.; Peters, M.; Sahara, D.; Schäfer, T.; Schill, E.; Schilling, F.; Schröder, E.; Selzer, M.; Stoll, M.; Wiemer, H.-J.; Wolf, S.; Zimmermann, M.; Kohl, T., Integrated Research as Key to the Development of a Sustainable Geothermal Energy Technology. *Energy technology* **2017,** *5* (7), 965-1006.

40. Meller, C.; Schill, E.; Bremer, J.; Kolditz, O.; Bleicher, A.; Benighaus, C.; Chavot, P.; Gross, M.; Pellizzone, A.; Renn, O.; Schilling, F.; Kohl, T., Acceptability of geothermal installations : A geoethical concept for GeoLaB [in press]. *Geothermics* **2017**.

41. Misaelides, P.; Fellhauer, D.; Gaona, X.; Altmaier, M.; Geckeis, H., Thorium(IV) and neptunium(V) uptake from carbonate containing aqueous solutions by HDTMA-modified natural zeolites. *Journal of radioanalytical and nuclear chemistry* **2017,** *311* (3), 1665-1671.

42. Nie, Z.; Finck, N.; Heberling, F.; Pruessmann, T.; Liu, C.; Lützenkirchen, J., Adsorption of Selenium and Strontium on Goethite: EXAFS Study and Surface Complexation Modeling of the Ternary Systems. *Environmental science & technology* **2017,** *51* (7), 3751-3758.

43. Pang, B.; Saurí Suárez, H.; Becker, F., Monte Carlo based study of radiation field in a deep geological repository for high-level nuclear waste with different host rock types. *Nuclear engineering and design* **2017,** *325*, 44-48.

44. Pang, B.; Saurí Suárez, H.; Becker, F., Reference level of the occupational radiation exposure in a deep geological disposal facility for high-level nuclear waste : A Monte Carlo study. *Annals of nuclear energy* **2017,** *110*, 258-264.

45. Petrov, V. G.; Fellhauer, D.; Gaona, X.; Dardenne, K.; Rothe, J.; Kalmykov, S. N.; Altmaier, M., Solubility and hydrolysis of Np(V) in dilute to concentrated alkaline NaCl solutions: formation of Na–Np(V)–OH solid phases at 22 °C. *Radiochimica acta* **2017,** *105* (1), 1-20.

46. Pidchenko, I.; Kvashnina, K. O.; Yokosawa, T.; Finck, N.; Bahl, S.; Schild, D.; Polly, R.; Bohnert, E.; Rossberg, A.; Göttlicher, J.; Dardenne, K.; Rothe, J.; Schäfer, T.; Geckeis, H.; Vitova, T., Uranium Redox Transformations after U(VI) Coprecipitation with Magnetite Nanoparticles. *Environmental science & technology* **2017,** *51* (4), 2217-2225.

47. Polly, R.; Heberling, F.; Geckeis, H., Quantum Chemical Investigation of the Selenite Incorporation into the Calcite (10-14) Surface. *The journal of physical chemistry <Washington, DC> / C* **2017,** *121* (37), 20217.

48. Preočanin, T.; Namjesnik, D.; Brown, M. A.; Lützenkirchen, J., The relationship between inner surface potential and electrokinetic potential from an experimental and theoretical point of view. *Environmental chemistry* **2017,** *14* (5), 295-309.

49. Quinto, F.; Blechschmidt, I.; Perez, C. G.; Geckeis, H.; Geyer, F.; Golser, R.; Huber, F.; Lagos, M.; Lanyon, B.; Plaschke, M.; Steier, P.; Schäfer, T., Multiactinide Analysis with Accelerator Mass Spectrometry for Ultratrace Determination in Small Samples : Application to an in Situ Radionuclide Tracer Test within the Colloid Formation and Migration Experiment at the Grimsel Test Site (Switzerland). *Analytical chemistry* **2017,** *89* (13), 7182-7189.

50. Ratnayake, S. Y.; Ratnayake, A. K.; Schild, D.; Maczka, E.; Jartych, E.; Luetzenkirchen, J.; Kosmulski, M.; Weerasooriya, R., Chemical reduction of nitrate by zerovalent iron nanoparticles adsorbed radiation-grafted copolymer matrix. *NUKLEONIKA* **2017,** *62* (4).

51. Regenspurg, S.; Schäfer, T., Workshop "Geothermal fluids in saline systems". *Geothermal Energy* **2017**, *5* (1), 18.

52. Sauri Suarez, H.; Pang, B.; Becker, F.; Metz, V., Monte-Carlo based comparison of the personal dose for emplacement scenarios of spent nuclear fuel casks in generic deep geological repositories. *Atw* **2017,** *62* (6), 384-390.

53. Schill, E.; Genter, A.; Cuenot, N.; Kohl, T., Hydraulic performance history at the Soultz EGS reservoirs from stimulation and long-term circulation tests. *Geothermics* **2017,** *70*, 110-124.

54. Skerencak-Frech, A.; Trumm, M.; Fröhlich, D. R.; Panak, P. J., Coordination and Thermodynamics of Trivalent Curium with Malonate at Increased Temperatures : A Spectroscopic and Quantum Chemical Study. *Inorganic chemistry* **2017,** *56* (17), 10172-10180.

55. Stoll, M.; Huber, F. M.; Schill, E.; Schäfer, T., Parallel-plate fracture transport experiments of nanoparticulate illite in the ultra-trace concentration range investigated by Laser-Induced Breakdown Detection (LIBD). *Colloids and Surfaces A : Physicochemical and Engineering Aspects* **2017,** *529*, 222-230.

56. Teles, P.; Nikodemová, D.; Bakhanova, E.; Becker, F.; Knežević, Ž.; Pereira, M. F.; Sarmento, S., A Review of Radiation Protection Requirements and Dose Estimation for Staff and Patients in CT Fluoroscopy. *Radiation protection dosimetry* **2017,** *174* (4), 518-534.

57. Vespa, M.; Dähn, R.; Huthwelker, T.; Wieland, E., Soft X-ray absorption near-edge investigations of Mg-containing mineral phases relevant for cementitious materials. *Physics and chemistry of the earth* **2017,** *99*, 168-174.

58. Vitova, T.; Pidchenko, I.; Fellhauer, D.; Bagus, P. S.; Joly, Y.; Pruessmann, T.; Bahl, S.; Gonzalez-Robles, E.; Rothe, J.; Altmaier, M.; Denecke, M. A.; Geckeis, H., The role of the 5f valence orbitals of early actinides in chemical bonding. *Nature Communications* **2017,** *8*, 16053.

59. Wagner, C.; Mossini, E.; Macerata, E.; Mariani, M.; Arduini, A.; Casnati, A.; Geist, A.; Panak, P. J., Time-Resolved Laser Fluorescence Spectroscopy Study of the Coordination Chemistry of a Hydrophilic CHON [1,2,3-Triazol-4-yl]pyridine Ligand with Cm(III) and Eu(III). *Inorganic chemistry* **2017,** *56* (4), 2135-2144.

60. Wilden, A.; Lumetta, G. J.; Sadowski, F.; Schmidt, H.; Schneider, D.; Gerdes, M.; Law, J. D.; Geist, A.; Bosbach, D.; Modolo, G., An Advanced TALSPEAK Concept for Separating Minor Actinides - Part 2 : Flowsheet Test with Actinide-spiked Simulant. *Solvent extraction and ion exchange* **2017,** *35* (6), 396-407.

61. Zang, A.; Stephansson, O.; Stenberg, L.; Plenkers, K.; Specht, S.; Milkereit, C.; Schill, E.; Kwiatek, G.; Dresen, G.; Zimmermann, G.; Dahm, T.; Weber, M., Hydraulic fracture monitoring in hard rock at 410 m depth with an advanced fluid-injection protocol and extensive sensor array. *Geophysical journal international* **2017,** *208* (2), 790-813.

62. Zimina, A.; Dardenne, K.; Denecke, M. A.; Doronkin, D. E.; Huttel, E.; Lichtenberg, H.; Mangold, S.; Pruessmann, T.; Rothe, J.; Spangenberg, T.; Steininger, R.; Vitova, T.; Geckeis, H.; Grunwaldt, J.-D., CAT-ACT - A new highly versatile x-ray spectroscopy beamline for catalysis and radionuclide science at the KIT synchrotron light facility ANKA. *Review of scientific instruments* **2017,** *88* (11), 113113.

Invited talks

63. Altmaier, M., *Recent advances on aquatic radionuclide chemistry at KIT-INE*. Seminar Talk at Florida State University, Miami, USA, **2017**.

64. Altmaier, M., *Research overview KIT/INE*. Actinide and Brine Chemistry in a Salt Repository Workshop (V) Convention Center, Ruidoso NM, USA., **2017**.

65. Altmaier, M., *Thermodynamik und Speziation von Actiniden bei höheren Temperaturen*. 3. Projektstatusgespräch zur BMBF-geförderten Nuklearen Sicherheitsforschung, Dresden, Germany, **2017**.

66. Fellhauer, D.; Gaona, X.; Altmaier, M., *Redox chemistry of Pu abd Np under alkaline to hyperalkaline pH conditions*. Annual Goldschmidt Conference, Paris, France, **2017**.

67. Fellhauer, D.; Gaona, X.; Petrov, V.; Dardenne, K.; Rothe, J.; Altmaier, M., *Recent advances in Np(V) solubility and speciation in repository relevant chloride solutions*. International Workshop on Actinide and Brine Chemistry in a Salt-Based Repository (ABC-Salt V), Ruidoso, USA, **2017**.

68. Gaona, X.; Yalcintas, E.; Baumann, A.; Polly, R.; Dardenne, K.; Rothe, J.; Altmaier, M.; Geckeis, H., *Aquatic chemistry and thermodynamics of technetium: redox processes, solubility and complexation*. ACS Meeting, Washington DC, USA, **2017**.

69. Geckeis, H., The road to a high-level radioactive waste repository in Germany – research issues from the view point of a nuclear chemist. Laboratory on Nuclear Environmental Chemistry, Peking University, China, **2017**.

70. Geckeis, H., *The Institute for Nuclear Waste Disposal (INE)*. North China Electric Power University, Beijing, China, **2017**.

71. Geckeis, H., *Research at the Institute for Nuclear Waste Disposal (INE)*. Institute of Chemistry, Chinese Academy of Sciences, Beijing, China, **2017**.

72. Geckeis, H., *The Institute for Nuclear Waste Disposal (INE)*. European Summer School Radiochemistry and Nuclear Instrumentation, Strasbourg, France, **2017**.

73. Geckeis, H.; Bouby, M., *Role of nanoparticle formation in the environmental behavior of actinides*. Workshop, Membrane Technology Department - Seminar, KIT, Karlsruhe, Germany, **2017**.

74. Geist, A., *Highly efficient actinides stripping agents developed in European research programs*. EU-Japan Symposium on Back-End Systems for Reduction of Radiotoxicity and Final Waste Volume, Tokyo Institute of Technology, Tokyo, Japan, **2017**.

75. Geist, A., Minor actinide separations chemistry developed in Europe: evolution and current trends. Japan Atomic Energy Agency, Tokai, Japan, **2017**.

76. Geist, A., SO$_3$-Ph-BT(B)P, highly efficient complexing agents for actinide ions: insights from basic studies applied to process development. ACTINIDES 2017, Sendai, Japan, **2017**.

77. Geist, A., Why we created hydrophilic BT(B)P ligands - and basic science's non-negligible role therein. Helmholtz-Zentrum Dresden-Rossendorf, **2017**.

78. Heberling, F., Untersuchungen zur Struktur und Ladung von Mineral-Wasser-Grenzflächen mittels Röntgen-Oberflächendiffraktionsmethoden und Zetapotentialmessungen am Beispiel von Calcit. Annual Workshop of the working group "Induced Polarization" of the German Geophysical Society, Aachen, Germany **2017**.

79. Kienzler, B., Site selection process in Germany and overview on disposal related R&D at Karlsruhe Institute of Technology. Florida International University, Miami, USA, **2017**.

80. Kienzler, B., *Situation in Germany and site selection process*. International Workshop on Actinide and Brine Chemistry in a Salt-Based Repository (ABC-Salt V), Ruidoso, USA, **2017**.

81. Lützenkirchen, J., *Water Structure at Solid/Liquid Interfaces*. Universität Granada, Granada, Spain, **2017**.

82. Lützenkirchen, J., Some experimental values on various silica-titania systems - Coupled second harmonic generation and streaming potential measurements - Column experiments on Teflon to elucidate the role of hydroxide ions at inert interfaces. Universität Twente Twente, The Netherlands, **2017**.

83. Plaschke, M.; Geckeis, H.; Lagos, M.; Gompper, K.; Geyer, F. W.; Quinto, F.; Walschburger, C., *Massenspektrometrische Verfahren in der Radionuklidanalytik*. 20. Sommerschule der Landesanstalt für Personendosimetrie und Strahlenschutzausbildung des Landes Mecklenburg-Vorpommers (LPS), Berlin, Germany, **2017**.

84. Schäfer, T., *Reactive transport and the fate of radionuclides in geochemically perturbed systems*. Johannes-Gutenberg- Universität Mainz (JGUM), Institut für Kernchemie, Kolloquium invited by Prof. Tobias Reich. **2017**.

85. Vitova, T., *Insights into the actinide speciation and electronic structure using An M4,5 HR-XANES and 3d4f RIXS*. AnXAS 2017: 8th WORKSHOP Speciation, Techniques, and Facilities for Radioactive Materials at Synchrotron Light Sources, University of Oxford, UK, **2017**.

86. Vitova, T., *Speciation and electronic structure studies of actinides using An M4,5 HR-XANES and 3d4f RIXS*. Seminar at Ecole Polythechnique Federale de Lausanne (EPFL), Switzerland, **2017**.

87. Vitova, T., *X-ray absorption spectroscopy*. Summer School 2017 Non-Equilibrium Dynamics of Condensed Matter in the Time Domain, St. Peter-Ording, Germany, **2017**.

88. Vitova, T., *X-ray absorption spectroscopy* European Summer School Radiochemistry and Nuclear Instrumentation (low level radioactivity) Strasbourg, France, **2017**.

89. Vitova, T., *Introduction to the FEFF code for experimentalists* ASEAN Workshop on XANES Simulations and In-s/tu XAS Experiments, Nakhon Ratchasima, Thailand, **2017**.

Oral and poster presentations

90. Abdelmonem, A.; Lützenkirchen, J., Coupling non-linear optical spectroscopy and surface chemistry: Towards new insights in atmospheric chemistry and aerosols. European Geosciences Union, General Assembly 2017, Vienna, Austria, **2017**.

91. Adam, N.; Gaona, X.; Altmaier, M.; Geckeis, H., Solubility of Th(IV) and U(VI) in the presence of selected organic cement additives and model compounds: Screening experiments in alkaline NaCl, MgCl$_2$ and CaCl$_2$ solutions. 16th International Conference on the Chemistry and Migration Behaviour of Actinides and Fission Products in the Geosphere (Migration), Barcelona, Spain, **2017**.

92. Adam, N.; Keskitalo, M.; Pfeuffer-Rooschüz, J.; Adam, C.; Panak, P., *Interaction of human serum albumin (HSA) with Cm(III) studied by time-resolved laser fluorescence spectroscopy*. Actinides Conference, Sendai, Japan, **2017**.

93. Ait Mouheb, N.; Montoya, V.; Schäfer, T., *Modelling of radionucleides migration in the low pH cement/clay interface*. 7th PhD Meeting on Reactive Transport (modeling & experiments) - UFZ, Leipzig ,Germany, **2017**.

94. Ait Mouheb, N.; Montoya, V.; Schild, D.; Adams, C.; Joseph, C.; Schäfer, T., Experimental and modelling studies of low pH cement / clay interface processes: Characterization and sorption properties of low pH cements. 2nd Annual Workshop of the CEBAMA project, Espoo, Finland, **2017**.

95. Altmaier, M., *Geochemistry / TDB Update: An-borate, iron, An-organics*. NEA Salt Club 7, Middelburg, Netherlands, **2017**.

96. Altmaier, M.; Brandt, F.; Brendler, V.; Chiorescu, I.; Colas, E.; Curtius, H.; Endrizzi, F.; Franzen, C.; Gaona, X.; Grive, M.; Hagemann, S.; Koke, C.; Kulik, D. A.; Krüger, S.; Lee, J.-Y.; Maiwald, M.; Panak, P. J.; Skerencak-Frech, A.; Steudtner, R.; Thoenen, T., *ThermAc, a collaborative project investigating aquatic chemistry and thermodynamics of actinides at elevated temperature conditions*. Actinide and Brine Chemistry in a Salt Repository Workshop (V), Convention Center, Ruidoso NM, USA, **2017**.

97. Altmaier, M.; Brandt, F.; Brendler, V.; Chiorescu, I.; Colas, E.; Endrizzi, F.; Gaona, X.; Gray, A.; Grive, M.; Hagemann, S.; Huittinen, N.; Koke, C.; Kulik, D. A.; Krüger, S.; Lee, J.-Y.; Maiwald, M.; Miron, G. D.; Panak, P. J.; Poonoosamy, J.; Skerencak-Frech, A.; Steudtner, R.; Thoenen, T., *Aquatic chemistry and thermodynamics of actinides at elevated temperature: research within THERMAC, a German collaborative project*. Actinides 2017, Sendai, Japan, **2017**.

98. Altmaier, M.; Brandt, F.; Brendler, V.; Chiorescu, I.; Colas, E.; Endrizzi, F.; Gaona, X.; Gray, A.; Grive, M.; Hagemann, S.; Huittinen, N.; Koke, C.; Kulik, D. A.; Krüger, S.; Lee, J.-Y.; Maiwald, M.; Miron, G. D.; Panak, P. J.; Poonoosamy, J.; Skerencak-Frech, A.; Steudtner, R.; Thoenen, T., *ThermAc – a German collaborative project on aquatic chemistry and thermodynamics at elevated temperatures*. Migration 2017 - 16th International Conference on the Chemistry and Migration Behaviour of Actinides and Fission Products in the Geosphere, Barcelona, Spain, **2017**.

99. Altmaier, M.; Costa, D.; Felmy, A.; Moog, H. C.; Pabalan, R.; Ragoussi, M.; Reed, D. T.; Runde, W.; Thakur, P.; Voigt, W., State-of-the-art report within the NEA-TDB to assess modeling and experimental approaches in aqueous high ionic strength solutions. Migration 2017 - 16th International Conference on the Chemistry and Migration Behaviour of Actinides and Fission Products in the Geosphere, Barcelona, Spain, **2017**.

100. Altmaier, M.; Montoya, V.; Duro, L.; Valls, A.; Holt, E.; Claret, F.; Mäder, U.; Grambow, B.; Idiart, A., *CEBAMA- an EC HORIZON 2020 Project on cement based-materials*. 16th International Conference on the Chemistry and Migration Behaviour of Actinides and Fission Products in the Geosphere (MIGRATION 2017) Barcelona, Spain, **2017**.

101. Altmaier, M.; Montoya, V.; Duro, L.; Valls, A.; Holt, E.; Claret, F.; Mäder, U.; Grambow, B.; Idiart, A., *CEBAMA – an EC Horizon 2020 funded collaborative Research Project on Cement-Based-Materials*. Actinide and Brine Chemistry in a Salt Repository Workshop (V), Convention Center, Ruidoso NM, USA, **2017**.

102. Altmaier, M.; Montoya, V.; Duro, L.; Valls, A.; Holt, E.; Claret, F.; Mäder, U.; Grambow, B.; Idiart, A., *CEBAMA – a Horizon2020 project on cement-based-materials*. Migration 2017 - 16th International Conference on the Chemistry and Migration Behaviour of Actinides and Fission Products in the Geosphere, Barcelona, Spain, **2017**.

103. Baumann, A.; Yalcintas, E.; Gaona, X.; Altmaier, M.; Geckeis, H., *Redox behaviour, solubility and hydrolysis of ⁹⁹Tc(IV) in dilute to concentrated alkaline NaNO₃-NaCl systems*. 16th International Conference on Chemistry and Migration Behaviour of Actinides and Fission Products in the Geosphere - MIGRATION-2017, Barcelona, Spain, **2017**.

104. Baumann, A.; Yalcintas, E.; Gaona, X.; Polly, R.; Dardenne, K.; Prüssmann, T.; Rothe, J.; Altmaier, M.; Geckeis, H., *Thermodynamic description of Tc(IV) solubility and carbonate complexation in alkaline systems.* 16th International Conference on Chemistry and Migration Behaviour of Actinides and Fission Products in the Geosphere - MIGRATION-2017, Barcelona, Spain, **2017**.

105. Beck, A.; Bahl, S.; Dardenne, K.; Geckeis, H.; Vitova, T., *Immobilization of a Cs- and Re-rich waste simulate in different host matrices.* European Summer School 2017, Radiochemistry & Nuclear Instrumentation (Low Level Radioactivity), Strasbourg, France, **2017**.

106. Becker, F.; Suarez, H. S.; Pang, B.; Metz, V.; Geckeis, H., *Monte-Carlo simulations for individual dosimetry in disposal facilities for spent nuclear fuel.* Research on Radioactive Waste Management : Ethics - Society - Technology, Final ENTRIA Conference, Braunschweig, Germany, **2017**.

107. Bourg, S.; Geist, A.; Adnet, J.-M.; Rhodes, C.; Hanson, B., *GENIORS, a new European project addressing Gen IV integrated oxide fuels recycling strategies.* Proc. Internat. Conf. GLOBAL 2017 (Nuclear Energy Innovation to the Carbon-Free World), Seoul, Korea, **2017**.

108. Brandauer, M., Magnet Rod Filter Analysis for the Treatment of Radioactive Waste from the Abrasiv Water Jet Cutting. Physical Separation Conference 2017, Falmouth UK, 2017.

109. Brandauer, M., *Ausstieg aus der Kerntechnik. Und nun? Rückbau!* "Junge Talente- Wissenschaft und Musik", KIT&Förderverein, Medien und Wissenschaft e.V., **2017**.

110. Brandauer, M., Expert Mission on Site Preparation for Decommissioning and Site Management during Decommissioning. IAEA Expert Mission to Hengyang Hunan 421001 P.R. China, **2017**.

111. Brandauer, M.; Geckeis, H.; Gentes, S.; Heneka, A.; Krauß, C.; Plaschke, M.; Schild, D.; Tobie, W., *Improvement of a Seperaion Method for the Reduction of Secondary Waste from the Water Abrasice Suspension Cutting Technique.* Decommissioning Workshop by IAEA, NEA, OECD-HRP and Institute for Energy Technology, Halden, Norway, **2017**.

112. Brandauer, M.; Geckeis, H.; Gentes, S.; Heneka, A.; Krauß, C. O.; Plaschke, M.; Schild, D.; Tobie, W., Monte-Carlo based study of the personal dose for an emplacement scenario of spent nuclear fuel canisters in a generic geological repository. 48. Jahrestagung Kerntechnik, Berlin, Germany, **2017**.

113. Brandauer, M.; Geckeis, H.; Gentes, S.; Heneka, A.; Krauß, C. O.; Plaschke, M.; Schild, D.; Tobie, W., Untersuchung der Strömungsverläufe in einem Magnetfilter zur Minimierung von Sekundärabfall der Wasser-Abrasiv-Suspensions-Schneidtechnik. 48. Jahrestagung Kerntechnik, Berlin, Germany, **2017**.

114. Brandauer, M.; Geckeis, H.; Gentes, S.; Heneka, A.; Krauß, C.-O.; Plaschke, M.; Schild, D.; Tobie, W., *Improvement of a separation method for the reduction of secondary waste from the waterjet abrasive suspension cutting technique.* Workshop on Current and Emerging methods for Optimising Safety and Efficiency in Nuclear Decommissioning, Sarpsborg, Norway, **2017**.

115. Brandauer, M.; Martens, A., *Innovative Reinforced Concrete Decontamination and Abrasive Waste Treatment Technologies.* 15th EPRI International Decommissioning Workshop, Lyon, France, **2017**.

116. Brandauer, M.; Starflinger, J.; Gentes, S.; Langlois, R.; Waters, K., *Magnet Rod Filter Analysis for the Treatment of Radioactive Waste from the Abrasiv Water Jet Cutting.* Physical Separation Conference 2017, Falmouth, UK, **2017**.

117. Cevirim, N.; Yalcintas, E.; Gaona, X.; Dardenne, K.; Altmaier, M.; Geckeis, H., *Redox chemistry and solubility and hydrolysis of uranium in reducing dilute to concentrated saline systems* Migration Conference, Barcelona, Spain, **2017**.

118. Cevirim, N.; Yalcintas, E.; Gaona, X.; Dardenne, K.; Altmaier, M.; Geckeis, H., *Solubility of U(VI) in dilute to concentrated KCl solutions.* Migration Conference, Barcelona, Spain, **2017**.

119. Cousseau, F.; Kaiser, S.; Gentes, S.; Engelmann, D.; Hess, U.; Kisling, M., *Development of a tool system for the surface decontamination of reinforced concrete structures.* Kontec 2017, Dresden, Germany, **2017**.

120. Dagan, R.; Herm, M.; Metz, V.; Becker, M., *Determination of minor actinides in irradiated fuel rod components.* 48th Annual Meeting on Nuclear Technology (AMNT 2017) Berlin, Germany, **2017**.

121. Dardenne, K.; Altmaier, M.; Baumann, A.; Cevirim, N.; Fellhauer, D.; Gaona, X.; Rothe, J.; Tasi, A.; Yalcintas, E.; Bruno, J.; Grivé, M.; Colàs, E.; Geckeis, H., *X-ray absorption fine structure (XAFS) determination of radionuclide speciation in aquatic media* ACTINIDE XAS 2017, 8th WORKSHOP on Speciation, Techniques, and Facilities for Radioactive Materials at Synchrotron Light Sources, University of Oxford, UK, **2017**.

122. Dardenne, K.; Prüssmann, T.; Rothe, J.; Vespa, M.; Vitova, T.; Geckeis, H., *Radionuclide research at the KIT synchrotron source ANKA. The INE Beamline and ACT experimental stations.* 8th Workshop on Speciation, Techniques, and Facilities for Radioactive Materials at Synchrotron Light Sources, Oxford, UK, **2017**.

123. Delavernhe, L.; Kupcik, T.; Joseph, C.; Montoya, V.; Glaus, M. A.; Schuhmann, R.; Emmerich, K.; Schäfer, T., *Multitracer (HTO, $^{36}Cl^-$, $^{85}Sr^{2+}$) diffusion in compacted natural and reduced-charge dioctahedral smectites* 7th Conference on Clays in Natural and Engineered barriers for radioactive waste confinement, Davos, Switzerland, **2017**.

124. Fellhauer, D.; Montoya, V.; Schepperle, J.; Gaona, X.; Metz, V.; Altmaier, M.; Geckeis, H., *Radionuclide source term estimations for generic nuclear waste repositories within the ENTRIA project.* International Workshop on Actinide and Brine Chemistry in a Salt-Based Repository (ABC-Salt V), Ruidoso, USA, **2017**.

125. Fellhauer, D.; Montoya, V.; Schepperle, J.; Gaona, X.; Metz, V.; Altmaier, M.; Geckeis, H., *Estimation of radionuclide source terms for generic nuclear waste repositories within the ENTRIA project.* ENTRIA Final Conference, Braunschweig, Germany, **2017**.

126. Fellhauer, D.; Montoya, V.; Schepperle, J.; Gaona, X.; Metz, V.; Altmaier, M.; Geckeis, H., *Estimation of radionuclide source terms for generic nuclear waste repositories within the ENTRIA project.* 16th International Conference on the Chemistry and Migration Behaviour of Actinides and Fission Products in the Geosphere (MIGRATION 2017), Barcelona, Spain, **2017**.

127. Foerstendorf, H.; Mayordomo, N.; Jordan, N.; Lutezenkirchen, J.; Alonso, U.; Missana, T.; Schmeide, K., *The surface processes of Se(IV) on α-alumina in the presence of carbonate.* 16th International Conference on the Chemistry and Migration Behaviour of Actinides and Fission Products in the Geosphere (Migration), Barcelona, Spain, **2017**.

128. Galán, H.; Núñez, A.; Sánchez, I.; Munzel, D.; Müllich, U.; Cobos, J.; Geist, A., Influence of gamma radiation on extraction systems based on diglycolamides and water soluble SO_3-Ph-BTP such the Euro-GANEX process. 21st International Solvent Extraction Conference, ISEC 2017, Miyazaki, Japan, **2017**.

129. Galanzew, J.; Pidchenko, I.; Geckeis, H.; Vitova, T., *Determination of U(V) stability in 1.5 M Na_2CO_3 aqueous solution using in-situ spectroelectrochemical cell.* European Summer School 2017, Radiochemistry & Nuclear Instrumentation (Low Level Radioactivity), Strasbourg, France, **2017**.

130. Gaona, X.; Altmaier, M.; Geckeis, H., Impact of organic ligands on the solubility of actinides under repository-relevant pH / Eh conditions. Migration Conference, Barcelona, Spain, **2017**.

131. Gaona, X.; Cevirim, N.; Böttle, M.; Yalcintas, E.; Ait Mouheb, N.; Montoya, V.; Rabung, T.; Altmaier, M., *Update on beryllium activities in KIT-INE: solubility, hydrolysis and uptake by cement.* 2nd Annual Workshop of the CEBAMA project, Espoo, Finland, **2017**.

132. Gaona, X.; Cevirim, N.; Böttle, M.; Yalcintas, E.; Altmaier, M., *Solubility and hydrolysis of beryllium in NaCl and KCl systems.* Migration Conference, Barcelona, Spain, **2017**.

133. Gaona, X.; Endrizzi, F.; Lee, J. Y.; Fellhauer, D.; Altmaier, M., Effect of elevated temperatures on actinide solubility and speciation - studies performed by KIT-INE within the German project ThermAc. 253rd American Chemical Society National Meeting and Exposition, San Francisco, USA, **2017**.

134. Gaona, X.; Fellhauer, D.; Lee, J.-Y.; Hinz, K.; Petrov, V.; Vespa, M.; Dardenne, K.; Rothe, J.; Silver, M. A.; Reed, D.; Albrecht-Schmitt, T. E.; Altmaier, M.; Geckeis, H., *Role of Np(V) solid phases in the solution chemistry of neptunium under alkaline pH conditions.* ACS Meeting, Washington DC, USA, **2017**.

135. Gaona, X.; Schepperle, J.; Yalcintas, E.; Fellhauer, D.; Cevirim, N.; Altmaier, M.; Geckeis, H., *Impact of carbonate on the solubility of An(IV) under alkaline to hyperalkaline pH conditions.* ACS Meeting, Washington DC, USA, **2017**.

136. Gaona, X.; Yalcintas, E.; Baumann, A.; Polly, R.; Altmaier, M.; Geckeis, H., *Chemistry of technetium in dilute to concentrated saline systems: redox processes, solubility and complexation.* 253rd American Chemical Society National Meeting (ACS), San Francisco, USA, **2017**.

137. Geist, A., New trends in water soluble actinide stripping agents to be pursued in the upcoming EURATOM GENIORS programme. 41st Annual Actinide Separations Conference, Argonne National Laboratory, Lemont, USA, **2017**.

138. Geist, A.; Modolo, G.; Müllich, U.; Taylor, R.; Whittaker, D.; Wilden, A.; Woodhead, D., *The extraction of An(III), Ln(III) and HNO_3 by a TODGA solvent: equilibrium modelling.* 21st International Solvent Extraction Conference, ISEC 2017, Miyazaki, Japan, **2017**.

139. Gentes, S., *Innovationspotential bei Abbruch und Rückbau*. Fachforum Energie des Tagesspiegels, Berlin, Germany, **2017**.

140. Gentes, S., *Forschungsarbeiten zum Rückbau von kerntechnischen Anlagen*. Tagung für die Junge Generation in der Kerntechnik, „Zwischen Forschung, Rückbau und Entsorgung – aktuelle Aufgaben in der Kerntechnik", Karlsruhe, Germany, **2017**.

141. Gonzalez-Robles, E.; Herm, M.; Müller, N.; Dardenne, K.; Rothe, J.; Schild, D.; Dagan, R.; Metz, V., *Composition of radionuclide containing solid phases on the inner surface of zircaloy-4*. Scientific Basis for Nuclear Waste Management Symposium 2017, Sydney, Australia, **2017**.

142. Hain, K.; Steier, P.; Eigl, R.; Froehlich, M.; Golser, R.; Hou, X.; Lachner, J.; Qiao, J.; Quinto, F.; Sakaguchi, A., *First Study of Anthropogenic U-233/U-236 Ratios in Environmental Reservoirs*. AMS 14 – 14th International Conference on Accelerator Mass Spectrometry, Ottawa, Canada, **2017**.

143. Hain, K.; Steier, P.; Eigl, R.; Froehlich, M. B.; Golser, R.; Hou, X.; Lachner, J.; Qiao, J.; Quinto, F.; Sakaguchi, A., $^{233}U/^{236}U$ – *A new tracer for environmental processes?* Vilnius, Lithuania, **2017**.

144. Hain, K.; Steier, P.; Eigl, R.; Golser, R.; Hou, X.; Lachner, J.; Qiao, J.; Quinto, F.; Sakaguchi, A., *Analysis of $^{233}U/^{236}U$ in environmental samples*. Deutsche Physikalische Gesellschaft (DPG)-Frühjahrstagung 2017, Mainz, Germany, **2017**.

145. Heberling, F.; Metz, V.; Weber, J.; Böttle, M.; Curti, E.; Klinkenberg, M.; Brandt, F.; Geckeis, H., *Barite recrystallizatuion in the presence of ^{226}Ra and ^{133}Ba*. Migration Conference, Barcelona, Spain, **2017**.

146. Held, S.; Nitschke, F.; Schill, E.; Eiche, E.; Morata, D.; Kohl, T., *Hydrochemistry and genesis of the hot spring fluids of Villarrica Geothermal system in the Andes of Southern Chile*. 41st Geothermal Research Council Annual Meeting (GRC) & GEA GeoExpo+ 2017, Salt Lake City, USA, **2017**.

147. Heneka, A.; Krauß, C. O., Magnetseperation von Korngemischen zur Minimierung von Sekudärabfällen beim WASS- Verfahren. KTG, **2017**.

148. Heneka, A.; Krauß, C. O.; Brandauer, M.; Geckeis, H.; Gentes, S.; Plaschke, M.; Schild, D.; Tobie, W., *Improvement of a separation method for the reduction of secondary waste from the waterjet abrasive suspension cutting technique*. 3rd PETRUS-ANNETTE PhD and Early-Stage Researchers Conference, Lisboa, Portugal, **2017**.

149. Herm, M.; Gonzalez-Robles, E.; Böttle, M.; Müller, N.; Bohnert, E.; Dagan, R.; Caruso, S.; Papaioannou, D.; Kienzler, B.; Metz, V.; Geckeis, H., ^{14}C *present in zircaloy-4 cladding and stainless steel sampled from an irradiated UO$_2$ fuel rod segment - inventory and chemical form after release*. GDCh Wissenschaftsforum Chemie, Berlin, Germany, **2017**.

150. Herm, M.; Müller, N.; Dardenne, K.; Rothe, J.; Schild, D.; Dagan, R.; Metz, V.; Gonzalez-Robles, E., *Comparison of calculated and measured radionuclide inventory of a zircaloy-4 cladding tube plenum section*. Scientific Basis for Nuclear Waste Management Symposium 2017, Sydney, Australia, **2017**.

151. Hess, U.; Weber, M.; Gentes, S.; Engelmann, D.; Cousseau, F.; Kisling, M., *Entwicklung eines Werkzeugsystems für die Oberflächendekontamination von Stahlbetonstrukturen*. Kontec 2017, Dresden Germany, **2017**.

152. Jähnichen, S.; Degering, D.; Haas Nüesch, R.; Heberling, F.; Schäfer, T.; Scheiber, J.; Seibt, A., *Scaling formations in a geothermal plant in the Upper Rhine Valley: From fluid to solid composition*. Annual Goldschmidt Conference, Paris, France, **2017**.

153. Jones, J. E.; Adam, C.; Geist, A.; Kaden, P.; Martin, L. R.; Natrajan, L. S.; Sharrad, C. A., *DTPA-amino acid conjugates, complexing agent and buffer in a single molecule: towards a simplified TALSPEAK process*. 21st International Solvent Extraction Conference, ISEC 2017, Miyazaki, Japan, **2017**.

154. Jones, J. E.; Adam, C.; Kaden, P.; Martin, L. R.; Geist, A.; Natrajan, L. S.-.; Sharrad, C. A., *Towards a simplified TALSPEAK process using DTPA-amino acid conjugates*. 41st Annual Actinide Separations Conference, , Argonne National Laboratory, Lemont, USA, **2017**.

155. Jones, J. E.; Langford, M. H.; Geist, A.; Panak, P. J.; Kaden, P.; Adam, C.; Adam, N.; Sharrad, C. A.; Martin, L.; Natrajan, L. S., *Modified DTPA ligand systems for simplified trivalent actinide-lanthanide separations based on the TALSPEAK process*. 253rd ACS National Meeting and Exposition, San Francisco, USA, **2017**.

156. Kaiser; Gentes; Engelmann; Geimer; Hess; Dekena; Braun; Kisling; Edelmann; Cousseau, *Definierter Abtrag hochbewehrter Stahlbetonstrukturen (DefAhS)*. 48th Annual Meeting on Nuclear Technology (AMNT 2017) Berlin, Germany, **2017**.

157. Kaiser; Hess; Cousseau; Braun; Engelmann, *Defined Removal of Highly Reinforced Concrete Structures* 48th Annual Meeting on Nuclear Technology (AMNT 2017) Berlin, Germany, **2017**.

158. Kaiser; Hess; Cousseau; Braun; Engelmann, *Definierter Abtrag hochbewehrter Stahlbetonstrukturen (DefAhS)*. "Neue Entwicklungen im Strahlenschutz und ihre Anwendung in der Praxis", TÜV SÜD, München, Germany, **2017**.

159. Kerry, T.; Sharrad, C.; Banford, A.; Carey, T.; Geist, A.; Thompson, O.; Schild, D., *Understanding Actinide Binding Mechanisms and Speciation on Stainless Steel*. WM2017 Symposia, Phoenix, USA, **2017**.

160. Kienzler, B., *Corrosion of canister material in salt brines: Summary of results*. International Workshop on Actinide and Brine Chemistry in a Salt-Based Repository (ABC-Salt V), Ruidoso, USA, **2017**.

161. Kienzler, B., *Microbial effects: Past considerations in Germany*. International Workshop on Actinide and Brine Chemistry in a Salt-Based Repository (ABC-Salt V), Ruidoso, USA, **2017**.

162. Klacic, T.; Heberling, F.; Lützenkirchen, J.; Delac, I.; Namjesnik, D.; Preocanin, T., *Surface potential of calcite in aqueous medium*. 25th Croatian meeting of chemists and chemical engineers, Poreč, Croatia, **2017**.

163. Koke, C.; Skerencak-Frech, A.; Panak, P., Fluoreszenzspektroskopie von Cm(III)-Halogenid und -Pseudohalogenidkomplexen im Temperaturbereich von T= 25-200°C. GDCh Wissenschaftsforum, Berlin, Germany, **2017**.

164. Koke, C.; Skerencak-Frech, A.; Panak, P., Fluorescence Spectroscopy of Aqueous Cm(III) Halide and Pseudohalide Complexes at Elevated Temperatures. ACTINIDES Conference, Sendai, Japan, **2017**.

165. Koll, D.; Busser, C.; Deneva, B.; Faestermann, T.; Gomez-Guzman, J.-M.; Hain, K.; Korschinek, G.; Krieg, D.; Lebert, M.; Ludwig, P.; Quinto, F., *Recent Developments for AMS with Medium Mass Isotopes at the Munich Tandem Accelerator*. AMS 14 – 14th International Conference on Accelerator Mass Spectrometry, Ottawa, Canada, **2017**.

166. Krauß, C.; Brandauer, M.; Geckeis, H.; Gentes, S.; Heneka, A.; Plascheke, M.; Schild, D.; Tobi, W., *Magnetseperation von Korngemischen zur Minimierung von Sekudärabfällen beim WASS- Verfahren*. VDI Konferenz, **2017**.

167. Krauß, C.; Gentes, S., Improvement of a Seperaion Method for the Reduction of Secondary Waste from the Water Abrasice Suspension Cutting Technique. Kontec 2017, Dresden, Germany, **2017**.

168. Krauß, C.; Gentes, S., Study of magnetic filter system for the reduction of secondary waste from the water abrasive suspension cutting technique. 48th Annual Meeting on Nuclear Technology (AMNT 2017) Berlin, Germany, **2017**.

169. Krauß, C. O.; Brandauer, M.; Geckeis, H.; Gentes, S.; Heneka, A.; Plaschke, M.; Schild, D.; Tobie, W., *Magnet separation for the reduction of secondary waste from the waterjet abrasive suspension cutting technique*. 3rd PETRUS-ANNETTE PhD and Early-Stage Researchers Conference, Lisboa, Portugal, **2017**.

170. Krauß, C.-O.; Brandauer, M.; Geckeis, H.; Gentes, S.; Heneka, A.; Plaschke, M.; Schild, D.; Tobie, W., *Verbesserung eines Separationsverfahrens zur Behandlung des Sekundärabfalls der Wasser-Abrasiv-Suspensions-Schneidtechnik*. 13. Internationales Symposium 'Konditionierung radioaktiver Betriebs- und Stilllegungsabfälle' (KONTEC 2017), Dresden, Germany, **2017**.

171. Lee, J.-Y.; Fellhauer, D.; Gaona, X.; Dardenne, K.; Johnsen, A. M.; Altmaier, M., *Solid phase transformation of Np(V) at elevated temperature in NaCl, CaCl2 and MgCl2 solutions*. 16th International Conference on the Chemistry and Migration Behaviour of Actinides and Fission Products in the Geosphere (Migration '17), Barcelona, Spain, **2017**.

172. Lützenkirchen, J., Specific ion effects on μm-size alumina particles: A surface complexation to describe shifts of isoelectric points and levels of zeta-potentials. AMAM-ICAM 2017, 2nd International Conference on Applied Mineralogy & Advanced Materials – 13th International Conference on Applied Mineralogy, Castellaneta Marina - Taranto, Italy, **2017**.

173. Lützenkirchen, J., *Surface charge of selected silica particles*. 4. Nationaler Workshop "Induzierte Polarisation", Aachen, Germany, **2017**.

174. Lützenkirchen, J.; Finck, N., Treatment of temperature dependence of interfacial speciation by speciation codes and temperature congruence of oxide surface charge. Goldschmidt Conference, Paris, France, **2017**.

175. Magnusson, D.; Malmbeck, R.; Geist, A., *Development of an improved GANEX 2nd cycle using a modified TDDGA extracting agent*. 21st International Solvent Extraction Conference, ISEC 2017, Miyazaki, Japan, **2017**.

176. Metz, V., *Near field evolution and radionuclide migration in generic spent nuclear fuel repositories.* Interdisciplinary Research on Radioactive Waste Management: Ethics - Society - Technology, Braunschweig, Germany, **2017**.

177. Metz, V., *Sicherheitsforschung am KIT-INE zur Entsorgung nuklearer Abfälle.* Tagung für die Junge Generation in der Kerntechnik: „Zwischen Forschung, Rückbau und Entsorgung – aktuelle Aufgaben in der Kerntechnik", Eggenstein-Leopoldshafen, Germany, **2017**.

178. Modolo, G.; Wilden, A.; Lumetta, G. J.; Levitskaia, T. G.; Casella, A. J.; Hall, G. B.; Law, J.; Geist, A., *Demonstration of an advanced TALSPEAK process for actinide(III)/lanthanide(III) separation.* 21st International Solvent Extraction Conference, ISEC 2017, Miyazaki, Japan, **2017**.

179. Montoya, V.; Ait Mouheb, N.; Schäfer, T.; Metz, V., *Reactive transport model in the low pH cement / bentonite interface and effects on radionuclide migration.* 2nd Annual Workshop of the CEBAMA project, Espoo, Finland, **2017**.

180. Montoya, V.; Fellhauer, D.; Metz, V.; Geckeis, H., Reactive transport modelling: near field evolution and radionuclide migration in generic spent nuclear fuel repositories. ENTRIA Final Conference, Braunschweig, Germany, **2017**.

181. Montoya, V.; Fellhauer, D.; Metz, V.; Geckeis, H., *Repository near field evolution and radionuclide migration studied by reactive transport modelling.* ENTRIA Final Conference, Braunschweig, Germany, **2017**.

182. Montoya, V.; Fellhauer, D.; Metz, V.; Geckeis, H., *Repository near field evolution and radionuclide migration studied by reactive transport modelling.* 16th International Conference on the Chemistry and Migration Behaviour of Actinides and Fission Products in the Geosphere (MIGRATION 2017), Barcelona, Spain, **2017**.

183. Montoya, V.; Kupcik, T.; Van Laer, L.; Glaus, M. A.; Marques Fernandes, M.; Baeyens, B.; Bruggeman, C.; Maes, N.; Schäfer, T., Sorption of Sr, Co and Zn on Na-illite: batch sorption experiments and modelling including some reference measurements on compacted clay samples 7th Conference on Clays in Natural and Engineered barriers for radioactive waste confinement, Davos, Switzerland, **2017**.

184. Moog, H. C.; Altmaier, M.; Bok, F.; Brendler, V.; Gaona, X.; Marquardt, C.; Montoya, V.; Richter, A.; Scharge, T.; Thoenen, T.; Voigt, W.; Yalçintaş, E., *THEREDA – Thermodynamic Reference Database.* ENTRIA Final Conference, Braunschweig, Germany, **2017**.

185. Mossini, E.; Macerata, E.; Scaravaggi, S.; Wagner, C.; Panak, P. J.; Geist, A.; Boubals, N.; Charbonnel, M.-C.; Arduini, A.; Volpi, S.; Casnati, A.; Mariani, M., *UV-Vis and TRLFS study of the outstanding An/Ln selectivity of PyTri ligands under GANEX process conditions.* 5th International Nuclear Chemistry Congress, INCC 2017, Göteborg, Sweden, **2017**.

186. Müller, S., Untersuchungen zum Geometrieeinfluss auf Hartmetalllamellen beim Betonfräsen, Paper. Kontec 2017, Dresden, Germany, **2017**.

187. Müller, S.; Gentes, S., *Untersuchungen zum Geometrieeinfluss auf Hartmetalllamellen beim Betonfräsen.* 48th Annual Meeting on Nuclear Technology (AMNT 2017) Berlin, Germany, **2017**.

188. Müller, S.; Gentes, S., *Untersuchungen zum Geometrieeinfluss auf Hartmetalllamellen beim Betonfräsen, Vortrag.* 48th Annual Meeting on Nuclear Technology (AMNT 2017) Berlin, Germany, **2017**.

189. Muñoz, A. G.; Beuth, L. R.; Finck, N.; Moog, H.; Schäfer, T., Iron corrosion in concentrated saline solutions at high T and p conditions: thermodynamic predictions and kinetic evaluations in high-level radioactive waste rock repositories. 231st ECS Meeting (Electrochemical Society), New Orleans, USA, **2017**.

190. Nie, Z.; Finck, N.; Heberling, F.; Pruessmann, T.; Liu, C.; Lützenkirchen, J., *Adsorption of selenium and strontium on goethite: surface complexation modeling of the ternary system* AMAM-ICAM 2017, 2nd International Conference on Applied Mineralogy and Advanced Materials, 13th International Congress on Applied Mineralogy, Castellaneta Marina, Italy, **2017**.

191. Nie, Z.; Finck, N.; Heberling, F.; Pruessmann, T.; Liu, C.; Lützenkirchen, J., *Adsorption of Selenium and Strontium on Goethite: Surface Complexation Modeling of the Ternary System.* AMAM-ICAM 2017, 2nd International Conference on Applied Mineralogy & Advanced Materials – 13th International Conference on Applied Mineralogy, Castellaneta Marina - Taranto, Italy, **2017**.

192. Pidchenko, I.; Schild, D.; Prüssmann, T.; Montoya, V.; Gaona, X.; Bohnert, E.; Rothe, J.; Baker, R.; Vitova, T., Study of neptunium(V) carbonate reactivity in the Na-K-U(VI)-CO$_3$-H$_2$O system: first application of Np M5 HR-XANES for characterization of Np oxidation states. 16th International Conference on the Chemistry and Migration Behaviour of Actinides and Fission Products in the Geosphere, Barcelona, Spain, **2017**.

193. Polly, R., *Computational studies of surfaces.* Thul School, Forschungszentrum Jülich, Germany, **2017**.

194. Polly, R.; Schimmelpfennig, B.; Pidchenko, I.; Vitova, T.; Geckeis, H., *Quantum Chemical Investigation of the Incorporation of Uranium(V) into Magnetite*. Jahrestagung FG Nuklearchemie, GDCH Wissenschaftsforum, Berlin, Germany, **2017**.

195. Preocanin, T.; Brkljaèa, Z.; Namjesnik, D.; Lützenkirchen, J., *Quartz-Water Interface - Complementary Experimental and Molecular Dynamics Study*. 12th International Symposium on Electrokinetics, Dresden, Germany, **2017**.

196. Quinto, F., *Ultratrace analysis of radionuclides by AMS*. Lecture at the European Summer School - Radiochemistry and nuclear instrumentation (low level radioactivity), Strasbourg, France, **2017**.

197. Quinto, F.; Blechschmidt, I.; Garcia Perez, C.; Geckeis, H.; Geyer, F.; Golser, R.; Huber, F.; Lagos, M.; Lanyon, B.; Plaschke, M.; Steier, P.; Schäfer, T., *Investigating the long-term behaviour of actinides in repository relevant conditions with the multi-actinides analysis and AMS*. Institute of Geological Sciences, University of Bern, Switzerland, **2017**.

198. Quinto, F.; Blechschmidt, I.; Garcia Perez, C.; Geckeis, H.; Geyer, F.; Golser, R.; Huber, F.; Lagos, M.; Lanyon, B.; Plaschke, M.; Steier, P.; Schäfer, T., *Multi-actinide analysis with AMS applied to in-situ radionuclide tracer tests at the Grimsel Test Site*. Lawrence Livermore National Laboratory, Livermore, USA, **2017**.

199. Quinto, F.; Faestermann, T.; Gómez Guzmán, J.-M.; Hain, K.; Korschinek, G.; Ludwig, P.; Plaschke, M.; Schäfer, T.; Steier, P.; Geckeis, H., *A novel analytical method for the ultra-trace determination of actinides and ^{99}Tc in natural water samples with Accelerator Mass Spectrometry*. 16th International Conference on the Chemistry and Migration Behaviour of Actinides and Fission Products in the Geosphere (Migration 2017), Barcelona, Spain, **2017**.

200. Quinto, F.; Geyer, F.; Lagos, M.; Plaschke, M.; Schäfer, T.; Geckeis, H., *AMS status on Run 13-05 and LIT*. Project Kollorado e2 Meeting, Karlsruhe, Germany, **2017**.

201. Quinto, F.; Geyer, F.; Lagos, M.; Plaschke, M.; Schäfer, T.; Steier, P.; Geckeis, H., *Investigating the long-term behaviour of actinides in repository relevant conditions with the multi-actinides analysis and AMS*. ENVIRA2017 - the International Conference on Environmental Radioactivity, Vilnius, Lithuania, **2017**.

202. Ratnayake, S.; Ratnayake, A.; Schild, D.; Maczka, E.; Jartych, E.; Luetzenkirchen, J.; Kosmulski, M.; Weerasooriya, R., *Chemical reduction of nitrate by zerovalent iron nanoparticles adsorbed radiation grafted copolymer matrix*. International Conference on Applications of Radiation Science and Technology (ICARST 2017), Vienna, Austria, **2017**.

203. Reed, D.; Altmaier, M., *Actinide and brine chemistry in salt repositories: Updates from ABC Salt (V)*. 8th US/German Workshop on Salt Repository Research, Design, and Operation, Middelburg, Netherlands, **2017**.

204. Sakai, A.; Koikegami, H.; Weisenburger, S.; Roth, G.; Kanehira, N.; Komamine, S., Comparison of Advanced Melting Process for HLW Vitrification, Joule-Heated Ceramic-Lined Melter (JHCM) and Cold-Crucible Induction Melter (CCIM). 25th International Conference on Nuclear Engineering, Volume 7: Fuel Cycle, Decontamination and Decommissioning, Radiation Protection, Shielding, and Waste Management : Mitigation Strategies for Beyond Design Basis Events, ASME, New York (NY): Shanghai, China, **2017**.

205. Schäfer, T.; Rinderknecht, F.; Huber, F.; Leone, D.; Garcia, C.; Quinto, F.; Heck, S.; Lanyon, B.; Blechschmidt, I., *Bentonite erosion and colloid mediated radionuclide transport: experiments and modelling*. Clay Conference, Davos, Switzerland, **2017**.

206. Schepperle, J.; Fellhauer, D.; Gaona, X.; Dardenne, K.; Rothe, J.; Schild, D.; Altmaier, M.; Geckeis, H., *Characterisation and solubility behavior of $Na_2Pu_2O_7.H_2O(cr)$ in dilute to concentrated NaCl-NaOH solutions*. International Workshop on Actinide and Brine Chemistry in a Salt-Based Repository (ABC-Salt V), Ruidoso, USA, **2017**.

207. Schepperle, J.; Fellhauer, D.; Schramm, T.; Gaona, X.; Dardenne, K.; Rothe, J.; Schild, D.; Altmaier, M.; Geckeis, H., *Pu(VI) solubility and hydrolysis in alkaline NaCl solutions*. 16th International Conference on the Chemistry and Migration Behaviour of Actinides and Fission Products in the Geosphere (Migration 2017), Barcelona, Spain, **2017**.

208. Schepperle, J.; Yalcintas, E.; Fellhauer, D.; Cevirim, N.; Gaona, X.; Altmaier, M.; Geckeis, H., *Hydroxo-carbonate complex formation and solubility of tetravalent actinides at alkaline pH conditions*. 16th International Conference on the Chemistry and Migration Behaviour of Actinides and Fission Products in the Geosphere (Migration 2017), Barcelona, Spain, **2017**.

209. Tasi, A. G.; Gaona, X.; Fellhauer, D.; Rabung, T.; Rothe, J.; Grivé, M.; Colàs, E.; Bruno, J.; Källström, K.; Altmaier, M.; Geckeis, H., *Redox. Solubility and sorption behavior of plutonium in the presence of isosaccharinic acid and cement*. Migration Conference, Barcelona, Spain, **2017**.

210. Taylor, R.; Bourg, S.; Boxall, C.; Carrott, M.; Geist, A.; Hanson, B.; Malmbeck, R.; Modolo, G.; Rhodes, C.; Sarsfield, M.; Sharrad, C.; Tinsley, T.; Whittaker, D.; Wilden, A., *Progress towards reference routes for recycling actinides in future nuclear fuel cycles*. 21st International Solvent Extraction Conference, ISEC 2017, Miyazaki, Japan, **2017**.

211. Tromm, W.; Brandauer, M., *KIT Arbeiten zum Rückbau Cluser*. 1. Workshop des Rückbau Cluster, **2017**.

212. Trumm, M.; Lindqvist-Reis, P.; Schimmelpfennig, B., *Spin-orbit effects in Eu(III)/Am(III) water clusters*. 16th International Conference on the Chemistry and Migration Behaviour of Actinides and Fission Products in the Geosphere (Migration), Barcelona, Spain, **2017**.

213. Vitova, T., *Calculations of XANES/HR-XANES spectra with the FEFF9 code*. The CAT-ACT beamline for catalyses and radioactive research at ANKA: Opening workshop KIT, Karlsruhe, Germany, **2017**.

214. Vitova, T., *HR-XANES studies at the actinide M4,5 edges*. The CAT-ACT beamline for catalyses and radioactive research at ANKA: Opening workshop KIT, Karlsruhe, Germany, **2017**.

215. Yakubov, Y.; Brandauer, M., *Alternative Methods for Decomissioning and Decontamination of pipes with small diameter*. 48th Annual Meeting on Nuclear Technology (AMNT 2017), Berlin, Germany, **2017**.

216. Yalcintas, E.; Baumann, A.; Gaona, X.; Altmaier, M.; Geckeis, H., *Thermodynamic studies with Tc at KIT–INE: inputs to THEREDA database*. ABC-Salt Workshop, Actinide Brine Chemistry, Ruidoso, USA, **2017**.

217. Yalcintas, E.; Cevirim, N.; Gaona, X.; Reed, D. T.; Altmaier, M., Redox behavior of U(VI)/U(IV) and solubility of U(IV) in repository relevant dilute to concentrated solutions in the absence and presence of complexing ligands. ACS National Meeting - San Francisco 2017, San Francisco, USA, **2017**.

218. Yalcintas, E.; Cevirim, N.; Gaona, X.; Reed, D. T.; Dardenne, K.; Altmaier, M., *Redox chemistry and solubility of uranium in dilute to concentrated NaCl systems: impact of carbonate and EDTA*. ABC-Salt Workshop, Actinide Brine Chemistry, Ruidoso, USA, **2017**.

219. Yalcintas, E.; Reed, D. T.; Gaona, X.; Altmaier, M., *Impact of EDTA on the solubility and redox behaviour of uranium in dilute to concentrated NaCl solutions*. 16th International Conference on the Chemistry and Migration Behaviour of Actinides and Fission Products in the Geosphere, Barcelona, Spain, **2017**.

220. Yalcintas, E.; Scheinost, A. C.; Gaona, X.; Altmaier, M.; Geckeis, H., *Technetium interaction with Fe(II)-minerals analysed by spectroscopy and thermodynamics*. Goldschmidt conference, Paris, France, **2017**.

221. Zellmann, E., Status of developement and experience in implementation of nuclear technology management NTM prgrammes at KIT. INMA, IAEA, **2017**.

222. Zimina, A.; Dardenne, K.; Doronkin, D.; Lichtenberg, H.; Pruessmann, T.; Rothe, J.; Vitova, T.; Geckeis, H.; Grundwaldt, J. D., *CAT-ACT - A highly versatile X-ray spectroscopy beamline for catalysis and radionuclide science at KIT*. GeCatS Infoday "Synchrotron Radiation and Neutrons for Catalysis, Materials Research and Development", Frankfurt,Germany, **2017**.

Proceedings

223. Altmaier, M.; Montoya, V.; Duro, L.; Valls, A., Proceedings of the First Annual Workshop of the HORIZON 2020 CEBAMA Project. *KIT Scientific report* **2017,** *KIT-SR 7734*.

Reports

224. Geckeis, H.; Altmaier, M.; Fanghänel, S. Annual Report 2016 - Institute for Nuclear Waste Disposal (KIT Scientific Reports ; 7743); **2017**.

225. Gentes, S.; Kramer, C.; Böhnke, D.; Ehrlich, S.; Emami-Far, H.; Kretz, S.; Krauss, C.-O.; Weber, M. Abschlussbericht FoRK: Technische, wirtschaftliche, soziale und politische Folgen durch den Rückbau eines Kernkraftwerks auf regionaler und lokaler Ebene; **2017**.

226. Heide, B. Numerical Calculation of Specific Energy Distribution of I-125 in Water with Geant4, Using Different Frequency Distributions; **2017**.

227. Herm, M.; de Visser-Tynova, E.; Heikola, T.; Ollila, K.; Gonzalez-Robles, E.; Böttle, M.; Müller, N.; Bohnert, E.; Dagan, R.; Caruso, S.; Kienzler, B.; Metz, V. *Final report on C-14 release from steels under low pH and acidic conditions (D2.16)*; **2017**.

228. Herm, M.; Gonzalez-Robles, E.; Böttle, M.; Müller, N.; Bohnert, E.; Dagan, R.; Caruso, S.; Kienzler, B.; Metz, V. *Report on C-14 release speciation from stainless steel under acidic conditions (D2.11)*; **2017**.

229. Herm, M.; Sakuragi, T.; Gonzalez-Robles, E.; Böttle, M.; Müller, N.; Bohnert, E.; Dagan, R.; Caruso, S.; Kienzler, B.; Metz, V. *Final report on ^{14}C release and speciation from zircaloy (D3.15)*; **2017**.

230. Kienzler, B. 50 Jahre Forschungs- und Entwicklungsarbeiten zur Endlagerung im KIT. (KIT Scientific Reports; 7723); **2017**.

231. Kienzler, B. F&E-Arbeiten zur Korrosion von Endlager-Behälterwerkstoffen im INE (KIT Scientific Reports; 7729); **2017**.

232. Kienzler, B. Flüssige hochradioaktive Abfälle: Verglasung und andere Optionen. (KIT Scientific Reports; 7730); **2017**.

233. Kienzler, B. Schwach- und mittelradioaktive Abfälle: Organische Matrices. (KIT Scientific Reports; 7731); **2017**.

234. Kienzler, B.; Swanson, J. S. Microbial Effects in the Context of Past German Safety Cases (KIT Scientific Reports; 7744); **2017**.

235. Manara, D.; Konings, R.; Kloosterman, J. L.; Tkaczyk, A.; Heybroek, V.; Fazio, C.; Metz, V.; Sanchez-Espinoza, V. H.; Cuervo, D.; Coeck, M.; Ricotti, M.; Heath, S.; Legrady, D.; Streit, M.; Hyvärinen, J. *Evaluation Report of the Student Research Experiences instrument". Graduate and Executive Nuclear Training and Lifelong Education - GENTLE, Deliverable D2.4.* ; **2017**.

Dissertations

236. Bahl, S. P. Advanced chemical and structural Characterization of Nuclear Waste Materials related to the Nuclear Fuel Cycle. *Ph.D. thesis*, Karlsruher Institut für Technologie (KIT), **2017**.

237. Kern, P. Elastomerreibung und Kraftübertragung beim Abscheren von aktiv betriebenen Vakuumgreifern auf rauen Oberflächen. *Dissertation,* KIT Scientific Publishing, **2017**.

238. Rinderknecht, F. R. Bentonite erosion and colloid mediated transport of radionuclides in advection controlled systems. *Ph.D. thesis*, Karlsruher Institut für Technologie (KIT), **2017**.